The Analysis Of The Platinum-Group Elements By Neutron Activation Analysis And Their Behaviour In Fire-Assay And Natural Igneous Melts In The Presence Of A Carbonaceous Volatile Phase.

by

Iain McDonald

A thesis presented for the degree of Doctor Of Philosophy,

in the Department of Geological Sciences, University of Cape Town.

August 1993

Declaration

I, the undersigned, declare that the studies contained in this thesis represent my own work and have not been submitted for a degree at another university. Appendices three, four and five of comprise research papers which were written in collaboration with others. The extent of my involvement in each of these papers is shown in the table below.

Appendix	Authors	Title Or Subject	% Contribution By I.McDonald
3	Watterson & McDonald	NAA for the precious metals.	40%
4	McDonald, Hart & Tredoux	Analysis of the PGE in S. African kimberlites by fire-assay & NAA	70%
5	McDonald, Tredoux, Lindsay Hart and de Wit	Transport of the PGE by CO under magmatic conditions.	80%

Signed ..... on the 10th day of August 1993 in Cape Town.

This thesis is dedicated to my mother, Georgina McDonald, and my brother, Stewart McDonald, for all their love and support over the last four years.

Where the vulture glides descending,
On an asphalt highway bending,
Through libraries and museums,
Galaxies and stars.

Through the windy halls of friendship,
Past the rose clipped by the bullwhip,
The motel of lost companions waits,
With heated pool and bar.

But me, I'm not stopping there,
Got my own row left to hoe,
Just another line,
In the fields of time.

When the thrasher comes I'll be stuck in the sun,
Like the dinosaurs enshrined,
But I'll know the time has come,
To give what's mine.

Neil Young 1979

Abstract.

The studies presented in this thesis can be divided into three sections. The first reviews the general chemistry and analytical chemistry of the PGE, with particular reference to the neutron activation analysis (NAA) procedures employed at the Schonland Research Centre. The merits of instrumental NAA, radiochemical NAA and nickel sulphide (NiS) preconcentration with NAA are reviewed. The NiS-NAA procedure offers the possibility of determining all of the PGE in a single aliquot and the large sample sizes employed largely eliminate problems associated with the heterogeneous distribution of the PGE in rocks which affect the instrumental and radiochemical NAA procedures. Several improvements were made to existing NiS-NAA procedures during the course of this work which allow a significant improvement in detection limits for all of the PGE. A preliminary standardization of a new PGE reference material, Wits-1, was carried out using these procedures and estimated standard concentrations are reported.

In section two, it was found that the presence of carbon in fire-assay melts produces significant losses of the PGE to the volatile phase which follow the trend Ir > Rh ~ Os > Ru ~ Pt > Pd. Radiotracer experiments confirmed the losses to the volatile phase and showed that the volatile species were preferentially adsorbed in a non-polar solvent (toluene). This indicated that the species involved might be non-polar. Infrared analysis of the non-polar toluene trap suggested the presence of metastable carbonyl compounds and these may be the species involved in transporting the PGE from the melt to the volatile phase. It is suggested that the formation of carbonyl compounds at low pressures may be promoted by an extremely fine degree of division of the PGE (possibly as metallic clusters) in the silicate melt.

Analogies are drawn between the fire-assay experiments and the case of basalts which have incorporated carbonaceous material, either from near-surface sediments or from surface vegetation, and which then degas at high temperature and atmospheric pressure. It is suggested that significant amounts of PGE might be lost from the melt to the volatile phase under these conditions. Literature data

on PGE-enriched aerosols does strongly support or deny the proposed reaction and analyses of aerosols emitted from basalts containing carbon will have to be made before any firm conclusions are possible.

In section three it is shown that the PGE signatures obtained from hypabyssal kimberlites from Brazil and southern Africa show significant differences between kimberlites emplaced into the craton and those emplaced outwith the craton. This is attributed to the contamination of kimberlitic melts passing through the craton with material from PGE-enriched, metallic pods which may have been exhumed from the deep mantle into the earliest oceanic and subsequently continental lithosphere.

The PGE patterns of Group II and isotopically transitional kimberlites may be modelled as contamination of a melt, with a fractionated (LTPGE enriched) PGE signature, with the unfractionated pod material. Group I kimberlites appear to have formed via the contamination of a PGE-poor melt with the pod material. This differences in the PGE signature of these melts does not appear to support an asthenospheric source for kimberlites. Rather it is suggested that the signatures reflect source regions which are chemically distinct in terms of PGE, in the lower lithosphere.

Acknowledgements

Let's not beat around the bush. The task of writing a PhD thesis is rarely a pleasant one. The end of it is pleasant but I remember too many late night shifts over the last three years for me to go dopey eyed with pleasure about my experience at this stage. There were several times where I wanted to pack the whole thing in and consign it to the dustbin of history, but thankfully good sense prevailed. That I made it through to the end is largely thanks to the following crew of characters.

Thanks firstly to my supervisors. Maarten de Wit got me out of of one mess in 1990 and dumped me in another one, this project. He allowed me to pursue my own thoughts and gave me the freedom to follow whatever topic I considered to be interesting. The diversity of subjects discussed in this thesis is a reflection of that. For that degree of freedom, a great trip to Barberton in 1991 and for a (well deserved) mutilation of the first draught of chapter 8, he has my sincere thanks. Marian Tredoux was the sounding board for most of my ideas on PGE geochemistry. With the aid of liberal amounts of red pen she pointed out where I had to fill the gaps in my arguments and helped assemble many of the ideas in this thesis into their final form. For her diligence with my writing and for helping set a record of 45 seconds in ^{104m}Rh Decay Time Hall Of Fame at SAFARI-1, she has my deepest thanks. Last but not least comes Rodger Hart, who managed the NAA facilities at Schonland Centre in Johannesburg. Our extended discussions on football, women, art, politics and (occasionally) geology helped me survive the ups and downs of continual labwork. Thanks Rodger.

Financial support during the course of this thesis was provided by a J.W. Jagger scholarship from the University of Cape Town. I would also like to thank the Geological Survey of South Africa for supporting the PGE lab at Schonland Centre through grants to Rodger Hart.

My colleagues for most of the last three years at Schonland Centre deserve special thanks. Particularly John Beer, who helped me fix pumps and furnaces when they gave out. Hugo Andeweg, who taught me to appreciate and understand the

detector systems. Rodger Fearick solved my computing problems and always had an answer for whatever problem I dropped into his lap. Raju Kala helped with the neutron source irradiations and numerous other little jobs and Carl Erasmus was a veritable goldmine of information on NAA and PGE analysis. Very special thanks to Ashok Damarupashad and Sam Masala, who shared an office with me. I will remember our discussions on sport, politics and all the rest for a long time.

Thanks to the Schonland footballers; Elias, Eddy, Simon, Mervyn, Raju, Sha, Mike, Bransby, Silas, Sampson, Johannes, Martin, Matthew, Louis, Thabo, William, Haresh, Sanjiv, Osborne, Peter, Jacob, Ray, Ashok, Stewart, Paul and Zeblon. Thanks guys, we had some great games.

Thanks to the folks at AER, namely Annagret Tegen, Silas Hlapolosa and especially Christine Müller, for allowing me continual use of their analytical balance and for picking me up when I was feeling down.

My warmest thanks go to my two fellow foreign legionnaires and true friends, Elias (Partisan) Haddad and Erich (Baron) Muskat. Their humour and their company during the long nights spent in the lab was what got me through in the end and I'm in their debt for that.

Thanks to Id Software for Wolfenstein 3D, although the guy that designed the maze of secret doors on level 8 in Operation Eisenfaust deserves to be put up against a wall and shot. Thanks also to Dynamix Software for Aces Of The Pacific and Red Baron. The latter saw Captain Papandreau, Captain Snoopy and Baron Muskat locked in aerial combat over the fields of France well into the night.

The folks at BPI Geophysics (now sadly departed). Johan Kruger was the first to point me in the direction of the Bushveld Pt pipes. Craig Smith and Fanus Viljoen have been a never-ending source of kimberlite samples and good advice and chapter 8 exists in its final form thanks to discussions with them. Thanks guys.

Thanks to Julian, Peter, Tony, Andrew, Barry, Colin, Susan and Caroline for helping make the Bozz a cheery place to drink when the rigours of science became too much to bear.

Thanks to Brad Lifegiver, Chong, Fritz Bred-und-Butta, Kronos Nobrain, Smarx, Dumb-pirate Robert, Clutch Ballcox, Bogey Trapspringer, Shaggy, Artie Fufkin (Polymer Records), Lou Carpenter, and Di Haw (in reality Ashley, Greg, Robbie, Antonio, Linton, Daryl, Neil, Stewart, John, Brian, Dean and Graham) for some sanity-saving Dungeons and Dragons games over the last three years.

The following people at AEC (Pelindaba) deserve special thanks. Marco Andreoli was always full of good ideas and at times was often more enthusiastic about my work than I was. Arno Faanhof, Franki Fouché, Don Bogart, Don Robertson, Org Exley, John MacDonald and Piet Louw helped arrange Rh irradiations and provided me with technical information on the SAFARI-1 reactor. Thanks also to SAFARI-1 for behaving itself reasonably well over the last three years.

Finally, thanks to the folk at my "home" university in Cape Town, namely Cornel and Ginny de Ronde, Protea Hirschel, Luiz Bizzi, Jeff Loen, Kevin Faure and Nick Steven, who helped make the times in between all the labwork so much more enjoyable.

List Of Abbreviations.

(1) Pressures and temperatures are expressed in megapascals (MPa) and degrees centigrade (°C);

(2) All chemical elements, salts and compounds are expressed by their IUPAC approved formulae;

(3) PGE = Platinum Group Elements (Os, Ir Ru, Rh, Pt, Pd);
HTPGE = High Temperature PGE (those with elemental melting points >2000°C [Os, Ir, Ru]);
LTPGE = Low Temperature PGE (those with elemental melting points <2000°C [Rh, Pt, Pd]);

(4) REE = Rare Earth Elements (La, Ce, Pr, Nd, Pm, Sm, Eu, Gd, Tb, Dy, Ho, Er, Tm, Yb, Lu);

(5) ppm = parts per million (10^6) ie. $mg.kg^{-1}$;
ppb = parts per billion (10^9) ie. $\mu g.kg^{-1}$;

(6) NAA = Neutron activation analysis;
INAA = Instrumental NAA;
RNAA = Radiochemical NAA;

(7) XRF = X-ray Fluoresence Spectrometry;
XRD = X-ray Diffraction;
PIXE = Particle Induced X-ray Emission;

(8) ICP-MS = Inductively Coupled Plasma (source) Mass Spectrometry;

(9) NiS = Nickel sulphide;
NiS-NAA = Nickel sulphide fire-assay followed by NAA;

(10) RSD = Relative standard deviation, defined as Y/Z
where Y = the standard deviation of a dataset from the mean value
and Z = the mean value of the dataset;
COV = Coefficient of variation. This is the RSD expressed as a percentage ie. (Y/Z) x 100%;

(11) Ge(Li) = Ge semiconductor doped with Li atoms;
HPGe = High Purity Ge, containing $<10^{10}$ impurity atoms per cm^3 of Ge;

(12) AEC = Atomic Energy Corporation of South Africa Ltd.;

(13) MORB = Mid-ocean ridge basalt;
OIB = Ocean island basalt;
CFB = Continental flood basalt;

(14) K/T = Cretaceous-Tertiary, particularly used in discussing the boundary between these periods;

(15) BA = Bon Accord Ni-rich body from the Barberton greenstone belt.

Table Of Contents

List Of Figures.

List Of Tables

Chapter 1

Introduction And Historical Review.

The platinum-group elements (PGE) are a suite of six transition metals occupying the second and third rows of group VIII of the the periodic table. The six PGE, ruthenium (Ru), osmium (Os), rhodium (Rh), iridium (Ir), palladium (Pd) and platinum (Pt), along with gold (Au) are collectively known as the "noble metals". This term arises from their observed lack of reactivity with simple aqueous reagents such as acids and alkalis. The most striking geochemical feature of the PGE is their rarity in the Earth's crust (Cotton and Wilkinson 1980; Westland 1981). The PGE typically occur in most rocks in concentrations of a few parts per billion (ppb) and this has presented the single most difficult obstruction to studies directed at understanding their behaviour in geological processes (Crocket 1981). However, despite these low general concentrations, some geological processes are able to concentrate the PGE into particular horizons or bodies of rock (Naldrett 1981) or even into the volatile phase of an igneous melt (Zoller et al. 1983). Some geochemical processes which might effect such transport and concentration are discussed in this thesis.

The earliest known use and working of Pt is on the ancient Thebes Casket. Heiroglyphs fashioned from an alloy of the PGE, presumably collected along with gold from alluvial deposits, are found on the 2700 year old artifact, and Pt, again probably collected from alluvial gravels, was used in conjunction with gold in South America long before the arrival of the Spanish in the 16th century (Robson 1985). However, the first systematic investigation of the chemical and physical properties of the PGE springs from the time of the Spanish conquest. The name platinum derives from the unfortunately rather derogatory term "platina" meaning "little silver". The metal's restricted workability; the fact that its alloys were very much less malleable than gold and could not be smelted using the equipment available at the time, meant that it was viewed as very much less valuable than gold (Robson 1985). In fact the major use of "platina" during the 16th and 17th centuries was as part of counterfeiting operations (de Ment and Drake 1949), filling the centres of hollowed out gold bars. "Platina" was much

superior to lead for these activities due to its specific gravity, which is much closer to that of gold. This practice lead to the banning of all exports of "platina" from the New World by the Spanish government and all known stocks were dumped at sea (de Ment and Drake 1949).

It was not until the middle of the eighteenth century that formal chemical investigation of natural "platina" nuggets was carried out. In 1751, Scheffer, a Swedish assayer and director of the Stockholm mint, and in 1752, Watson, an English chemist, both published accounts which recognised "platina" as a new element. The substance was given its formal name platinum and the symbol Pt by Bergman in 1771 (Hunt 1977). During research on the purification of platinum, Wollaston demonstrated that the "element" described in the previous studies was in fact an alloy. In 1803, Wollaston isolated two new elements. The first was named palladium (Pd). The name was taken from the asteroid Pallas which had been discovered a year earlier. The second new element was rhodium (Rh), from the greek rodon (ροδον) meaning rose. This name came from the red colour of Rhodium's compounds (Greenwood and Earnshaw 1984).

These discoveries were followed in 1804 by Tennant's isolation of two more elements from the residue left over after crude platinum was treated with aqua regia. Iridium (Ir) was named by Tennant from the greek Iris (Ιρισ), goddess of the rainbow, after the variety of colour of its salts. And osmium (Os) from the greek osme (οσμε), meaning smell, on account of the odour of its volatile tetroxide (Greenwood and Earnshaw 1984). In 1827, Osann announced the discovery of three more new elements, pluran, ruthen and polin. which he claimed to have isolated from the residue left after dissolution of platinum ore from the Ural Mountains. However Osann's claim was disputed by his co-worker Berzelius and it was rejected (de Ment and Drake 1949). In 1844, K.Klaus repeated Osann's experiment and showed that although Osann's ruthen oxide was very impure, it did contain a new element, and out of respect for Osann he named it ruthenium (Ru), after Ruthenia, the latin for Russia (Greenwood and Earnshaw 1984).

Prior to the Industrial Revolution, the highly refractory nature of the PGE limited their uses primarily to jewellery and for decorating personal possessions (Robson 1985). This state of affairs was dispelled with the invention of the oxyhydrogen blowpipe by Hare in the middle of the nineteenth century. This development

meant that for the first time, the PGE could be melted and fashioned into any desired form. Since that time the platinum metals industry has blossomed and has expanded tremendously (de Wit 1985; Hartley 1991).

Between 1828 and 1841, platinum was used in imperial Russia for coinage purposes, but owing to the impossibility at that time of stabilising the price of the metal, its use was abandoned (Wagner 1929). Around the turn of the century, the PGE rapidly found uses in temperature measuring instruments and for inert and high temperature laboratory equipment. In the early years of this century, recognition of their role as catalysts extended their application into the bulk manufacture of chemicals, notably the manufacture of sulphuric and nitric acids (Greenwood and Earnshaw 1984; Hartley 1991).

Since the Second World War, the PGE have found yet more extensive uses as technology has expanded. They now have a wide range of applications ranging from dental alloys, autocatalysts and electrical components, as well as uses in the fine chemical and glass industries. Platinum jewellery remains popular, especially in the far east, and more recently a wide range of platinum bullion products have been mooted alongside gold as an investment commodity (Greenwood and Earnshaw 1984; Robson 1985). There is a growing interest in the use of the PGE in fuel cells (de Wit 1985; Hartley 1991) and it is likely that this will provide another huge market for the PGE in the near future.

The primary sources of the PGE for the world economy have changed with time. The principal supplier of raw platinum to Europe up to 1820 was Colombia. In 1822, exploitable reserves of the PGE were proven in the alluvial goldfields of the Ural Mountains in Russia. Production of platinum metals from Ekaterinburg (renamed Sverdlovsk under communist rule) began in 1824 (Wagner 1929) and by 1827 Russia had succeeded Colombia as the world's largest producer (Robson 1985). In 1888, PGE were discovered in the Ni-Cu ores of the Sudbury Massif in Canada, and in 1927 alluvial platinum was found in Goodnews Bay in Alaska. These deposits however were completely overshadowed by Hans Merensky's discovery in 1925 of the extensive PGE horizons of the Bushveld Complex of the Transvaal, South Africa (Wagner 1929). This single deposit broke the reliance on alluvial gravels and firmly established magmatic sulphide deposits as the primary source of the PGE. Today, the Republic of South Africa and the Russian Republic,

through its Noril'sk-Talnakh magmatic sulphide deposit, remain the world's largest producers of the PGE. (Naldrett 1981; de Wit 1985).

Political sensitivities and fears about the stability of supply from South Africa and, more recently, the former Soviet Union, have turned PGE ores into a prime exploration target (De Wit 1985; Morrisey 1988; R. Boyd pers. comm. 1992). Canada continues to supply a significant fraction of world production as a by-product of the Sudbury Ni-Cu ores, and 1987 saw the start of mining at the United States' first major source of the PGE, the Stillwater Complex of Montana. Other potential deposits, notably the Penikat intrusion in Finland and the Leka intrusion in Norway, have been the subject of recent exploration programs (Alapieti and Lahtinen 1986; Boyd et al. 1992). One other notable candidate is the Dufek Complex in Antarctica. After the Bushveld Complex, this is the second largest igneous intrusion in the world (De Wit and Kruger 1990). It has not yet been explored, but the feasibility of Pt mining in such an environment, should a deposit be found, has been discussed by De Wit (1985).

The physics and chemistry of many of the geological processes which have been inferred to transport and concentrate the PGE are not well constrained (E.D. Kinloch pers. comm. 1991). This stems in large part from the restricted nature of our database for the distribution of the PGE in most common rock types (> 90% of PGE studies deal only with with occurrences in basic and ultrabasic rocks; Tredoux 1990). Even the concentration processes inferred to have occurred to produce an intensely studied deposit such as the Merensky Reef of the Bushveld Complex are a matter of heated debate (Campbell et al. 1983; Campbell and Barnes 1984; Boudeau et al. 1986; Stumpfl and Ballhaus 1986).

This thesis can be regarded as being split into three principal sections. The intention of the first five chapters is to summarize our existing knowledge of PGE chemistry and evaluate the various techniques which can be used for the analysis of the PGE at ppb levels. Included is a chapter on the theory of the principal analytical technique employed in this study, instrumental neutron activation analysis (INAA), and an outline of some modifications made by the author to previous PGE analysis procedures.

Section two, comprising chapters six and seven, assesses the problem of how the PGE might be transported and concentrated into a volatile phase, particularly in

igneous systems which are poor in sulphide. Evidence will be presented to show that in the absence of a sulphide melt, the PGE may show strong associations with carbon. It would appear that under certain conditions, the carbon association and the postulated transport of the PGE as volatile carbonyls or related species, may be competitive with the extraction of the PGE by a sulphide melt. A reaction mechanism is proposed and suggested as a possible means for generating Ir enrichments in the aerosols emitted from volcanic events. The inter-PGE fractionation trends predicted from the fire-assay experiments are compared with natural igneous rocks which are believed to have interacted with large amounts of carbonaceous volatiles.

Section three comprises chapter eight. This section examines the concentrations of PGE found in kimberlite rocks and discusses the role of PGE geochemistry in understanding the formation of various types of kimberlite and their interactions with the lithosphere. Chapter nine is a final summary which draws on the conclusions of the previous chapters and makes recommendations for future research.

Chapter 2.

The Inorganic Chemistry And Geochemistry Of The PGE.

2.1. Introduction.

The PGE, along with Fe, Co and Ni, comprise Group VIII of the periodic table (see Figure 2.1). The PGE are members of the d or transition block of the periodic table and they display all of the associated properties of transition metals. They contain d outer electron orbitals which are only partly filled. All of the PGE show variable oxidation states and display coloured ions and compounds in one if not all of these oxidation states (Cotton and Wilkinson 1980). As they are metallic elements, they display all of the properties normally expected of metals, namely the formation of alloys, a degree of malleability and ductility and the ability to conduct heat and electricity.

Group IIIa	Group IVa	Group Va	Group VIa	Group VIIa	Group VIII			Group Ib	Group IIb
Sc	Ti	V	Cr	Mn	Fe	Co	Ni	Cu	Zn
Y	Zr	Nb	Mo	Tc	Ru	Rh	Pd	Ag	Cd
La	Hf	Ta	W	Re	Os	Ir	Pt	Au	Hg

Figure 2.1.: The position of the Group VIII metals within the d block of the periodic table.

The chemical reactions of this group of elements with simple chemical reagents have been intensively studied. Their general and coordination chemistry is well reviewed by Livingston (1975), Cotton and Wilkinson (1980), Westland (1981) and Greenwood and Earnshaw (1984). Beamish (1966), Beamish and Van Loon (1972; 1977), Crocket (1981) and Lenahan and Murray-Smith (1986) discuss the analytical chemistry of the PGE.

It should be emphasized that many of the reactions and notes on PGE reactivity contained within this chapter pertain only to the general or laboratory chemistry of the PGE. Reactions which can be performed under well constrained laboratory conditions are not always representative of the reaction chemistry which occurs in the geological environment. Local geological conditions will exert a strong influence on possible reaction pathways and any inferences drawn from laboratory experiments should always be seen in this light.

2.2. Physical Properties Of The PGE.

In some respects, the six PGE resemble one another in their chemical behaviour. This behaviour often differs markedly from their first row counterparts Fe, Co and Ni. A summary of some of the chemical and physical properties of the Group VIII elements is presented in Table 2.1. , below. The data is drawn from Livingston (1975), Cotton and Wilkinson (1980), Westland (1981), and Greenwood and Earnshaw (1984) and the reader should consult these references for more specific information.

Table 2.1.: Summary of physical properties of the Group VIII metals

	Fe	Ru	Os	Co	Rh	Ir	Ni	Pd	Pt
Atomic Number	26	44	76	27	45	77	28	46	78
Atomic Weight	55.85	101.70	190.2	53.93	102.91	199.22	58.69	106.42	195.1
Electronic Configuration	[Ar] $3d^6\ 4s^2$	[Kr] $4d^6\ 5s^2$	[Xe] $5d^6\ 6s^2$	[Ar] $3d^7\ 4s^2$	[Kr] $4d^8\ 5s^1$	[Xe] $5d^7\ 6s^2$	[Ar] $3d^8\ 4s^2$	[Kr] $4d^{10}$	[Xe] $5d^9\ 6s^1$
Lattice Structure	bcc/fcc	hcp	hcp	hcp/fcc	fcc	fcc	fcc	fcc	fcc
Density ($g.cm^{-3}$)	7.87	12.41	22.59	8.90	12.39	22.56	8.91	12.01	21.45
Melting Point (°C)	1535	2334	3050	1495	1967	2454	1455	1555	1768
Boiling Point (°C)	2750	4045*	5025*	3100	3760	4550*	2920	2940	4170
ΔH_{fus} ($kJ\ mol^{-1}$)	13.8	25.5	31.7	16.3	21.6	26.4	17.5	17.6	19.7
ΔH_{vap} ($kJ\ mol^{-1}$)	340	--	738	382	494	622	375	362	469
Electronegativity	1.8	2.2	2.2	1.8	2.2	2.2	1.8	2.2	2.2
Oxidation State (Highest)	+6	+8	+8	+5	+6	+6	+4	+4	+6
(Most Common)	+2 or +3	+3	+4	+2 or +3	+3	+3	+2	+2	+2 (+4)

* indicates that there is ± 100°C uncertainty on this measurement,
hcp = hexagonal close packed, bcc = body centred cubic, fcc = face centred cubic

The stereochemistry of the Group VIII metals is commonly that of octahedral coordination, but in the lower oxidation states, a variety of planar, tetrahedral or trigonal bypyramidal geometries are found. The divalent ions of the Ni group, (Ni^{2+}, Pd^{2+} and Pt^{2+}) all show a strong preference for a D_{4h} or square planar geometry. D_{4h} symmetry is characteristic of the d^8 outer electron configuration. Monovalent Rh and Ir compounds also have a d^8 electron configuration and those with a coordination number of four will also favour a square planar geometry.

Several general trends are immediately apparent from Table 2.1. and these can be summarized as follows:

(1) There is a general decrease in the range of available oxidation states exhibited as one moves from the Fe group to the Ni group. The most common oxidation state generally also decreases as one moves in this direction.
(2) There is a progressive decrease in the melting points of the metals from the Fe-Ru-Os triad to the Ni-Pd-Pt triad.
(3) The lattice structure of the metals changes from bcc/hcp in the Fe-Ru-Os group to fcc in the Ni-Pd-Pt group. This affects the mechanical properties of the metals quite strongly. The hcp metals, Ru and Os are much less malleable than their cubic close packed neighbours and can only be worked after special preparation and even then, only with great difficulty.
(4) There is a general decrease in density in the second and third row triads with Ru>Rh>Pd and Os>Ir>Pt. This is the opposite of the density trend among the first row triad, where Fe<Co<Ni. Os and Ir are the densest naturally occurring elements in the periodic table.
(5) The metallic and electronic properties of the metals suggest a grouping based on the groups Fe-Ru-Os (a sum of 8 s and d electrons), Co-Rh-Ir (a sum of 9 s and d electrons) and Ni-Pd-Pt (a sum of 10 s and d electrons). This classification is the one most commonly adopted by inorganic, and particularly, organometallic chemists to explain similarities in oxidation states, stereochemistries, exchange reactions, paramagnetic strengths and some catalytic properties.

Other schemes for grouping the PGE have been suggested, principally to account for some of their grouped occurrences in nature. Barnes et al. (1985) saw the metals Os, Ir and Ru as Ir associated (IrPGE) and Rh, Pt and Pd as Pt associated (PtPGE) without defining any physical property which caused such a

discrimination. Cabri (1972) and Wedepohl (1978) group the PGE on the basis of atomic weight or density. This yields the heavy triad of Os-Ir-Pt and the lighter triad of Ru-Rh-Pd. Melting point was first used as a discriminant by Naldrett et al. (1979). At the time, these authors drew no particular significance to it but the idea was resurrected by Tredoux et al. (1986) in an attempt to explain the apparent separation of the PGE during igneous melting. Tredoux et al. (1986) define a high temperature PGE (HTPGE) group comprising, Os-Ir-Ru, and a low temperature PGE (LTPGE) group made up of, Rh-Pt-Pd.

It is this author's opinion that none of the subdivisions of the PGE adopted above can be taken as a universal guide-line for PGE behaviour. Each of the groupings or divisions is applicable only to a certain set of conditions. Outside of those conditions, behaviour of individual PGE might be very different. For example, low temperature solution chemistry will be much more strongly influenced by the electronic and complexing properties of the metals with respect to aqueous or organic species than a consideration of the melting points of the metals. Equally, when one is attempting to decide which metals might separate from the other PGE during high temperature igneous melting then obviously a consideration of their melting points would appear to be more useful than their electronic bonding properties. Logic, and some knowledge of the prevailing conditions, should dictate which classification or grouping of the metals might best fit a given situation and which physical or chemical property might exercise the principal control on the final PGE distribution.

2.3. Reactivity And Chemical Behaviour Of The Platinum Group Metals.

2.3.1. Formation Of Alloys.

As can be seen from Table 2.1., Os and Ru possess a hexagonal symmetry while the other PGE have a cubic symmetry. Although this difference in crystallography is the strongest factor limiting solid solution in binary and ternary alloys (Blum et al. 1989), it was noted by Berlincourt et al. (1981) that despite this, the PGE have a general tendency to be mutually soluble in one another and can substitute for one another in alloys and compounds with other elements. Table 2.2. summarizes those metals which show complete and restricted solid solutions with the individual PGE.

Table 2.2.: Summary of metal-PGE solid solutions. Data from Berlincourt et al. (1981) and references therewithin.

	Lattice Structure	Complete Solid Solution	Partial Solid Solution
Ru	h.c.p.	Os, Fe, Ni	Pt, Rh, Ir, Pd
Os	h.c.p.	Ru, Fe, Ni	Pt, Rh, Ir
Rh	f.c.c.	Pt, Pd, Ir, Ni, Cu	Ru, Os, Fe
Ir	f.c.c.	Pt, Pd, Rh, Ni, Fe	Ru, Os, Sn
Pd	f.c.c.	Pt, Rh, Ir, Ni, Cu	Ru, Fe, Bi, In, Sn, Pb
Pt	f.c.c.	Pd, Rh, Ir, Ni, Cu, Fe	Ru, Os, In, Sb, Sn

Natural PGE alloys contain many of the metals listed in Table 2.2. as major or minor components. Cabri (1981) has compiled the most extensive list of known PGE alloys, to date. About 100 different species have been listed.

As is apparent from Table 2.2., in the presence of iron metal, all of the PGE can display some siderophile behaviour (Sun 1982). It would appear that this process may cause considerable fractionation of the individual PGE. Using Fe alloys containing 1-2% Ni, Fleet and Stone (1991) were able to show that the overall siderophile tendency appears to be Os ≥ Ir > Pt > Ru > Rh » Pd. The estimated partition coefficients, between Fe alloy and FeS, for the individual PGE vary over at least 2 orders of magnitude (1-2 for Pd and possibly 1000 for Os and Ir).

Blum et al. (1988) examined the behaviour of Os, Ir, Ru and Pt during the oxidation of Fe-Ni alloy. They found that Os and Ru exsolved from the Fe-Ni alloy phase to form discrete nuggets of Os-Ru alloy. Pt was retained in the Fe-Ni alloy and was not present in any other phase. Ir showed intermediate behaviour and was found to be present in both the Fe-Ni alloy and in the Os-Ru nuggets.

Berlincourt et al. (1981) showed that due to the different crystal structures present, Os-Fe and Ru-Fe alloy compositions had a very restricted range. In contrast, Pt-Fe and Ir-Fe alloy compositions could be quite variable. Depending on the temperature, Pt can accommodate between 17 and 50 atomic % Fe in solid solution. Ir is somewhat less flexible. It can accommodate between 40 and 60 atomic % Fe in solid solution. The compatibility of crystal structures (hcp:fcc vs. fcc:fcc) and the capacity for non-ideality in these alloy systems may explain why Pt

appears to be preferentially retained within the Fe-Ni alloy phase at the expense of Ir, Os and Ru.

2.3.2. Reaction With Acids And Alkalis.

The six PGE are relatively unreactive towards simple aqueous reagents such as dilute acids or alkalis (Beamish 1966; Cotton and Wilkinson 1980; Westland 1981). Additional oxidants or mixtures of strong acids are usually required. Table 2.3. summarizes the best solvent(s) for each metal.

Table 2.3.: Summary of the best acid/base solvents for the PGE (after Cotton and Wilkinson 1980).

Element	Best Solvent(s)
Os	Alkaline oxidising fusion
Ru	Alkaline oxidising fusion
Ir	Conc. HCl + $NaClO_3$ at 125-150°C
Rh	Hot conc. H_2SO_4 or conc. HCl + $NaClO_3$ at 150°C
Pt	Aqua Regia (3 volumes HCl : 1 volume HNO_3)
Pd	Conc. HNO_3 or HCl + Cl_2

Hot, concentrated mineral acids will slowly dissolve Pd, Ru and Os. The latter however is only attacked when in a very finely divided form. Ru and Os acid dissolutions tend to be very slow even above 100°C and the metals are generally best dissolved by an alkaline oxidising fusion using $KClO_3$ or a combination of NaOH and Na_2O_2 (Cotton and Wilkinson 1980). Rhodium and iridium can be dissolved in concentrated HCl with an additional oxidant or under a pressure of oxygen, but in general they are hardly attacked at all by most acids or combinations of acids alone, even when the metals are finely divided (Greenwood and Earnshaw 1984).

Pt and Pd are rather more reactive than the other metals. Both are rapidly attacked by fused alkali oxides and peroxides. Pd can be dissolved in nitric acid to yield $Pd(NO_3).(OH)_2$. In the massive state, this reaction is quite slow but it can be promoted by the presence of oxygen or oxides of nitrogen. Finely divided Pd will slowly dissolve in HCl but the reaction requires the presence of oxidants such as free chlorine or oxygen. Pt is considerably more resistant to dissolution by acids and is not attacked by any single mineral acid. Mixtures of acids such as aqua regia tend to be more effective. Aqua regia will dissolve Pd rapidly and Pt quite

readily. The combination of acids in a mixture such as aqua regia is more effective in attacking the PGE than either of the components alone for two reasons (Westland 1981): firstly, the mixture generates chlorine and nitrosyl chloride, both of which are very powerful oxidants, and secondly, the excess HCl in the mixture complexes with metal ions produced, making the corrosion products stable. However, it is notable that alloys of Pt with the other PGE are considerably less reactive than pure Pt alone.

The hypochlorite ion is another powerful oxidant, capable in theory of oxidising all of the PGE. In fact, both ruthenium and osmium dissolve in hypochlorite solution but the reagent is less effective towards the other PGE as these quickly form surface layers of a protective, insoluble oxide at high pH and Eh which effectively prevents further attack (Westland 1981). It should be emphasized then, that the resistance of some PGE to attack by these oxidising solutions in many cases is <u>not</u> due to the supposedly "noble" character of the metals as defined by their high electrode potentials. The behaviour of a metal under oxidation is often more fundamentally controlled by the kinetics of each reaction system (Westland 1981). Slow reactions will make the PGE appear "noble" but they can be attacked and dissolved by a number of reagents. The behaviour of the various PGE species in acidic and basic solutions is discussed in section 2.4.

2.3.3. Reactions With Oxygen And The Halogens.

All of the PGE, unlike gold, react with oxygen at elevated temperatures to yield a variety of mono-, di-, tri- and tetroxides. Alcock and Hooper (1960) demonstrated that although volatile oxides are formed by all of the metals when they are heated in air, their oxide pressures are very low except in the case of OsO_4. The PGE oxides usually dissociate again on strong heating. They are generally rather inert to aqueous acids and can be reduced back to the metal again by reaction under a stream of hydrogen.

The most active gas phase components for the PGE at elevated temperatures are the halides, fluorine and chlorine. The PGE metals or their alloys at red heat are completely attacked by a stream of chlorine (Westland 1981; Cotton and Wilkinson 1980). The action of fluorine at high temperatures on the PGE leads to the formation of highly oxidised and reactive PGE fluorides. In these compounds the metals typically attain oxidation states in excess of +4.

The most important PGE halide compounds are the hexafluorides. Of these, only that of Pd is not yet known (Cotton and Wilkinson 1980). The PGE hexafluorides are prepared by direct fluorination of the metals at elevated temperatures and moderate pressures (<10 atmospheres). The PGE species decrease in stability in the order Os > Ir > Pt,Rh > Ru. The compounds react violently to heat and to ultraviolet radiation, dissociating into fluorine and the lower PGE fluorides. PtF_6 is one of the most powerful oxidising agents known. It was found to be powerful enough to oxidise the inert gas xenon (Xe), creating a variety of novel xenon fluorides. The reaction suggested by Bartlett et al. (1973) is shown in equation (2a) below:

$$Xe + 2\,PtF_6 \longrightarrow [XeF^+]\,[PtF_6^-] + PtF_5 \longrightarrow [XeF^+]\,[Pt_2F_{11}^-] \qquad \text{...equation (2a)}$$

All of the PGE hexafluorides are exceptionally reactive substances. The vapours hydrolyse with water vapour and can react violently with liquid water. IrF_6 will react with water to give HF, O_2, O_3 and IrO_2. OsF_6 reacts to give OsF_5 , OsO_4 and HF. PtF_6 and RhF_6 react with glass at room temperature and all of the PGE hexafluorides will attack silica at high temperatures.

The pentafluorides and lower order PGE fluorides can be obtained by controlled fluorination of the metal or by decomposition of the hexafluorides. These compounds, like the hexafluorides, are generally highly reactive and are violently hydrolysed by interaction with water. Only RhF_3 and IrF_3 are relatively stable (ie non-explosive) in the presence of water (Cotton and Wilkinson 1980).

The other PGE halides, most notably the chlorides, are formed by direct interaction between the metals and gas at high temperatures. In contrast to the fluorides, the higher halides of this group are more stable and they form from the the lower halides on heating. Except for the chlorides of Pt and Pd, the other anhydrous halides are generally insoluble in water and rather inert to other reagents apart from HCl. Some of the most common chloride, bromide and iodide species are listed in Table 2.4., below.

$PtCl_2$ and $PdCl_2$ are very soluble in HCl, forming $[PtCl_4]^{2-}$ and $[PdCl_4]^{2-}$. These species can undergo a variety of reactions with species such as amines and phosphines to give complexes of the forms $Pd(Cl)_2(NH_3)_2$ and $[Pd(NH_3)(Cl)_2]_2$.

Table 2.4.: Summary of anhydrous halides of the PGE (after Cotton and Wilkinson 1980).

Oxidation State	Ru	Os	Rh	Ir	Pd	Pt
+2	unknown	unknown	unknown	unknown	$PdCl_2$	$PtCl_2$
	-	-	-	-	$PdBr_2$	$PtBr_2$
	-	-	-	-	PdI_2	PtI_2
+3	$RuCl_3$	$OsCl_3$	$RhCl_3$	$IrCl_3$	unknown	$PtCl_3$
	$RuBr_3$	$OsBr_3$	$RhBr_3$	$IrBr_3$	-	$PtBr_3$
	RuI_3	OsI_3	RhI_3	IrI_3	-	PtI_3
+4	unknown	$OsCl_4$	unknown	$IrCl_4$(?)	unknown	$PtCl_4$
	-	$OsBr_4$	-	$IrBr_4$(?)	-	$PtBr_4$
	-	-	-	IrI_4(?)	-	PtI_4

The PGE are stabilized in these high oxidation states by an interaction with surrounding "hard" ligands such as the halides and oxygen. The "hard" interaction takes place by electron sharing and a direct sigma-type bonding. However the compounds are generally only partly ionic. The structures tend to be molecular units which are strongly controlled by shared halogens or halogen bridges, rather than metal-metal bonds.

As can be seen from the examples noted above, the "noble" character of the PGE can be overcome and they can be made into highly reactive, oxidised species.

2.3.4. Reactions With Sulphur And Other P Block Elements.

In nature, the PGE generally do not appear to show much association with "hard" ligands. They appear more often to be stabilized by the "soft" acids of the P block of the periodic table, forming a wide variety of sulphides, tellurides or arsenides. The "soft" interaction is more covalent in character and involves electron orbital overlap rather than direct electron sharing. The compounds formed by this interaction are therefore partially covalent.

Direct heating of the metals with elements such as S, Se, Te, P, As, Bi, Sn or Pb under carefully selected experimental conditions produces dark, often semimetallic solids (Livingston 1975; Westland 1981). These compounds are resistant to attack by alkalis and all single mineral acids other than nitric acid (Cotton and Wilkinson 1980). Many of the PGE compounds which have been produced in this manner are poorly characterised and, as in many natural

systems, it would appear that numerous phases, including non-stoichiometric compounds and solid solutions are probably present depending on the reaction conditions (Westland 1981). Cabri (1981) and Berlincourt et al. (1981) present a comprehensive review of natural compounds of, and phase relations between, the PGE and many P block elements.

In addition, some PGE sulphides can also be prepared by bubbling H_2S gas into PGE salt solutions. $PtCl_4^{2-}$ and $PtCl_6^{2-}$ yield PtS and PtS_2 by equations (2b) and (2c).

$$PtCl_4^{2-} + H_2S = PtS + 2\,HCl + 2\,Cl^- \quad \text{...equation (2b)}$$
$$PtCl_6^{2-} + 2\,H_2S = PtS_2 + 4\,HCl + 2\,Cl^- \quad \text{...equation (2c)}$$

Pd^{2+} solutions produce PdS when treated with H_2S. Rh^{3+} and Ir^{3+} solutions precipitate amorphous, hydrated sulphides which are assumed to have the general formula $M_2S_3.(nH_2O)$. Their exact compositions are not known.

2.4. Solution Chemistry Of The PGE.

2.4.1. Species In Acid Solutions.

The PGE can display extensive solution chemistry with a wide variety of complexing ligands. In acid media, the most important complexes are the halometallates (Westland 1981; Mountain and Wood 1988). Strongly chlorine co-ordinated complexes such as $IrCl_6^{3-}$, $RuCl_6^{3-}$ and $PdCl_4^{2-}$ predominate in acid media but gradually convert to aquachloro complexes as pH is increased. In complexes such as $RhCl_6^{3-}$, chloro groups are successively removed to yield ions such as $[RuCl_5(H_2O)]^{2-}$ and $[RuCl_4(H_2O)_2]^-$. If the pH is rapidly increased into the range 4-7.5, this triggers the precipitation of hydrated oxides such as $OsO_2.nH_2O$, $Ir_2O_3.nH_2O$ and $PdO.nH_2O$ etc. The $[PtCl_6]^{2-}$ ion is less susceptible to hydrolysis and requires pH values in excess of 8 before it will precipitate Pt as a hydrated oxide. During PGE analysis and also during refining operations, this resistance to hydrolysis is used as a method of separating Pt from the other PGE (Westland 1981). Apart from chloride, there are a number of other ions such as **Br** , **I** , and NO_2 , which can complex the PGE under acidic and oxidising conditions.

The multiple component Eh-pH diagram for Pt shown as an example in Figure 2.2. provides a convenient way to express the stabilities of different Pt species in

solution or as solids, as a function of pH and the oxidising potential of the system. Starting with an acid solution containing $PtCl_4^{2-}$, an increase in pH and sequential hydrolysis to precipitate hydrated oxides might be represented by arrow A in Figure 2.2.. Bubbling H_2S through an acidic solution of $PtCl_4^{2-}$ (as discussed in section 2.3.4.), or the reaction between an, acidic, Pt bearing solution and sulphide crystals, would reduce the Eh of the system, making species such as PtS and PtS_2 stable. This reaction might be represented by arrow B on the diagram.

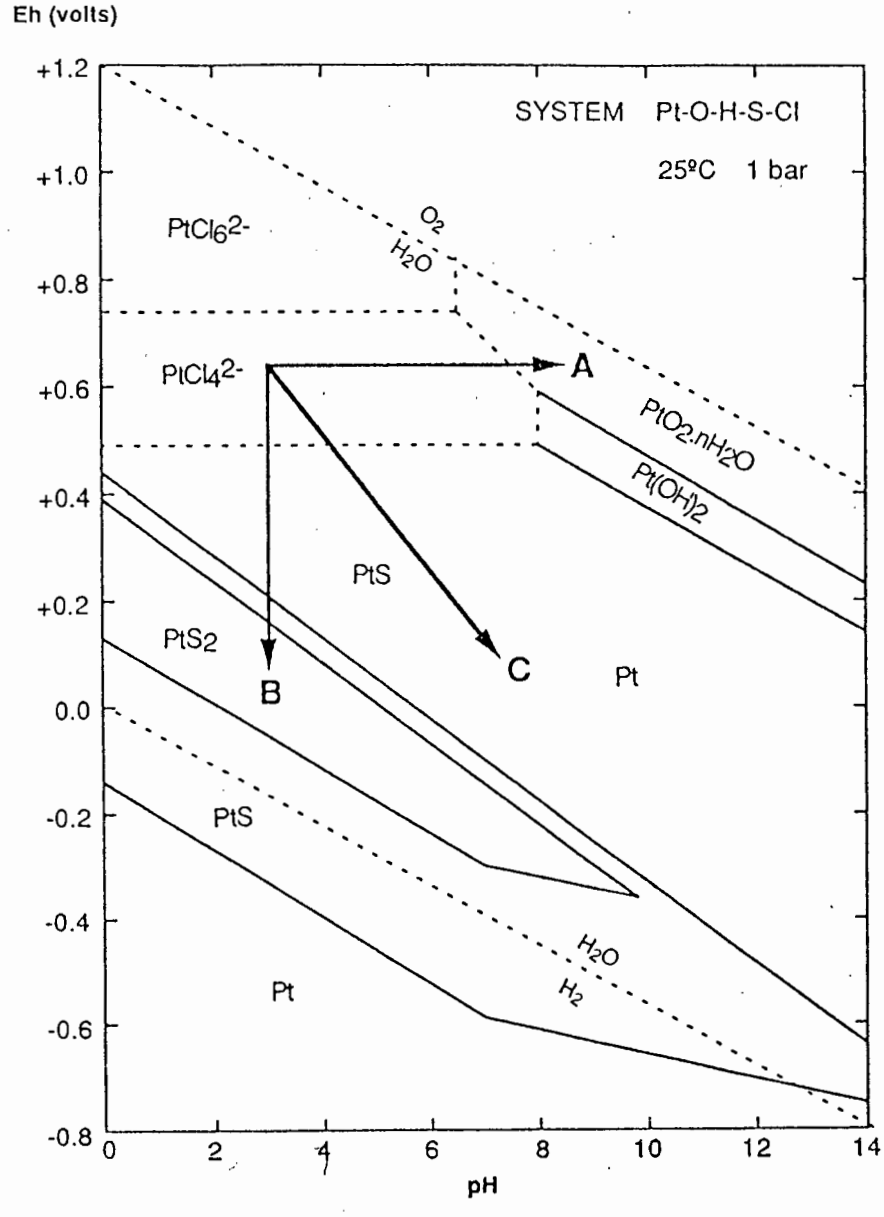

Figure 2.2.: Eh-pH diagram for Pt at 25°C. Modified after Brookins (1987) and Mountain and Wood (1988). The assumed activities of the dissolved species are: Pt = 10ppb, S = 0.1m and Cl = 1m.

Reactions such as the reduction of $PtCl_4^{2-}$ by alcohols or aldehydes, where pH is increased while Eh is reduced, resulting in conditions well within the stability field of the pure metal, might be represented by arrow C on the diagram.

The Eh-pH diagrams for the other PGE reveal similar trends. The stability fields for the pure metals are large and the PGE are only stable in solution under extremely acidic and oxidising conditions. Changes in either Eh or pH can rapidly cause the PGE to precipitate from solution.

2.4.2. Species In Neutral And Alkaline Solutions.

Simple PGE aquo ions only exist in the absence of any competing polarised ligands and are therefore not considered to be of much significance in real solutions (Westland 1981). Mountain and Wood (1988) suggested that PGE hydroxides might be important species in near neutral to strongly alkaline pH conditions. Sassani and Shock (1990) disputed this contention and their thermodynamic modelling appeared to indicate that Pd chloride complexes would dominate over hydroxide complexes well into alkaline conditions (pH >8). However, the experimental work of Wood (1991) seems to confirm that hydroxide ions of Pt and Pd might well be the dominant species in many near neutral solutions and possibly in seawater as well.

Other ions which might be important in alkaline and particularly sulphide rich alkaline solutions include CN^-, NH_3, SCN^- and HS^- (Mountain and Wood 1988; Davidson 1990). In cyanide solutions, $Pd(CN)_4^{2-}$ is known to be an exceptionally stable complex (Westland 1981) but little other data is available and the conditions required to stabilize other PGE complexes of this type are not well known. Oxidising Eh conditions will destroy many of these complexes, precipitating the PGE as metals (Hartley 1991; C.S. Erasmus pers. comm. 1991). The role these complexes might play in natural solutions is probably rather limited.

2.5. Organometallic PGE compounds.

2.5.1. Introduction.

For many years this has been a field of intensive study for inorganic chemists and a vast number of compounds have been synthesized and described. However, it has been a field which has been rather neglected by most geochemists. Despite

elevated concentrations of the PGE found in some petroleums, coals and fly ashes (Goldschmidt 1954; Saxby 1969; Chyi 1982; van der FLier Keller 1991), the possibility of a strong association between carbon and the PGE has only been seriously addressed from the early-1980s onwards.

The most striking feature of most organometallic compounds is that the oxidation state of the metal is usually very low. Formation of these compounds generally takes place under strongly reducing conditions. In contrast to the common oxidation states found in co-ordination chemistry (see Table 2.1.) the metal often has a neutral or even a slightly negative charge. Organometallic interactions take place between the metal and various neutral ligands. Bonding generally takes place by the overlap of π electron orbitals between metal and ligand (Crabtree 1988). This overlap allows charge to be transferred from the metal to empty, so-called π-acceptor, orbitals on the ligand, giving rise to a strong covalent bond. Species capable of taking part in π-bonding with transition metals such as the PGE include CO, CN, NO_2 , alkanes, alkenes, aromatic rings, H , trialkyl phosphines (PR_3), SCN and $SC(NH_2)_2$.

Hunt (1977), Johnson (1980), and Crabtree (1988) review many features of general organometallic chemistry. Livingston (1975), Cotton and Wilkinson (1980), Greenwood and Earnshaw (1984) and Pruchnik (1990) contain more specific discussions of the organometallic chemistry of the PGE.

The number of PGE compounds in the organometallic field alone, is enormous. However for the purposes of this thesis, only one group of organometallic PGE compounds, the carbonyls and related species, will be discussed in detail. The extreme volatility of most carbonyls, and the conditions under which they might form, may have important implications for the behaviour of the PGE during some magmatic processes (see chapter 6). Therefore it is important to provide the reader with detailed information on these species at this stage.

2.5.2. PGE Carbonyls And Related Compounds.

The existence of transition metal carbonyls, that is metals complexed with carbon monoxide (CO), has been known for more than a century (eg. Mond et al. 1890). However, it took 22 years after the discovery of $Ni(CO)_4$, for the properties of any PGE carbonyls to be described by Mond et al. (1910). The most notable feature of

this group of compounds is their extreme volatility, which is highly unusual for compounds containing such heavy metal atoms (Abel and Stone 1970). The carbonyls which Mond and his co-workers produced were liquids or metastable solids at room temperature and most of them rapidly became gaseous above 60°C.

Since the 1920's a wide variety of PGE carbonyls and carbonyl derivatives have been prepared and described. Abel and Stone (1970), Hieber (1970), Cotton and Wilkinson (1980), Greenwood and Earnshaw (1984) and Pruchnik (1990) provide general reviews of PGE carbonyl chemistry. Tripathi et al. (1975) summarize the chemistry of Os and Ru carbonyls; and in a companion paper (Tripathi et al. 1976), the same authors present a detailed review of Rh, Ir, Pt and Pd carbonyls. They note, in particular, that while many carbonyls of Rh, Ir and Pt have been made, there are relatively few Pd carbonyl compounds and those that do exist have always been very difficult to prepare.

Classical PGE carbonyl syntheses involved the reaction of the metal with CO under high pressure (0.1-30 MPa) and temperature (50-450°C) (eg. Mond et al. 1910; Hieber and Bader 1928). The simple binary species $Os(CO)_5$ and $Ru(CO)_5$ could be prepared by this method. In contrast to Ni, which readily forms $Ni(CO)_4$, similar binary carbonyls of Pt and Pd are rather unstable and only polynuclear species, containing more than one atom of Os or Ru, have been well characterised (Greenwood and Earnshaw 1984; Mingus and Wales 1991).

It was later found that the use of PGE oxides, halides and sulphides as the starting materials, along with Cu or Ag catalysts, led to faster reactions, under less extreme conditions, than were possible before (eg. Hieber and Bader 1928, Hieber and Fischer 1940). For example it was found that OsO_4 could be converted to the carbonyl as follows:

$$OsO_4 + 9CO \xrightarrow[180°C]{10\ MPa\ CO} Os(CO)_5 + 4CO_2 \qquad \text{...equation (2d)}$$

Laurite (RuS_2) could be carbonylated in the presence of Cu:

$$RuS_2 + 5CO + 2Cu \xrightarrow[200°C]{20\ MPa\ CO} Ru(CO)_5 + 2CuS \qquad \text{...equation (2e)}$$

In the solid state, Rh and Ir chlorides reacted to form di- and tetracarbonyls:

$$2RhCl_3 + 8CO + 3Cu \xrightarrow[200^{o}C]{20\ MPa\ CO} Rh_2(CO)_8 + 3CuCl_2 \qquad \text{...equation (2f)}$$

$$4RhCl_3 + 12CO + 6Cu \xrightarrow[200^{o}C]{30\ MPa\ CO} Rh_4(CO)_{12} + 6CuCl_2 \qquad \text{...equation (2g)}$$

$Ni(CO)_4$ was synthesised from a reaction between CO and nickel sulphide in an alkaline solution by Manchot and Gall (1929) and since the late 1940's, reactions carried out in solution have been the preferred method of preparation for most PGE carbonyls (Abel and Stone 1970). In solution, Rh and Ir chlorides reacted with CO under relatively mild conditions to yield carbonyl halides

$$2RhCl_3.3H_2O + 4CO \xrightarrow[100^{o}C]{0.1\ MPa\ CO} Rh_2(CO)_4Cl_2 \qquad \text{...equation (2h)}$$

$$2IrCl_3.H_2O + 4CO \xrightarrow[100^{o}C]{1\ MPa\ CO} Ir_2(CO)_4Cl_2 \qquad \text{...equation (2i)}$$

These are very stable compounds which serve as precursors for making more complex species. Subsequent reactions of the carbonyl halides with CO at higher pressures gave rise to the tetracarbonyls $Rh_4(CO)_{12}$ and $Ir_4(CO)_{12}$. Although Pt does not form a stable monocarbonyl, $PtCl_4$ in solution can react with CO as follows to form a stable carbonyl halide.

$$PtCl_4 + 2CO + Cu \xrightarrow[250^{o}C]{10\ MPa\ CO} Pt(CO)_2Cl_2 + CuCl_2 \qquad \text{...equation (2j)}$$

Hieber and Bader (1928) also reported the synthesis of $Pt(CO)_2Cl_2$ via a direct reaction between finely divided Pt and mixture of CO and dry Cl_2. It was discovered that $Pt(CO)_2Cl_2$, along with many other PGE carbonyls and carbonyl halides was stable in accompanying CO or CO_2 atmospheres and could be sublimed as the temperature was increased. It appears that the introduction of halides stabilizes Pt and Pd compounds at the expense of Ni. There are no known carbonyl halides of Ni whereas several unstable and stable Pt and Pd species are known (Greenwood and Earnshaw 1984).

It is interesting to note that the carbonyl halides of the PGE show similar volatilities to the pure carbonyls and depending on the pressures of CO and Cl_2 it appears likely that a mixture of true halides, carbonyl halides and carbonyls might co-exist in the gas phase.

It is clear from the equations shown above that PGE carbonyls can display a wide variety of **mononuclear** (eg, $Os(CO)_5$), **binuclear** (eg. $Rh_2(CO)_8$) and **polynuclear** (eg. $Rh_4(CO)_{12}$) forms. The higher forms consist of clusters of metal atoms, held together by metal-metal bonds, which are also bonded to CO groups (Cotton and Wilkinson 1980; Mingos and Wales 1991). For example, when $Os_3(CO)_{12}$ crystals are heated in a sealed tube, CO is evolved and a number of cluster carbonyls containing between 5 and 11 Os atoms are formed (Mingos and Wales 1991). The structures of $Os_5(CO)_{16}$ and $Os_6(CO)_{18}$ are shown in Figure 2.3.

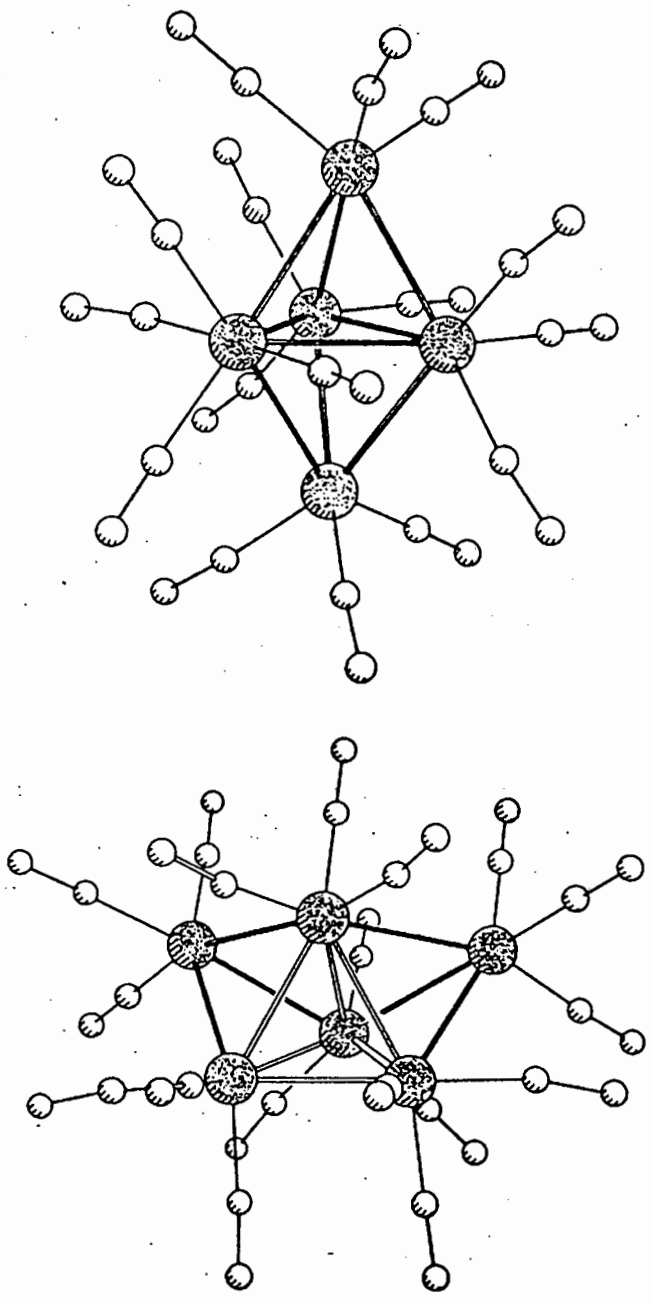

Figure 2.3.: Structures of some polynuclear Os carbonyls. From Cotton and Wilkinson (1980)

Inter-PGE fractionation is a common feature and there may be large differences in the behaviour of the individual metals, frequently influenced by one dominant physical or chemical property. Table 2.5. contains a generalized summary of physical properties which are most likely to cause differences in individual PGE behaviour under some of the conditions discussed in this chapter.

Table 2.5.: Summary of physical properties likely to cause variations in chemical behaviour between individual PGE.

Chemical Environment	Possible Controlling Physical Property
Alloy Formation	1. Lattice Structure
Co-ordination Chemistry	1. Oxidation State Of Metal 2. Electronegativity 3. Symmetry Of Complex
Solution Chemistry	1. Oxidation State Of Metal 2. Ligand Polarization
Organometallic Chemistry	1. Electron Configuration 2. Symmetry

In conclusion then, when one attempts to explain a PGE distribution either in the laboratory or in nature, the foremost question should always be: What is the controlling factor or factors most likely to have brought this about ? Only when all of the possible properties which might exert a dominant control over that particular situation are clearly identified and evaluated, can any prediction or modelling of PGE behaviour be made with confidence.

Chapter 3

Overview And Theory Of Neutron Activation Analysis.

3.1. Introduction.

Activation analysis is a method for the sensitive analysis of a wide variety of chemical elements, from major components to trace or ultratrace impurities. It is carried out by the production of radioactive isotopes via nuclear capture reactions with stable isotopes of the elements of interest. Quantitative analysis is achieved by the measurement of radiations emitted by the desired product radioisotopes.

A variety of nuclear particles may be employed as probes in activation analysis. These particles include photons, neutrons, and charged particles such as protons, and alpha particles. Selection of the type of nuclear particle to be used in a given nuclear capture reaction is influenced by the probability of capture of the incident particle by the target isotope and by the intensity of incident particles produced by available irradiation facilities. Although the use of charged particles and focussed charged particle beams has become increasingly popular, for many reasons, Instrumental Neutron Activation Analysis (INAA), using thermal neutrons, is still the most widely employed activation technique.

Neutrons can be produced by a number of physical processes and several of these have been employed as sources of the particles in activation analysis. These sources vary considerably in their neutron emission intensity, the so-called "neutron flux". The flux or intensity of the neutron bombardment is an important factor in determining the activity induced into the target sample, and hence, how accurately the radiations emitted by the active sample, can be measured.

Relatively small, portable neutron sources can be made using nuclides undergoing spontaneous fission (eg, Cf-252), or those which produce neutrons by photonuclear reactions such as Be. In addition, accelerators can be used to accelerate charged particles which then yield beams of neutrons by reaction with suitable targets. Portable and accelerator based sources typically yield neutron

fluxes of between 10^6 and 10^9 neutrons cm^{-2} sec^{-1} (Watterson and McDonald 1991). While fluxes of this magnitude are sufficient to activate a number of highly sensitive elements, notably , manganese, vanadium and several lanthanides, the irradiation periods required are often quite long and more powerful neutron sources are generally required to activate most other elements (Bowen and Gibbons 1963; Koeberl 1992).

The production of neutrons during the fission of heavy nuclei, first noted by Halban et al. (1939), is the basic principle behind the operation of a nuclear reactor. The fission of U-235 produces, on average, 2.47 neutrons for each uranium atom decomposed. The corresponding figure for Pu-239 is 2.91 neutrons (Bowen and Gibbons 1963). By concentrating the fissionable fuel and controlling the neutron density by the use of suitably placed moderators, it is possible to obtain very high neutron fluxes within the core of a reactor. Nuclear reactors, using fissionable fuel, are capable of generating neutron fluxes in excess of 10^{12} neutrons cm^{-2} sec^{-1} and are the presently preferred irradiation facility for neutron activation analysis.

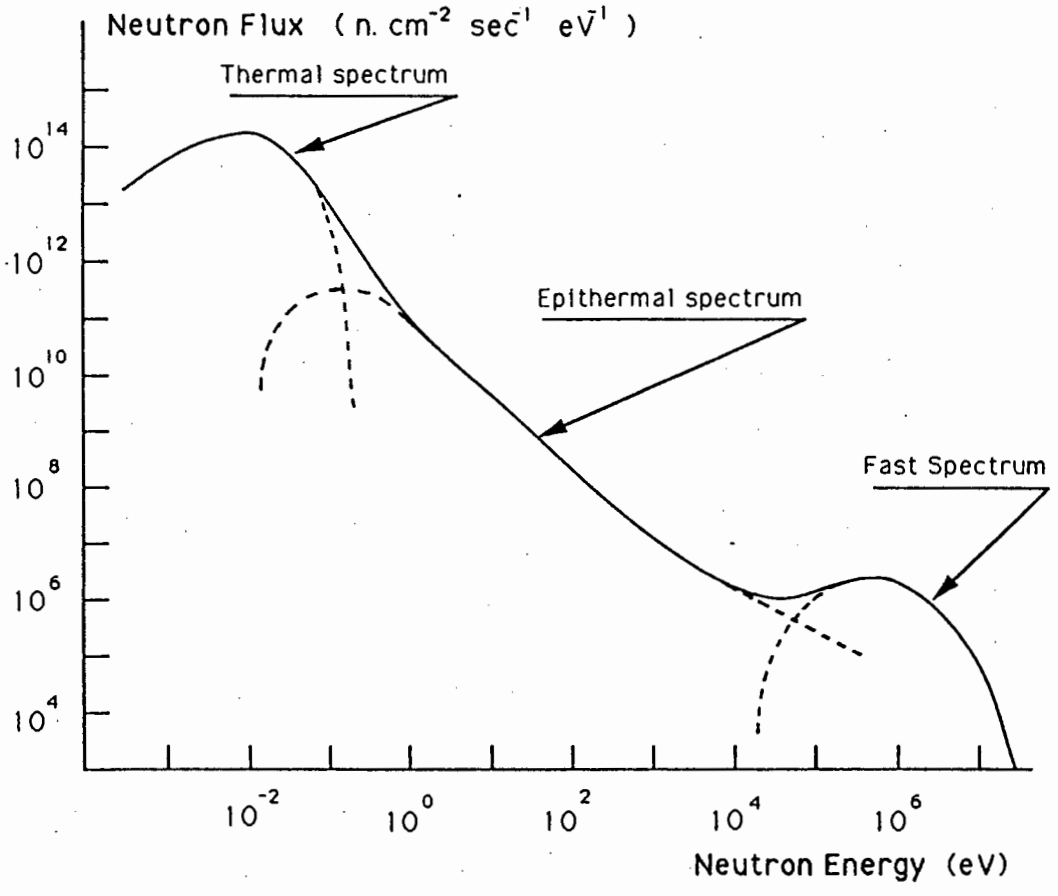

Figure 3.1.: Schematic spectrum of SAFARI 1 reactor neutron flux distribution (modified from Watterson 1975).

However, there are a number of differences compared to smaller sources associated with the use of reactors for activation analysis. Unlike the smaller neutron sources where the proceeding reactions allow only a very narrow range of neutron energies, the fission neutron energy spectrum for a reactor is very wide. Typically, the range is from 0.01eV to 15 MeV. These neutron energies can broadly be classified as **thermal** (less than 0.1 eV), **epithermal** (0.1eV to 0.1 MeV) and **fast** (0.5 to greater than 15 MeV). The neutron energy spectrum for the SAFARI-1 reactor of the Atomic Energy Corporation of South Africa is shown in Figure 3.1. 95 % of the neutron flux inside the reactor is in the thermal region. As will be explained in the following section, this high proportion of slow to fast neutrons makes the SAFARI-1 reactor very suitable for INAA purposes. More detailed information on the SAFARI-1 reactor is contained in Appendix 1.

3.2. Instrumental Neutron Activation Analysis - Theory.

3.2.1. The Process Of Activation.

Nuclear reactions are generally presented in the form,

$$X(a, b\gamma)Y \qquad \text{...equation (3a)}$$

where
- **X** is the "parent" or target isotope
- **Y** is the radioactive "daughter" isotope
- **a** is the incident particle with which the sample material is bombarded, e.g. neutrons, or protons
- **b** is any light particle which may be emitted during the reaction e.g. β particles, or α particles
- γ are any "prompt" gamma rays (energies of 0.01 to 3 MeV) which may be emitted during the reaction.

Since its discovery by Lea (1934), the radiative capture (n , γ) reaction has been the most widely employed and important reaction in INAA. This is a reaction in which the excited nucleus becomes de-excited and passes into a lower energy state by the emission of one or more "prompt" gamma rays. The resulting "daughter" product of this de-excitation, the species Y in equation (3a) above, is usually radioactive.

The nuclear reaction in INAA is a function of two steps. The first is the capture of a neutron by the target (parent) nucleus. The binding energy (ε) of a nucleus in MeV, which is the energy required to split it into its component protons and neutrons, is given by the simple formula (Bowen and Gibbons 1963):

$$\varepsilon = 931\,(\,1.008145\,Z + 1.008986\,N - M\,) \qquad \text{...equation (3b)}$$

where Z = the number of protons in the nucleus (atomic number)
N = the number of neutrons in the nucleus
M = the mass of the nucleus (relative to O^{16} = 16.000)

If the binding energy per nucleon, ε/(Z+N), is plotted against the mass number M, the curve shown in Figure 3.2. is obtained. This indicates that for all but the lightest nuclei, the binding energy per component nucleon (or per added neutron) is 8 +/- 1 MeV (Koeberl 1992).

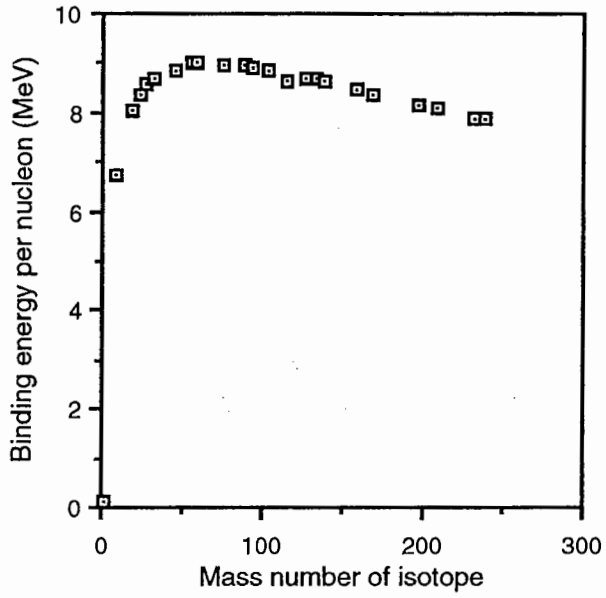

Figure 3.2.: Plot of Binding Energy Per Nucleon vs. Mass Number for selected nuclei. Note the narrow range of binding energies for isotopes greater than 20 atomic mass units.

As they carry no charge, neutrons can penetrate atomic nuclei without having to overcome any Coulomb barrier. A nucleus which captures a neutron increases its energy by about 8 MeV due to nuclear binding. By conservation of momentum, it also acquires any kinetic energy which the colliding neutron might have possessed. The species formed by this reaction has a certain lifetime during which it remains in an excited state due to the interaction and the capture of the neutron

by the nucleus. This reaction and the resulting de-excitation of the nucleus can proceed in a number of differing ways as shown below

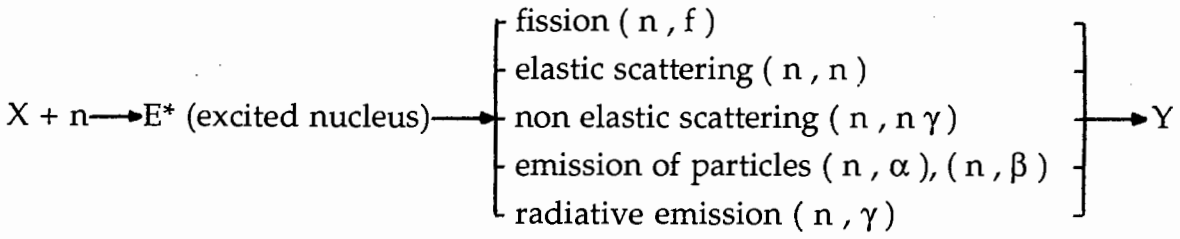

The mode of de-excitation is dependant on the excitation energy of the excited nucleus, and hence, on the kinetic energy of the incident neutron. Slow, thermal neutrons, which have mean energies around 0.025 to 0.04 eV, generally give rise to radiative capture (n , γ) reactions, while the emission reactions such as (n , α) mostly arise with fast neutrons. This is because it takes much less energy to expel a photon than a particle from the nucleus.

Fast neutrons can give rise to all of the reactions noted above. Many sputtering reactions such as (n , 2n) have a threshold energy of around 10 MeV, while if 100 MeV neutrons are used, fission reactions can be induced in most elements, where the target nuclei are broken down into a number of lighter nuclides. Unfortunately these high energy neutron reactions often generate a high number of side reactions which can contribute to sizeable background activities. This seriously hampers the sensitivity and usually makes the analysis unnecessarily complicated. There are several reasons for using mainly thermal neutrons for analytical work. These can be summarized broadly as follows:

1. The narrow range of thermal neutron energies means that any errors due to uncertainties in the neutron energy spectrum are minimized.
2. The general availability of large fluxes of thermal neutrons in modern research reactors.
3. The large nuclear capture cross sections generally prevalent for the radiative capture of thermal neutrons.

Point 3 is especially important in INAA. The nuclear capture cross section is a measure of the probability that a collision with an activating particle will occur and produce a desired nuclear reaction. As shown in Figure 3.3., for a large range of slow neutron velocities, the cross sections for capture reactions are generally

proportional with $1/Velocity_{neutron}$ and decrease with increasing neutron energy. Thus thermal neutron capture cross sections are generally high when compared with capture cross sections for faster neutrons.

However at higher neutron energies so called neutron resonance peaks occur. These are also shown in Figure 3.3. The capture cross section for the reaction increases very rapidly within a restricted energy range and then falls again very quickly. These resonance peaks have small widths at half height, generally on the order of 0.1eV.

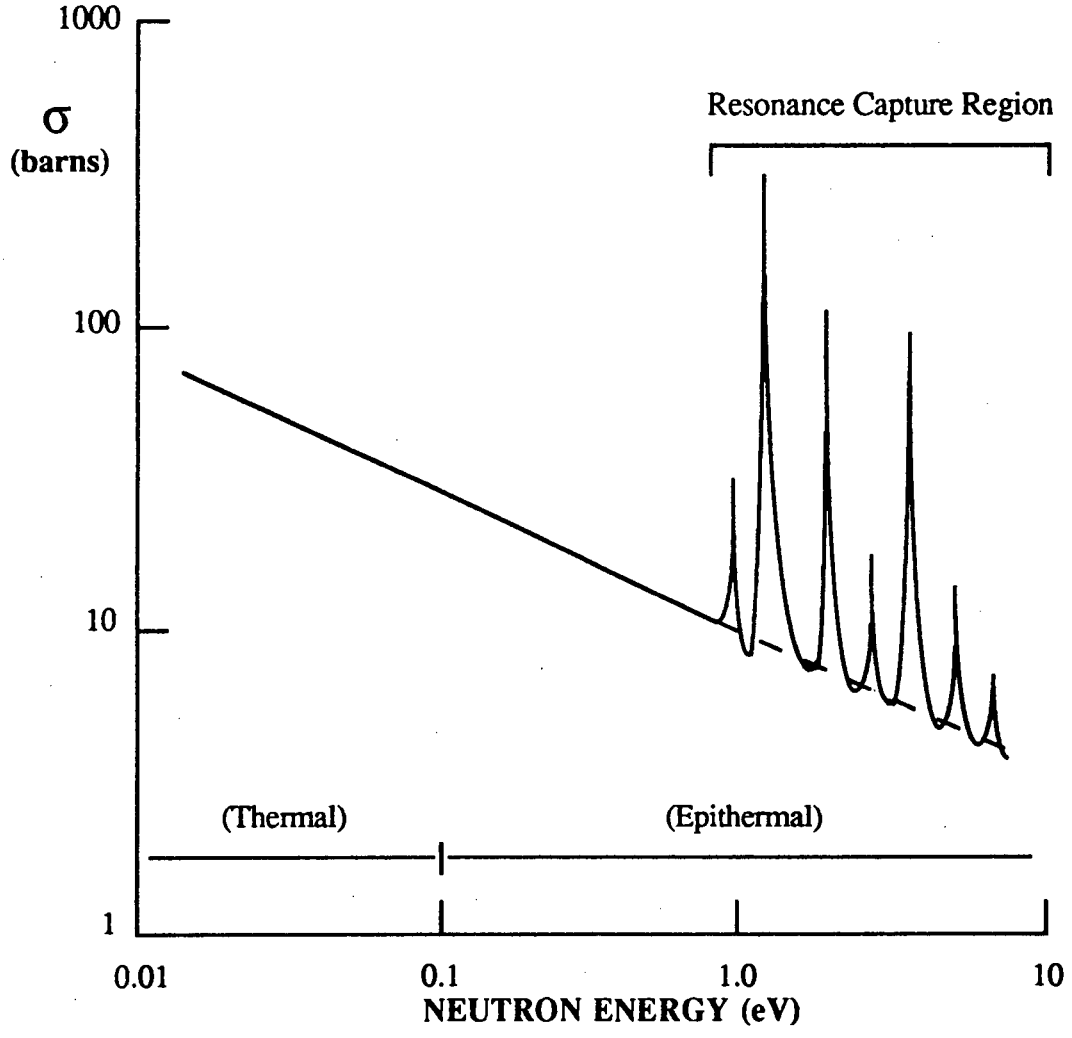

Figure 3.3. Plot of neutron capture cross section (σ) against low incident neutron energies for a capture reaction. Note the increased capture cross sections in the resonance energy region.

The occurrence of particularly large resonance peaks for some elements means that an irradiation with epithermal neutrons can sometimes lead to a greater production of daughter radionuclei than is the case with a purely thermal

neutron irradiation. This has lead to the calculation of so-called "advantage factors" for different elements for epithermal irradiation. These "advantage factors" vary considerably from reactor to reactor, as each reactor will have its own distinctive neutron energy spectrum. However, the low epithermal neutron fluxes produced by the SAFARI-1 reactor in the positions used for PGE irradiation (see Appendix 1, p.240) do not offer significant advantages over thermal neutrons for these elements (Tredoux 1990).

3.2.2. The Production And Decay Of Radioisotopes.

The induced activity from the irradiation is measured in terms of the decay of the number of atoms of the radioactive daughter product (Y) present. This radioactive nuclide has a characteristic mode of decay and energy pattern of emitted radiations during the decay process. The radionuclide will decay to another daughter product, usually stable, by a number of possible processes summarized below.

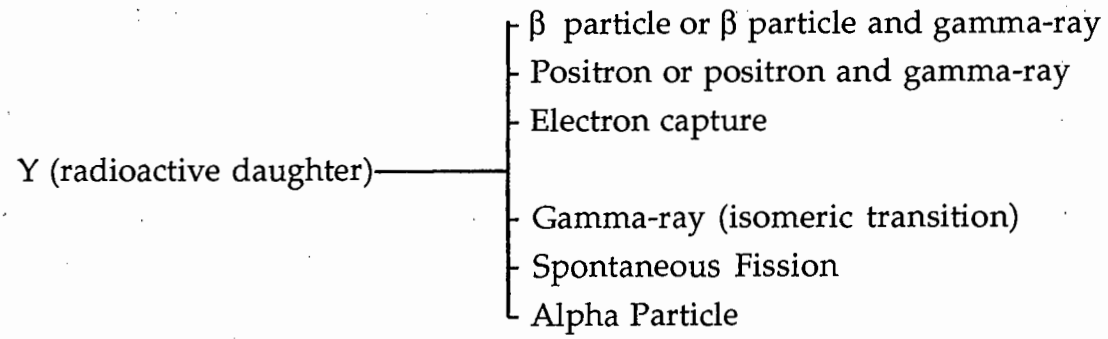

Radioactive decay is a purely random process which is independant of external chemical or physical factors. The probability that a given radionuclide (Y) will decay is fixed and is independent of the presence or absence of other radioactive nuclei (Bowen and Gibbons 1963; Adams and Dams 1970). The variation in the number of radioactive nuclei with time is given by the relationship:

$$\frac{dN}{dt} = -\lambda N \qquad \text{equation (3.2.2.1)}$$

where N = the number of radioactive atoms at any time t
λ = radioactive decay constant of the radionuclide concerned

Integration of equation (3.2.2.1) gives

$$N = N_0 e^{-\lambda t} \qquad \text{equation (3.2.2.2)}$$

where N_0 = the number of radioactive atoms present at time $t = 0$

The process therefore follows an exponential curve, as shown in Figure 3.4.

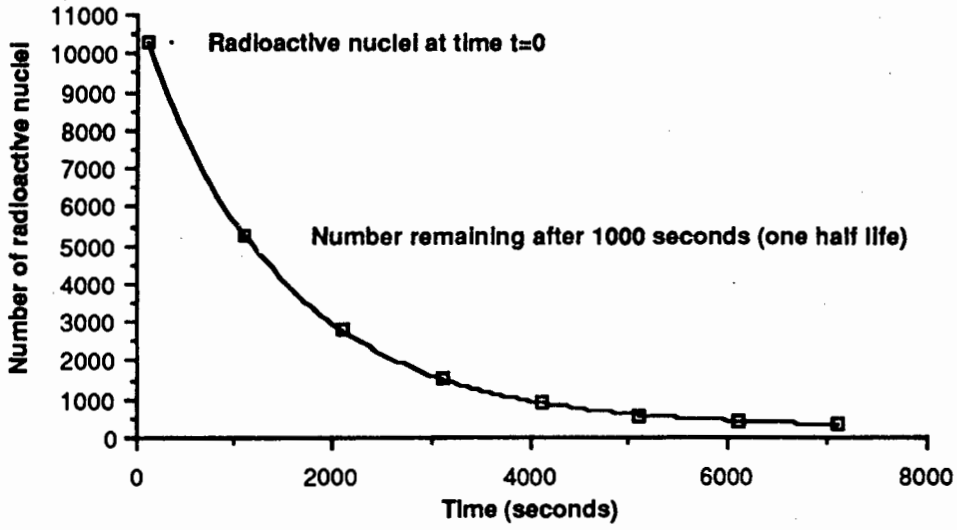

Figure 3.4.: Plot of the number of radioactive nuclides against time for a radionuclide with a half life of 1000 seconds. This shows the the exponential nature of the decay process as defined by equation (3.2.2.2.)

Instead of numbers of atoms it is more convenient to measure the rate of decay, or the activity at a time t. This is given the symbol A and is expressed as:

$$A = \lambda N \qquad \text{equation (3.2.2.3)}$$

The activity at any time t is proportional to N, so by equation (3.2.2.2):

$$A = A_0 e^{-\lambda t} \qquad \text{equation (3.2.2.4)}$$

where A_0 = activity of the sample at decay time $t = 0$. This is the time at the end of the irradiation and is therefore a measure of the activity induced into the sample by that irradiation.

If the time ($t_{1/2}$) is measured during which A_0 decreases to half its value,

$$0.5\, A_0 = A_0 e^{-\lambda t_{1/2}} \qquad \text{equation (3.2.2.5)}$$

therefore,

$$\ln 2 = \lambda t_{1/2} \qquad \text{equation (3.2.2.6)}$$

so,

$$t_{1/2} = \frac{0.693}{\lambda} \qquad \text{equation (3.2.2.7)}$$

This time, $t_{1/2}$, is known as the *half life* of the radionuclide. It is a function of λ and is therefore also characteristic for the species under decay.

When a radioisotope is produced at a constant rate (eg. under bombardment by a constant neutron flux in a reactor), the rate of accumulation of the radionuclide is given by the difference between the rate of its production and the rate of its decay. Thus,

$$\frac{dN}{dt} = P - \lambda N \qquad \text{equation (3.2.2.8)}$$

where P = the rate of production of the radionuclide

The solution of equation (3.2.2.8) gives,

$$N = \frac{P}{\lambda}(1 - e^{-\lambda t}) + N_0 e^{-\lambda t} \qquad \text{equation (3.2.2.9)}$$

P is a function of the irradiation conditions, the cross section of the capture reaction and the number of target nuclei present in the sample. It is expressed as:

$$P = \phi \sigma N_{tar} \qquad \text{equation (3.2.2.10)}$$

where ϕ = the neutron flux (neutrons cm^{-2} sec^{-1})
σ = capture cross section of the relevant reaction in barns ($cm^2 \times 10^{-24}$)
N_{tar} = the number of target atoms of the parent nuclide (X) in the sample

Unless we are reirradiating a previously irradiated sample, N_0, the number of radioactive atoms present initially, is zero. Therefore N can be expressed as,

$$N = \frac{\phi\sigma N_{tar}}{\lambda}(1 - e^{-\lambda t}) \qquad \text{equation (3.2.2.11)}$$

so, the activity of the radionuclides at any time during production is given by,

$$A = \lambda N = \phi\sigma N_{tar}(1 - e^{-\lambda t}) \qquad \text{equation (3.2.2.12)}$$

When the activity of the radionuclides being produced is plotted against the half life of their decay, the growth curve shown in Figure 3.5. is obtained. A saturation level of activity, where the rate of production is balanced by the rate of decay, is obtained within about 1%, after an irradiation period equivalent to 8 half lives. Irradiation times longer than one half life become increasingly inefficient,

where the returns in activity are not matched by the amounts of flux put in. Therefore, unless it is vital to obtain the maximum activity possible, it is rather pointless to irradiate beyond a period of one half life, as seven times more flux will only produce twice as much activity.

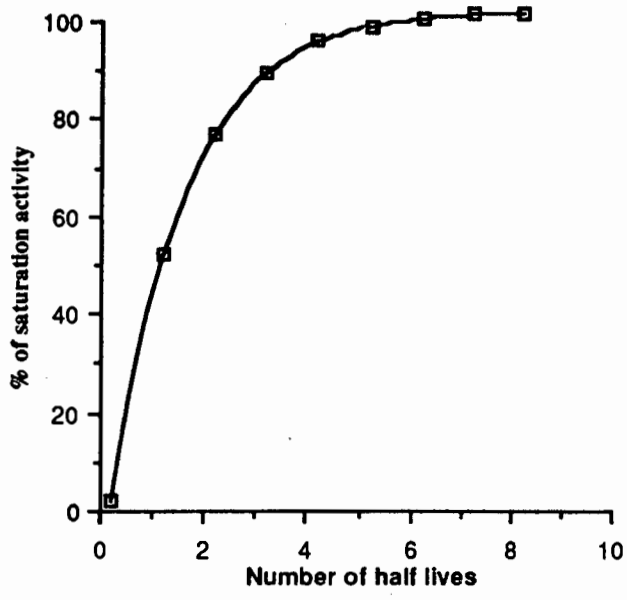

Figure 3.5. Growth of activity as a fraction of the saturation activity, plotted against the half life of the activated species.

Therefore, the activity of the radionuclides produced at the end of the irradiation period, or the Induced Activity (A_o) is given by

$$A_o = \phi\sigma N_{tar} (1 - e^{-\lambda t_{irr}}) \qquad \text{equation (3.2.2.13)}$$

where t_{irr} = the time of the irradiation.

In principle then, from a study of the activity of a radionuclide as it decays, it should be possible to relate that activity back to an initial induced activity, and thence, using the nuclear characteristics of the capture reaction, to a concentration of the parent nuclide. The practicalities of this procedure are discussed in section 3.4.

3.3. The Detection Of Emitted Gamma Radiation.

All of the decay processes outlined at the start of section 3.2.2., are accompanied by the the emission of "delayed" gamma and/or X-rays. The pattern of energies of these "delayed" gamma-ray and X-ray photons are characteristic for a given

radionuclide (Adams and Dams 1970; Koeberl 1992). It is the measurement of these characteristic rays, exclusive of any others, which allows the eventual quantification of the abundance of a particular radionuclide in an irradiated sample.

Gamma-ray spectroscopy has much wider application in INAA than X-ray spectrometry and is the more commonly used technique. The gamma-rays emitted by a decaying radionuclide are spread over a much wider range of energies (30-3000 keV) than X-rays (2-90 keV) and are subject to much fewer losses by absorption in the sample matrix. Thus the intensities of gamma peaks are higher than those of X-rays and the resolution of such peaks by solid state detectors is much better. These features are of great importance in the detection and measurement of radiations emitted from the complex matrices that are typical of geological materials.

All nuclear detection measurements are based on detection of the interaction of the emitted radiations with the crystalline matter of the detector. The detection methods are generally based on excitation or ionisation of atoms within the detector via the passage of a charged particle. In the energy range from 10 eV to 5 MeV, electromagnetic radiations (including gamma-rays) give rise to energetic electrons by one of three separate processes; the Photoelectric Effect, Compton Scattering and Pair Production. Details of these processes and a discussion of the detector systems employed during the analytical work is contained in Appendix 2.

3.4. Calculation Of Concentration In Activation Analysis.

The activity of detected gamma-rays of a known energy is directly proportional to the disintegration rate of the daughter radionuclide (Y). In theory, if we can measure the absolute activity (A) of the radionuclide at a time (t) after irradiation, and we know the decay constant (λ) for that radionuclide, then it is possible to calculate the activity initially present at the end of the irradiation (A_o) by equation (3.2.2.4).

Then, if all of the nuclear parameters and the precise conditions of the irradiation are known, equation (3.2.2.13) can be solved from first principles for N_{tar}. This gives the number of atoms of the parent nuclide (X) in the sample. Most elements however are not monoisotopic so that N_{tar} only represents some

fraction (f) of the total number of atoms of that element actually present in the sample. However, in the cases of those elements and those geological processes for which it is safe to assume that stable isotopic fractionation did not occur, f is a constant for all samples and the concentration of the parent nuclide (X) can be taken as representative of the elemental abundance. This is known as "absolute activation analysis".

In many cases though, parameters such as f, Φ, σ and the absolute disintegration rate (A) are not well constrained or are difficult to measure with sufficient accuracy (Bowen and Gibbons 1963; Adams and Dams 1970; Koeberl 1992). This is a particular problem for the PGE, whose nuclear dataset is rather incomplete (Tredoux 1990). Thus large errors are usually inherent when using the "absolute analysis" technique for the analysis of the PGE.

These uncertainties can be removed by use of a comparative method. In this case the activity of a gamma ray of specific energy from a sample of unknown concentration is converted to an initial activity (A_0) using equation (3.2.2.4). This initial activity is compared with other calculated initial activities from one or more standards of known concentration. If one standard is employed for comparison this reduces the comparison to equation (3c) below.

$$\frac{\text{weight of element in sample}}{\text{weight of element in standard}} = \frac{\text{activity in sample}}{\text{activity in standard}} \qquad \text{...equation (3c)}$$

Conveniently, a calibration curve of initial activity vs concentration is drawn up from measurements of the activities of several standards. The activity measured from a sample of unknown concentration will intersect the curve at some point. This point is projected onto the concentration axis and the concentration of the element in the sample can be determined. This is shown in Figure 3.6.

The standards employed are usually either synthetic solutions prepared from a stoichiometric salt of the desired element or well calibrated rock powders. If one considers the presumed penetrative power of gamma-ray radiations then in theory the exact matching of matrices between standards and unknowns is not critical (Koeberl 1992). This assumption is not wholly correct and the analyst should bear the following factors in mind when selecting the standards to be used;

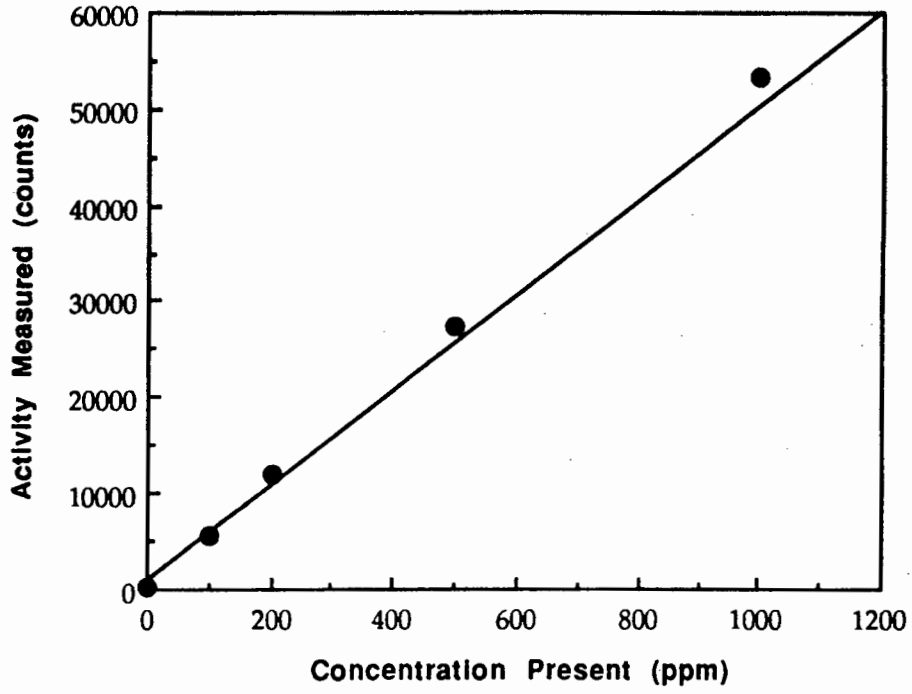

Figure 3.6 : A typical calibration curve showing the linear relationship between the activity of a radionuclide and the concentration of the same element in the standard.

1. Gamma-ray activity from an undesired matrix component, present in the sample but not in the standard (or vice versa) may interfere with the desired gamma-ray peaks in that spectra. This introduces an uncertainty in the determination of the element of interest which might be difficult to correct for.

2. Particular care should be taken if samples or standards contain high amounts of elements which have high gamma-ray absorption eg. U or Th. These samples taken as bulk, will therefore have high self absorption and the pattern of gamma-rays reaching the detector might not be entirely representative of the decay processes going on within the sample.

3. A fairly close match (less than an order of magnitude) between the concentration levels of the standards and the unknowns is considered critical. The relationship between activity and concentration in practice would appear at least in part to be curvi-linear (Hall and Bonham-Carter 1988; M. Tredoux pers comm. 1990). Thus unknowns falling within the range of values occupied by the standards can be very well constrained, but those several times higher or lower in concentration could be subject to serious errors.

An example of the latter point, where this matching of standards and expected values of unknowns was not taken into account is shown in Table 3.1. This was a trial analysis on a Schonland Centre internal standard (PWS-5). The analyst (the author) constructed a calibration curve from solid dilutions of the noble metal standard SARM-7 which comprised values 5 to 10 times lower than those expected in the samples of PWS-5. The results are often consistent but the uncertainties of the calibration curve mean that they deviate substantially, sometimes by more than a factor of 2, from the expected values.

Table 3.1.: Summary of data from internal standard PWS-5 run with poorly matched standards. All values are in parts per billion. "n.d." indicates that the element was not detected and "nda" indicates that no data is available for that element. Expected values for PWS5 are taken from Tredoux (1990).

	Concentration Present						
Sample	**Os**	**Ir**	**Ru**	**Rh**	**Pt**	**Pd**	**Au**
PWS-5 (1)	n.d.	3.0	42	nda	481	1150	240
PWS-5 (2)	n.d.	2.8	40	nda	453	1130	320
PWS-5 (3)	3.2	2.6	48	nda	465	1100	380
PWS-5 (4)	n.d.	3.6	46	nda	443	1180	271
Expected Values	**<5**	**3.9**	**112**	**nda**	**655**	**1739**	**157**

Gijbels and Hoste (1971) note that the most accurate results can be obtained using INAA if the analyst is well aware of its principles and also its limitations. These limitations include:

1. Chemical Limitations. It is not possible to distinguish the different chemical forms adopted by a given element within the sample. The information gained concerns the quantity of an element in the entire sample. There is no indication of the distribution of the element throughout individual phases.

2. Nuclear Limitations. INAA concerns itself with the measurement of radiations from the products of certain primary nuclear reactions. As discussed previously, interference from other nuclear reactions is possible and should be considered. Primary, secondary or second order reactions from other radioactive species may mask those of an element of interest. In addition there may be interference during irradiation from elements which have a high capacity for neutron self shielding or absorption.

3. Spectroscopy And Equipment Limitations. This is notably the level to which the unwanted Compton continuum in the measured gamma ray spectrum can be suppressed and the extent to which individual gamma ray peaks can be resolved from each other and from the background on different spectrometers.

4. Time Factor. This is the time required for the decay of short lived radioactive species before those with longer active half lives can be resolved from the spectrum and measured. This is a feature created by the physics of the decay process and is inherent in INAA. Results, although very accurate, are sometimes gathered over a period of weeks, not minutes.

5. Standardisation. This reflects the accuracy with which any standards, irradiated along with the unknown samples, can be measured and suitable calibrations determined.

6. Health Hazards. Working with any irradiated material always carries a certain level of risk. The need to observe radiological safety precautions at all times is paramount.

3.5. Summary.

In summary, the most important analytical features of thermal neutron activation are its excellent sensitivity, selectivity and accuracy, even down to very low concentrations. It is a multielement technique which typically can yield information on more than 30 elements present in many geological materials from a single irradiation. In addition, there are the added potential advantages of freedom from external, ie non irradiated, contamination and non destruction of the sample material. The latter is particularly important if only very small amounts of sample material are available. Chemical techniques generally destroy a sample in order to get the species of interest into solution whereas after INAA and a suitable decay period, an irradiated sample can be safely handled and subjected to additional analyses to gain information on more elements.

Due to their very favourable neutron capture cross sections, Ir and Au can often be determined instrumentally. However, the low levels of the PGE in most geological materials generally make either chemical separation after irradiation or a chemical preconcentration before irradiation necessary if data for Os, Ru, Rh, Pt

and Pd are sought. Post irradiation treatment destroys the sample but has the advantage of being free from external, ie non-irradiated, contamination. In the case of preconcentration, both of the advantages of freedom from external contamination and non destruction of the sample are lost. The merits of both pre-irradiation and post-irradiation analysis procedures, as applied to the PGE, are described in greater detail in the next chapter.

Chapter 4

Determination Of The PGE And Gold By Neutron Activation Analysis.

4.1. Introduction.

Since the late 1950's , a large variety of analytical procedures based on NAA have been suggested and applied for the PGE and Au. All of the PGE and Au can undergo neutron capture reactions to produce radionuclides. The (n,γ) reactions which are most important in analysis are listed in Table 4.1.

Table 4.1.: Summary of nuclear data for the analytically important neutron capture reactions of the PGE and Au. Gamma-ray energies listed in order of decreasing intensity. Nuclear and isotopic data from Mughabghab et al. (1981) and Mughabghab (1984). Gamma-ray energies taken from Reus and Westmeier (1983). The radionuclides used for the analytical work in this thesis are shown with an asterisk.

Stable Target Isotope	Target Isotopic Abundance, %	Capture Cross Section (barns)	Radionuclide Produced	Half Life	Principle γ Rays (keV)
^{102}Ru	31.6	1.30	^{103}Ru*	39.4 d	**497**, 610
^{104}Ru	18.6	0.47	^{105}Ru	4.4 h	**724**, 469, 676
^{103}Rh	100	139	^{104g}Rh	42.3 s	**556**, 19
		11	^{104m}Rh*	4.34 m	**51**, 20, 23
^{108}Pd	26.7	0.20	^{109m}Pd	4.69 m	**189**, 21, 23
		12.2	^{109}Pd*	13.5 h	22, 25, **88**
^{190}Os	26.4	13.0	^{191}Os*	15.4 d	65, **129**, 63
^{192}Os	41.0	2.07	^{193}Os	30.5 h	65, **139**, 460
^{191}Ir	37.3	925	^{192}Ir*	73.8 d	**316**, 468, 308
^{193}Ir	62.7	112	^{194}Ir	19.2 h	**328**, 293
^{196}Pt	25.3	0.74	^{197}Pt	18.3 h	77, **191**, 69
^{198}Pt	7.2	3.7	^{199}Au*	3.14 d	**158**, 208, 71
^{197}Au	100	98.6	^{198}Au*	2.70 d	**412**, 676

Notation for half lives; s = seconds, m = minutes, h = hours, d = days

The most analytically useful gamma-rays for each isotope are underlined in Table 4.1.. In some cases this is the most intense ray, however due to interference

problems often a gamma-ray of lesser intensity, which is free of interference has to be adopted. The choice of peak can be particularly problematic when the most intense gamma-ray is of low energy (10-70keV). This region of the spectrum is not well resolved on many spectrometers and often contains a large amount of Compton background and X-rays which may interfere with peaks of interest. For example, the 65keV peaks of ^{191}Os and ^{194}Os are not used for the analysis of Os in the presence of the other PGE because they suffer interference from the Kα X-rays of Pt and Au (C.S. Erasmus pers. comm. 1991).

Crocket (1971) defined a concept called the *production factor* (PF) which offers a useful comparison of induced activities for a variety of different irradiation periods. The production factor is defined as:

$$PF = \frac{\sigma.f}{W} (1-e^{-\lambda t_{irr}}) \qquad \text{...equation (4.1.1)}$$

where f = isotopic abundance of the target nuclide
W = isotopic mass of the target nuclide
(definitions of other symbols are the same as those given in section 3.2.2.)

The production factor is directly proportional to the induced activity (A_o), as defined in equation (3.2.2.13), and compares relative activities per unit mass of target element for irradiation periods of the same time and neutron flux (Crocket 1971). Production factors for the isotopes in Table 4.1., calculated for irradiation periods of 10 minutes, 24 hours and 7 days are shown in Table 4.2.

For short irradiation periods of a few minutes, only the ^{104}Rh radioisotopes and, to a lesser extent ^{194}Ir, are significantly activated. Production of ^{104}Rh reaches saturation very rapidly and sensitivity is unaffected by longer irradiations. With an irradiation period of 24 hours, the relative noble metal activities are Rh > Ir > Au > Pd > Os > Ru > Pt. Longer irradiation periods of up to seven days do not change the order much: Rh > Au > Ir > Pd > Os > Pt ~ Ru, but the absolute sensitivities of the determinations are greatly increased for all elements except Rh and Pd (Crocket and Cabri 1981). In the case of the SAFARI-1 reactor, PGE samples can be irradiated for maximum periods of 12 or 24 hours depending on the irradiation facility (see Appendix 1) and therefore the one day production factors shown in Table 4.2. offer the best guide to the relative sensitivities which can be obtained.

Table 4.2.: Summary of production factors for PGE and Au radioisotopes listen in Table 41.1, calculated for irradiation periods of 10 minutes, 24 hours and 7 days (after Crocket 1971).

	Production Factor		
Radionuclide	**10 minutes**	**24 hours**	**7 days**
^{103}Ru	0.000053	0.0076	0.05
^{105}Ru	0.0023	0.088	0.090
^{104g}Rh	134.9	134.9	134.9
^{104m}Rh	8.52	10.7	10.7
^{109m}Pd	0.038	0.049	0.049
^{109}Pd	0.025	2.15	3.0
^{191}Os	0.00056	0.08	0.50
^{193}Os	0.0017	0.18	0.42
^{192}Ir	0.012	1.7	11.4
^{194}Ir	0.22	20.0	36.3
^{197}Pt	0.00061	0.06	0.095
^{199}Au	0.00020	0.03	0.11
^{198}Au	0.089	11.3	41.7

Table 4.2. also shows that the induced activities for PGE neutron capture reactions can vary over more than three orders of magnitude, from Ir and Rh, the most sensitive to Ru and Pt, the least sensitive. This large variation in sensitivity, as well as the very short half lives of the Rh daughter radionuclides, present some of the most significant problems in the analysis of the PGE by NAA (Crocket and Cabri 1981; see also Appendix 3)

The published NAA procedures for trace analysis of the PGE in rocks can be grouped into three general categories; (1) those which employ INAA alone, with no chemical treatment prior to or after irradiation (e.g. Gijbels 1971); (2) those in which radiochemistry and a post-irradiation separation of the PGE from the matrix is carried out (e.g. Crocket et al. 1968, Stockman 1983); and (3) those which involve a chemical preconcentration of the PGE before irradiation (e.g. Hoffman et al. 1978, Erasmus et al. 1982b). Each of these approaches has inherent advantages and disadvantages and each will be briefly reviewed in the following sections.

4.2. Non-destructive INAA.

INAA, with no added chemistry, has not been particularly successful for the determination of all of the PGE in a single aliquot of rock sample. To date, only partial analyses have been performed. The high neutron capture cross sections of ^{198}Au and ^{192}Ir and long half-life of the latter isotope means that Au and Ir can be routinely determined at the ppb level in many rock materials (Gijbels 1971; Crocket and Cabri 1981; Koeberl 1992). However, the rock matrix contains numerous other elements which produce radionuclides whose gamma-rays either swamp or seriously interfere with those emitted by the other PGE (Shazali 1988). The short half-lives of both ^{104}Rh isotopes and the need to resolve their peaks from a very high initial background makes an analysis for Rh by INAA almost impossible, and it is usually ignored (Crocket and Cabri 1981).

In addition, uranium in the sample can undergo fission to produce the fission fragments ^{103}Ru, and ^{109}Pd and these can seriously interfere with measurement of the same isotopes produced by (n,γ) reactions. This is particularly apparent in the analysis of silicic rocks with high U contents such as granites, and corrections must be applied to the Ru and Pd data (Crocket 1971; Ganapathy 1980). The problem is less serious for basic rocks, ultrabasic rocks and meteorites and generally corrections are not necessary for these samples (Crocket 1971). A summary of other irradiation products, with similar half lives to the analytical PGE isotopes, which can interfere with their principle gamma-ray peaks is shown in Table 4.3.

While noting many of the above points, Shazali (1988) carried out a study of the feasibility of INAA as applied to the noble metal standard SARM-7, which is known to contain high levels of PGE (Steele et al. 1975). Short irradiation periods (60-300 seconds) produced a high Compton background from which no ^{104}Rh peaks could be discerned. A longer irradiation period and subsequent decay permitted the determination of ^{192}Ir and ^{198}Au, but no traces of long lived activities from Os, Ru, Pt and Pd were observed.

It would appear that in the light of the problems associated with resolving the PGE photopeaks from background and from interfering species, INAA has a very limited applicability to the analysis of the PGE in most rocks. Although Os and Ru have been analysed in some meteorites and chondritic material by INAA

(Elmann et al. 1970; Scott et al. 1973), in the majority of rock samples, only Ir and Au can be detected instrumentally.

Table 4.3.: Summary of the main PGE and Au isotopes employed during analysis and potential interfering species of similar half-life. The means of production of the interference is also shown.

PGE Radionuclide	Principle γ-ray (keV)	Interfering Radionuclides	Interfering γ-ray (keV)	Production of Interference
^{104m}Rh	51.4	none	-	-
^{109}Pd	88.0	^{176m}Lu	88.3	(n,γ)
		^{109}Pd	88.0	U-fission
^{191}Os	129.4	^{177m}Lu	128.6	(n,γ)
		^{169}Yb	130.6	(n,γ)
^{199}Au	158.3	^{117m}Sn	158.4	(n,γ)
		^{47}Ca	159.4	(n,γ)
^{192}Ir	316.5	^{177m}Lu	319.2	(n,γ)
		^{51}Cr	320.1	(n,γ)
^{198}Au	411.8	none	-	-
^{103}Ru	497.1	^{131}Ba	496.3	(n,γ)
		^{103}Ru	497.1	U Fission

4.3. Radiochemical Neutron Activation Analysis.

It is clear from the previous section, that successful determination of all six PGE in a single aliquot by NAA, requires a separation of the PGE from their geological matrix. RNAA procedures employ carriers which consist of an inactive amount of the same element which is being determined. After irradiation of the sample, chemical separations are performed to remove the element of interest from the remainder of the sample, with the active atoms embedded within the larger mass of carrier. By virtue of the fact that chemical separations are carried out <u>after</u> irradiation of the sample, RNAA offers several advantages over other separation procedures. These can be summarized as follows:

(1) The final material obtained for gamma-ray counting is often very pure, containing only the radionuclides of interest plus the inactive carrier. Background is therefore largely eliminated, peak resolution is greatly improved and low limits of detection can be attained.

(2) Post-irradiation chemistry greatly reduces the possibility of environmental contamination and virtually eliminates any reagent blank.

(3) Corrections can be made for losses in the procedure via the use of tracers to determine the chemical yield of the separation process. Complete recovery of PGE by the carrier material is therefore not essential.

However it must be stressed that the approach of applying corrections by calculation of chemical yields relies on the important assumptions that (a) losses for individual samples can be accurately measured; (b) that complete isotopic equilibrium has taken place between the active species and the carrier (van Loon 1985); and (c) the separations operate with the same efficiency for the PGE in the sample (usually sulphides or alloys) as the PGE in the tracer material (metal sponge or a PGE-halide salt). If losses are variable or if isotopic equilibrium was not attained, then any corrections may be subject to error.

Over the last 30 years a large number of RNAA procedures have been applied to the analysis of the PGE in rocks. Early procedures such as those developed by Brown and Goldberg (1949) and Vincent and Smalls (1959) were elaborate affairs which separated and purified individual PGE. The poor energy resolution of the first generation of NaI(Tl) gamma-ray detectors meant that the final products had to be as pure as possible to prevent interferences (Crocket and Cabri 1981; Perlman 1981). With the development of the present generation of high purity Ge detectors, which offer vastly improved resolution, this problem has gradually fallen away and group separations of the PGE are now the preferred approach.

Nadkarni and Morrison (1974) used a noble metal specific ion exchange resin, Sfarion NMRR, to separate the PGE and Au from the base metals, and claimed that it could be used for the determination of all six PGE from a single aliquot. Although this method has been employed by other authors, eg. Kyte et al. (1980), it has been heavily criticised by Apt and Gladney (1975) and by Tredoux (1990). The latter author found that only Ir, Pt and Pd could be reliably determined using the procedure outlined by Nadkarni and Morrison (1974).

Pernicka and Wasson (1987) determined Re, Os, Ru, Pt and Au in a number of iron meteorites using RNAA. After irradiation they leached the samples with aqua regia. The resulting solution was oxidised and OsO_4, RuO_4 and Re_2O_7 were

distilled under nitrogen, trapped in 4N NaOH, and counted. Solvent extraction into ethyl acetate was used to separate gold (including the ^{198}Au and ^{199}Au) from the aqua regia. The gold was precipitated with hydrazine, collected on glass filters and counted.

De Bruin (1992) noted that RNAA can potentially offer the greatest accuracy and the greatest sensitivity of any analytical technique but the need for dedicated facilities and highly skilled staff can make it very expensive in terms of both facility and labour costs. When applied to the noble metals, RNAA suffers from the drawback that radiological health considerations place a severe constraint on the amount of material which can be irradiated (Crocket and Cabri 1981). At most only a few grams of material can be used in the analysis and the extremely heterogeneous distribution of the PGE in many rocks, the so-called "nugget effect" (Erasmus et al. 1982), means that this small amount of sample material may not be truly representative of the bulk material, making reproducibility of results very difficult.

RNAA comes into its own when it is applied to specialized samples or to cases where there is very little material available for analysis, eg. meteorite chips or tektites (C. Koeberl pers. comm. 1992). However, the literature indicates that there does not presently appear to be a reliable, rapid RNAA procedure which can determine all of the PGE and Au in a single, geologically representative, aliquot of sample material (Crocket and Cabri 1981; Tredoux 1990).

4.4. Preconcentration Methods.

Preconcentration methods for the PGE and Au can be broadly divided into two categories. Those which collect the precious metals from a large mass of molten sample material (fire-assay) and those in which preconcentration, usually via leaching, is performed on solid samples. Preconcentration via fire-assay has been used since biblical times for the determination of the precious metals (Lenahan and Murray-Smith 1986; Laws 1991). As early as 300 BC, Theophrastus referred to the method of Pb collection for the testing of gold as a "trial by fire". These simple fire-assay procedures have proved remarkably successful and still continue to be used on a regular basis in modern laboratories.

Preconcentration procedures which do not utilise fire-assay are relatively new and various procedures are presently being investigated and developed (Laws 1991). The most important procedures, of both types, in use at present and those which might find wider application in the future are discussed in greater detail in the following sections.

4.4.1. Lead (Pb) Fire-Assay.

The oldest fire-assay procedure for the preconcentration of the PGE and Au is collection by Pb and it is still widely used in the gold and platinum mining industries (Lenahan and Murray-Smith 1986; Laws 1991). The collection process is carried out by fusion of the sample in a clay crucible with a flux of sodium carbonate, fused borax and silica. A reducing agent such as maize meal, and Pb oxide (litharge) are also added. During the fusion, the litharge is reduced to Pb, forming a "Pb rain" which collects the PGE and Au as the Pb droplets fall through the melt to gather at the bottom of the crucible. When fusion is complete, the melt is poured into a cast iron mold and allowed to cool. This allows the Pb button at the base of the mold to effectively separate from the silicate slag. The button is then hammered and cupelled into silver (Ag) at 960°C to remove the bulk of the Pb and then again at 1300°C to remove the silver. This leaves a final prill which contains the PGE and Au. The Pb fire-assay procedure is described in detail by Beamish and van Loon (1977), van Wyk and Dixon (1983) and Lenahan and Murray-Smith (1986).

Serious and highly variable losses of Os, Ru and Ir as volatile oxides have been shown to occur during the silver cupellation step (Watterson et al. 1971; Lenahan and Murray-Smith 1986). Au prills have been used to improve the collection of Ir but losses of Os are still extremely high (van Loon 1984). Therefore Pb fire-assay generally does not allow the determination of all six PGE.

Preconcentration by Pb collection and Ag cupellation was used by Rowe and Simon (1971) to determine Pt and Pd in a variety of rocks. Pb fire-assay buttons were analysed directly, without cupellation, using NAA by Turkstra et al. (1970) and De Wet et al. (1971). The Pb matrix was found to be very non-ideal for NAA due to high self absorption of γ-rays in the button (Watterson et al. 1971). The assay buttons therefore had to be reduced in weight from 20-30 grams to 50-1500mg by prolonged heating, prior to irradiation. Ir, Rh, Pt, Pd, Au and Ag were detected in the Pb button. Os and Ru were not detected due to losses during

heating of the Pb (De Wet et al. 1971). However, since these early studies, there have been few examples of the combined use of Pb fire-assay and NAA reported in the literature.

4.4.2. Nickel Sulphide Fire-Assay.

In view of the problems with Pb fire-assay for the quantitative collection of all of the PGE, various other collectors have been investigated. Excellent reviews of this topic and the other collectors which have been tested are given by van Loon (1984) and Laws (1991). The close association between the PGE and magmatic nickel sulphides in nature lead to the development of a technique by Robért et al. (1971) whereby nickel sulphide (NiS) was used as a collector for the PGE and Au. 50 grams of rock sample is melted at 1000°C using a mixture of sodium carbonate, borax, nickel carbonate and sulphur. This mixture produces two immiscible melts; a borosilicate melt containing silica, alumina and most of the major elements present in the sample; and a dense NiS melt. The sulphide phase descends through the less dense silicate melt, in principle extracting the PGE and Au from the silicate. These elements are present in the final assay button. A diagram of the contents of the crucible after NiS fire-assay are shown in Figure 4.1.

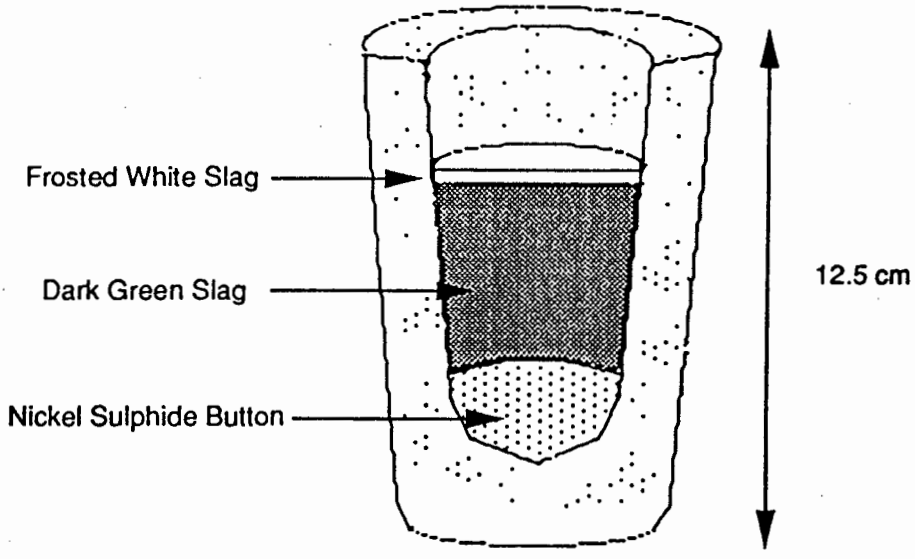

Figure 4.1 : Diagram of the interior of the crucible after NiS fire-assay.

After fire-assay, Robért et al. (1971) dissolved the assay button in hot, concentrated HCl. The main reaction taking place in solution during this process is:

$$NiS + 2HCl = NiCl_{2\,(aq)} + H_2S\,(g) \qquad \text{...equation (4a)}$$

Os, Ir, Ru and Rh are believed to remain unattacked by the HCl. Pt and Pd may be attacked but the hydrogen sulphide given off during this reaction strongly inhibits dissolution of Pt and Pd, as they will continually be reprecipitated as sulphides (see section 2.3.4.). When dissolution of the NiS was complete, the solution was allowed to cool and then filtered through a micropore (0.45µm pore size) filter paper to collect the insoluble PGE residue. The residue was then dissolved in HCl and hydrogen peroxide and Robért et al. (1971) used colorimetry and atomic absorption spectroscopy to determine the concentrations of the PGE and Au

Since the mid-1970's there have been several other techniques applied to the analysis of the PGE residue. Hoffman et al. (1978) were the first to use NAA for the analysis of the PGE residue without a subsequent acid-peroxide dissolution. The filter paper with the residue from the NiS dissolution was simply sealed, irradiated and analysed directly by NAA. Inductively coupled plasma atomic emission spectroscopy (ICP-AES) and inductively coupled plasma mass spectrometry (ICP-MS) have been used in the analysis of the dissolved residue (Barnes and Diallo 1986; Date et al. 1987; Jackson et al. 1990). More recently, XRF has also been applied to the direct analysis of the filtered residue (Eddy et al. 1991).

Although the samples used by Hoffman et al. (1978) in their study were predominantly sulphide ores which contained elevated levels of PGE, the limits of detection which they calculated for the NiS-NAA method suggested that it could be applied to the analysis of unmineralized rocks. This possibility was tested by Erasmus et al. (1982) who developed a procedure based on three separate irradiations and determined the PGE concentrations in 22 samples of unmineralized rocks from the western Bushveld Complex.

A compromise between the procedures of Hoffman et al. (1978) and Erasmus et al. (1982) was adopted by Davies and Tredoux (1985) in an effort to streamline the procedure and allow a greater throughput of samples. The two irradiation

periods (1 hour for the determination of ^{109}Pd, ^{198}Au and ^{199}Au, and a further 12 hours for the determination of ^{103}Ru, ^{191}Os and ^{192}Ir) employed by Erasmus et al. (1982) were replaced with a single 6 hour irradiation. This had the effect of increasing the background under the 88 keV peak of the short lived ^{109}Pd isotope, raising the detection limit for Pd from 2 to 4 ppb (Tredoux 1990). The overall lowering of flux also made resolution of the 129 keV peak of ^{191}Os very difficult and Os was sometimes not detected.

Robért et al. (1971) concluded that the NiS fire-assay method offered the following advantages over Pb collection:

(1) The NiS method achieves a quantitative extraction of all six PGE from the silicate matrix. This conclusion has subsequently been confirmed by Hoffman et al. (1978) and Shazali et al. (1987).
(2) Samples which are rich in sulphide can be treated without an initial roasting, minimising any losses of Os by conversion to OsO_4.
(3) Ni rich samples can be treated without leaching by HCl, preventing potential losses of Au and possibly Pd.

With the development of sophisticated techniques such as NAA and ICP-MS for the analysis of the PGE residue, the added advantage of extremely low detection limits can be added to this list.

4.4.3. Other Preconcentration Methods.
Although fire-assay remains the most common method of preconcentration for the noble metals, a number of new methods based on leaching of the noble metals from the rock matrix into solution have been developed and are becoming more widely accepted (Mallet 1986; Laws 1991). Procedures employing an initial fusion of the rock sample with lithium tetraborate (eg. Barnes and Diallo 1986) followed by leaching of the fusion crust, or direct leaching of the powdered silicate material (eg. Nicolas 1985) have both been applied.

Once the noble metals are in solution, solvent extraction procedures can be used to extract the PGE and Au from the other metals. ICP-OES, ICP-MS, ion chromatography (IC) and graphite furnace atomic absorption spectroscopy (GFAAS) are the most commonly employed instruments for the analysis of the noble metal extract. Detection limits which have been obtained from these

studies are generally on the order of 10 ppb, slightly higher than NiS fire-assay and ICP-MS (Laws 1991).

However, these procedures suffer from a similar problem to RNAA, ie that large amounts of material cannot be used. Typically the masses of material which can be taken for analysis are on the order of 5 grams or less (Laws 1991). The presence of the "nugget effect" (see section 4.4.1) suggests that similar problems with reproducibility may occur due to the fact that a relatively small amount of material may not be truly representative of the noble metal concentrations in the bulk of the sample.

Recently, Perry et al. (1992) have suggested a new procedure for the determination of the PGE and Au based on the dry chlorination of large samples (up to 250 grams) which may solve this problem. Samples are heated with chlorine gas at 570ºC and the PGE and Au are converted to soluble chlorides. These species are then taken up in distilled water and analysed by ICP-MS. To date, NAA has not been used in conjunction with any of these studies, primarily because the liquid nature of the noble metal extracts makes the use of strictly solution based analysis techniques more applicable.

It seems highly likely that techniques for the liquid or gas extraction and preconcentration of the noble metals will enjoy an increasingly important role in the future, particularly if they can be applied to large samples. Whether such techniques will ultimately replace fire-assay remains to be seen. Any application of NAA in this field will probably be quite limited.

4.5. Analysis Of The PGE By NAA At The Schonland Centre.

Mitchell (1982) outlined a set of hypothetical ideal criteria for any trace analytical method or technique. In order to qualify as ideal the technique should offer the following:

(1) Unequivocal identification of each of the desired elements in the presence of all other elements,
(2) Qualitative and quantitative multielement determination,
(3) Sub-nanogram detection limits,
(4) No matrix, interelement or interference effects,

(5) The technique should be instrumental and non destructive (ie. no chemical treatment of the sample),
(6) Negligible instrumental or reagent blank,
(7) Absolute quantitative results or realistic calibrations with available reference standards.

For the analysis of the PGE, a further note should be added:

(8) The technique should have the capacity to analyse a truly representative sample.

INAA, RNAA and preconcentration-NAA methods for the analysis of the six PGE are compared and evaluated in terms of the Mitchell (1982) criteria in Table 4.4.. A plus sign indicates that the method meets that condition very well, a zero indicates that method meets the condition adequately or at least offers no major disadvantages, and a negative sign indicates that the method does not meet that condition. A totals column, representing the addition of the various advantages and disadvantages is also given in the table.

As Table 4.4. shows, the NiS fire-assay method, in theory, offers only slightly more advantages than RNAA, most important of which are, the ability to process a representative aliquot of sample material, and the possibility of determining all six PGE from that single aliquot. RNAA procedures were investigated at Schonland Centre by Erasmus et al. (1982b) and Tredoux (1990). These studies indicated that reliable results could only be obtained for three or four of the PGE and it was concluded that these methods did not offer any significant advantages in terms of sensitivity or precision over preconcentration via NiS fire-assay.

Table 4.4.: Evaluation of the analysis techniques for the PGE in terms of the Mitchell (1982) criteria. See text for further details.

	Ideal Analysis Technique Criteria								
	1	**2**	**3**	**4**	**5**	**6**	**7**	**8**	**Total**
INAA	–	0	0	–	+	+	+	–	0
RNAA	–	+	+	+	–	+	+	–	+2
Pb fire-assay	–	+	+	–	–	–	+	+	0
NiS fire-assay	+	+	+	0	–	–	+	+	+3

Since 1982, the NiS fire-assay and NAA (NiS-NAA) method has been the one most commonly applied to the analysis of the PGE and Au at Schonland Centre. All of the analyses for the PGE in unknown samples carried out in this thesis were performed using modified versions of the Nis-NAA methods published by Davies and Tredoux (1985) and de Wit and Tredoux (1988).

Modifications to the above methods were required because the sensitivity achieved was still not sufficient to obtain data for all six PGE in unmineralized rocks on a routine basis. Problems with high initial background under the 88 keV peak of ^{109}Pd and poor resolution of the ^{103}Ru and ^{191}Os peaks at 497keV and 129 keV respectively, meant that these elements were reported only in a few favourable cases (see section 4.4.2). For example Davies and Tredoux (1985) reported no Os data in their study. In later studies based on the same method, Lee and Tredoux (1986) also did not report any Os data and could only detect Pd in 7 out of the 40 samples analysed and Borg et al. (1988) reported only 4 cases out of 30 where data for five PGE plus Au (Rh was not analysed) were obtained. The method outlined by de Wit and Tredoux (1988) suffered from similar problems (non detection of Os and high background interference on Pd). It should be stressed however that when applied to samples with individual noble metal contents of $\geq$ 5 ppb, both of the above methods were generally effective for all of the metals.

Crocket (1981), Barnes et al. (1985) and Tredoux et al. (1989b) have strongly emphasized the need for data on all six PGE in a sample in order to put real constraints on any geochemical modelling. As such modelling was conceived as being an integral part of this thesis from the beginning it therefore seemed logical to develop and refine a method based on the existing NiS fire-assay and NAA procedures which could obtain data for all of the PGE on a routine basis. This work is expanded and detailed in the following section.

4.6. Development And Modification Of The NiS-NAA Procedure.

Improvements to the existing methods are still very much an ongoing process, with slight modifications being tried with each new batch of samples. Summaries of the present procedure and the one employed by De Wit and Tredoux (1988) are shown in Figure 4.2. A detailed list of the analytical apparatus and many of the changes made to the previous procedures are documented in Appendix 4, which

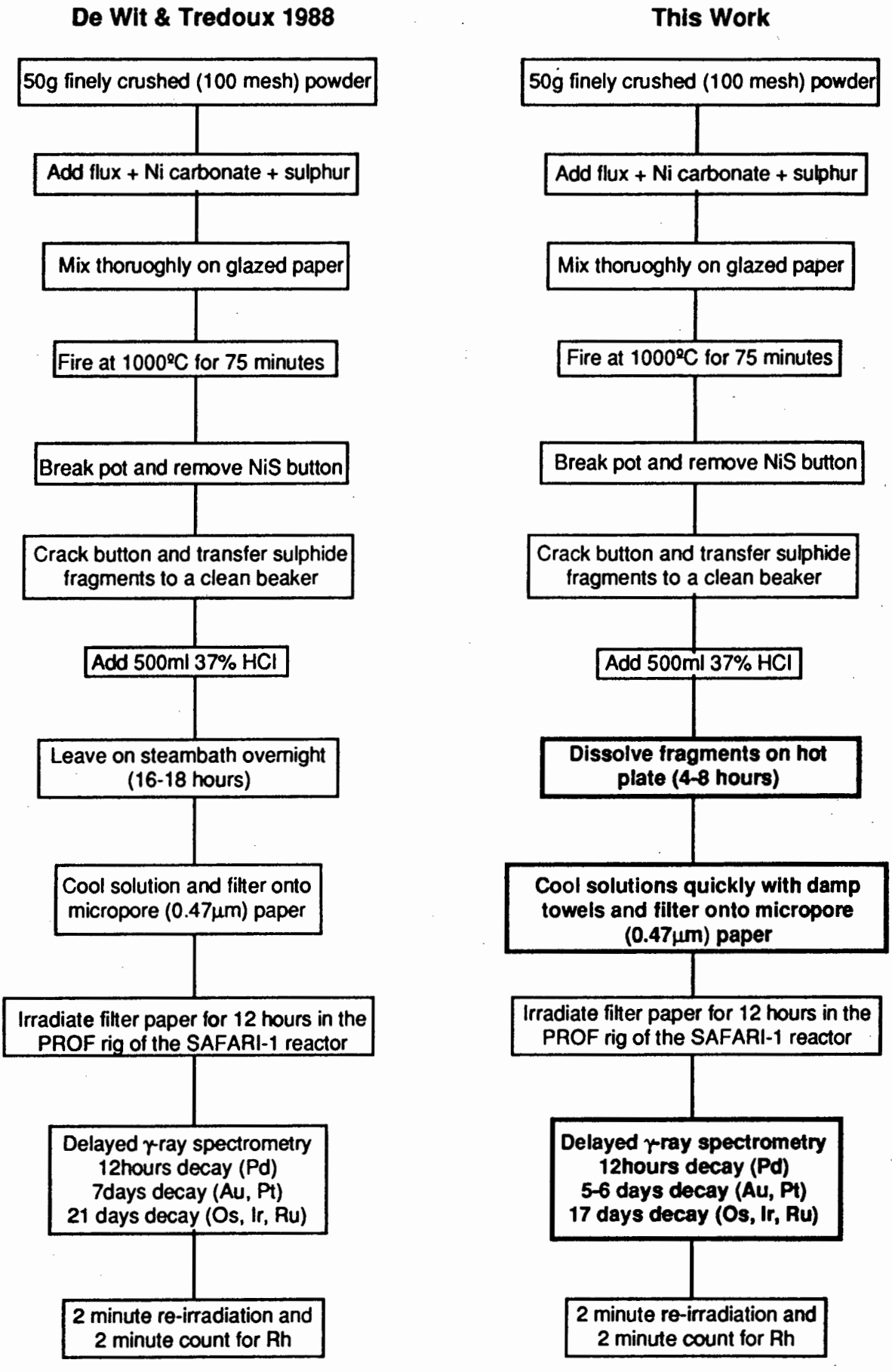

Figure 4.2: Summary of analytical procedures employed by De Wit and Tredoux (1988) and in this study. Principle changes made in this study are highlighted in bold text.

deals more specifically with the analysis of the PGE in kimberlites, and the reader will be referred to this appendix whenever necessary. Several lines of enquiry were followed during the optimization of the analytical procedure and these are described in the following sections.

4.6.1. NiS Fire-Assay Step.

It was found that the procedure originally described by Robért et al. (1971) and Hoffmann et al. (1978) was effective for most of the sample analysed during the course of this thesis. No particularly chromite-rich samples were analysed and the relative merits of Li tetraborate vs. Na tetraborate flux mixtures (eg. Borthwick and Naldrett 1983; Lee and Parry 1988; Parry et al. 1988; Tredoux 1990) for these samples was not investigated and will not be addressed here. Losses of noble metals occuring during NiS fire-assay of normal basic rocks are discussed in Appendix 4.

Particular problems did arise during the fire-assay with samples which were either very rich in MgO (harzburgites and dunites) or had high levels of carbonate (kimberlites and carbonatites). Problems with the fusion of carbonate-rich samples were previously noted by Tredoux et al. (1989b) and Tredoux (1990). The "normal" flux mixture (taken from Robért et al. 1971) was not able to melt these samples properly and modifications to the flux mixture had to be made. This is explained in greater detail in Appendix 4.

4.6.1. Removal Of Unwanted Background During Gamma-Ray Spectrometry.

As the NiS-NAA procedure involves a number of chemical preconcentration steps before irradiation, the material which is irradiated is very likely to contain a number of elements other than the noble metals. In order to understand whether these additional elements might seriously interfere with the analysis, one must first determine which elements are present on the final filter paper, what their sources are, what effects their radionuclides might have on the PGE analytical peaks and whether they can be removed.

It is the opinion of this author that the high background interference which affected the detection limits for Pd, Ru and Os in the studies carried out by Lee and Tredoux (1986), Borg et al. (1988) and de Wit and Tredoux (1988) was strongly linked to the amount of insoluble residue left after dissolution of the NiS assay button. In order to determine which species might be involved, an old filter

paper which had been prepared and sealed (but not irradiated) using the method of de Wit and Tredoux (1988), was irradiated under the same irradiation conditions employed by these authors and counted. It was found that in addition to peaks from the activated PGE, the gamma spectrum of the irradiated plastic vial, filter paper and residue contained peaks from the following isotopes:

6-8 hours decay: ^{24}Na, ^{42}K, ^{51}Cr, ^{56}Mn, ^{64}Cu, ^{65}Ni, ^{76}As, ^{82}Br, ^{122}Sb, ^{140}La, ^{152m}Eu, ^{153}Sm, ^{187}W, ^{197}Hg

7-8 days decay: ^{24}Na, ^{51}Cr, ^{58}Co (Ni), ^{60}Co, ^{75}Se, ^{76}As, ^{82}Br, ^{122}Sb, ^{124}Sb, ^{140}La, ^{152g}Eu, ^{153}Sm, ^{182}Ta, ^{203}Hg

20 days decay: ^{46}Sc, ^{51}Cr, ^{58}Co (Ni), ^{59}Fe ^{60}Co, ^{65}Zn, ^{75}Se, ^{76}As, ^{82}Br, ^{123m}Te(?), ^{124}Sb, ^{134}Cs, ^{140}La, ^{141}Ce, ^{152g}Eu, ^{182}Ta, ^{203}Hg

Shazali (1988) also reported the presence of some of the above species in the irradiated residue. He commented that activities from these species may interfere with or increase the background beneath the PGE gamma-ray peaks and have a serious effect on detection limits. Any reduction in this unwanted activity would therefore be desirable.

In order to determine the source(s) of these additional species and their relative contributions to the final background, an empty polyethylene irradiation vial, a clean cellulose nitrate filter paper, the residue left after evaporation of 20ml of 37% HCl, and 100mg of powdered NiS button were irradiated separately and then counted. The species detected in these separate fractions are summarized in Table 4.5.

Table 4.5. shows that, rather as expected, the chalcophile metals such as Cu, Zn, and Ni and the chalcogenide elements (Se, As and Sb) which were detected in the final PGE-bearing residue have their source in the NiS button and that the alkali metals and rare earths come from the HCl. Cr is a contaminant in all of the components bar the HCl, where it was beneath the limit of detection. Hg salts still find application in the pulp paper industry (Friberg and Vostal 1972; Cotton and Wilkinson 1980) and therefore it was not surprising to find small amounts of Hg in the filter paper. Br is present in both the filter paper and the HCl in high concentrations and peaks from the ^{82}Br isotope persist even after 3 weeks decay.

This feature has previously been noted in polycarbonate filter papers used for aerosol analysis (McDonald 1991c).

Table 4.5.: Summary of species detected in representative fractions of the materials which are irradiated and counted after dissolution and filtering of the NiS button.

Irradiation Vial	Filter Paper	Acid Residue	Nickel Sulphide
^{24}Na	^{24}Na	^{24}Na	^{24}Na
^{51}Cr	^{51}Cr	^{42}K	^{51}Cr
^{182}Ta	^{82}Br	^{46}Sc	^{58}Co (Ni)
^{187}W	^{134}Cs	^{51}Mn	^{60}Co
	^{203}Hg	^{82}Br	^{65}Ni
		^{134}Cs	^{65}Zn
		^{140}La	^{75}Se
		^{141}Ce	^{76}As
		^{152g}Eu	^{124}Sb
		^{153}Sm	

4.6.2.1. Species Present In The Irradiation Vial And Filter Paper.

Radiolytic degradation of the cellulose nitrate filter papers during the irradiation produced a mass of tiny, brittle fragments. It proved impossible to quantitatively transfer all of the fragments to clean counting vials, therefore samples had to be counted in the irradiated vials. This meant that activity from the vial could not be eliminated and, like the activity from the filter paper itself, was an inherent feature of the analytical blank.

None of the species detected in the vials or the filter papers seriously interferes with the ^{109}Pd activity. After a few days, the only significant activities from the vial and the filter paper are those from ^{51}Cr, ^{82}Br and ^{203}Hg. A compton edge from the 320 keV peak of ^{51}Cr may occur between 182-140 keV and this may interfere with the 158 keV peak of ^{199}Au, similarly, the 279 keV peak of ^{203}Hg may produce a compton edge between 155-120 keV which might potentially interfere with the 129 keV peak of ^{191}Os. In practice however, the low concentrations of Cr and Hg in the vial and in the paper indicate that any interference is probably negligible. It is therefore safe to conclude that counting samples in irradiated vials did not significantly affect the determination of the PGE.

4.6.2.2. Species Present In The HCl.

The species produced on the cellulose nitrate filter paper by the HCl present more of a problem. The amount of HCl left on the paper after filtration is very dependent on the washing procedure (see Appendix 4). The Br content of the filter papers alone was found to be relatively consistent, therefore the total activity of ^{82}Br, along with the activities of ^{140}La and ^{152g}Eu, could be used to obtain a very crude measure of the amount of acidic material retained on the filter. It was found that variations in the activity of ^{82}Br did not bear any correlation to either the sample type or the amount of material on the filter paper. In fact it was often found that filter papers which appeared to be very clean and free of any residue, had higher ^{82}Br activities than filter papers which retained some residue.

During later experiments, it was found that the temperature of the washing water played a considerable role in the efficiency with which Br could be removed from the filter paper. The manufacturers (Sartorius) specifications note that the cellulose nitrate fibres begin to disintegrate in solutions above 60°C, therefore this established ceiling temperature for the washing solutions. The final wash with 500ml of distilled water should be carried out above 45°C in order to achieve the most effective removal of Br from the filter paper.

The use of larger volumes of water for washing was also investigated and this is shown in Figure 4.3. The ^{82}Br activity was reduced to values close to those obtained for the filter paper alone, quite effectively with 500ml of water, as long as the water temperature was kept above 45°C. Washing with larger volumes of water did not significantly reduce the ^{82}Br activity beneath this value, suggesting that Br not bound up within the filter paper itself is present in a relatively soluble form.

The activities of ^{140}La and ^{152g}Eu showed a very broad correlation with the amount of residue left on the filter paper. Significant activities of these species were present on some filters which had been washed with up to 1500ml of distilled water, suggesting that that these elements may have been trapped on the filter paper in an insoluble form. This possibility is discussed in greater detail in the following section.

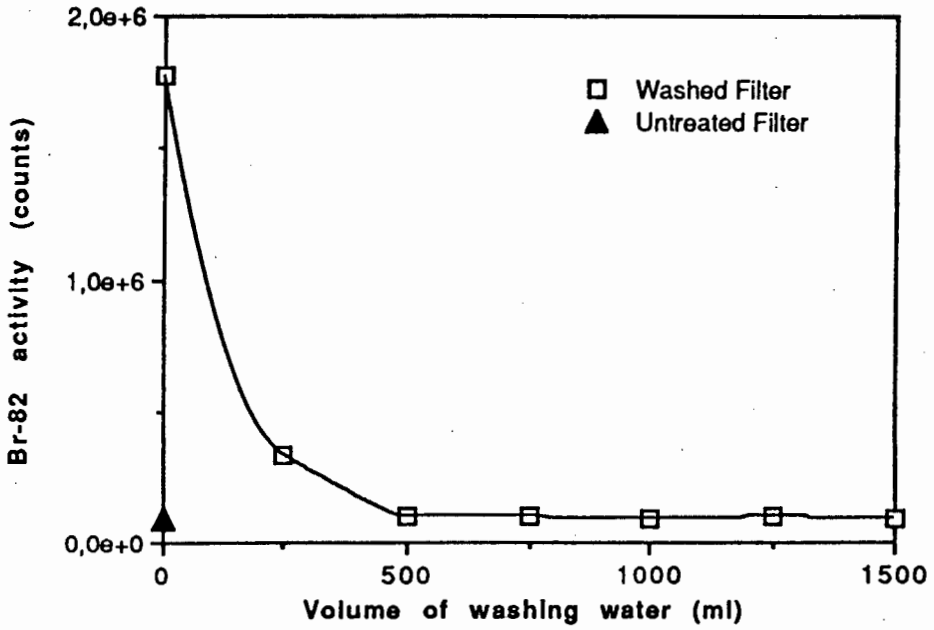

Figure 4.3.: Summary of ^{82}Br activity on washed filter papers compared to untreated, blank filters.

4.6.2.3. Species Present In The Residue.

Excluding the Br background, by far the most significant problem was activity generated by undissolved material from the NiS button. The 1988 filter paper which was analysed was very dark and contained a lot of undissolved material. Apart from PGE species, the strongest peaks were found to come from ^{51}Cr, ^{60}Co, ^{58}Co(Ni), ^{76}As, ^{75}Se and ^{124}Sb respectively. High activities from all of the above species in the first count produced a very high Compton background underneath the 88 keV peak of ^{109}Pd. The peak just penetrated the steep shoulder of a rise in the background and was not identified by the HEVESY peak-search algorithm (see Appendix 2).

High activity from the 320 keV peak of ^{51}Cr (and also the 316 keV peak of ^{192}Ir) produced a compton edge from 182-138 keV which partially obscured the 158 keV peak of ^{199}Au. On closer examination, the 158 keV peak also had a distinct tail, stretching up to 163 keV. A best-fit model of the total area using DISPLAY, a more sophisticated peak fitting routine than the HEVESY algorithm (R.W. Fearick pers. comm 1991), indicated the presence of two peaks, large peak at 158.2 keV and second, smaller peak at 159.5 keV which is probably ^{123m}Te. The presence of Te in the final residue raises the possibility that the 158 keV peak of ^{199}Au may be overestimated by the peak-fitting algorithm.

The comment made by Stockman (1983) that any interference by ^{123m}Te on ^{199}Au should be negligible because 1ng of ^{199}Au produces 1000 times more 158 keV gamma-rays than 1ng of ^{123m}Te, certainly cannot be applied to the NiS-NAA procedure. Te was detected in small quantities in the sulphur used for the fire-assay and is therefore likely to be present in all of the NiS assay buttons. Conversion of base metal telluride species to H_2Te gas in acids solutions is not very efficient (Greenwood and Earnshaw 1984) and therefore Ni, Cu or Zn tellurides might be expected to concentrate in any undissolved residue along with any PGE tellurides, possibly generating interference on the Pt determination.

A rather extreme example of this problem was encountered with a sample (NAM 219) which produced an abnormally high amount of dark residue. When this sample was irradiated, the spectrum recorded after 7 days decay showed a very strong peak at 159 keV, which was at first assumed to be ^{199}Au. Analysis of the LEPD spectrum is shown in Figure 4.4. The spectrum clearly shows the presence of peaks from Se (a companion chalcogenide to Te) as ^{75}Se, and ^{131}I. The latter species is produced from ^{130}Te which is activated to ^{131}Te. This subsequently decays with a 25 minute half-life to ^{131}I. A strong Te Kα x-ray peak at 27.5 keV is also present. Based on this information, it would appear that the peak at 159 keV is most probably from ^{123m}Te.

^{51}Cr can cause a small interference on the 316 keV peak of ^{192}Ir if the residue contains large amounts of Cr. If this occurs, the slightly less intense, 468 keV of ^{192}Ir, which is interference free, can be used as an alternative. The 129 keV peak of ^{191}Os and the 497 keV peak of ^{103}Ru are not directly interfered with by any of the major species in the residue but high background in the low energy region was found to obscure the 129 keV peak in some cases. In particularly dirty samples, the 511 keV positron annihilation peak can be abnormally wide and may affect the 497 keV peak.

As mentioned in section 4.6.2.2, significant activities from ^{140}La and ^{152g}Eu were also present on some filter papers even after extensive washing. Lanthanide chlorides can form sulphides when reacted with H_2S at high temperatures in the gas phase (Cotton and Wilkinson 1980). It is not known whether La or Eu sulphides might form in solution under the conditions employed during dissolution of the NiS button, but such a possibility is attractive in explaining their presence in the final insoluble residue. The strongest ^{140}La and ^{152g}Eu peaks

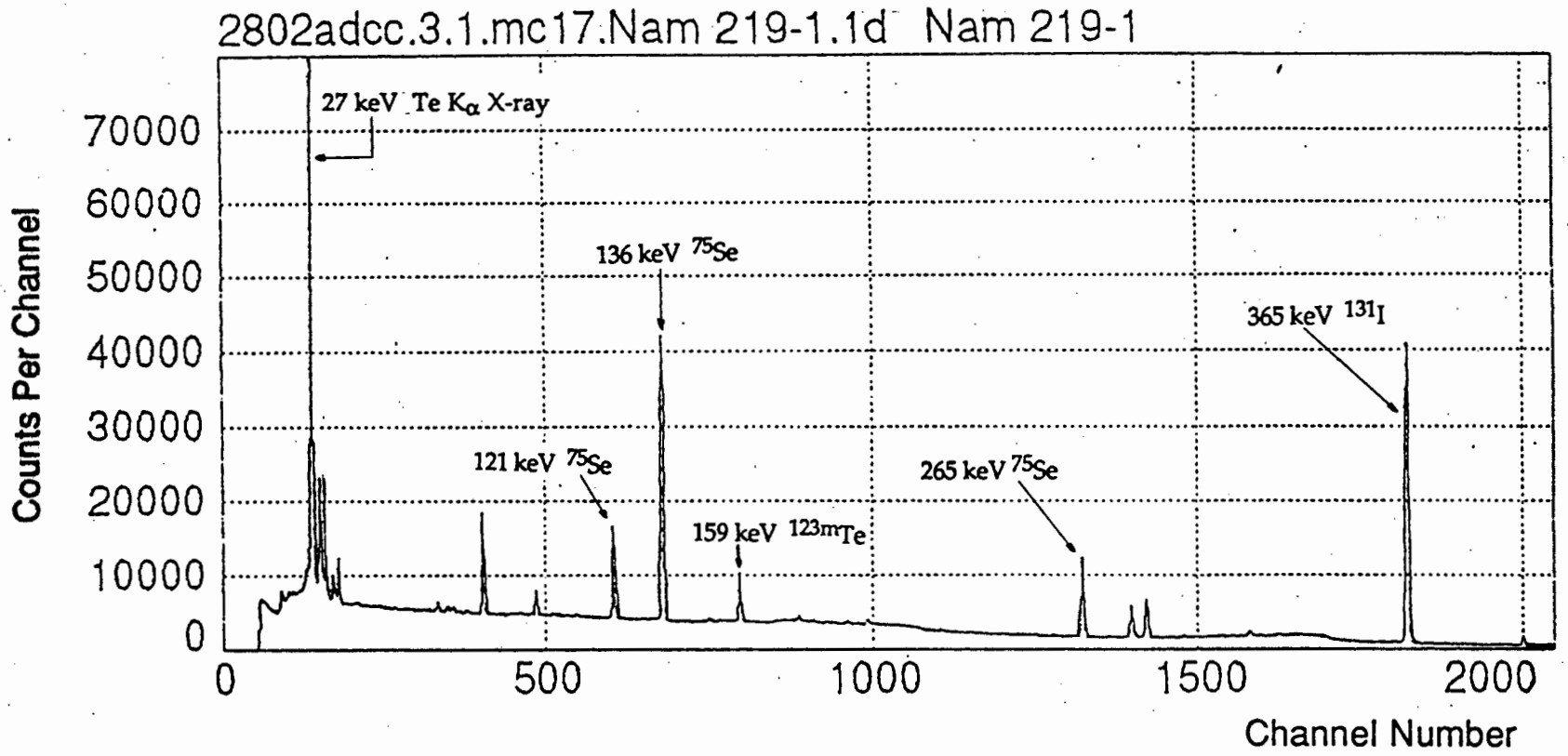

Figure 4.4.: Gamma spectrum produced by sample NAM 219 after 7 days decay. Spectrum recored on the LEPD which was calibrated for 0.2 keV per channel. Major peaks and their sources are shown.

were noted from those filter papers which had accumulated surface scum from the HCl (see section 4.6.3.), suggesting that some kind of reprecipitation process might be responsible for the accumulation of these elements on the filter paper.

Many of the species discussed in this section would appear to have been deposited on the filter paper via incomplete dissolution of the NiS button. Improvements in the dissolution procedure would therefore be expected to reduce this unwanted background and these are discussed in the next section.

4.6.3. Dissolution Of The Button.

4.6.3.1. Replacement Of Steambaths With Hot Plates.

The high amounts of insoluble residue which were sometimes left on the filter paper could be traced directly to the use of a steambath for the dissolution of the NiS button by Davies and Tredoux (1985) and de Wit and Tredoux (1988). It was found that the temperatures attained on steambaths were neither high enough to permit continuous dissolution, nor could the temperature be sufficiently controlled as occasional water pressure fluctuations sometimes caused the steambath to lose heat. Drops in temperature during the dissolution frequently led to the formation of a metallic grey scum on the surface of the solution. Once formed, the scum layer proved very difficult to redissolve, even with the addition of more HCl. During filtration, the scum produced a thick, oily grey mass on the final filter paper. This made folding and packing of the filter paper into an irradiation vial, without the loss of any material, very difficult.

In addition, dissolutions carried out with steambaths were found to be very slow. In many cases, samples had to be left overnight or for several days before they would dissolve. This meant that there might potentially be long periods where the PGE and Au were in contact with hot acid without the presence of a reducing atmosphere to stabilize them. There is some debate in the literature whether the PGE might dissolve under these conditions (Palmer and Watterson 1971; Hoffman et al. 1978; Shazali 1988; see also section 4.6.3.3 and Appendix 4) and in the light of this it was decided to try to minimise the period in which the PGE might be in contact with hot acid after H_2S evolution had ceased.

Steambaths were replaced with a hot plates in an attempt to solve this problem. It was found that the hotplates provided a much more even and controlled heating of the solution and that the time required to dissolve most NiS buttons was

considerably shortened. Buttons could be dissolved over periods of 4-8 hours which meant that the solutions could be monitored during a normal working day and filtered in the late afternoon or evening.

The higher temperatures which were obtained with the hot plates effectively prevented the formation of surface scum. The higher temperatures and more vigorous dissolution conditions rapidly broke up and redissolved any specks of scum which formed. On filtering, it was found that those solutions prepared on the hot plate gave much cleaner filter papers than those obtained from solutions which had been prepared with the steambath.

4.6.3.2. The End Point Of The Dissolution.

The end point of the dissolution was met when evolution of gas from the solution effectively ceases and a close examination of the insoluble particles on the base of the beaker also reveals no gas activity. A routine test was to turn up the temperature on the hot plate for 5-10 minutes. If this produced gas activity in any base metal sulphides then the residue was allowed to dissolve for another 20-30 minutes before being examined again. If there was no gas activity during the initial temperature rise, then it was judged that all of the base metals had dissolved and that the end point had been reached.

4.6.3.3. Te Coprecipitation.

Te coprecipitation procedures to reprecipitate any noble metals which pass into solution during the dissolution step have been outlined by Shazali et al. (1987) and Jackson et al. (1990). Such procedures have the effect of introducing a large amount of Te onto the final filter paper(s), which can cause a major interference with the 158 keV peak of ^{199}Au (Shazali 1988; see also section 4.6.2.3). Shazali et al. (1987) recommended the use of the less sensitive 208 keV peak of ^{199}Au as an alternative but this had the effect of dramatically raising the detection limit for Pt (see Table 4.7).

The advantages and disadvantages of introducing a Te coprecipitation step for very low level PGE analysis are discussed in Appendix 4 and slightly expanded here. In order to minimise losses of the PGE and Au during the dissolution step and obviate the need for Te coprecipitation, a rigorous approach to this step of the analysis was taken. The use of hot plates meant that the entire dissolution could generally be monitored by the analyst during the course of a day. With careful

monitoring and a close examination for the end point of the dissolution (see section 4.6.3.2), the solution could be removed, cooled and filtered without the PGE bearing residue standing in contact with the hot acid for lengthy periods.

NiS buttons containing irradiated Os, Ir, Pt, Pd and Au metals (Johnson Matthey Specpure sponges) as tracers were dissolved in HCl. Some solutions were removed from the hot plate and cooled when the end point the dissolution was reached, while others were allowed to stand for progressively longer times after gas activity from the solution had ceased. All of the solutions were filtered and the filter papers counted for ^{109}Pd, ^{193}Os, ^{194}Ir, ^{197}Pt and ^{198}Au on a Ge(Li) detector. The volume of filtrate was reduced under gentle heating to about 60 ml, cooled, sealed in a polythene bottle and counted on the same detector. Sample to detector distances were kept above 100 mm (C.S. Erasmus pers. comm. 1992) in order to minimize corrections for the differing sample geometries. The results are shown in Table 4.6.

Table 4.6.: Losses of PGE and Au during acid dissolution of NiS buttons. See text for further details.

Solution	% Activity Present				
	Os	Ir	Pt	Pd	Au
End Point					
Filter Paper*	100	99.6	100	98.6	97.0
Solution*	n.d.	0.4	n.d.	1.4	3.0
End Point + 6 hrs					
Filter Paper	100	99.5	100	96.2	92.9
Solution	n.d.	0.5	n.d.	3.8	7.1
End Point + 12 hrs					
Filter Paper	100	99.2	100	92.6	88.0
Solution	n.d.	0.8	n.d.	7.4	12.0
End Point + 18 hrs					
Filter Paper	100	99.3	95.5	89.9	84.7
Solution	n.d.	0.7	4.5	10.1	15.3

*** Average of 4 determinations.**

The results of this study are generally in line with the conclusions of Palmer and Watterson (1971) and Kuznetsov et al. (1974) that significant losses of Pt, Pd, and Au can occur during the dissolution, but only in the absence of a reducing (H_2S) atmosphere. It was concluded that provided the end point of the dissolution could be monitored and the solutions cooled and filtered quickly after this, any loss of PGE and Au to the solution would be minimised. Any improvements in PGE recovery produced by Te coprecipitation would not be matched by the adverse effect of high amounts of Te in the final residue. In view of the reduction in sensitivity for Pt after activation (and the other PGE due to higher overall background), Te coprecipitation was not employed for samples analysed during the course of this thesis.

4.6.4. Lower Limits Of Detection.

Limits of detection, defined as the smallest concentration which produces a net peak area of twice the standard deviation of the background beneath the peak of interest, for previously published NiS-NAA procedures are shown in Table 4.7.. Limits of detection for the modified procedure developed in this study are also shown in Table 4.7.. These limits pertain to both normal basic rocks and kimberlites, where due to the low PGE concentrations, 100 grams of material was taken for analysis (see Appendix 4).

Table 4.7.: Summary of detection limits for the PGE obtained by earlier authors and in this work using combined NiS-NAA procedures. All values are quoted in parts per billion.

	Os	Ir	Ru	Rh	Pt	Pd	Au
Hoffman et al. 1978	2	0.1	3	1	5	5	0.1
Erasmus et al. 1982b	0.5	0.05	2	0.5	5	2	0.05
Davies & Tredoux 1985*	3	0.1	5	1	5	4	0.1
Shazali et al. 1987	5	0.5	3	2	15	7	0.2
This work (50g sample)	0.4	0.01	2	0.6	3.8	1.5	0.002
This work (100g sample)	0.2	0.005	1	0.35	2.5	0.8	0.001

* M. Tredoux pers. comm. 1992.

The high limit of detection for Pt quoted by Shazali et al. (1987) is a direct consequence of the use of Te coprecipitation after dissolution of the NiS button. The use of the 208 keV peak of ^{199}Au has the effect of increasing the detection limit for Pt by a factor of three.

All of the values shown in Table 4.7 are "theoretical" detection limits, ie. they do not take into account any contribution from the reagent blank. Ir, Rh and Au, the most sensitive elements for NAA usually produce a quantifiable reagent blank and this is discussed in section 4.7. The role of the blank contribution in the calculation of the "real" limit of detection is discussed in Appendix 4.

4.7. Control Of The Reagent Blank.

As the NiS-NAA procedure involves a large amount of pre-irradiation chemistry, it is particularly vulnerable to contamination (Murphy 1976; Erasmus et al. 1982b). The major potential sources of contamination are (1) the lab environment (air purity and analytical equipment such as glassware); (2) the chemicals used; and the analysts themselves. Each of these potential sources is evaluated in the following sections.

4.7.1. Lab Environment.

The air in the PGE laboratory at Schonland Centre is not purified or filtered. The Witwatersrand region contains numerous mine dumps and small amounts of Au, and occasionally Ir, have been detected during monitoring of the air quality around Johannesburg and the Vaal Triangle (McDonald 1991c), suggesting that airborne contamination could be a potential hazzard. A comparison of blank values between Schonland Centre and laboratories in Europe showed that the European laboratories had higher Au blanks and lead Tredoux (1990) to conclude that airborne contamination did not seriously affect the blank. Although a small component of airborne contamination may be present, my experience in the laboratory generally confirms this conclusion provided considerable care is always taken to cover and shield samples from dust during all stages of the analysis.

Some laboratory equipment (eg. the jaw crusher and swing-mill bowl, borosilicate beakers for dissolutions and the filtering apparatus) was re-used during analysis and this introduced the possibility of cross-contamination. In order to minimize this, the swing-mill was cleaned with barren quartz between each sample crushing (see Appendix 4). Beakers were thoroughly washed with 50% HCl and distilled water after dissolutions had been completed. The sartorius glass filter funnels were cleaned with aqua regia and distilled water, and stored in 50% HCl when not in use.

Most importantly, samples where widely differing PGE contents were expected (ie mineralized and barren material) were purposely kept apart and treated as separate sample batches. Low level samples were always treated before high level samples and after the high level samples had been completed the laboratory was thoroughly cleaned before any new material was analysed.

4.7.2. Chemicals

The chemicals used during the fire-assay are undoubtedly the principal source of contamination. Nickel, whether in the form of Ni metal, NiO, or $NiCO_3$ powder always contains some traces of PGE. The PGE content of all of these Ni components can be extremely erratic (Shazali 1988; Tredoux 1990) and consecutive batches from the same supplier can vary considerably. As a matter of general policy, small quantities of powder were first purchased, tested for PGE content, and if this was sufficiently low, a larger quantity of the batch of powder was purchased. If the trial sample contained levels of PGE in excess of 2ppb of each metal, it was rejected and another batch of Ni was tested until one was found which was sufficiently clean.

Prior to the analysis of any unknown samples, seven batches of $NiCO_3$ from a variety of different suppliers had to be tested before one of sufficient purity was found. The results of these tests are shown in Table 4.8.

Following these trial determinations, 20kg of Labchem #2 $NiCO_3$ was purchased and this was used for the majority of analyses in this thesis. Shazali et al. (1988), Parry et al. (1988) and Jackson et al. (1990) have noted similar problems with the Ni used for fire-assay. An additional point is also worth noting; the carbonate powder was kept in a large bucket when not in use and it was found that blanks deteriorated very badly when using the last 2-3kgs of powder at the bottom of the bucket. Up to 20ppb of Os and Ir and 55ppb of Ru were found in some blanks and buttons prepared with this $NiCO_3$ fraction had to be discarded.

From this it would appear that the PGE particles in the $NiCO_3$ powder are present as relatively dense phases and over time they collect in the lowest layer of the powder. Since this was discovered, $NiCO_3$ batches are split up, kept in separate 500g containers and shaken before use so that PGE will only concentrate from a relatively small mass of material, keeping any blank to manageable levels.

Table 4.8.: Summary of blank determinations made on batches of nickel carbonate during 1990. "n.d." indicates not detected, "n.d.a" indicates no data available. All data in ppb.

	Concentration Present						
Nickel Batch	**Os**	**Ir**	**Ru**	**Rh**	**Pt**	**Pd**	**Au**
Nickel #1*	n.d.	0.057	n.d.	n.d.a	n.d.	n.d.	0.54
	n.d.	0.077	n.d.	n.d.a	n.d.	n.d.	0.81
Nickel #2	3.4	6.4	33	n.d.a	n.d.	n.d.	2.5
	2.9	6.2	25	n.d.a	n.d.	n.d.	2.7
Nickel #3	2.1	3.0	15	n.d.a	n.d.	n.d.	1.5
	3.5	3.6	23	n.d.a	n.d.	n.d.	1.6
	1.8	5.1	14	n.d.a.	n.d.	n.d.	1.7
Labchem #1	n.d.	0.05	5.6	n.d.a	n.d.	n.d.	0.75
	n.d.	0.07	6.8	n.d.a	n.d.	n.d.	1.2
	n.d.	0.10	6.1	n.d.a	n.d.	n.d.	1.3
Quadralab #1	n.d.	0.61	5.4	n.d.a	n.d.	n.d.	1.9
	n.d.	0.64	5.0	n.d.a	n.d.	n.d.	1.9
	n.d.	0.88	5.2	n.d.a	n.d.	n.d.	1.5
Chem.Smallpax #1	n.d.	0.36	2.5	n.d.a	12.2	n.d.	1.2
	n.d.	0.35	2.3	n.d.a	10.1	n.d.	1.1
Labchem #2	n.d.	0.52	n.d.	n.d.	n.d.	n.d.	0.78
	n.d.	0.43	n.d.	0.45	n.d.	n.d.	0.64
	n.d.	0.47	n.d.	0.42	n.d.	n.d.	0.60

* Although Ni #1 was very clean, only 1kg of material was still in stock by the time the determination was made.

The presence of anomalous concentrations of Ru in some batches of HCl was noted by Jackson et al. (1990). This may also have been the case with some batches of HCl used in this study but this could not be verified. Many of the blanks in Table 4.8. were analysed with the same batch of acid and it would appear that the principle cause of the variation is the $NiCO_3$ powder. It is my opinion that the amount of noble metals in the $NiCO_3$ outweighed any small contribution from the acid to the total blank.

4.7.3. The Analyst.

During processing of the samples, the analyst should take extreme care to (1) shield samples from dust or other external contamination; (2) prevent any cross-contamination; and (c) keep handling of the samples to a minimum, because sweat can add Na and Br to the surfaces of sample containers, increasing gamma-ray backgrounds after irradiation. If these tasks are performed with care and skill, the chances of obtaining a quantitative result from low level samples is greatly increased (Murphy 1976; C.S. Erasmus pers. comm 1990).

4.8. Conclusions.

Of the several methods for PGE analysis by NAA outlined in this chapter, non-destructive INAA has a very limited application due to very serious interferences from other, more abundant, elements in the rock. RNAA can produce very precise data with low limits of detection, but only three or four PGE may be analysed from single aliquot. In addition, RNAA suffers from the fact that, due to radiological health considerations, large amounts of sample material cannot be analysed and the heterogeneous distribution of the PGE in most rocks may make reproducibility of results very difficult.

NiS fire-assay preconcentration followed by NAA allows the analysis of large (and therefore more representative) samples and permits the determination of all six PGE in a single aliquot of sample. However the pre-irradiation chemistry inherent in this procedure introduces a number of species which may interfere with PGE peaks after irradiation. Noble metals in the reagents used for fire-assay also produce a significant reagent blank.

Samples rich in MgO and CO_2 may give problems during the fire-assay. The addition of larger quantities of acidic flux components may be required to produce a stable melt and a usable NiS button.

The use of a hot plate for dissolution of the NiS button is preferred over a steambath as this significantly reduces the amount of unwanted residue on the final filter paper. Careful monitoring of the dissolution by the analyst can do away with the need for Te coprecipitation, which has a serious effect on the determination of Pt. The reagent blank can only be minimized by the careful screening of all new batches of chemicals prior to their use in the analysis.

The NiS-NAA procedure outlined in this chapter offers significantly lower limits of detection than previous methods but suffers from the disadvantage that the analyst must adopt a very rigourous approach to the dissolution step. This makes the procedure less convenient in terms of an 8 hour working day than previous ones where the solutions were much less carefully monitored. The analyst must be prepared to weigh whether the advantages in sensitivity which are gained using this approach are worth the extra effort involved.

Chapter 5

Preliminary Standardisation Of Wits-1; A Potential Low Level PGE Reference Material.

5.1. Introduction.

Relatively few reference materials are presently available for use as PGE standards in routine analysis. Until recently, NAA was the only technique capable of achieving the sensitivities needed for common rocks. As shown in Table 5.1., only a few of the PGE have been analysed in common silicate standards and even in these cases there is considerable uncertainty over some values (Gijbels et al. 1971; Crocket 1981, Shazali 1988). Due to the short half lives of the ^{104m}Rh daughters and the extreme difficulties inherent in analysing the element by NAA, the absence of Rh data from these standards is also a very serious problem.

Table 5.1.: Summary of PGE analysed for in common silicate rock standards.

Standard	PGE Determined	Reference
BCR-1	Ir, Pd	Anders et al. 1988
DTS-1	Os, Ir, Ru	Gijbels et al. 1971
	Ir, Pt, Pd	Nadkarni and Morrison 1974
G-1	Os, Ir, Pd	Crocket et al. 1968
G-2	Pt, Pd	Rowe and Simon 1971
PCC-1	Os, Ir, Ru	Gijbels et al. 1971
	Os, Ir, Pt and Pd	Nadkarni and Morrison 1974
	Ir	Cummings et al. 1988
W-1	Os, Ir, Pd	Crocket et al.1968

A few meteorites such as Allende have been analysed for Os, Ir, Ru and Pt (Crocket 1969). Canada Centre for Mineral and Energy Technology (CANMET) produces the standards PTC-1 (a sulphide concentrate) and SU-1 (a Ni-Cu-Co ore) which have been certified for some of the precious metals but not all (Steger 1983). However, the only readily available geological reference material with certified values for all of the precious metals is the South African Bureau of Standards Pt ore SARM-7

(Steele et al. 1975; van Loon 1984; Jackson et al. 1990). This standard is a composite of several tonnes of mineralized Merensky Reef harzburgite and barren anorthosite taken from various mines situated around the eastern and western lobes of the Bushveld Complex (Steele et al. 1975).

PTC-1, SU-1 and SARM-7 are samples or concentrates of mineralized rocks and therefore contain concentrations of PGE several orders of magnitude higher than usually encountered in unmineralized samples. Extrapolating calibration curves for the calculation of concentrations over such a large range, can lead to very serious errors (see section 3.4.). In addition it has been shown by Fesq and Lee (1976) and by Erasmus et al. (1977) that the noble metals are not homogeneously distributed in small amounts (<1g) of SARM-7 and that large variations, on the order of 30%, may result from the use of such small sample sizes. Despite the above problems, SARM-7 remains the only available standard if data for all six PGE are sought (Van Loon 1984).

In order to achieve a range of concentrations which is more representative of the expected levels of PGE in basic and ultrabasic rocks, all analyses carried out at Schonland Centre have employed solid dilutions (1:10, 1:20 and 1:40) of large masses of SARM-7 as standards (eg. Erasmus et al. 1982b; Davies and Tredoux 1985; see also Appendix 4). In each study, the dilutant used was extra pure silica powder.

This approach requires great care on the part of the analyst to ensure that SARM-7 is completely homogenised prior to the extraction of 50-100g aliquots for dilution. Careful and vigorous mixing (3-4 hours on a shaker) is then required to ensure that SARM-7 is homogeneously distributed throughout the silica and that effective solid dilution has been achieved. The problems of heavy PGE particles sinking through a less dense powder matrix which were observed with the $NiCO_3$ (see section 4.7.2.) have also been found to apply to the diluted standards. Therefore it is very important that the standards should be reshaken in order to rehomogenise them prior to their use in fire-assay.

This approach, while allowing satisfactory calibrations to be obtained, is far from ideal and since the late 1980's there has been a consensus amongst PGE analysts that more samples with low levels of PGE should be analysed and certified for all six PGE (M. Tredoux pers. comm. 1991). This would allow more realistic calibrations to

to be drawn up, which more closely reflect the range of PGE concentrations expected from unmineralized rocks.

5.2. Preparation Of A PGE Reference Material At The Schonland Centre.

In 1987, after discussions between PGE analysts at the Geoplatinum-87 Conference in Milton Keynes, it was decided to attempt such a standardization at Schonland Centre. During the early 1988 approximately 1000 kg of a silicified and hydrated komatiite, was collected from close to the type section in the Komati River, south of Barberton, (Viljoen and Viljoen 1969). The komatiite sample, named Wits-1 was a rapidly quenched ultramafic lava flow which was expected to have an undifferentiated but also a fairly uniform PGE distribution. The komatiites in this area are not mineralized (Viljoen and Viljoen 1969b; Naldrett and Campbell 1982) and rather low concentrations of the individual PGE and Au (<15ppb) were expected.

Crushing was carried out at the National Institute for Metallurgy in Randburg using agate mills reserved for the crushing of low level samples (E. van Wyk, pers. comm. 1992). All of the powder was thoroughly mixed via rolling and shovelling for several days on large plastic sheets. After this, 5kg aliquots were removed and sealed in screw top plastic bottles. Prior to PGE analyses being performed, the major and common trace element composition of Wits-1 was determined using XRF and INAA. The results are shown in Tables 5.2 and 5.3.

Table 5.2.: Major element composition of Wits-1. XRF data based on the average of 9 aliquots, NAA data based on the average of 5 aliquots. Total iron expressed as Fe_2O_3.

			Analysis Method
Major Elements (wt %)	SiO_2	43.20	XRF
	TiO_2	0.26	XRF
	Al_2O_3	3.64	XRF
	Fe_2O_3*	11.93	XRF
	MnO	0.16	XRF
	MgO	28.46	XRF
	CaO	4.62	XRF, INAA
	Na_2O	0.21	XRF, INAA
	K_2O	0.01	XRF, INAA
	P_2O_5	0.02	XRF
	L.O.I.	8.29	Gravimetric
	Total	100.80	

Table 5.3.: Trace element composition of Wits-1. XRF data based on the average of 9 aliquots, NAA data based on the average of 5 aliquots..

			Analysis Method
Trace Elements (ppm)	Sr	21	XRF
	Rb	5.5	XRF
	Y	14	XRF
	Zr	24	XRF
	Cr	2820	XRF, INAA
	Ni	1680	XRF, INAA
	Co	97	INAA
	Sc	13	INAA
	Ta	4	INAA
	Sb	0.41	INAA
	As	1.7	INAA
	La	3.1	INAA
	Sm	0.25	INAA
	Eu	0.23	INAA
	Yb	0.47	INAA
	Lu	0.17	INAA

All XRF analyses were performed on a spectrometer in the Department of Geology of the University of the Witwatersrand. The analytical procedure adopted in this laboratory has been outlined by McCarthy (1978). INAA analyses were performed at Schonland Centre using a procedure modified from Erasmus et al. (1977). This is shown in Figure 5.1. INAA was carried out using the detectors and electronics described in Appendix 2.

5.3. Analysis For The PGE And Au In Wits-1.

5.3.1. NiS Fire-Assay And NAA.

To date, sixteen 50 gram aliquots of Wits-1 have been analysed successfully by NiS-NAA at Schonland Centre. An initial study which employed steambaths in the dissolution of the NiS button produced very dirty filter papers, which on irradiation produced a high background from which only Ir and Au could be resolved. There is considerable uncertainty associated with these partial analyses and it was decided not to include them in the subsequent discussion.

As previously outlined in section 4.6.3.1, the use of hotplates improved the analytical procedure and the data quality dramatically. The results of the 16 PGE determinations using the improved analysis procedure are shown in Table 5.4.

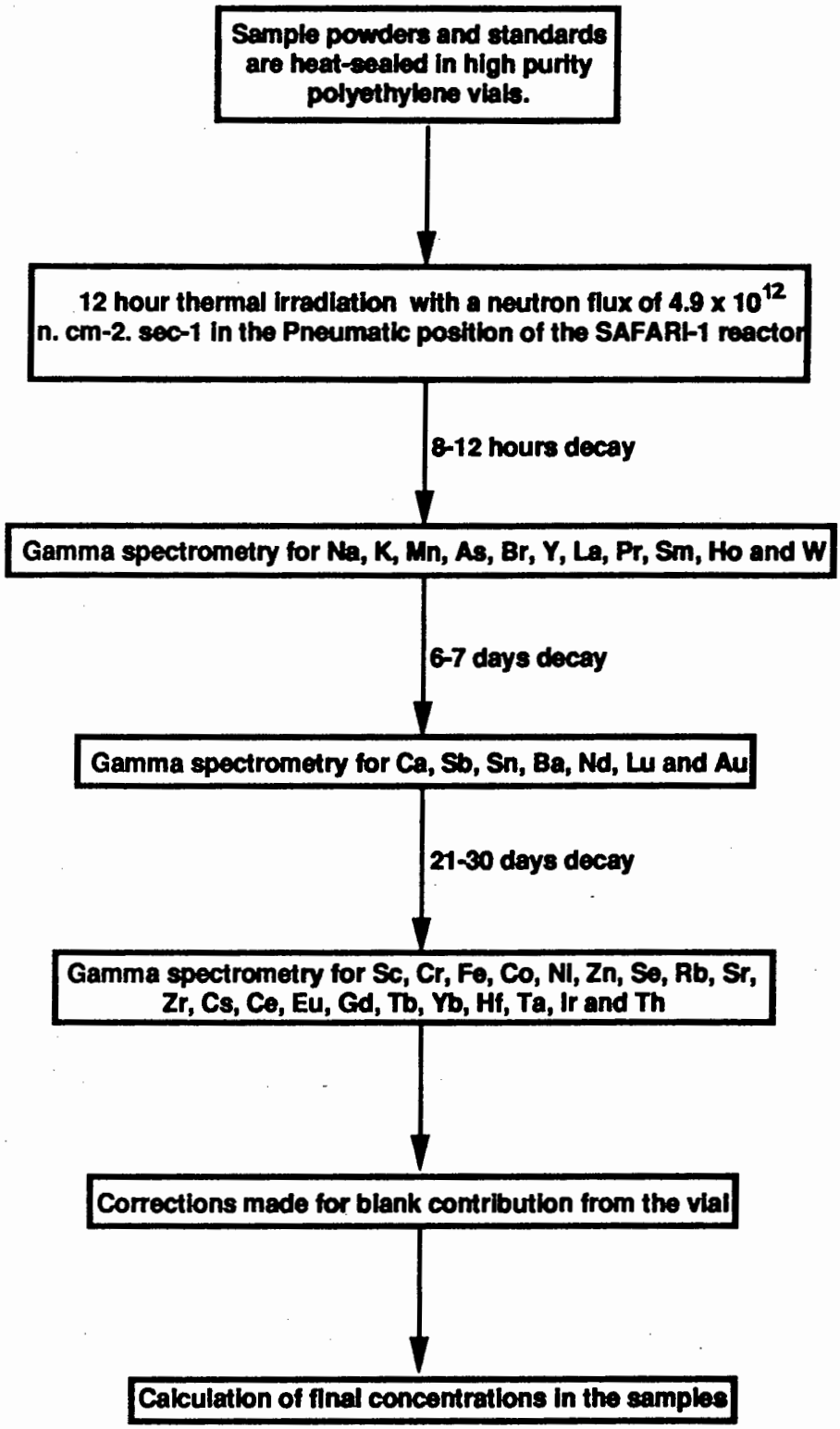

Figure 5.1 : Flow chart of the INAA procedure, modified from Erasmus et al. (1977).

Table 5.4: Summary of PGE and Au concentrations in Wits-1 as determined at Schonland Centre using NiS-NAA. "n.d." indicates that the element was not detected, "n d a" indicates no data available at present. All concentrations in parts per billion. Relative standard deviations for SARM-7 from Jackson et al. (1990) and coefficients of variation for 1:10 SARM-7 from Tredoux (1990).

	Concentration Present						
	Os	Ir	Ru	Rh	Pt	Pd	Au
Wits-1-1	n.d.	1.4	5.3	n d a	14.6	8.6	6.0
Wits-1-2	1.2	1.6	5.5	n d a	12.5	10.0	8.4
Wits-1-3	1.3	1.4	n.d.	n d a	19.4	10.1	5.2
Wits-1-4	1.7	2.0	6.3	n d a	20.8	8.4	3.4
Wits-1-5	1.2	1.8	5.3	n d a	21.1	10.0	4.0
Wits-1-6	1.6	1.6	6.0	1.3	10.5	8.4	6.8
Wits-1-7	1.5	1.4	5.2	1.1	17.7	8.9	5.3
Wits-1-8	1.3	1.3	4.9	1.2	14.2	8.5	2.0
Wits-1-9	1.3	1.2	4.0	1.2	11.7	5.9	3.8
Wits-1-10	1.3	1.5	6.3	n d a	10.5	8.0	5.4
Wits-1-11	1.7	1.5	5.6	n d a	9.9	7.1	5.7
Wits-1-12	1.5	1.4	6.0	1.4	12.1	8.7	4.9
Wits-1-13	1.4	1.3	5.9	1.2	9.0	6.9	7.0
Wits-1-14	1.4	1.5	5.3	n d a	11.8	7.4	4.7
Wits-1-15	1.6	1.4	5.2	1.3	12.9	8.0	4.1
Wits-1-16	1.5	1.6	5.6	1.4	14.1	8.1	2.2
MEAN (x)	**1.44**	**1.55**	**5.51**	**1.26**	**13.9**	**8.3**	**4.9**
Std.Deviation (σ)	**0.19**	**0.18**	**0.62**	**0.11**	**3.8**	**1.2**	**1.7**
Wits-1 C. O. V.*	**13.2%**	**12.0%**	**11.2%**	**8.7%**	**27.3%**	**14.3%**	**34.7%**
SARM-7 mean#	**63**	**74**	**430**	**240**	**3740**	**1530**	**310**
SARM-7 R.S.D.†	**18.0%**	**10.0%**	**14.0%**	**8.6%**	**13.5%**	**10.5%**	**19.8%**
1:10 SARM-7 C.O.V.*	**25.4%**	**13.2%**	**10.0%**	**n d a**	**18.4%**	**8.2%**	**46.0%**

* coefficient of variation, † relative standard deviation = $(\frac{\sigma}{x}).100\%$

preferred values from Steele et al. (1975)

As Table 5.4. shows, with the exception of Pt and Au, the coefficients of variation (COVs) between the results are <15 %, which compares very well with previously published COV's and relative standard deviations (RSDs) obtained from multiple analyses of SARM-7 and 1:10 dilutions of SARM-7 with silica. Although Wits-1 has

variation. Dilution of SARM-7 with silica, even taking care to ensure a vigorous mixing of the sample, would at best only preserve but most likely worsen, any initial inhomogeneity.

In SARM-7, Au is hosted as the native metal and as electrum, while the PGE are present as a combination of sulphides, tellurides, arsenides and alloy phases (Kinloch 1982). The silicate phases of SARM-7 contain only very low concentrations of the noble metals (Kinloch 1982; Lindsay 1989). A similar collection of host phases for the noble metals in Wits-1 appears unlikely due to the rapid quenching of the rock the absence of sulphide mineralization. The noble metals in Wits-1 are most probably hosted in the quenched silicate phases, either in solid solution (Ross and Keays 1979) or as physically entrained, sub-microscopic, alloy particles or clusters (Crocket and MacRae 1986; Lindsay 1989; Mathez and Peach 1989; Tredoux et al. 1991). The distribution of the PGE on a macroscopic scale in Wits-1 might therefore be more homogeneous than the micron to millimeter sized, PGE-rich, base metal sulphides and platinum-group minerals, and gold grains in the silicate matrix of SARM-7.

If this is the case, it implies that Wits-1 may be a much more useful noble metal standard than SARM-7 for analytical techniques such as INAA or RNAA, which employ small masses of sample material. However, some explanation must also be found for the apparent variation in the Pt and Au data. This is discussed in a later section.

5.3.2. NiS Fire-Assay And ICP-MS.

In order to check the data which was obtained by NiS-NAA at Schonland Centre, Wits-1 has also been analysed by two laboratories utilizing NiS fire-assay followed by ICP-MS. Two composite samples of 200g and 300g respectively were analysed by Johannesburg Consolidated Investment Company's Mineral Processing Research Laboratory (MPRL) at Knights, just outside Johannesburg and two 25g replicates of Wits-1 were analysed by Genalysis Laboratory Services in Western Australia. The MPRL procedure employed a hot dissolution of the filtered noble metal residue. This produces losses of Os by oxidation to OsO_4 and no Os data was reported. The Genalysis procedure utilized a cold dissolution which, in theory, retains the Os and Os data was reported. The results of these analyses are shown in Table 5.6.

mixing of the sample, would at best only preserve but most likely worsen, any initial inhomogeneity.

In SARM-7, Au is hosted as the native metal and as electrum, while the PGE are present as a combination of sulphides, tellurides, arsenides and alloy phases (Kinloch 1982). The silicate phases of SARM-7 contain only very low concentrations of the noble metals (Kinloch 1982; Lindsay 1989). A similar collection of host phases for the noble metals in Wits-1 appears unlikely due to the rapid quenching of the rock the absence of sulphide mineralization. The noble metals in Wits-1 are most probably hosted in the quenched silicate phases, either in solid solution (Ross and Keays 1979) or as physically entrained, sub-microscopic, alloy particles or clusters (Crocket and MacRae 1986; Lindsay 1989; Mathez and Peach 1989; Tredoux et al. 1991). The distribution of the PGE on a macroscopic scale in Wits-1 might therefore be more homogeneous than the micron to millimeter sized, PGE-rich, base metal sulphides and platinum-group minerals, and gold grains in the silicate matrix of SARM-7.

If this is the case, it implies that Wits-1 may be a much more useful noble metal standard than SARM-7 for analytical techniques such as INAA or RNAA, which employ small masses of sample material. However, some explanation must also be found for the apparent variation in the Pt and Au data. This is discussed in a later section.

5.3.2. NiS Fire-Assay And ICP-MS.

In order to check the data which was obtained by NiS-NAA at Schonland Centre, Wits-1 has also been analysed by two laboratories utilizing NiS fire-assay followed by ICP-MS. Two composite samples of 200g and 300g respectively were analysed by Johannesburg Consolidated Investment Company's Mineral Processing Research Laboratory (MPRL) at Knights, just outside Johannesburg and two 25g replicates of Wits-1 were analysed by Genalysis Laboratory Services in Western Australia. The MPRL procedure employed a hot dissolution of the filtered noble metal residue. This produces losses of Os by oxidation to OsO_4 and no Os data was reported. The Genalysis procedure utilized a cold dissolution which, in theory, retains the Os and Os data was reported. The results of these analyses are shown in Table 5.6.

Table 5.6.: Summary of ICP-MS data for Wits-1. All concentrations and abbreviations are as expressed in Table 5.4.. A comparison with Schonland Centre NiS-NAA data based on the analysis of 16 aliquots is also shown.

	Concentration Present						
	Os	Ir	Ru	Rh	Pt	Pd	Au
MPRL-Wits-1-1	n d a	6.0	19	28	36	26	58
MPRL-Wits-1-2	n d a	1.8	3.5	5.5	10.6	7.4	0.22
Genalysis-1	1.0	1.5	5	1.5	7	5	8
Genalysis-2	1.0	1.5	5	1.0	6	5	6
Schonland mean	1.44	1.55	5.5	1.26	13.9	8.3	4.9

5.3.3. Comparison Between NAA And ICP-MS Data.

The first analysis carried out at MPRL showed values for all of the noble metals which were well above any which had been obtained by NAA. The ICP-MS at MPRL is used routinely for a variety of PGE samples which range from bullion, to ore grade materials to unmineralized rocks and it was suggested that the very high values obtained in the first analysis could reflect either contamination or instrumental memory effects from much higher grade material. The second analysis which was carried out 4 months later, along with a group of very low-grade samples (F. Cruikshank pers.comm. 1992), shows a much better agreement with the NAA data. Only Rh and Au appear to show serious discrepancies.

The data from Genalysis Laboratory Services shows an excellent agreement with the Schonland Centre mean for Os, Ir, Ru, and Rh and a good correspondence with the MPRL data for Ir and Ru. Pt appears to be consistently higher by NAA than by ICP-MS while the Pd value of 5ppb obtained by Genalysis is slightly lower than the MPRL and Schonland values.

After conventional INAA analysis for non precious metal trace elements in Wits-1 had been carried out (see section 5.2), the sample was allowed to decay for 140 days to decrease activity from abundant radionuclides such as ^{51}Cr ($T_{1/2}$ = 51 days), ^{59}Fe ($T_{1/2}$ = 45 days) and $^{58}Co(Ni)$ ($T_{1/2}$ = 71 days). The Wits-1 aliquots were then recounted. The spectra recorded from each of the 5 aliquots showed a strong peak at 159 keV from Te as the long lived isotope ^{123m}Te ($T_{1/2}$ = 117 days). As noted in section 4.6.2.3., Te in the fire-assay reagents or in the sample may be deposited on

the final filter paper, producing ^{123m}Te after irradiation, which may cause a slight interference on the 158 keV peak of ^{199}Au. It therefore seems possible that some of the NAA results where very high concentrations of Pt (>15ppb) were reported, may in fact show a contribution from Te in Wits-1.

It is interesting to note that these high Pt values occur primarily in aliquots Wits-1-1 to Wits-1-7 which were analysed before the true nature of the Te interference on Pt became apparent and that in later aliquots, where more care was taken over the dissolution, a more consistent range of values between 9 and 14ppb was obtained. This would imply that the Schonland mean value for Pt in Wits-1, as calculated from all 16 aliquots, is probably slightly too high.

If one considers only the data from aliquots Wit-1-8 to Wits-1-16, the mean value for Pt becomes 11.8ppb with a COV of 15.2%. This gives an improved agreement with the Pt values derived by ICP-MS as well as with the COVs from the other PGE derived by NiS-NAA. If, as I believe, the analysis of these nine aliquots offers a closer approximation to the real Pt value in Wits-1, the results also suggest that in terms of sample homogeneity, Pt in Wits-1 is only slightly less homogenous than the other PGE.

The high COV shown by Au in the Schonland dataset is also reflected in the data obtained by ICP-MS. The MPRL and Genalysis data are more extreme than any of the values in the Schonland dataset and at present, the Schonland mean probably offers the best representation of the true concentration. It would appear that Au in Wits-1 is very heterogeneously distributed and the large observed variation is an inherent feature of the sample. The komatiites around the Komatii river, and throughout the Barberton region, have suffered greenschist facies metamorphism which locally concentrated Au in mineralized shear zones (de Wit et al. 1987). The apparently inhomogeneous distribution of Au in Wits-1 may be related to this metamorphism.

5.4.: Conclusions.

Repeated analyses of Wits-1 have vindicated many of the modifications made to the NiS-NAA procedure (especially the dissolution step) outlined in Chapter 4, and have shown that the improved procedure can be used to obtain high quality, reproducible data for all of the PGE and Au from a sample with relatively low

concentrations of the metals. Moderate to good agreement between the NiS-NAA data and analyses performed by ICP-MS has been shown for Os, Ir, Ru, Rh and Pd.

The presence of apparently significant amounts of Te in Wits-1 may cause some interference with the Pt determination if considerable care is not taken during the analysis. As a result of this, Pt concentrations determined by NiS-NAA may be slightly higher than the results obtained by ICP-MS. Au appears to be very heterogeneously distributed in Wits-1. Even with very large samples, there was very little agreement on the Au concentration between NiS-NAA and ICP-MS and also between the two ICP-MS procedures. The NiS-NAA data for Au lies between the values obtained by ICP-MS and at present appears to offer the closest estimate to the real Au concentration. The heterogeneous distribution of Au in Wits-1 is tentatively ascribed to greenschist facies metamorphism.

Based on the data discussed in this chapter, I would consider the present "best estimate" values for the noble metals in Wits-1 to be as follows:

Os	1.4 ppb
Ir	1.5 ppb
Ru	5.0 ppb
Rh	1.25 ppb
Pt	10 ppb
Pd	7.5 ppb
Au	4.9 ppb

Wits-1 is presently being analysed by a number of other laboratories using RNAA, NiS-NAA and ICP-MS techniques and a complete certification for all of the PGE and Au will hopefully be completed soon.

Wits-1 now serves as a very useful low-level internal noble metal standard in the Schonland Centre laboratory. More recently it has also been successfully included as an additional standard for Ru, Rh and Pd in order to more accurately fix the low concentration end of calibration curves.

In view of the consistency of the data so far, I would not expect the values for Os, Ir, Ru and Rh to be greatly altered with more data. More accurate Pt, Pd and Au data can probably be expected. A chondrite normalized plot of the "best estimate" Wits-1

data is shown in Figure 5.2. A comparison with data from other komatiites analysed by Crocket and MacRae (1986) and Brügmann et al. (1987) is also shown. This serves as an qualitative external check on the Wits-1 data. As Figure 5.2 indicates, the pattern obtained from Wits-1 does not appear to be greatly different from the other komatiites

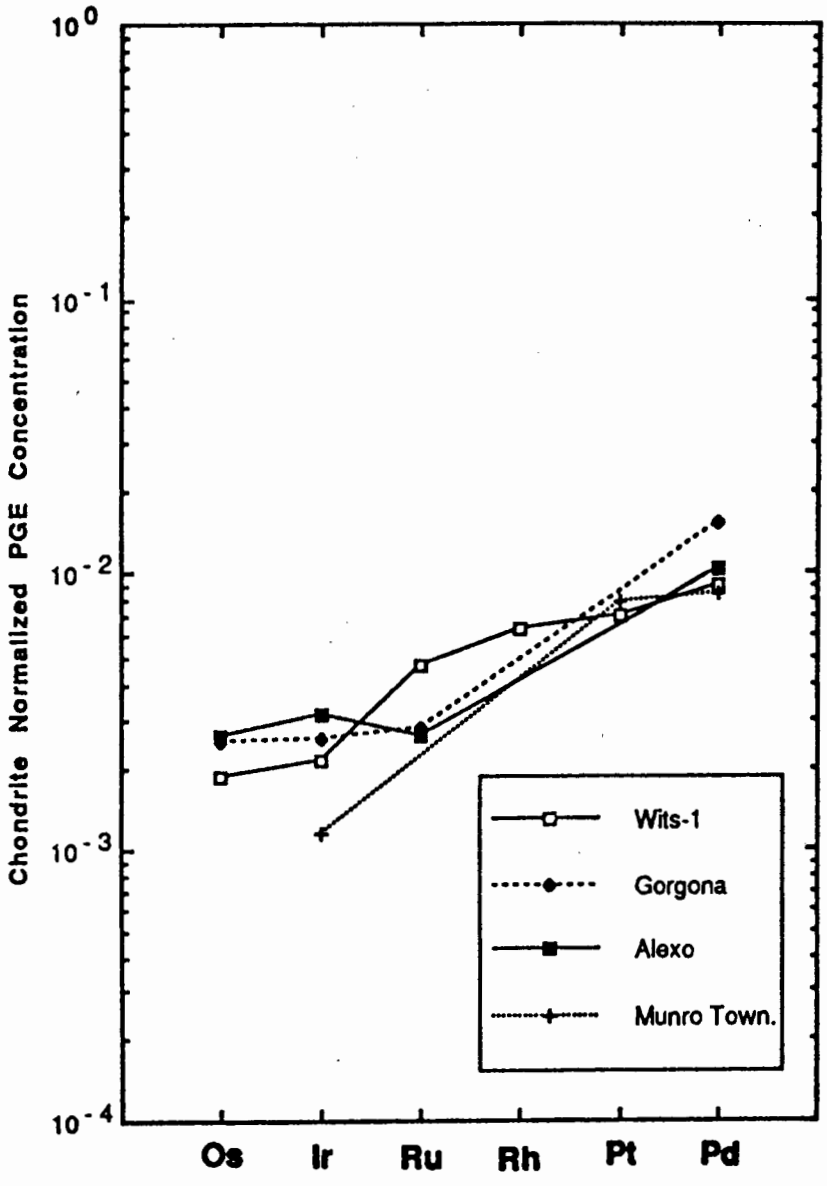

Figure 5.2.: Chondrite normalized PGE patterns for Wits-1 and other komatiites. Munro Township Flow data from Crocket and MacRae (1986) and Gorgona and Alexo Flow from Brügmann et al. (1987). Chondrite normalization values from Tredoux et al. (1989) as follows: Os 761ppb; Ir 710 ppb; Ru 1071ppb; Rh 201 ppb; Pt 1430 ppb; Pd 836 ppb; Au 218 ppb.

Chapter 6

The Volatile Transport Of The PGE In Fire-Assay Melts In The Presence Of A Carbonaceous Volatile Phase.

6.1. Introduction.

One of the most enigmatic geological environments from which the PGE have been recorded is the volatile aerosols emitted by some tholeiitic and alkali basaltic volcanos (Zoller et al. 1983; Finnegan et al. 1984; Koeberl 1989; Meeker et al. 1992). INAA of filters which trap the escaping aerosol gases indicate that noble metals like Au and Ir are enriched in the aerosols compared to the magma by factors in excess of 1000 (Olmez et al. 1986). Zoller et al. (1983) were the first to observe this phenomenon when they analysed the aerosols emitted during the 1982 eruption of Kilauea volcano on Hawaii.

Meeker et al. (1992) described particles of gold from Mount Erebus in Antarctica which had apparently quenched in the cooling gas plume and settled out under density within a few km of the vent. The Au particles had a characteristic quench morphology in which clusters of parallel growths terminated in reniform masses of octahedral crystals. Although Meeker et al. (1992) found that most of the Au appeared to be deposited within a few km of the active vent, analyses of Antarctic ice layers containing volcanic dust carried out by Koeberl (1989) revealed high concentrations of Ir and Au. This observation indicates that Ir and Au in the volcanic fallout from eruptions in the recent past could also have been carried much greater distances (up to 1500 km) from the inferred source volcano before the metals were deposited.

At present very little is known about the physicochemical nature of the PGE and Au in volcanic aerosols. Zoller et al. (1983) suggested that the Ir concentration of the Kilauea aerosols was related to the fluorine content of the gas and that the highly volatile compound IrF_6 might act as a transporting agent for the Ir. As discussed in section 2.3.3, IrF_6 and all of the PGE hexafluorides are highly reactive compounds which are very unstable in the presence of water and silica, breaking back down to HF and a mixture of oxide and metal species. Thermodynamic

calculations performed by Wood (1987) indicated that IrF_6 was not appreciably volatile in the presence of even a small amount of water due to the stability of the HF molecule. Wood (1987) concluded that it was unlikely that IrF_6 could be responsible for any appreciable Ir volatility in the Kilauea magma.

Schiffries (1982), Ballhaus and Stumpfl (1986) and Stumpfl and Ballhaus (1986) have suggested that pegmatoidal PGE mineralization in layered mafic complexes (LMC) can be explained via the transport of the PGE into the mineralized zones as chloride complexes in hydrothermal solutions. In view of this, Wood (1987) also investigated the potential volatility of a number of PGE chlorides under the conditions expected in magma chambers but reached the conclusion that significant PGE transport could only take place under extremely oxidising conditions and high partial pressures of chlorine.

Wood (1987) also noted that under the conditions where the PGE are sufficiently volatile as chloride complexes to account for transport in the vapour phase in amounts >1ppt, the base metals Fe,Ni, and Cu are many orders of magnitude more volatile. Therefore transport via chloride species alone would encounter difficulties in explaining the greater enrichments of the noble metals, compared to the base metals, in some PGE-rich zones of the LMC (eg the Picket Pin deposit; Mathez et al. 1986) and in the aerosols (Olmez et al. 1986). Whether the oxidising conditions and high Cl fugacities required by Wood's calculations are actually present in the magma chambers which formed the LMC or within the active vents which release Ir and Au, is a matter of continuing debate.

As outlined in section 2.5.2, the carbonyls of the PGE are extremely volatile compounds and Wood (1987) indicated that they could also be considered as a potential transporting species. Although not addressing the PGE in their study, Kerrich and Fyfe (1981) postulated that Au carbonyls might have acted as a transporting agent for Au in some graphite-bearing hydrothermal Au veins. McDonald et al. (1991a) carried out a preliminary study which indicated that losses of both the PGE and Au had occurred in NiS fire-assay melts to which carbon had been added and suggested that the generation of CO and noble metal carbonyls could explain this. Futhermore, they suggested that if these observations could be reliably extrapolated to the scale of a magma chamber, magmas containing reduced carbon (either from the mantle or derived from

crustal contamination) might show a similar transfer of the noble metals to the volatile phase.

A more detailed study of the role of carbon in NiS fire-assay melts, which involved more analyses and a close examination of the solid phases remaining after the fire-assay, was carried out by McDonald et al. (1991b) and is contained in Appendix 5. These authors speculated that a mechanism involving the transport of the PGE as carbonyls might explain the very curious Pt mineralization seen in transgressive metasomatic pipes in the eastern Bushveld Complex. An apparent association between Pt and graphite was commented on by Stumpfl and Rucklidge (1982) who were the first to suggest that the PGE may have been transported into the pipes as an organometallic complex.

In the light of the above, it was decided to expand the experiments carried out by McDonald (1991b) in order to examine how any losses of PGE from the fire-assay melt varied with different concentrations of carbon. From this information it would be possible to make an assessment of any variations in behaviour between the PGE under similar reaction conditions. This could indicate whether the pattern of PGE behaviour matched that expected from organometallic carbonyl chemistry ie. the metals showed behaviour compatible with their electronic configuration (Ru-Os, Rh-Ir and Pd-Pt; see section 2.2 and Table 2.5) or was completely different from it. These experiments are detailed in sections 6.2 to 6.4.

In addition, although carbonyls were proposed as the species responsible for the transport of the PGE, McDonald et al. (1991b) did not present any definite proof of this. Two sets of experiments to clarify the nature of any transporting species were also carried out and these are described in sections 6.5 and 6.6. A reaction model based on all of the experimental observations is presented in section 6.7. The application of this model to real igneous melts is discussed in chapter 7.

6.2. Outline Of Fire-Assay Experiments.

All of the experiments involved the reaction between a PGE-bearing silicate melt and carbon which had been added into the initial fusion charge. Unless noted otherwise, the components of the fire-assay charge were those outlined in Table 3 of Appendix 4. The source of carbon was Johnson Matthey 250 mesh Specpure graphite powder. McDonald et al. (1991b) added a fixed mass of 200mg of carbon

to the fire-assay charge. In this study, a range of carbon masses from 100mg to 600mg was investigated.

A fundamental assumption that the known differences between fire-assay melts and real igneous melts (much higher concentrations of Na, B and CO_2 in the fire-assay system) do not significantly affect the PGE reactions taking place within the system. The PGE do not form compounds with Na, B or CO_2 (Cotton and Wilkinson 1980; Hartley 1991) and do not show strong chemical compatibility with silicate minerals (Mathez and Peach 1989; Tredoux 1990) therefore I believe this to be a reasonable assumption.

Lindsay (1989) proposed a model indicating that the physical form of the PGE in silicate melts may be considered as submicroscopic clusters of <100 atoms (like micro-crystals) physically suspended within but chemically separate from the silicate liquid. Fractionation of the PGE into spinels or sulphide was viewed as a process of physical rather than chemical collection (Lindsay 1989). If this model is correct, and the clusters of PGE suffer only a physical interaction with the melt, then whether the melt is a natural silicate or an artificial borosilicate should not affect the clusters themselves and the assumption oultined above should hold true.

6.2.1. The Use Of Different Sample Matrices.

The range of noble metal concentrations in the sample material has to be considered carefully. A sample mixture of SARM-7 diluted 10 times with silica was used by McDonald et al. (1991b) for their experiments primarily because this mixture is also used as a routine calibration standard (see section 5.1) and it allowed a very easy comparison between carbon-spiked and carbon-free melts which initially contained the same amount of PGE. Using undiluted SARM-7 would probably allow a clearer discrimination of real losses from analytical uncertainty but would offer a very poor comparison with natural igneous melts which typically contain low PGE concentrations. In contrast, using a standard with low levels of PGE such as W-1, PCC-1 or Wits-1 would offer a closer comparison in terms of PGE concentrations with real melts but any losses would be much more difficult to resolve from the typical uncertainty on the determination of these low concentrations (see Table 5.5). The decision to use a 1:10 dilution of SARM-7 was therefore a compromise between using a sample composition which reflected the range of PGE concentrations in typical melts

(generally <10ppb) and using a sample with PGE concentrations high enough to enable a real discrimination between PGE losses caused by genuine reactions in the melt and analytical errors.

Diluting SARM-7 with pure silica powder produces a sample matrix with ~95% SiO_2, which is more siliceous than any normal igneous rock and it is therefore a very artificial composition. In order to obtain sample compositions more similar to real rocks, two other dilutants were used in addition to silica. The first dilutant used was Wits-1. The PGE concentrations of this material have been reasonably well established (see section 5.4.) and although there remains some doubt over the Au concentration it was felt that the noble metal concentrations resulting from such a mixture would be reasonably well constrained. The major element composition of this sample material is essentially "komatiitic".

SARM-7 was also diluted with an anorthosite sample called WP-4. This rock is a mottled anorthosite collected by the author from the Footwall #4 layer of the Western Platinum Mine, situated in the southwestern region of the Bushveld Complex. Viljoen and Scoone (1985) suggested that the anorthosites of the upper Critical Zone of the the Bushveld Complex host a large amount of trapped intercumulus liquid. If, as speculated by McDonald et al. (1991b), the PGE and Au might be concentrated in the intercumulus melt prior to their removal in a volatile phase, it was considered important to examine the behaviour of the metals with added carbon using this sample matrix. Six aliquots of sample were analysed by NiS-NAA and the PGE and Au concentrations are shown in Table 6.1.

Table 6.1.: Summary of PGE and Au data (in ppb) for anorthosite WP-4.

	Concentration Present						
	Os	**Ir**	**Ru**	**Rh**	**Pt**	**Pd**	**Au**
WP-4-1	0.50	0.61	0.91	0.36	4.3	3.9	0.52
WP-4-2	0.46	0.70	0.99	0.38	5.6	4.4	0.73
WP-4-3	0.59	0.72	1.1	n d a	4.7	4.0	0.68
WP-4-4	0.68	0.69	1.1	n d a	6.1	4.4	0.60
WP-4-5	0.49	0.66	0.95	n d a	6.0	3.8	0.69
WP-4-6	0.41	0.64	0.86	n d a	5.4	4.1	0.50
WP-4 Mean	0.52	0.67	0.98	0.37	5.4	4.1	0.62

6.2.2. The Presence Of Sulphide.

It was considered significant that the experimental data obtained by McDonald et al. (1991b; see Appendix 5) indicated that between 8 and 28% of the initial amount of noble metals could be lost from melts which also contained an immiscible sulphide phase. Distribution coefficients for the PGE and Au between sulphide and silicate melts ($D_{sulphide/silicate}$) are defined as:

$$D_{sulphide/silicate} = \frac{\text{concentration of PGE in sulphide}}{\text{concentration of PGE in silicate}} \qquad \text{...equation (6.1)}$$

Those calculated for natural systems are believed to be high, $>10^5$ (Campbell et al. 1983; Campbell and Barnes 1984; Mathez and Peach 1989). The tracer experiments detailed in Appendix 4 (data shown in Appendix 4, Table 2) which were carried out to test the efficiency of the extraction of the PGE and Au into the sulphide phase indicate that in the fire-assay melt, $D_{sulphide/silicate}$ for the PGE varies between 33 and 47. Extraction of Au into the sulphide is less efficient than for the PGE, with D values ranging between 15 and 21. These D values are significantly lower than the apparent values in natural melts and may reflect lack of equilibration in the system brought on by the relatively rapid quenching of fire-assay melt. The implications of this difference between natural and fire-assay melts will be discussed in section 6.7.

The losses of significant amounts of PGE and Au from fire-assay melts containing carbon and an immiscible NiS phase implies that whatever process removes the PGE and Au from the melt is competitive with the sulphide partitioning and therefore the $D_{vapour/silicate}$ must be relatively close to the fire-assay $D_{sulphide/silicate}$. In order to examine this hypothesis further, a series of parallel experiments was carried out using melts with accompanying sulphide and melts without a sulphide phase. Due to a restricted amount of WP-4, the "anorthositic" sample matrix was only used in one set of experiments, those in which carbon was allowed to react in the melt without the presence of immiscible sulphide.

6.2.2.1. Experimental Procedure For Sulphide-Bearing Melts.

Fire-assay charges containing sulphide were prepared as described in section 4.4.2 and Appendix 4 (Table 3). Carbon was added to the charge and mixed with the other components prior to firing. In some experiments, a considerable amount of carbon remained unreacted and was found to adhere to the sulphide (see section 6.3.2). The carbon was removed from the sulphide using distilled water and an

ultrasonic bath. The carbon suspended in the distilled water was then filtered onto a cellulose nitrate filter paper, sealed in a plastic vial and irradiated. The NiS button was dissolved in HCl and the residue was filtered, irradiated and counted as normal.

The slag remaining after the first fire-assay was carefully chipped out of the crucible onto glazed paper. The slag fragments were crushed to ~100 mesh in an agate swing mill and then subjected to a second NiS fire-assay under normal analytical conditions. The second NiS button was dissolved, filtered, irradiated and counted as normal. The concentrations of PGE in the first NiS button, the second NiS button and the carbon fraction were combined to yield the total amount of PGE remaining in the solidified phases after the initial reaction with carbon.

6.2.2.3. Experimental Procedure For Sulphide-Free Melts.

In experiments without sulphide, fire-assay took place as outlined in section 4.4.2, but no sulphur and $NiCO_3$ were added to the charge. Carbon was added and mixed with the sample material before firing. After the melt had cooled, the crucibles were cracked open and the chilled green or black slags were carefully chipped out with a hammer onto large sheets of glazed paper. The inside walls of the crucible were thoroughly scraped to remove the fragments of slag from the walls and if fragments of slag could not be detached from the crucible, those portions of the crucible wall were also included in the sample.

The slag and crucible fragments were then crushed to ~100 mesh in an agate swing mill. The entire contents of the crushing was then remelted along with the normal analytical masses of sulphur and $NiCO_3$. The sulphide button produced by this second firing was dissolved, filtered and analysed. The results of this analysis were used to calculate the concentrations of PGE and Au remaining in the first slag after the initial firing and reaction with carbon.

6.2.3. Experimental Terminology.

During the course of the experiments, a shorthand was developed by the author to briefly describe each sample as it passed through the sample processing stage and through post-irradiation handling. This shorthand will be used in subsequent discussions and it is therefore important to describe it here. The following abbreviations were used to describe the sample matrices:

SA	SARM-7 diluted 10 times with pure silica
WA	SARM-7 diluted 10 times with Wits-1
WP4A	SARM-7 diluted 10 times with WP-4

The following abbreviations were used to describe experiments carried out with and without a sulphide melt:

(C/S)	Carbon reacts and degases in the melt with an accompanying sulphide phase
(D/C)	Carbon reacts and degases in the melt, no sulphide.
(D)	Melt allowed to degas with no carbon and no sulphide
(N)	Normal NiS fire-assay conditions, no added carbon.

These groups of abbreviations were combined in order to describe each of the experimental conditions. For example, "WA(D/C)" would refer to carbon reacting in a sulphide-free melt of SARM-7 diluted with Wits-1. Similarly, "SA(C/S)" would correspond to carbon reacting in a sulphide-rich melt of SARM-7 diluted with SiO_2.

6.3. Qualitative Experimental Observations.

6.3.1. Gas Activity.

The most obvious difference between the melts containing carbon and those which contained no carbon was a much more vigorous release of gas from the carbon-bearing melts. Throughout the fusion and during cooling, the carbon-bearing melts bubbled very strongly whereas the carbon-free melts bubbled only sporadically. This first order observation was found to hold for all of the three sample matrices investigated and for the experiments carried out with and without sulphide. The difference in the gas activity therefore appeared to be strongly linked to the presence or absence of carbon in the melt.

Both CO and CO_2 are very insoluble in silicate melts (Stolper and Holloway 1988; Mathez 1989) and production of one or both of these components as the melt reacts with carbon is the most likely cause of the bubbling in the carbon-spiked melts. The presence of CO_2 was clearly indicated by the precipitation of $CaCO_3$ from lime water held over the degassing melts. The evolved gases were also

drawn through a silica glass nozzle held a few mm above the surface of the melt, along a plastic tube and into an aqueous solution of $PdCl_2$ with the use of a pump. The precipitation of a small amount of Pd from solution which was observed when the Pd solution was filtered, indicated that some CO was also present in the gas phase (Greenwood and Earnshaw 1984).

After cooling, the crucibles were broken open and the patterns of gas bubbles trapped in the slag were examined. There appeared to be significant differences in the populations of gas bubbles between the SA(C/S) and SA(N) slags. This is described in detail in Appendix 5 and is shown schematically in Figure 6.1, with a brief summary below:

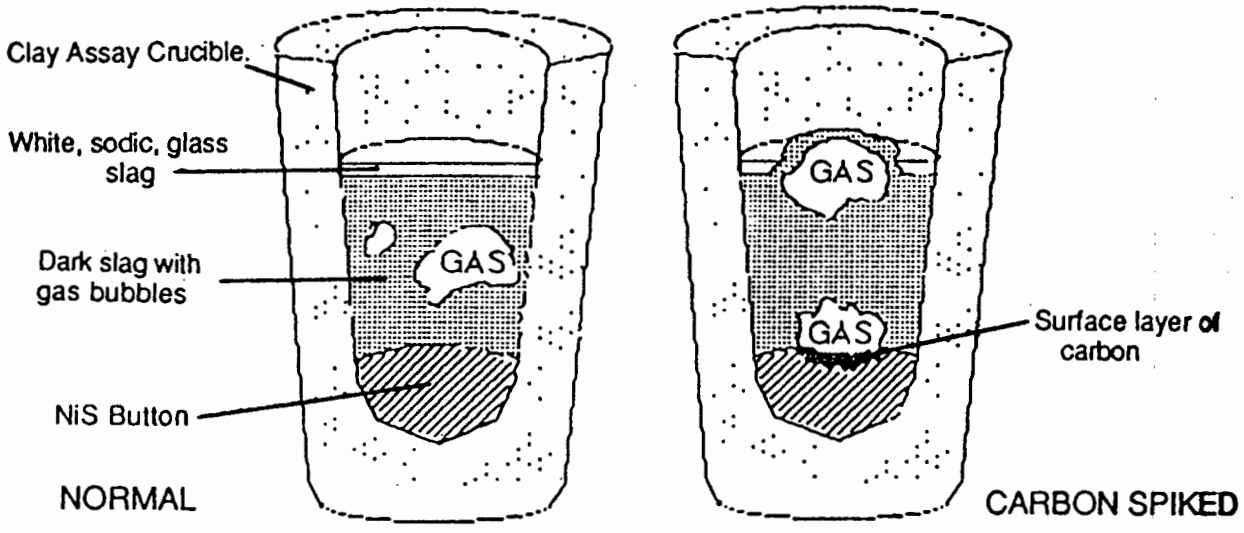

Figure 6.1.: Patterns of gas bubbles observed from carbon-spiked and carbon-free melts (from McDonald et al. 199b; Appendix 5).

In the slags produced from the SA(C/S) melts there appeared to be two separate phases of gas production and entrapment. The large gas bubble which was always present at the top of the slag appeared to be related to the degassing evident during the earliest phase of cooling. After removal from the furnace, the top surface of the melt undergoes a very turbulent phase where bubbles rise, burst and collapse. However, within 90-120 seconds, the top of the melt cools sufficiently to form a "semi-plastic" layer which does not burst, but rather arches

and domes upwards as gases are trapped and coalesce beneath it. This trapped gas almost certainly goes on to form the large gas bubble at the top of the slag.

SA(C/S) melts which had been spiked with between 200 and 300mg of carbon produced deformed (and sometimes fragmented) NiS buttons which, on removal, revealed traces of a number of gas bubbles trapped at the sulphide-slag interface. As will be described in more detail in section 6.3.2, carbon was also present at the interface between the trapped gas and the sulphide. In marked contrast, the WA(C/S) experiments produced large gas bubbles at the top of the slag but did not show any evidence for the presence of carbon, any damage to the sulphide button, or of gas bubbles at the sulphide-slag interface, no matter how much carbon was added to the initial mixture. This fundamental distinction between the SA(C/S) and WA(C/S) experiments is extremely important and is discussed in greater detail in section 6.7.

6.3.2. Carbon Deposition On And Fragmentation Of The SA(C/S) Buttons.

In addition to increasing the production of gas, the use of sequentially larger amounts of carbon in the SA(C/S) experiments caused progressively stronger and more intense fragmentation of the sulphide button. Masses of carbon less than 200mg, did not produce any visible damage to the button. There was an unbroken contact (and no evidence of any bubbles) between the sulphide and the slag. The addition of 200-300mg of carbon produced a broad depression on the top of the button and a bubble at the sulphide-slag interface. This depression (schematically shown in Figure 6.1.) was coated with a thin layer of very powdery, almost frothy, carbon.

The addition of masses of carbon greater than 300mg produces fragmented buttons with small gas bubbles above the sulphide fragments. This increasing fragmentation is shown diagrammatically in Figure 6.2. The fragmentation takes a relatively consistent form; namely one large mass of sulphide on the base of the crucible and a varying number of smaller sulphide fragments sitting above or around the large fragment. The mass of the large sulphide fragment decreases and the number of small fragments increases as more carbon is added to the initial mixture. The fragments from six SA(C/S) experiments were carefully collected and examined. The masses of the largest fragments, the number of smaller fragments and a comparison with normal SA(N) buttons are shown in Table 6.2.

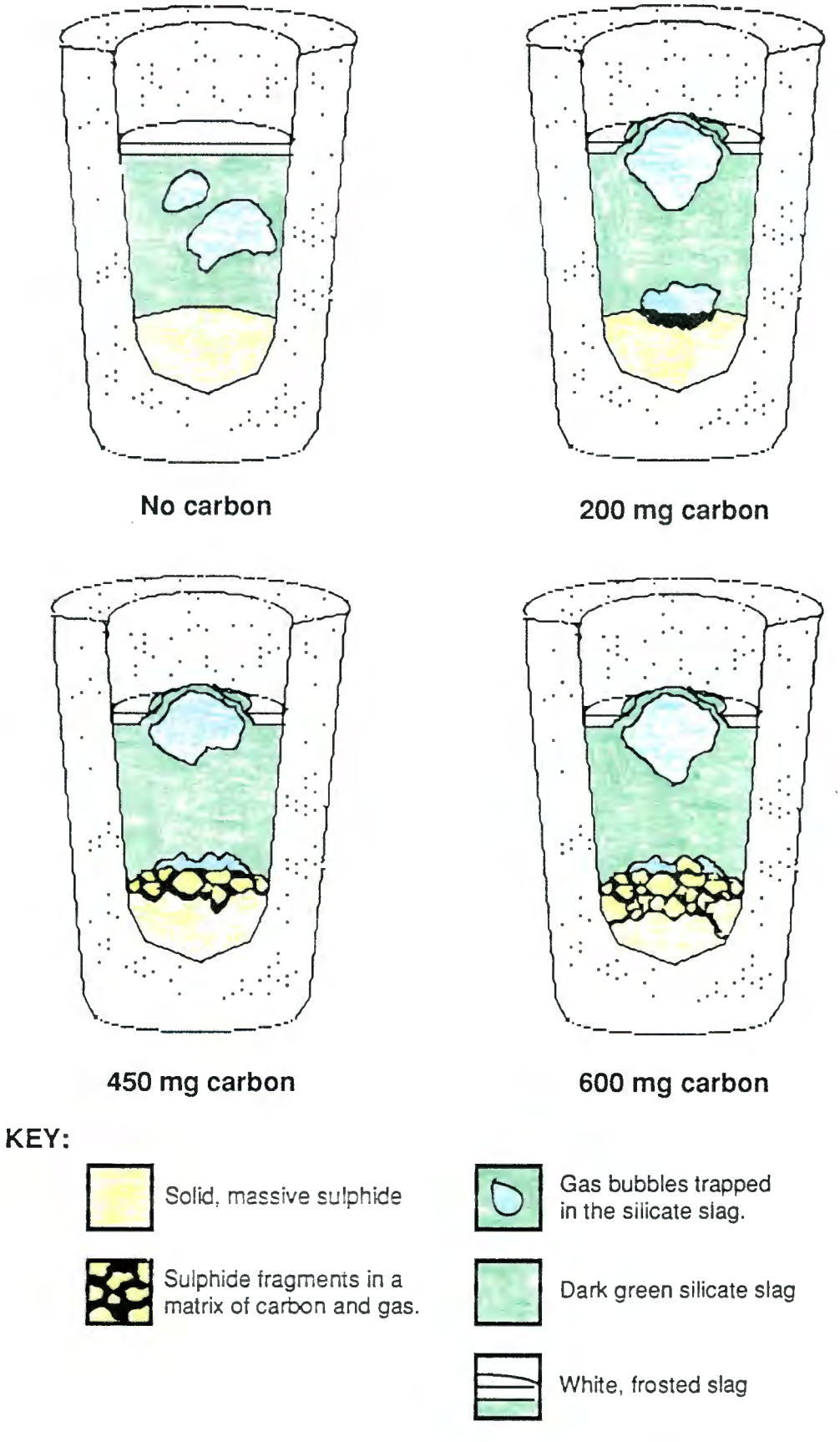

Figure 6.2 : Diagram showing the pattern of fragmentation observed in the NiS buttons from SA(C/S) melts with increasing masses of added carbon.

Table 6.2.: Masses of large sulphide fragments and number of secondary fragments as a measure of the degree of damage to the sulphide button caused by the addition of increasing masses of carbon.

Mass of carbon in melt	Mass of largest sulphide fragment	Number of small sulphide fragments
0 mg	24.29 g *	zero
300 mg	19.95 g	10
350 mg	16.82 g	39
400 mg	14.20 g	47
450 mg	12.01 g	74
500 mg	13.46 g	60
600 mg	12.39 g	77

* Average of 22 "normal" NiS button masses.

Both large and small fragments are covered with carbon on some or all of their faces. It is these carbon coatings or films which separate individual fragments. A reconstruction of the orientation of several sulphide fragments on top of a button produced from a melt containing 450mg of carbon is shown in Figure 6.3. There are visible gaps between the larger fragments which define the walls of carbon-filled channels. A jumbled mix of smaller, highly irregular sulphide fragments sits within the channels. The carbon between the sulphide fragments is very friable and crumbly and large gas pockets within the carbon are also occasionally evident. Therefore it would appear that a considerable amount of gas was also present in the carbon-filled channels between the large sulphide fragments.

Carbon was removed from the surfaces of the fragments using distilled water and an ultrasonic bath. Typically 10 minutes in the ultrasonic was sufficient to detach most of the carbon. After this cleaning, the fragments were closely examined. Most revealed faces which were comprised of very dark sandy brown sulphide. The dark colour could not be removed even after 60 minutes in the ultrasonic. It was considered highly likely that carbon, mixed with sulphide, was producing the dark colour. When the fragments were sliced open, polished and examined under a microscope, no carbon was observed within the bulk of the sulphide, but some very reflective films and spots were present on sulphide grain boundaries close to the fragment margins. This indicated that any carbon present in the sulphide fragments appeared to be primarily a surface or near-surface feature.

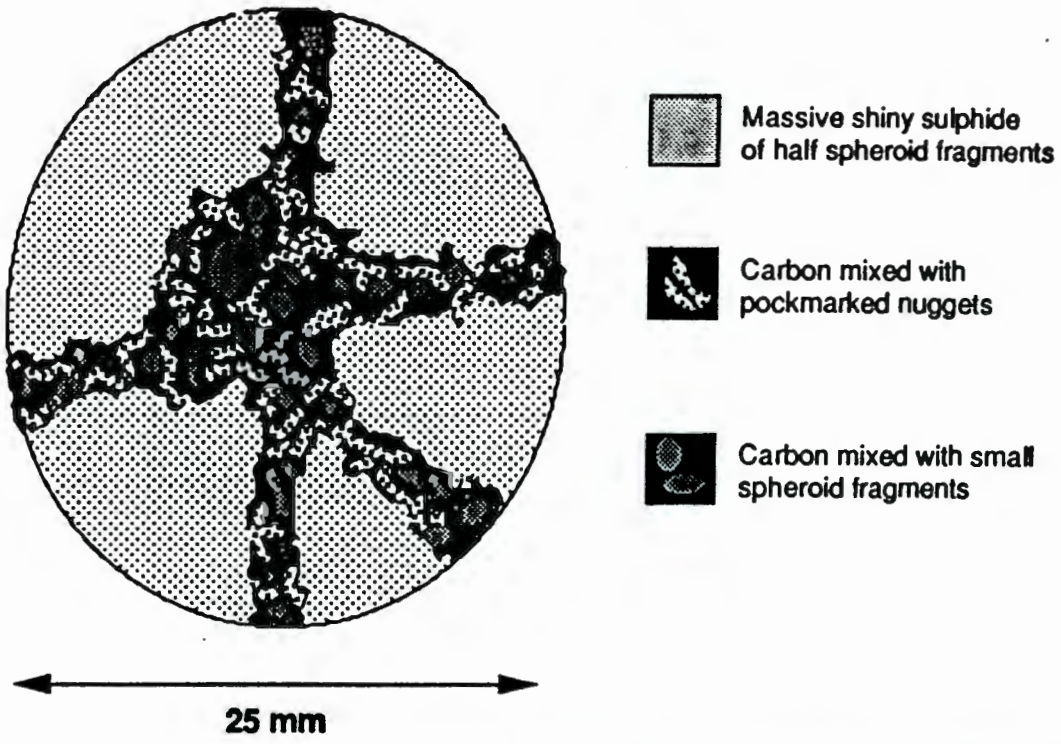

Figure 6.3.: Reconstruction of the SA(C/S) NiS button from a melt containing 450 mg of carbon. One half spheroid fragment above the centre of the button has been removed to show the distribution of carbon and fragments beneath.

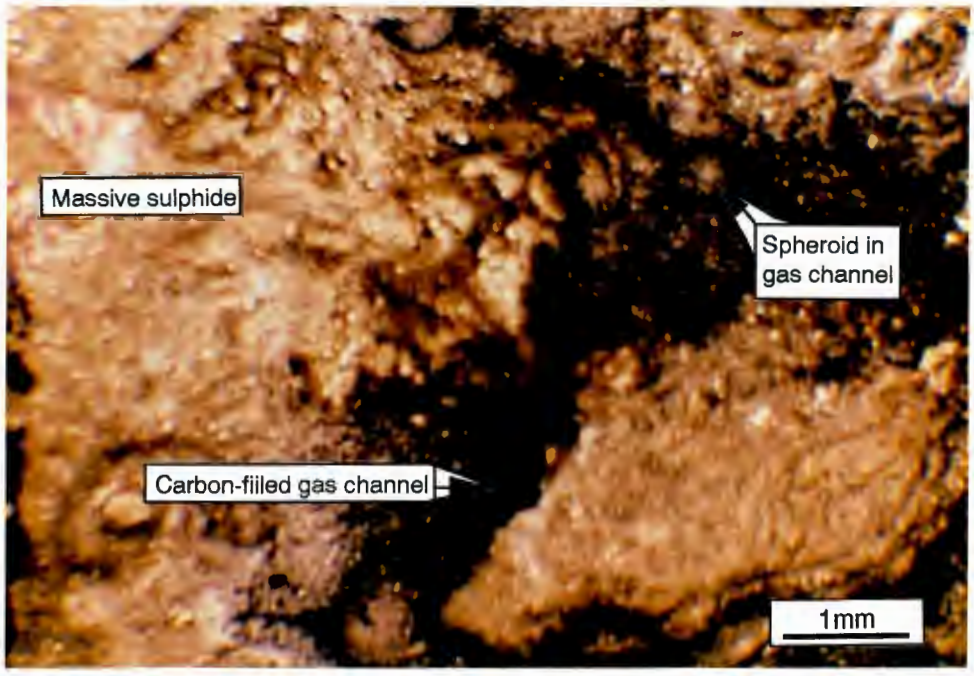

Figure 6.4 : Complex network of branching gas (?) channels (the dark lines) in a NiS button produced from a SA(C/S) melt contain ing 450 mg of carbon. Small sulphide spheroids are present in the channel junctions.

6.3.3. Gas (?) Channels Within The SA(C/S) Sulphide Buttons.

Carbon-filled channels and chimney structures were observed in many of the sulphide fragments produced from melts containing >350 mg of carbon. Individual channels are generally only a millimeter or slightly larger in diameter but are continuous on a millimeter scale and occasionally extend for more than a centimeter through the sulphide. The channels visibly branch and split into a large interconnected network which can sometimes extend across the width of the button. A network of connected channels is shown in Figure 6.4. Small spherical blobs of sulphide frequently occupy many of the major junctions of the network. A closer view of one of these spheroids is shown in Figure 6.5. The complexity of the channel network and the number of small spheroids present within it increases as the amount of carbon in the melt is increased.

Close to the surfaces of the button, the channels expand slightly to form chimney structures. The chimneys pierce the sulphide and are present on the surface as small circular depressions or craters with a central hole. A section through three chimneys close to one another is shown in Figure 6.6 and a closer view of an exposed chimney is shown in Figure 6.7. The chimney contains a highly irregular mixture of small spherical blobs of sulphide, similar to those found at the channel junctions, and material which is best described as very "frothy" sulphide. This is very dark sulphide which is very different in appearance to the solid sulphide on either side of the chimney, and is so intensely pockmarked and bubbled that it sometimes resembles a foam. Based on these observations it would appear that the chimneys were the sites for the (sometimes violent) release of gases from the button. The term *gas channel* will be used in subsequent discussions.

6.3.4. Pockmarks On The SA(C/S) Fragments.

The dark surfaces of many of the sulphide fragments are heavily pockmarked. The pockmarks are depressions of very shiny golden sulphide which contrast very strongly with the dark fragment surfaces. Pockmarks are especially evident on "frothy" sulphide in the centre of the gas channels. Small convex bumps are sometimes present along with the pockmarks on the sulphide surfaces. These bumps can be burst with a pin to produce shiny depressions identical to the surrounding pockmarks.

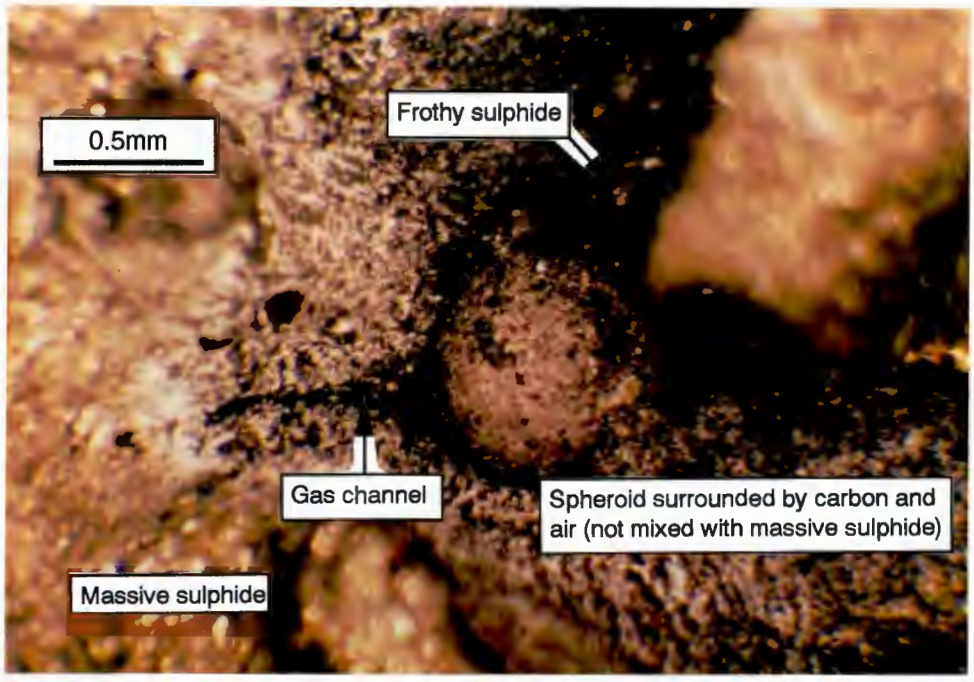

Figure 6.5 : Magnified view of lower left hand corner of Figure 6.4 showing a small sulphide spheroid in a junctions between two channels of the gas channel network.

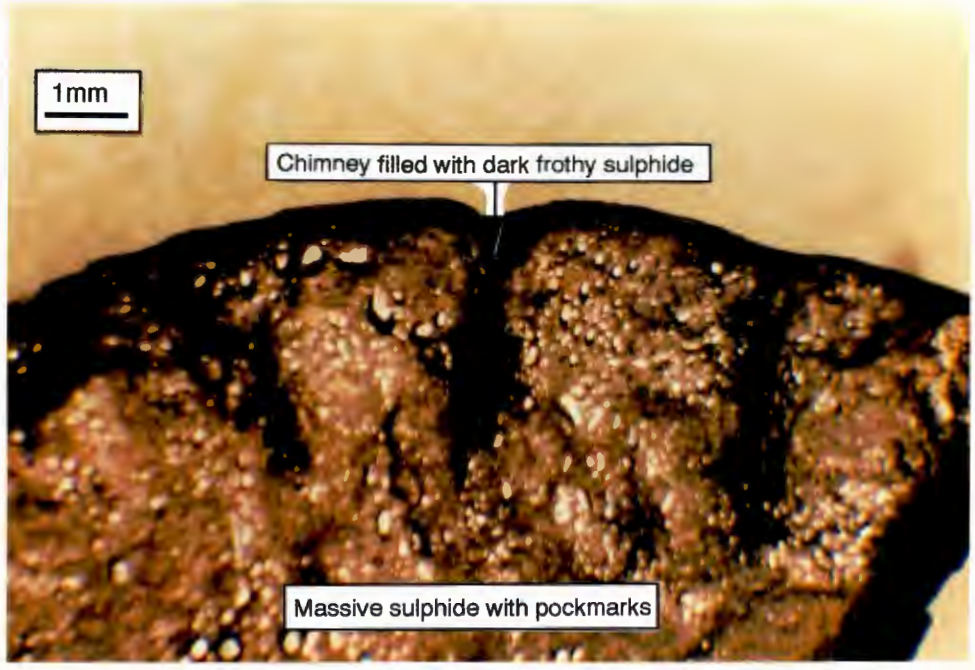

Figure 6.6: Exposed face of a sulphide button showing three chimneys in close proximity.

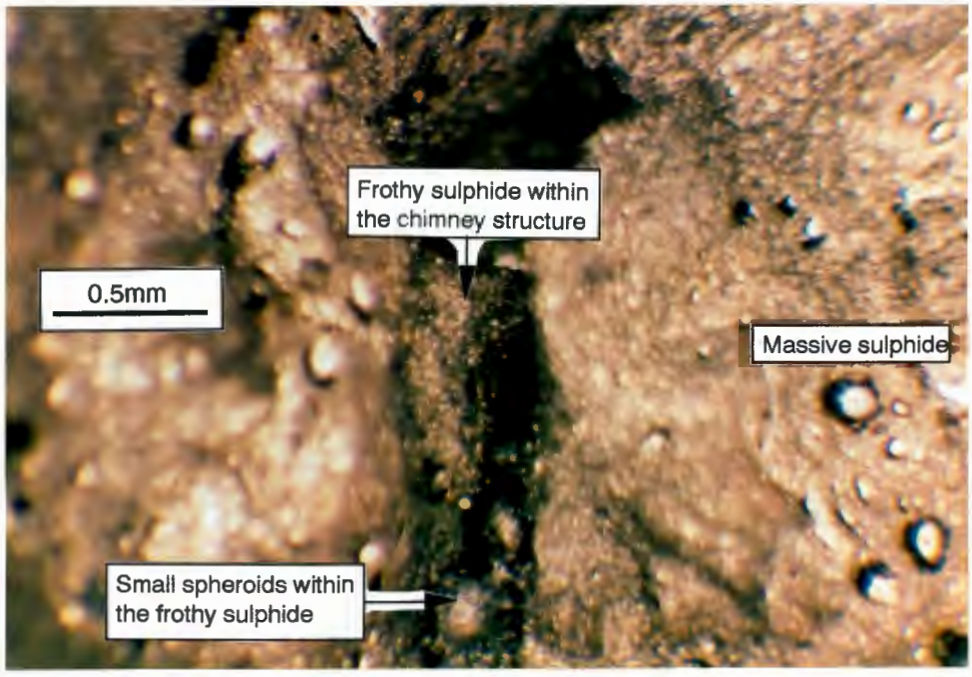

Figure 6.7 : Close-up view of the interior of a chimney. The chimney is filled with very dark, frothy sulphide. In the lower centre of the figure, two small spheroids are visible, mixed within the frothy sulphide . The sulphide on either side of the chimney shows slightly pockmarked surfaces but is essentially the massive and compact sulphide found in normal buttons.

This observation led to the conclusion that the pockmarks are the remnants of gas bubbles on the sulphide surface which have burst open. If this conclusion is correct, it would imply that all of the pockmarked surfaces of the fragments were sites where gas was being released from the sulphide. This observation appears to fit with the high density of pockmarks on the walls and on sulphide fragments within the gas channels.

6.3.5. Types Of Sulphide Fragment In SA(C/S) Buttons.

On the basis of shape and surface morphology, three distinct types of sulphide fragment have been recognised. These are classified as follows:

(1) *The Half Spheroid* - These fragments are almost half spheres which show two very different faces. The strongly curved surface of the sphere is smooth and shiny, blue/yellow or gold sulphide which has chilled against either the slag or the wall of the crucible. The other face of the half spheroid is dark sulphide. This face is usually flat or slightly convex and is heavily pockmarked. Half spheroids show a range of sizes from <0.5mm to >5mm across. As shown by Figure 6.3, the half spheroid fragments fit together to preserve the gross shape of the button,

with gas channels separating them. The occurrence of the pockmarks and gas features on the opposite face from the shiny, chilled sulphide could be indicative of gases being expelled away from a cooling front, forming a gas channel.

(2) *The Small Spheroid* - These fragments are complete spheres. They can be either very regular in shape or slightly deformed. Some small spheroids are shown in Figure 6.8. The whole of the outer surface of the spheroid is composed of dark sulphide. Pock marks are relatively uncommon and many of the spheroids appear quite smooth. The particles are generally small, <1mm across. The loose small spheroids are virtually identical to the spheroids which were examined in the chimneys and in the junctions of the gas channels (see Figures 6.5 and 6.7) and it seems likely that they were located within the gas channels prior to large-scale fragmentation of the sulphide.

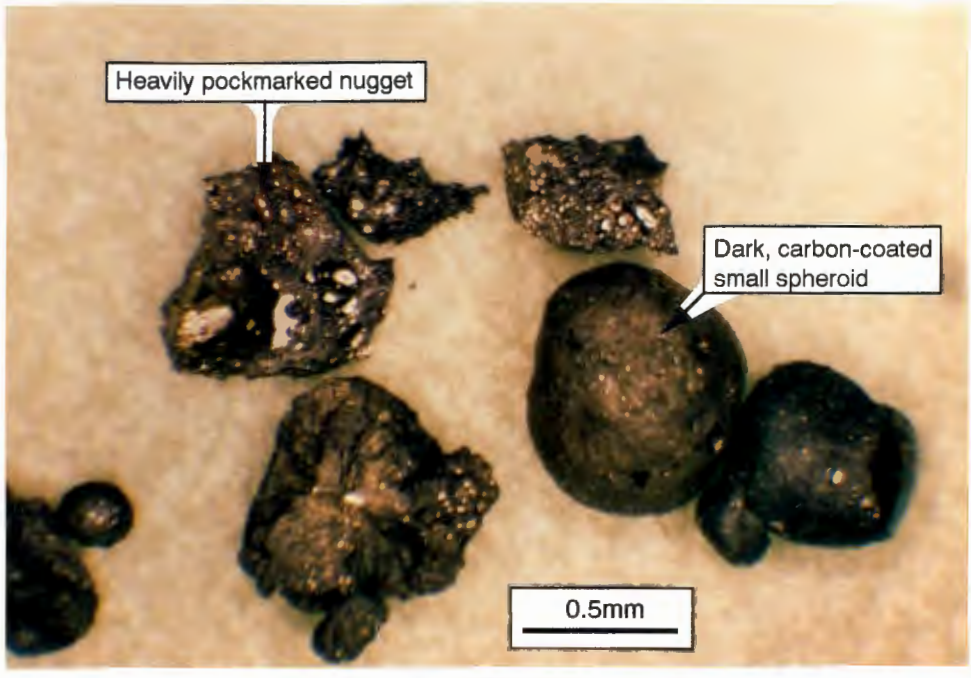

Figure 6.8 : A number of small spheroids (the round, dark blobs) and irregular, highly pockmarked nugget fragments.

Occasionally small spheroids (droplets ?) were found completely surrounded and enclosed in more massive, carbon-free sulphide away from the clearly defined gas channels with a thin layer of carbon and sometimes gas (now air) separating the small spheroid from the surrounding sulphide. The sulphide in the small spheroids had not been assimilated and mixed into the larger mass of sulphide

around it, apparently due to the presence of an impermeable interface between the two. The most obvious candidate for this interface appears to be the carbon layer.

The relative positions of the small spheroids and the surrounding massive sulphide suggest that carbon-coated droplets entered the carbon-free sulphide melt and the carbon layer or interface prevented mixing between the sulphide and the droplet from taking place. More carbon-free sulphide then descended to cover the small droplet. This implies that the carbon layer was present on the surface before the droplet (which later formed the small spheroid) entered the main mass of sulphide melt; and that the carbon coating may have formed within the silicate melt during settling of the sulphide droplet.

(3) *The Nugget* - Nuggets are highly irregular, flat fragments of intensely pockmarked sulphide which show a wide variety of forms and sizes. Some nugget fragments are shown in Figure 6.8. Nugget forms range from slightly irregular squares to highly irregular shapes such as "anvils", "triangles", "spearheads" and "spikes".

Nuggets show a wide range of sizes from <0.5mm to >4mm across. As indicated by Figure 6.3, nuggets are always found in the carbon-filled gas channels, sandwiched between half spheroids, when the fire-assay crucibles are first opened. In appearance, they are very similar to samples of the "frothy" sulphide which were removed from the interiors of the gas channels and this suggests that the nuggets are really fragments of "frothy" sulphide which were broken up and possibly redistributed as the gas channels widened and the button became fragmented.

Variations in the proportions of the three fragment types with increasing carbon are shown in Figure 6.9. The situation is initially dominated by half spheroids. As the carbon content increases, the proportion of nuggets rises slightly then falls back but the proportion of small spheroids increases rapidly until at 600 mg of carbon, the small spheroid form is most abundant type of fragment.

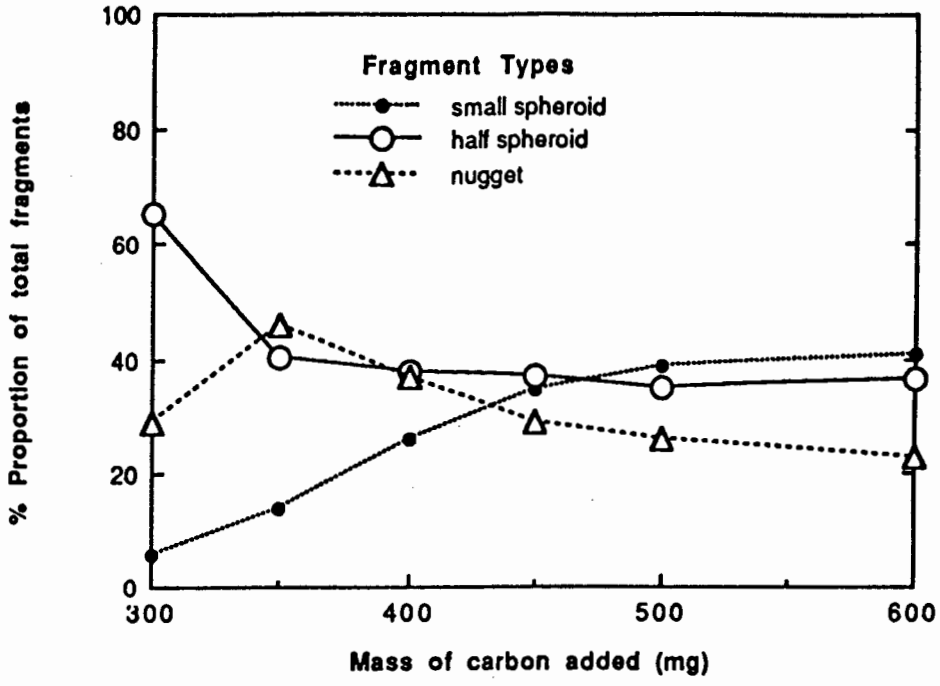

Figure 6.9 : Variation in fragment types with increasing masses of carbon.

6.3.6. Iron Rich Particles.

In some SA(C/S) and WA(C/S) experiments carried out using >450 mg of carbon, very tiny carbon-coated spheroids were sometimes found sandwiched between the walls of the assay crucible and the fragmented sulphide button. When these spheroids were cleaned in the ultrasonic, they did not resemble any of the particles previously described. All of the carbon was very easily removed by the ultrasonic, leaving clean and shiny surfaces, quite unlike the usual sulphide fragments. Typically the particles were very small, <0.4mm in diameter, and had a slightly silvery colour. All of the faces of the spheroids were shiny and none of the dark, carbon-bearing faces associated with the typical sulphide fragments were observed.

The spheroids were always found in tiny pits, cracks and depressions on the walls of the crucible and were often very difficult to remove, as if they were fixed or fused onto the walls. A PIXE x-ray spectrum obtained from the spheroids and the carbon layer in one the larger depressions of a crucible used in a SA(C/S) experiment with 600mg of carbon is shown in Figure 6.10(a). The spectrum shows that the spheroids contain large amounts of Fe, but without much Ni or S. This is very different from any of the other fragments where Ni and S produce the most intense x-ray peaks. Small amounts of other transition metals such as

Mn, Cr and Ti may also be present. Figure 6.10(b) is a spectrum of the thin film of slag which fills the depression and in which the shiny spheroids sit. This shows that the large peak from Si and the smaller Al peak in Figure 6.10(a) are probably x-rays derived from exitation of Si-rich SA slag around the edges of the spheroid.

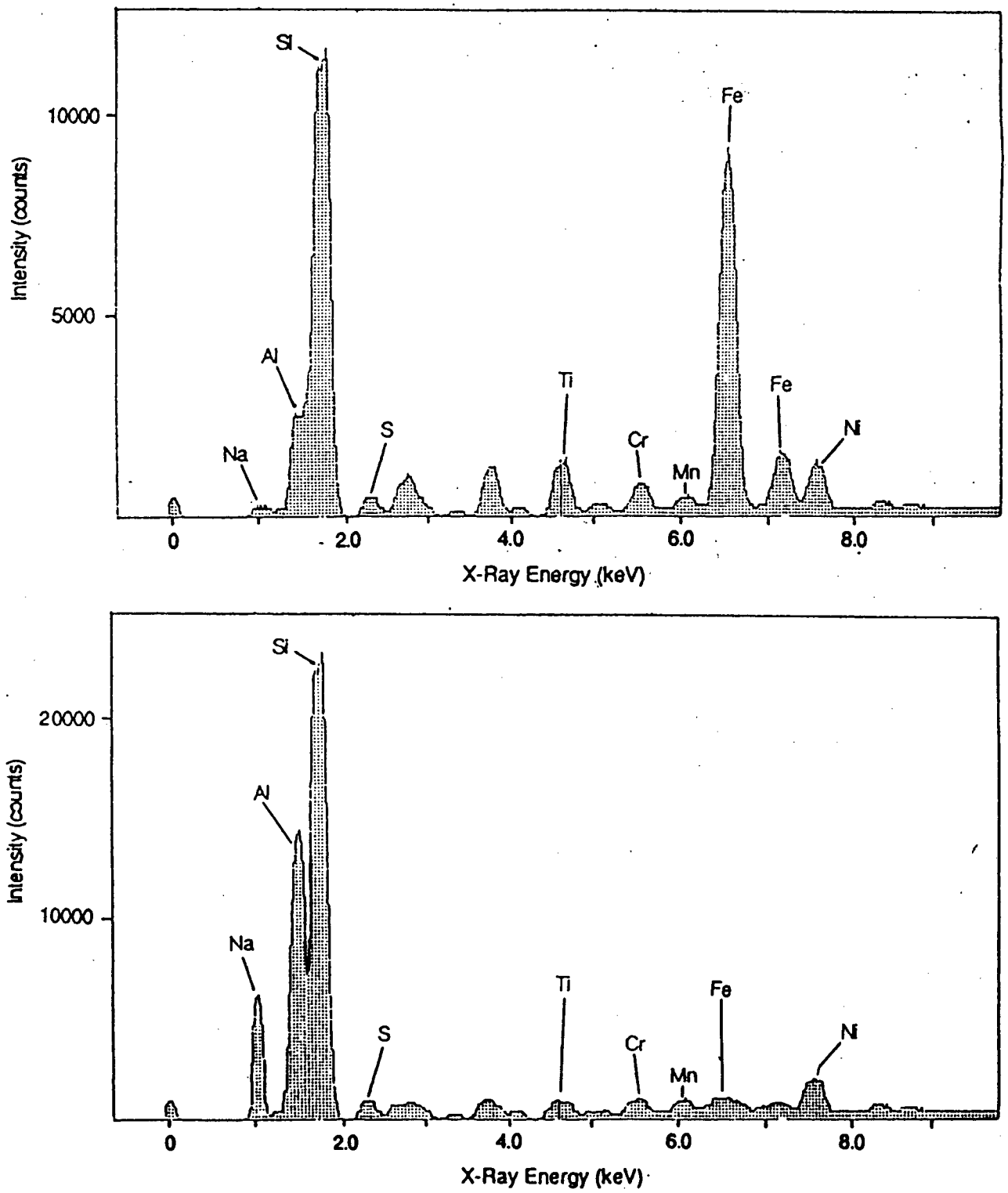

Figure 6.10.: X-ray spectrum of (a) Fe-rich spheroids and (b) slag on the wall of the assay crucible.

No such particles were observed during any of the fire-assays carried out without carbon. However, Shazali (1988) reported the presence of Fe-rich particles on the top surfaces of some NiS buttons during the fire-assay of SARM-7 but the x-ray spectra he obtained were very different to that shown in Figure 6.10(a). Ni and S were the dominant x-ray peaks while the Fe concentration was only 25% of the Ni concentration. The spheroids obtained here, show almost the opposite picture. The sulphur content of the spheroids appears too low for the Fe to be present as even a very Fe-rich sulphide phase and it seems possible that Fe may even be present as metal in these spheroids. The presence of siderophile metals such as Cr, Mn and Ti along with the Fe gives some support to this suggestion. If Fe is indeed present as the metal, this would imply that extremely reducing conditions could have prevailed during melting. This topic is discussed in greater detail in section 6.7.

6.4. Experimental Results.

The concentrations of PGE present in all of the solid phases (slag, sulphide or carbon) left after melting and reaction at 1000ºC were totalled and are shown in Tables 6.3. to 6.8. These tables clearly show that losses of the PGE were observed in all but one of the samples to which carbon had been added. Percentage losses of PGE in the carbon-spiked melts relative to the average of the normal (N) fire-assay melts using the same sample matrix are also presented as a separate column on each table.

Plots of the percentage losses of PGE versus the carbon content of the melt for the SA and WA sample mixtures are shown in Figures 6.11 to 6.16. Taking those melts containing sulphide first, the SA(C/S) and the WA(C/S) experiments show a relatively consistent picture for all of the metals. The SA(C/S) experiments show patterns of PGE losses with increasing carbon which define smooth, pseudo-parabolic curves. Losses of PGE reach a maxima between 250 and 350 mg of carbon, but thereafter decline as greater masses of carbon are used. With sulphide present, Ru shows higher losses (~40%) than the other PGE (21-28%). At high carbon concentrations, almost all of the Pd and Rh remains in the melt and is collected by the sulphide.

In contrast, the losses of PGE observed in the WA(C/S) experiments also define smooth curves but the losses do not appear to decline as higher masses of carbon

Table 6.3.: Os concentrations and percentage losses based on analyses of the solid phases left after fire-assay. Percentage losses are calculated relative to the normal (N) solid products for the particular sample matrix.

Sample	Carbon Added	Os Conc.	% Os Lost		Sample	Carbon Added	Os Conc.	% Os Lost
SA(N)	0	6.6	0.0		WA(N)	0	8.1	0.0
	0	6.3	0.0			0	7.7	2.5
	0	6.0	4.8		WA(C/S)	100	6.7	15.3
SA(C/S)	100	5.6	11.1			200	6.2	21.5
	100	5.7	9.5			300	5.9	25.3
	150	5.3	15.8			400	5.7	27.9
	200	5.3	15.8			500	5.1	35.4
	200	5.0	20.6			600	4.9	37.6
	250	5.0	20.6					
	300	4.6	26.9		WA(D)	0	n.d.	100.0
	350	4.8	23.8			0	0.4	94.9
	400	5.1	19.0		WA(D/C)	100	n.d.	100.0
	400	5.0	20.6			100	n.d.	100.0
	450	5.3	15.8			150	n.d.	100.0
	500	5.4	14.2			200	0.8	89.8
	600	5.7	9.5			200	0.9	88.6
						300	2.1	73.4
SA(D)	0	n.d.	100.0			300	1.6	79.7
	0	n.d.	100.0			350	3.1	60.7
SA(D/C)	100	n.d.	100.0			400	3.5	55.6
	150	n.d.	100.0			400	3.9	50.6
	200	n.d.	100.0			450	4.5	43.0
	200	n.d.	100.0			500	3.9	50.6
	250	0.5	92.0			500	3.6	54.4
	300	0.9	85.1			600	2.5	68.4
	350	1.4	77.8			600	2.5	68.4
	400	2.3	63.5					
	450	2.5	60.3		WP4A(N)	0	7.0	0.0
	500	2.0	68.1		WP4A(D)	0	n.d.	100.0
	600	1.7	73.1		WP4A(D/C)	100	n.d.	100.0
						300	0.7	90.0
						500	1.5	78.6

Table 6.4.: Ir concentrations and percentage losses based on analyses of the solid phases left after fire-assay. Percentage losses are calculated relative to the normal (N) solid products for the particular sample matrix.

Sample Type	Carbon Added	Ir Conc.	% Ir Lost		Sample Type	Carbon Added	Ir Conc.	% Ir Lost
SA(N)	0	7.6	0		WA(N)	0	8.9	0.0
	0	7.3	1.7			0	8.9	0.0
	0	7.4	0		WA(C/S)	100	7.8	12.8
SA(C/S)	100	6.7	9.4			200	7.0	21.0
	100	6.6	10.8			300	6.5	27.0
	150	6.2	16.2			400	6.6	25.6
	200	6.0	18.9			500	6.5	27.0
	200	5.8	21.6			600	6.3	29.2
	250	5.8	21.6					
	300	6.0	18.9		WA(D)	0	7.3	17.9
	350	6.0	18.9			0	7.5	15.7
	400	6.2	16.2		WA(D/C)	100	0.99	88.9
	400	6.3	14.9			100	0.75	91.6
	450	6.3	14.9			150	0.66	92.5
	500	6.6	10.8			200	0.64	92.8
	600	6.9	6.7			200	0.59	93.3
						300	0.46	94.8
SA(D)	0	5.5	25.7			300	0.48	94.6
	0	5.3	28.4			350	0.36	95.9
SA(D/C)	100	4.5	39.2			400	0.28	96.8
	150	4.4	40.5			400	0.30	96.6
	200	3.9	47.3			450	0.32	96.4
	200	4.0	45.9			500	0.27	96.9
	250	3.8	48.6			500	0.29	97.2
	300	3.6	51.4			600	0.25	97.1
	350	3.3	55.4			600	0.26	97.2
	400	3.1	58.1					
	450	3.0	59.5		WP4A(N)	0	8.0	0.0
	500	2.7	63.5		WP4A(D)	0	7.6	5.0
	600	2.7	63.5		WP4A(D/C)	100	2.3	71.3
						300	1.2	85.0
						500	1.0	87.5

Table 6.5: Ru concentrations and percentage losses based on analyses of the solid phases left after fire-assay. Percentage losses are calculated relative to the normal (N) solid products for the particular sample matrix.

Sample	Carbon Added	Ru Conc.	% Ru Lost		Sample	Carbon Added	Ru Conc.	% Ru Lost
SA(N)	0	43.0	2.3		WA(N)	0	50.0	0.0
	0	46.0	0.0			0	48.0	2.0
	0	43.1	2.3		WA(C/S)	100	41.3	15.7
SA(C/S)	100	38.0	13.7			200	39.2	20.0
	100	37.5	14.7			300	38.8	20.8
	150	35.3	19.8			400	36.4	25.7
	200	32.3	26.5			500	34.4	29.8
	200	30.1	31.6			600	35.0	28.6
	250	28.2	35.8					
	300	26.8	39.0		WA(D)	0	44.3	7.7
	350	26.4	40.1			0	43.9	8.5
	400	26.2	40.5		WA(D/C)	100	28.0	41.7
	400	26.7	39.3			100	30.8	35.8
	450	29.2	33.6			150	28.7	40.2
	500	31.4	28.7			200	25.3	47.3
	600	33.3	24.6			200	23.0	52.1
						300	21.1	56.0
SA(D)	0	38.4	12.7			300	19.8	58.8
	0	38.6	12.3			350	20.9	56.5
SA(D/C)	100	34.1	22.5			400	18.2	62.1
	150	33.7	23.4			400	18.8	60.8
	200	31.5	28.4			450	17.9	62.7
	200	31.8	27.7			500	16.8	65.0
	250	28.2	35.9			500	16.5	65.6
	300	29.2	33.6			600	14.7	69.4
	350	27.0	38.6			600	15.7	67.3
	400	24.6	44.0					
	450	22.1	49.8		WP4A(N)	0	44.1	0.0
	500	19.2	56.4		WP4A(D)	0	42.2	4.3
	600	19.0	56.8		WP4A(D/C)	100	31.8	27.9
						300	22.5	49.0
						500	17.5	60.3

Table 6.6.: Rh concentrations and percentage losses based on analyses of the solid phases left after fire-assay fire-assay. Percentage losses are calculated relative to the normal (N) solid products for the particular sample matrix. "nda" indicates no data available.

Sample Type	Carbon Added	Rh Conc.	% Rh Lost		Sample Type	Carbon Added	Rh Conc.	% Rh Lost
SA(N)	0	24.2	1.2		WA(N)	0	25.5	0
	0	24.5	0.0			0	25.3	1.2
SA(C/S)	100	19.1	22.0		WA(C/S)	100	22.8	11.1
	150	18.3	25.3			200	20.6	19.5
	200	17.9	26.9			300	20.2	21.1
	250	17.5	28.6			400	19.3	24.6
	300	19.3	21.2			500	18.2	28.9
	400	20.7	15.5			600	17.6	31.3
	500	22.1	9.8					
	600	24.1	1.6		WA(D)	0	22	13.4
						0	22.2	12.6
SA(D)	0	18.0	26.5		WA(D/C)	100	9.1	64.2
	0	18.3	25.3			200	8.2	67.8
SA(D/C)	100	13.6	44.4			250	7.1	72.1
	150	12.4	49.2			300	6.3	75.2
	200	12.3	49.6			400	6.2	75.6
	250	12.1	50.4			450	6.4	74.8
	300	11.2	54.1			500	6.8	73.3
	400	10.6	56.6			600	5.9	76.8
	500	9.6	60.6					
	600	9.0	63.1		WP4A(N)	n.d.a.	n.d.a.	n.d.a.
					WP4A(D)	n.d.a.	n.d.a.	n.d.a.
					WP4A(D/C)	n.d.a.	n.d.a.	n.d.a.

Table 6.7.: Pt concentrations and percentage losses based on analyses of the solid phases left after fire-assay. Percentage losses are calculated relative to the normal (N) solid products for the particular sample matrix.

Sample	Carbon Added	Pt Conc.	% Pt Lost		Sample	Carbon Added	Pt Conc.	% Pt Lost
SA(N)	0	387	0		WA (N)	0	397	0
	0	395	0			0	389	1.0
	0	379	2.1		WA(C/S)	100	330	16.0
SA(C/S)	100	359	7.2			200	320	18.6
	100	356	8.0			300	302	23.2
	150	336	13.2			400	307	21.9
	200	329	15.0			500	310	21.1
	200	321	17.0			600	302	23.2
	250	294	24.0					
	300	290	25.1		WA(D)	0	382	2.8
	350	290	25.1			0	385	2.0
	400	314	18.9		WA(D/C)	100	316	19.6
	400	306	20.9			100	328	16.5
	450	319	17.6			150	282	28.2
	500	332	14.2			200	235	40.2
	600	354	8.5			200	210	46.6
						300	180	54.2
SA(D)	0	338	12.7			300	176	55.2
	0	305	21.1			350	162	58.8
SA(D/C)	100	276	28.7			400	149	62.1
	150	196	49.4			400	131	66.6
	200	238	38.5			450	133	66.2
	200	246	36.4			500	127	67.7
	250	199	48.6			500	135	65.6
	300	192	50.4			600	123	68.7
	350	166	57.1			600	117	70.2
	400	174	55.0					
	450	156	59.7		WP4A(N)	0	382	0
	500	153	60.4		WP4A(D)	0	370	3.1
	600	149	61.5		WP4A(D/C)	100	290	24.1
						300	139	63.6
						500	110	71.2

Table 6.8.: Pd concentrations and percentage losses based on analyses of the solid phases left after fire-assay. Percentage losses are calculated relative to the normal (N) solid products for the particular sample matrix.

Sample	Carbon Added	Pd Conc.	% Pd Lost		Sample	Carbon Added	Pd Conc.	% Pd Lost
SA(N)	0	152	1.3		WA(N)	0	168	0.0
	0	154	0.0			0	162	1.8
	0	156	0.0		WA(C/S)	100	148	10.5
SA(C/S)	100	140	9.2			200	138	16.1
	100	143	7.2			300	130	21.0
	150	137	11.1			400	128	22.2
	200	132	14.4			500	121	26.3
	200	127	17.6			600	122	26.1
	250	126	18.3					
	300	123	20.4		WA(D)	0	153	7.3
	350	121	20.9			0	152	7.8
	400	129	16.3		WA(D/C)	100	108	34.5
	400	133	13.6			100	105	36.4
	450	141	8.5			150	87.8	46.8
	500	144	6.6			200	78.6	52.4
	600	153	0.6			200	68.6	58.4
						300	63.7	61.4
SA(D)	0	146	5.2			300	63.6	61.3
	0	143	7.1			350	61.0	63.0
SA(D/C)	100	142	7.8			400	66.0	60.0
	150	138	10.4			400	64.0	61.2
	200	137	11.0			450	61.8	62.5
	200	131	14.9			500	59.0	64.2
	250	125	18.8			500	56.6	65.7
	300	124	19.5			600	56.0	66.1
	350	120	22.1			600	57.3	65.3
	400	119	22.7					
	450	111	27.9		WP4A(N)	0	159	0
	500	108	29.9		WP4A(D)	0	152	4.4
	600	104	32.5		WP4A(D/C)	100	114	28.3
						300	74.3	53.3
						500	63.8	59.1

are used. Losses vary between 23% for Pt to 37% for Os. Only Os and Rh have curves which are still sloping at 600mg of carbon, suggesting that further losses may be possible. The curves for the other metals visibly flatten out (possibly as if the reaction is slowing or reaching saturation) but unlike the SA(C/S) experiments, the observed losses of PGE show no signs of decreasing.

For all of the metals, the (D/C) experiments, which were carried out in the absence of a sulphide melt, show greater losses than were obtained with the (C/S) experiments. Extremely large losses of Os (up to 100%) were observed from the SA(D), WA(D) and WP4A(D) melts. In the absence of carbon or sulphide, the $NaCO_3$:borax flux produces a highly oxidised melt (E. van Wyk pers. comm. 1992) and it is very possible that large scale losses of Os as the volatile oxide OsO_4 took place in these melts whereas smaller losses were observed with the other PGE.

Apart from Os, losses of PGE in the (D) experiments were always greater for the SA melt than for the WA or WP4A melts. All of the compounds in the SA fusion mixture ($NaCO_3$, borax and SiO_2) contain elements in very high oxidation states, therefore the capacity of these major components to buffer any excess oxygen (eg the air inside the powders) is very limited and the oxidation of PGE in the melt may take place quite readily. In contrast, the WA and WP4A sample matrices are real rocks and contain a variety of elements such as Fe, Mn, Cr, Ti, P and S in low oxidation states which can become further oxidised, soaking up free oxygen in the melt and restricting the potential for PGE oxidation.

The order of losses from highest to lowest in the (D) experiments is; Os » Ir ~ Rh > Pt ~ Ru ~ Pd. This order roughly resembles the order of the volatilities of the PGE and Au as oxides (Alcock and Hooper 1960 and section 2.3.3) and suggests that the losses of the PGE and Au from these relatively oxidising melts may be explained by conversion of the metals to oxide species.

As carbon is added, Os shows markedly different behaviour to the other PGE. Losses of Os from the melt initially remain very high but then rapidly fall as the amount of carbon is increased. A reversal in this trend takes place at 450 mg of carbon and thereafter the loss of Os is seen to increase again between 500 and 600 mg of carbon. This is suggestive that carbon in the melt may be having two effects on the Os. Increasing masses of carbon react with oxygen to produce CO and CO_2, reducing the amount of oxygen available to convert Os to OsO_4 and

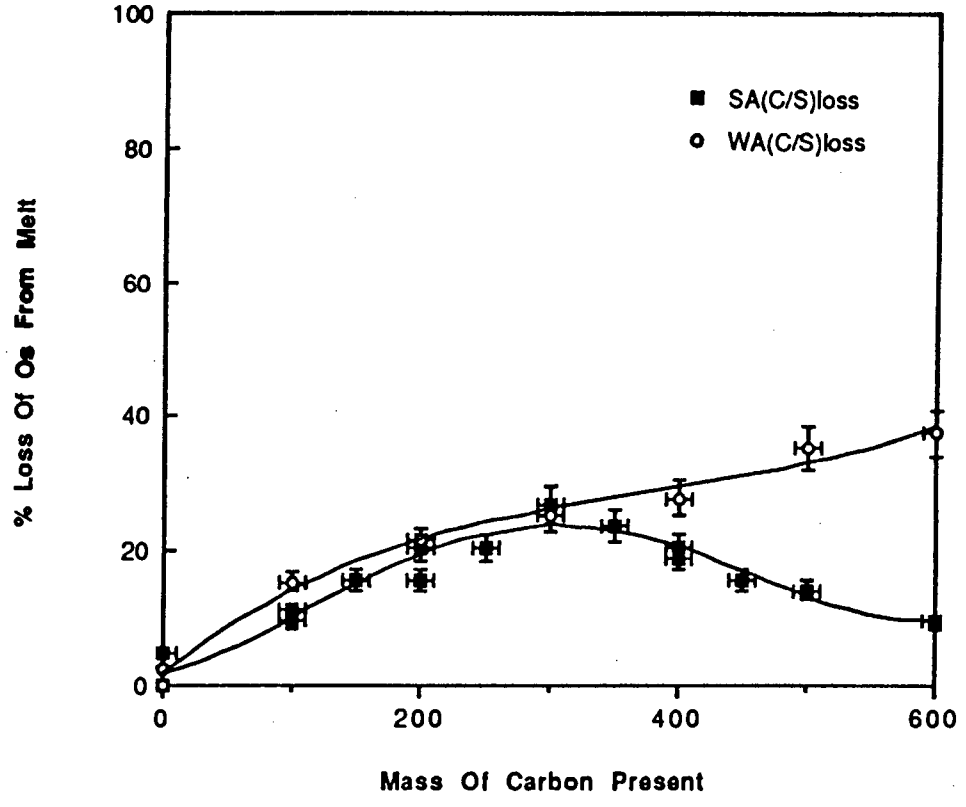

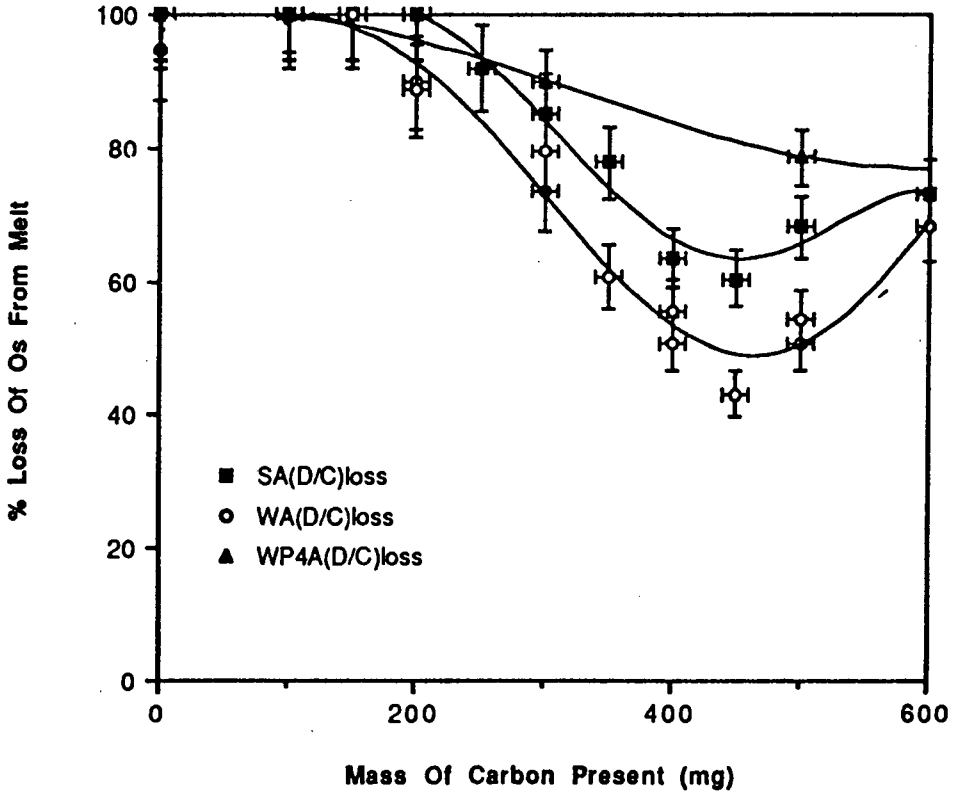

Figure 6.11 : Percentage losses of Os plotted against mass of added carbon for (C/S) and (D/C) experiments. The error on the carbon mass is ~10mg. Errors on concentrations and losses are taken from the 191-Os counting statistics.

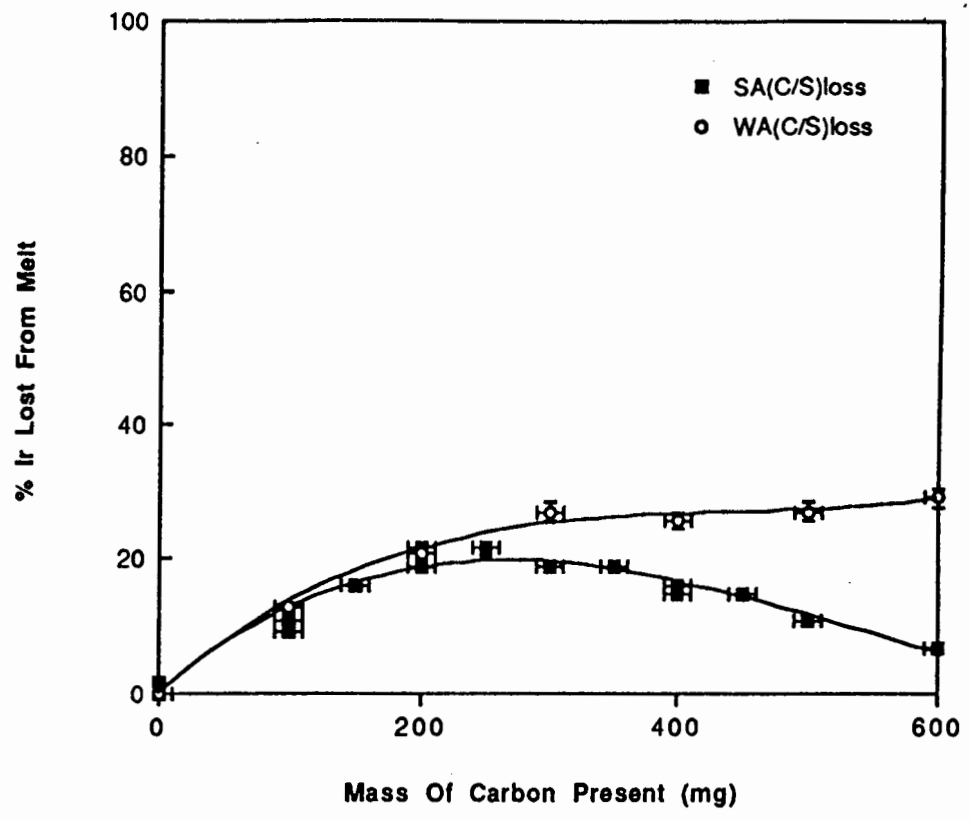

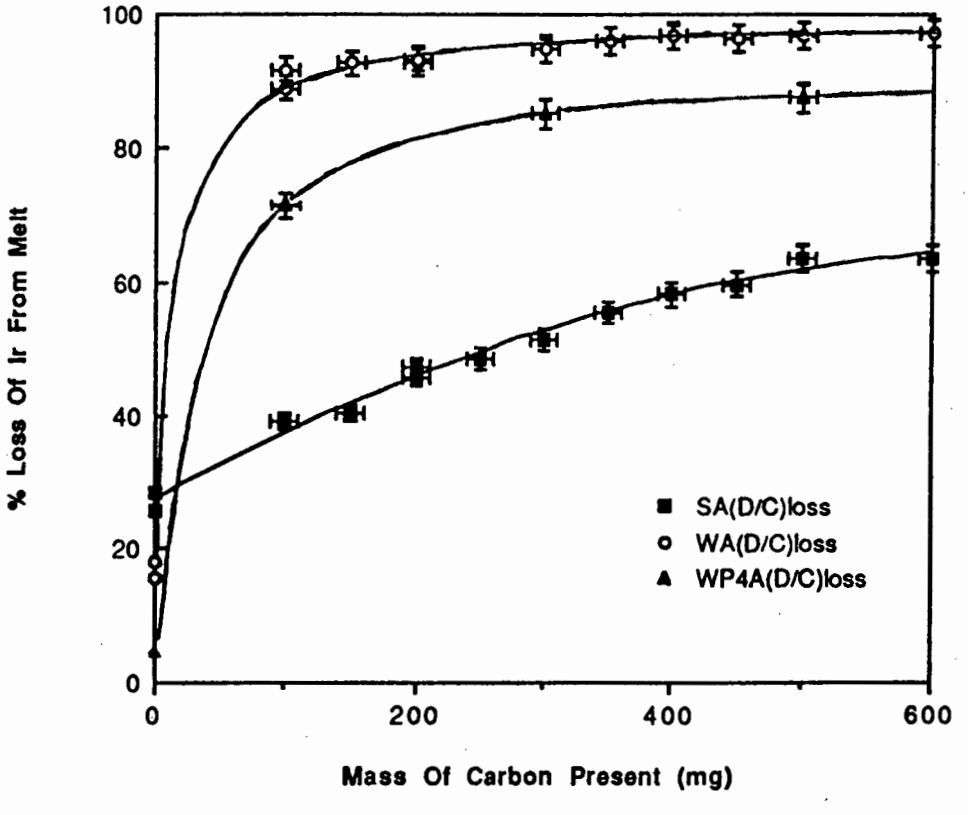

Figure 6.12 : Percentage losses of Ir plotted against mass of added carbon for (C/S) and (D/C) experiments. The error on the carbon mass is ~10mg. Errors on concentrations and losses are taken from the 192-Ir counting statistics.

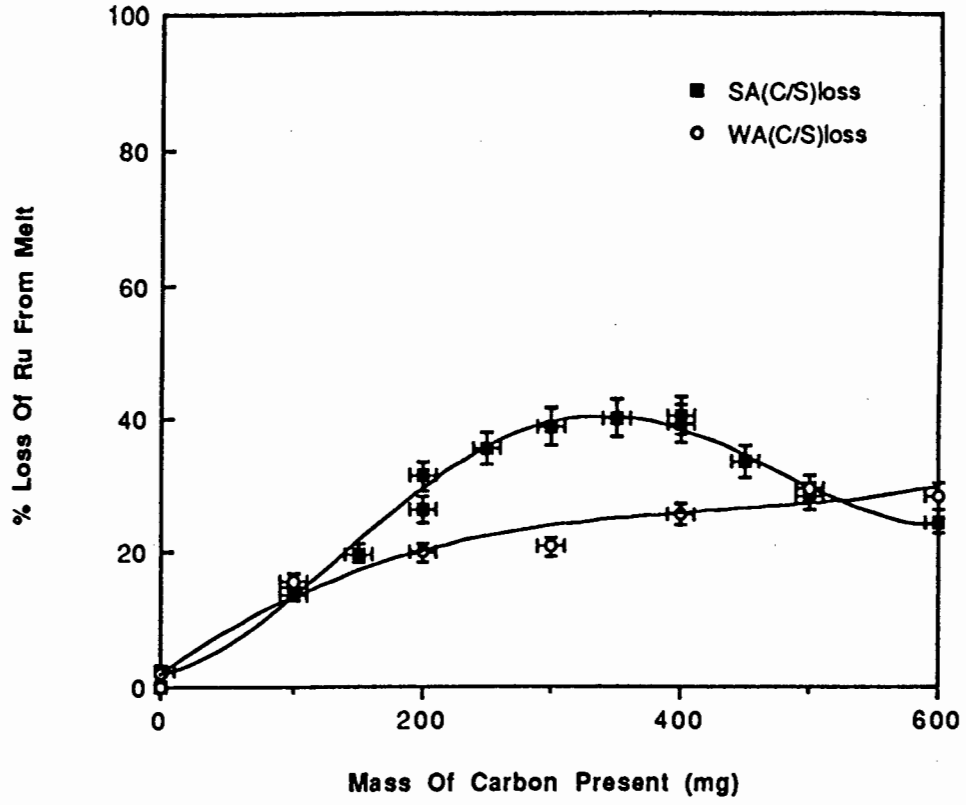

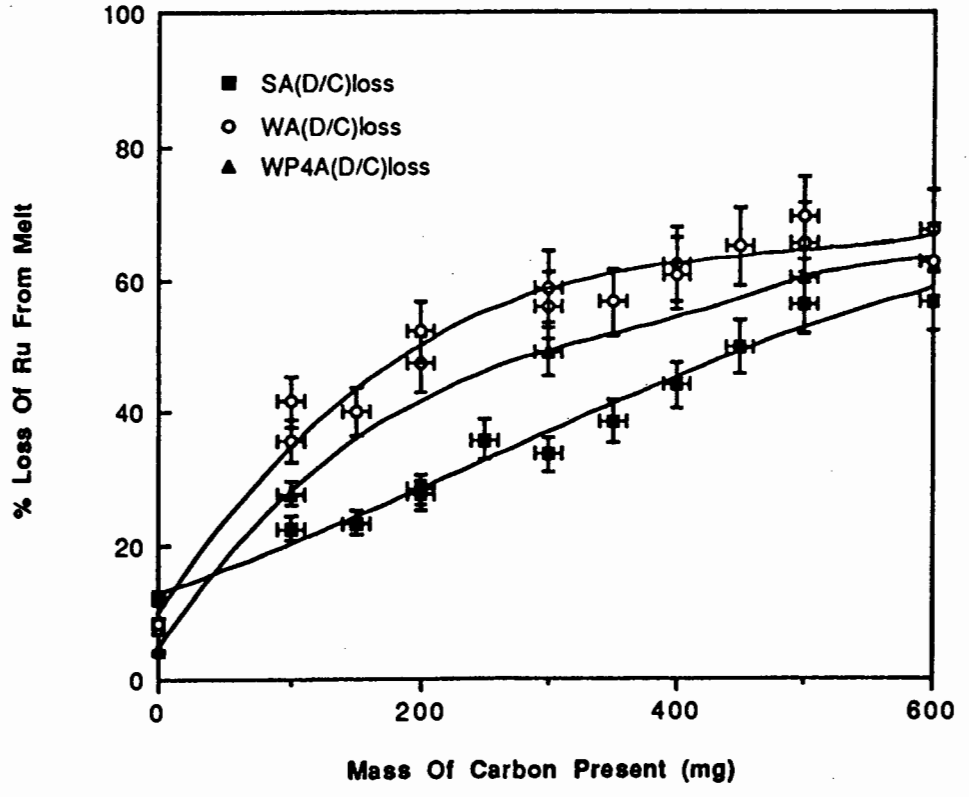

Figure 6.13 : Percentage losses of Ru plotted against mass of added carbon for (C/S) and (D/C) experiments. The error on the carbon mass is ~10mg. Errors on concentrations and losses are taken from the 103-Ru counting statistics.

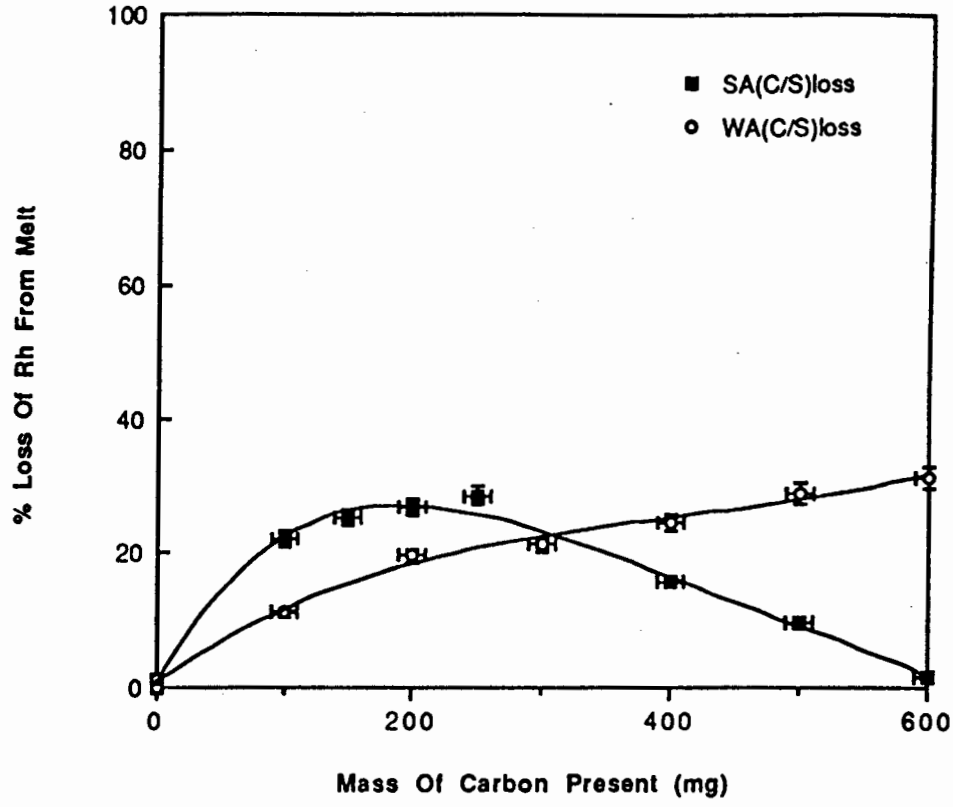

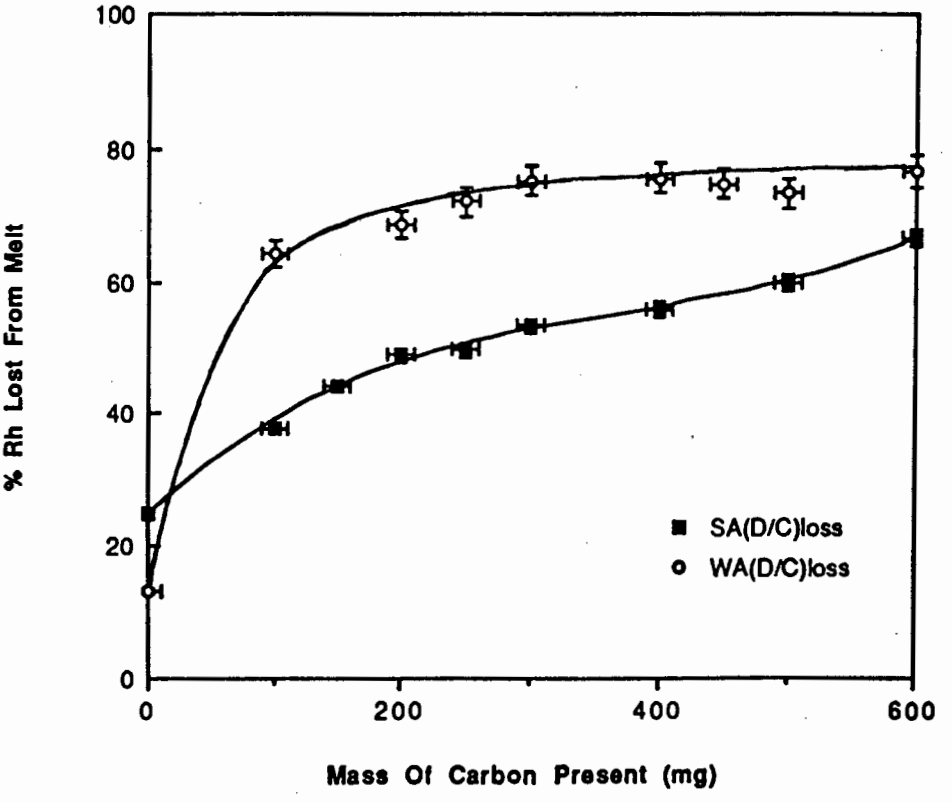

Figure 6.14 : Percentage losses of Rh plotted against mass of added carbon for (C/S) and (D/C) experiments. The error on the carbon mass is ~10mg. Errors on concentrations and losses are taken from the 104m-Rh counting statistics.

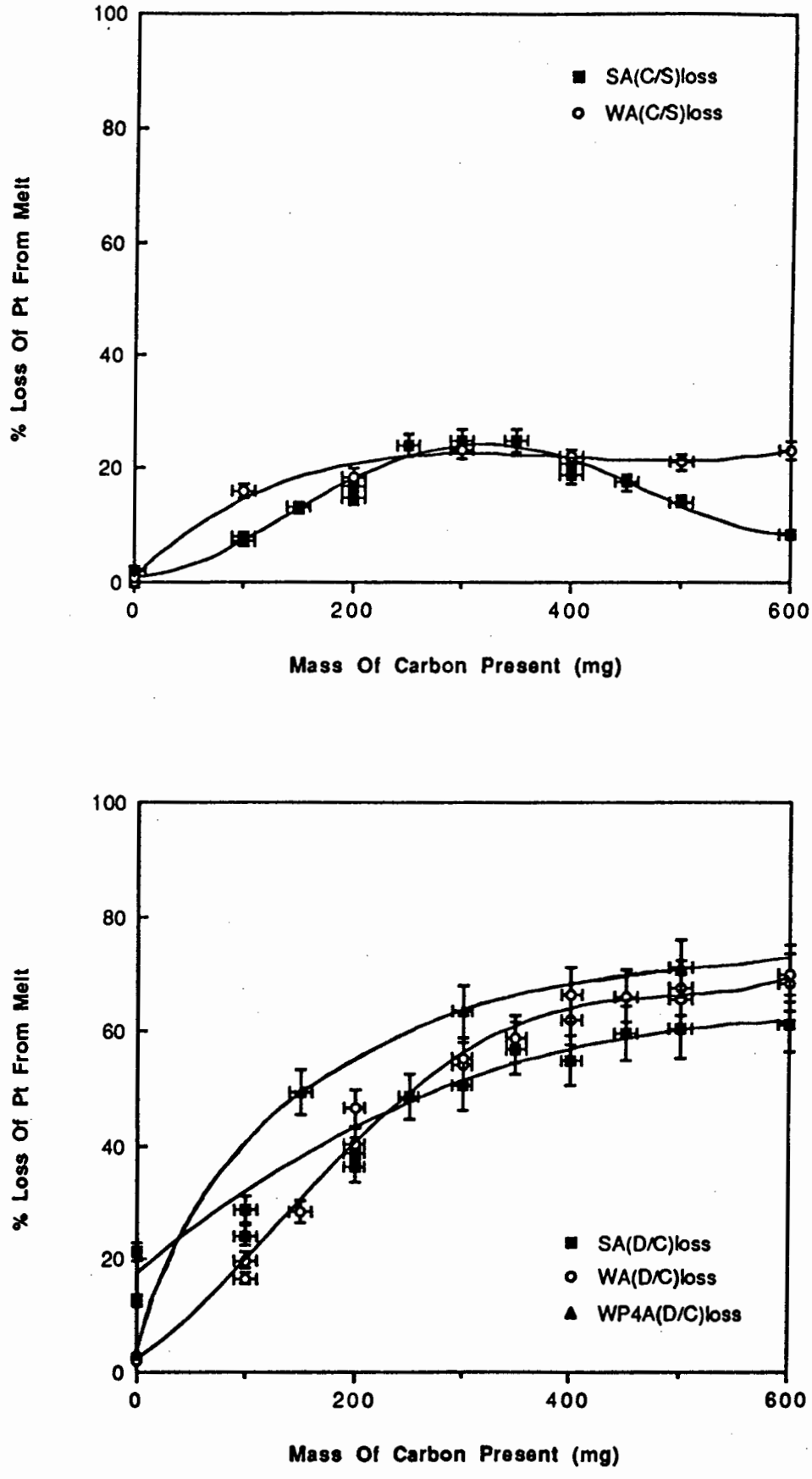

Figure 6.15 : Percentage losses of Pt plotted against mass of added carbon for (C/S) and (D/C) experiments. The error on the carbon mass is ~10mg. Errors on concentrations and losses are taken from the 199-Au (Pt) counting statistics.

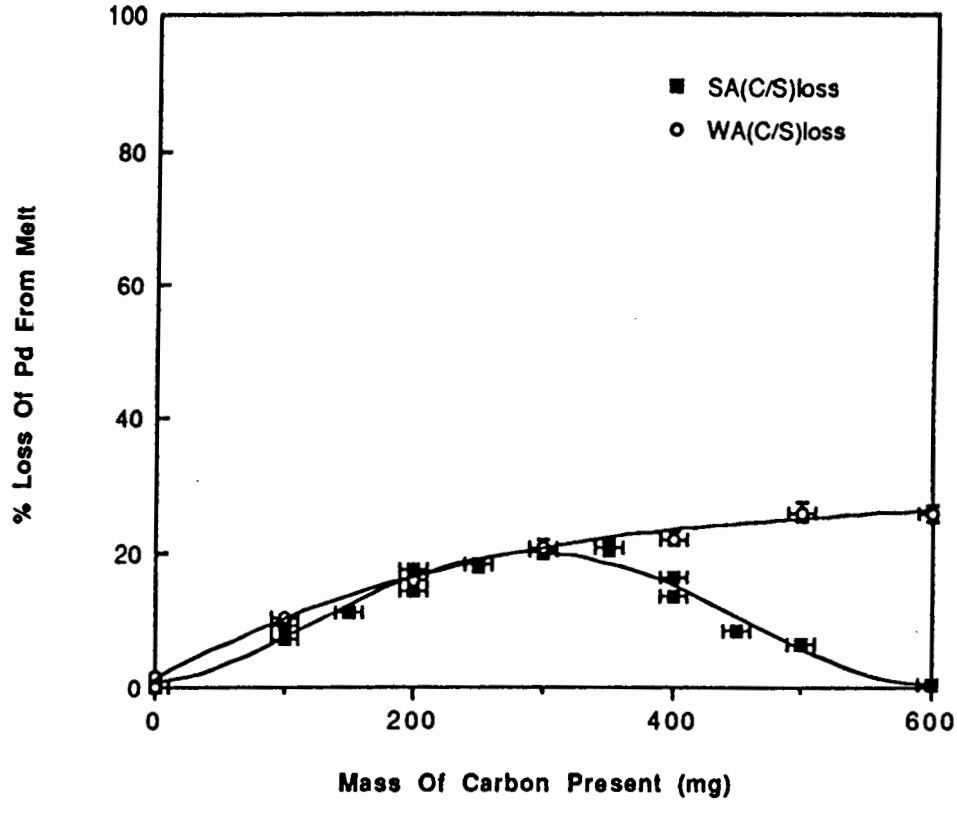

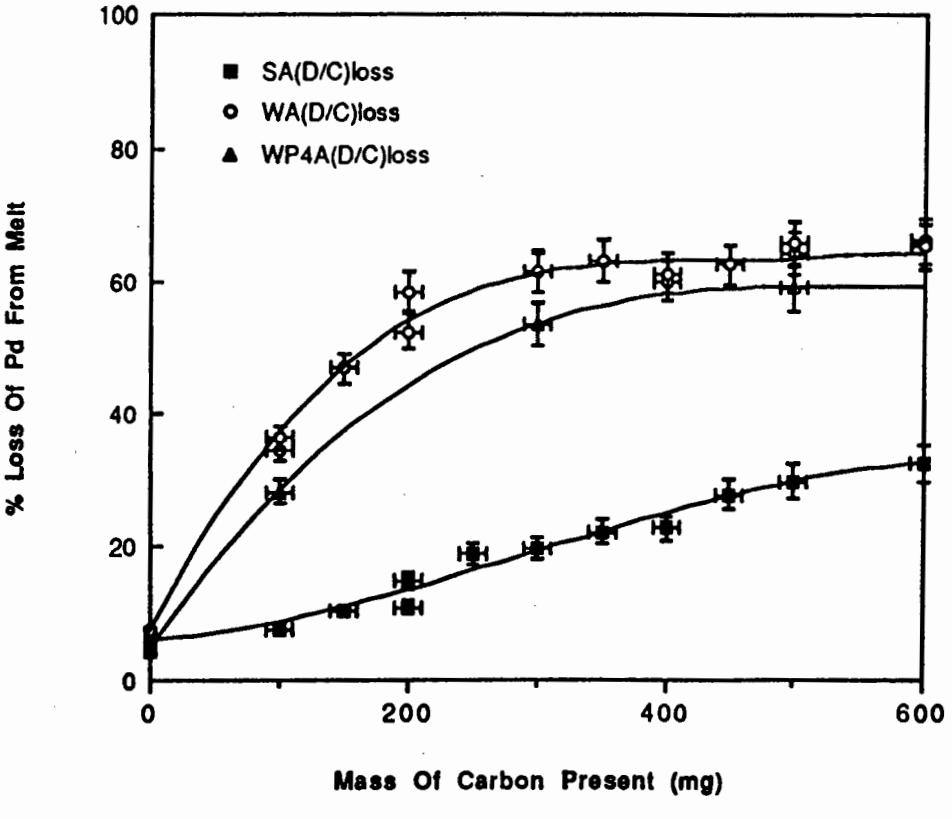

Figure 6.16 : Percentage losses of Pd plotted against mass of added carbon for (C/S) and (D/C) experiments. The error on the carbon mass is ~10mg. Errors on concentrations and losses are taken from the 109-Pd counting statistics.

causing the %loss of Os to fall. And then at high carbon concentrations, a reaction similar to that for the other PGE may become dominant, causing loss of Os as another chemical species.

The other PGE show patterns of loss which define smooth curves. The curves are steep initially but flatten out at higher carbon concentrations. Losses of the PGE are always greater in the WA and WP4A samples than those obtained with the highly siliceous SA sample matrix. The losses measured for Ir in the WA(D/C) and WP4A(D/C) experiments are particularly spectacular. The addition of small masses of carbon (100 mg) produces large losses of Ir until >95% of the Ir is mobilized into the volatile phase. Rh behaves in a similar manner to Ir with a very rapid removal of the metal from the melt at low carbon concentrations, followed by a flattening of the curve until 75-76% of the Rh is lost to the volatile phase. For Ru, Rh, Pt and Pd, up to 65% of the PGE initially present, can be mobilized into the volatile phase.

The few data points which do exist for the WP4A sample matrix indicate that it produces similar effects to the WA sample matrix, although the absolute losses are often slightly lower. With the exception of Os, the curves obtained from the WA(D/C) and WP4A(D/C) experiments rise quickly and flatten out at higher carbon concentrations, while the curves from the SA(D/C) experiments rise much more slowly and only flatten out above 450 mg of carbon. This may indicate a slightly slower rate of reaction taking place in the SA(D/C) system compared to the WA(D/C) and WP4A(D/C) experiments.

In summary, the data indicate that the PGE in the SA(C/S) and WA(C/S) melts show very different behaviour at high carbon concentrations. The reversal in the trend of increasing PGE loss seen in the SA(C/S) melts coincides with the appearance of gas channels and small spheroids in the fragmented buttons, while there is an absence of small spheroids, gas channels and no apparent reversal of PGE losses in the WA(C/S) experiments. This observation is suggestive of a link between the reversal of the PGE losses and the presence of gas channels and/or small spheroids in the button.

In the absence of sulphide, losses of all of the PGE increase. Sulphide clearly acts as a retainer for the PGE in the melt and without it, the PGE are much more free to react and enter the volatile phase. With no sulphide or carbon present, Os may

be readily lost as an oxide species. The addition of carbon reduces this loss intially but at high carbon concentrations, the Os loss increases again, in a manner similar to the other metals. The losses of PGE in the (D/C) experiments decrease in the order Ir > Rh ~ Os > Ru ~ Pt ~ Pd. This overall trend and particularly the similarity in behaviour between Ir and Rh (an initally very steep loss curve which flattens very quickly) is suggestive that the principle control on the reaction is the electronic configuration of the metals. This might indicate the generation of organometallic species.

6.5. Radiotracer Experiments.

6.5.1. Introduction.

The data from the carbon-spiked experiments indicates that PGE were being lost from the melt to the volatile phase and the pattern of the losses might be explained by the formation of an organometallic species. Both of these suggestions were addressed by using radiotracers. If radioactive PGE present in the melt could be removed, transported and then subsequently trapped and analysed then this approach would offer clear proof that the PGE were entering the volatile phase and were not somehow being accidently missed during the analysis of the solidified melt phases.

In addition, it was hoped to obtain some additional information on whether any PGE species in the volatile phase were organometallic. Different liquids have different selectivities towards ionic and non-polar molecules and these will trap these different species preferentially. Pernicka and Wasson (1987) used 4 molar NaOH in a cooled trap to collect OsO_4 and RuO_4 from a nitrogen atmosphere during RNAA. NaOH solutions also convert PGE chloride species into insoluble oxides (Cotton and Wilkinson 1980). NaOH was therefore used as a trapping agent with the knowledge that it could trap dominantly ionic PGE oxide and chloride phases.

Hinkley (1991) found that chilled methanol acted as a collector for transition metals such as Cu, Cd and Pb from volcanic gases and methanol was therefore investigated as a collector in these experiments. Organometallic species, carbonyls in particular, tend to be very soluble in non-polar organic solvents such as benzene, toluene or ether (Livingstone 1975; Cotton and Wilkinson 1980; Crabtree 1988). Toluene was therefore used as an indicator of potentially non-polar

organometallic species carried in the gas phase. The order of the liquids in the traps (whether NaOH came before toluene or vice versa) was also investigated.

6.5.2. Experimental Outline.

Approximately 0.2 grams of Os, Pt and Pd, as chlorides dissolved in aqua regia, were pipetted onto 10 grams of extra pure silica powder lying flat in a pyrex test tube with a gas outlet aperture. 0.1 grams of Ir was added in a similar fashion. The silica powder was dried under an infrared lamp for 2 hours. The top of the test tube was fitted to a gas inlet joint and connected to a hydrogen gas (Afrox >95% H_2) cylinder. The gas supply was turned on and the metal chlorides were reduced under hydrogen at ~600ºC for 2 hours to obtain the metals in the form of a very finely divided sponge on the silica powder.

Approximately 1.5 grams of silica containing the PGE was weighed into a 2.5 ml irradiation vial and the vial was sealed. Three such irradiation vials were prepared, sealed inside a water filled irradiation container and irradiated for 96 hours in a neutron flux of 5.6×10^6 $n.cm^{-2}.sec^{-1}$ using a ^{252}Cf source as described by Pillay et al. (1990). After irradiation, the vials containing the noble metals were packed into cylindrical, 22 ml vials in the centre of counting bottles. The small vials were kept in the geometrical centre of the central vial by the use of foam spacers (see Figure 6.17).

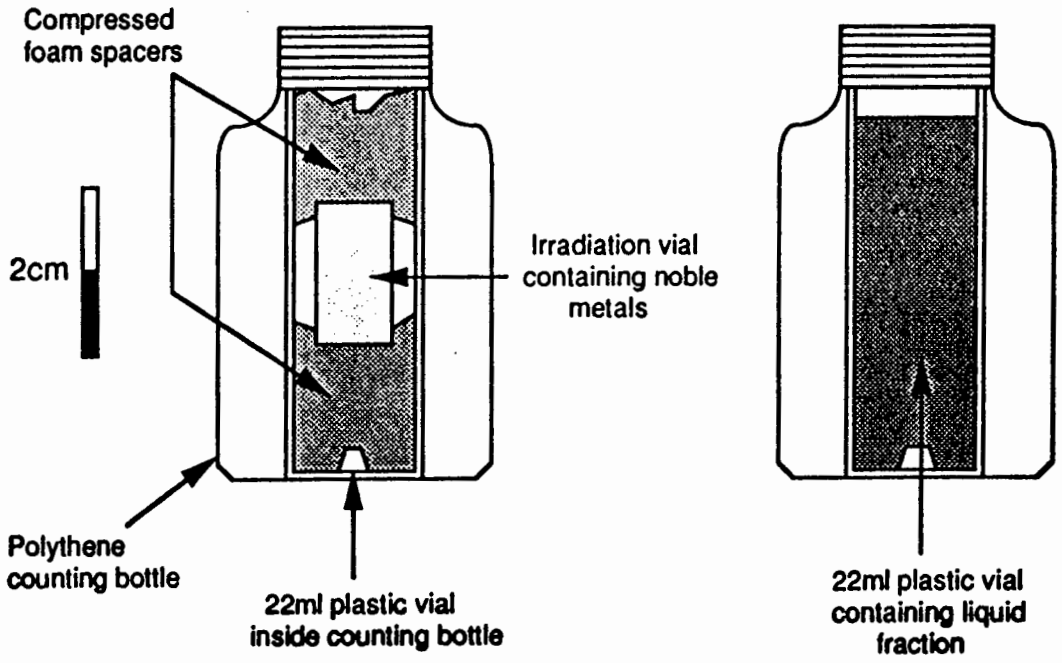

Figure 6.17.: Geometries used for counting of the of irradiated platinum metals and the liquid fractions in the counting bottles during radiotracer experiments.

Each sample was counted for 60 minutes on a Ge(Li) detector to determine the activities of ^{109}Pd, ^{193}Os, ^{194}Ir and ^{197}Pt present. A sample to detector distance of 80mm was used for this measurement in order to minimize geometry corrections (Watterson 1975) between the powders and the liquid (trap) samples to be counted later, after firing. After counting, the vials were opened and the contents added to previously prepared fire-assay mixtures. Due to the small size of the radiochemistry furnace and the small porcelain crucibles which were to be used, the reagents used in these mixtures had to be scaled down by a factor of ten from the normal procedures. Carbon was kept at 60 mg for two experiments (one with sulphide and the other without sulphide) and was not used in the third where losses due to degassing in the absence of both carbon and sulphide were investigated.. The full sample mixtures used in the three radiotracer experiments are summarized in Table 6.9, below:

Table 6.9.: Summary of the inactive and activated components used in the radiotracer fire-assay experiments.

	Experiment Type	Sample Mixture
Experiment 1	SA(C/S)	3 grams $NaCO_3$ 6 grams borax 1.25 grams sulphur 3.5 grams $NiCO_3$ 0.5 grams SARM-7 6.0 grams SiO_2* 60 mg carbon
Experiment 2	WA(D/C)	3 grams $NaCO_3$ 6 grams borax 0.5 grams SARM-7 4.5 grams Wits-1 1.5 grams SiO_2* 60 mg carbon
Experiment 3	WA(D)	3 grams $NaCO_3$ 6 grams borax 0.5 grams SARM-7 4.5 grams Wits-1 1.5 grams SiO_2* (no carbon)

* fraction containing irradiated noble metals

The contents of each crucible were mixed with a clean glass rod behind a lead wall in a fume cupboard. After mixing, the crucibles were sealed inside a plastic

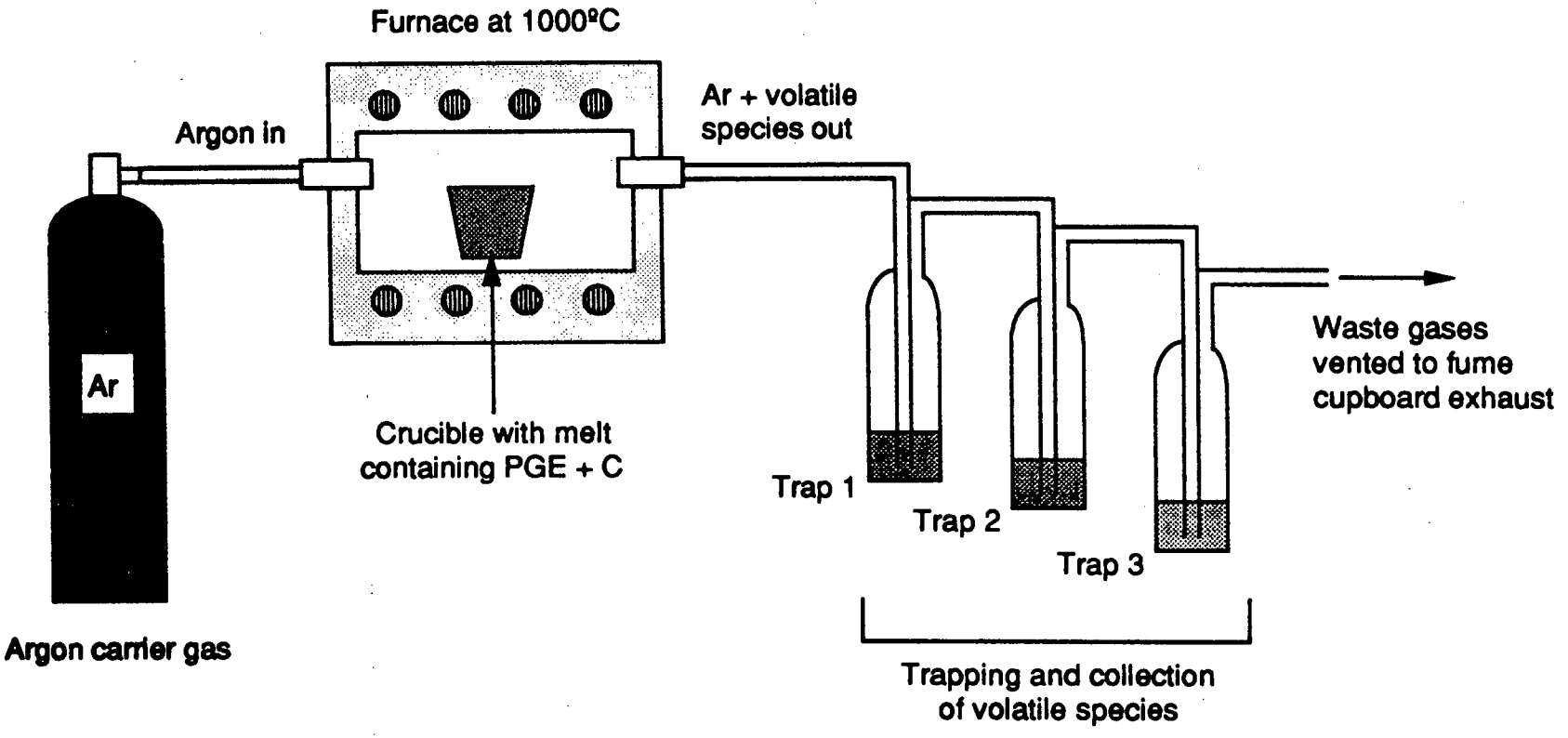

Figure 6.18 : Schematic arrangement of the experimental apparatus used in the radiotracer experiments.

container to contain any spillages of powder which might occur during storage, prior to transfering them to the furnace.

A diagram of the experimental apparatus used for the radiotracer experiments is shown in Figure 6.18. A Naber L47T furnace was modified to allow only single inlet and outlet apertures. These apertures were cylindrical tubes on the front door and on the rear panel of the furnace. Rubber bungs were smoothed to fit into both of the tubes to form a tight seal. After freezing in liquid nitrogen, holes were drilled through both rubber bungs and the rubber was allowed to warm and up and re-expand. After the rubber had reached ambient temperature, 10 cm lengths of silica glass tubing (7mm diameter) were gently forced through the drilled holes. Finally, Dow Corning high vacuum grease was smeared into the outside join between the glass tubing and the rubber to form a complete seal. When the bungs were firmly in place, any gas flowing into the furnace through the tube in the front door could only escape via the tube at the rear.

The external end of the front section of glass tubing was connected through a length of clear plastic tubing to the nozzle and needle valve of a cylinder containing Argon. The external end of the rear section of glass tubing was connected via plastic tubing to the inlet section of a distillation train. A similar Os distillation unit, comprising three cylindrical traps, has been described by Schoeller and Powell (1955) and Tredoux (1990). Individual 15 ml volumes of 4M NaOH, methanol and toluene were placed in the three traps and the distillation train was reassembled.

A single crucible containing irradiated metals was placed into the centre of the furnace at 1000°C. The furnace doors were closed, the valve to the argon cylinder was opened and argon was allowed to flow through the furnace to form both an inert atmosphere for any reactions taking place in the crucible and also an inert carrier gas for any gaseous products released from the melt. The argon, plus any gaseous products passed through the furnace, through the traps, and were vented to the fume hood. Argon was passed over the melt continuously for 90 minutes. At the end of this time, the valve to the argon cylinder was closed, the furnace was opened and the crucible removed.

The liquid contents of each trap were poured into individual 22ml vials and sealed. The vials were then inserted into the centres of marked counting bottles

(see Figure 6.17) and the activities of any metals present in the traps were determined on a Ge(Li) detector. Each bottle was counted for 60 minutes using the same sample:detector distance as was used for the initial count of the irradiated metals. This distance has the effect of minimizing differences in vertical geometry (see Figure 6.17) between the liquid fractions and the small irradiation vials. The measured activities of noble metals in each trap, calculated as a percentage relative to the activity initially added to the sample mixture, are shown in Table 6.10.

Table 6.10 : Percentage activities† of noble metals found in the liquid traps expressed relative to the initial activity of the metals added to the sample mixture.

		Trap 1 (NaOH)	Trap 2 (Toluene)	Trap 3 (Methanol)
Expt. 1 SA(C/S)	Os	7	14	n.d.
	Ir	3	9	1
	Pt	4	10	2
	Pd	2	7	n.d
		(Toluene)	(Methanol)	(NaOH)
Expt. 2 WA(D/C)	Os	19	4	n.d.
	Ir	23	6	2
	Pt	13	5	n.d.
	Pd	9	4	n.d.
		(NaOH)	(Toluene)	(Methanol)
Expt. 3 WA(D)	Os	28	4	3
	Ir	2	>0.5	n.d.
	Pt	n.d.	n.d.	n.d.
	Pd	n.d.	n.d.	n.d.

$$\text{† \% activity} = \frac{\text{activity of PGE in trap}}{\text{activity of PGE initially added to melt}} \times 100\%$$

6.5.3. Discussion.

Table 6.10 shows that in the case of experiments 1 and 2, where carbon was present in the melt, each of the PGE under investigation became volatile and

were carried from the melt into the traps. Significantly more PGE were mobilized in the WA(D/C) experiment than the SA(C/S) experiment, which is in agreement with the analyses of the solid melt phases shown in section 6.4. In experiment 3, where the melt was allowed to degas without carbon or sulphide present, Os was very strongly mobilized from the melt into the NaOH trap while Ir showed very much less mobility. Pt and Pd were not detected in any of the traps under the conditions of experiment 3. This observation that losses of PGE increase in the order Os » Ir > Pt, Pd is also in accord with losses calculated from the solid phases.

The preferential trapping of Os in the NaOH trap during experiment 3, coupled with the lack of reducing species (carbon or sulphur) in the melt is highly suggestive that the Os may have been lost as OsO_4. In the experiments which employed carbon in the melt, most of the trapped Os was present in the toluene fraction, which,as outlined above, is more suggestive of a non-polar and possibly organometallic compound.

In experiments 1 and 2, the relative positions of the NaOH and toluene traps were altered to see whether any differences in behaviour could be observed with either the toluene or the NaOH as the first trap in the train. It was observed that the majority of the noble metals were trapped in the toluene fraction regardless of whether it was used as the first trap or not. In experiment 2, where toluene was used in trap one and NaOH was used in trap three, Table 6.10 shows that the toluene removed most of the trapped Os, Ir, Pt and Au, methanol removed almost all of the rest and only a small amount of Ir reached the NaOH trap.

The results of experiments 1 and 2 strongly indicate that whatever chemical species is transporting the noble metals from the carbon-spiked melts into the traps, is clearly more soluble in the non-polar toluene than in any of the other liquids. This is strongly suggests that the transporting species itself may be non-polar.

6.6. Infrared Spectroscopy On The Organic Fraction.

6.6.1. Introduction.

Graphite added to the initial sample mixture provides the most obvious source of carbon for any volatile organometallic PGE compounds. Because carbon is added to the mixture in a very simple form, it seems highly likely that carbon

compounds generated in the melt will also be very simple compounds. Simple di-elemental species such as the oxides CO and CO_2, the sulphide CS_2, or methane (CH_4) are the most obvious candidates.

Both CO and CO_2 have been detected in the gases evolved from cooling melts so it is clear that they are present. Gibbs free energy calculations show that the reaction between C and S to form CS_2 is not thermodynamically favoured below 820°C. Furthermore, the reaction is strongly inhibited by the presence of any chalcogenide metals (Ni, Cu, Zn, Fe) which deplete the sulphur concentration by forming sulphides at much lower temperatures. It therefore seems unlikely that much CS_2 will be generated in either the (C/S) experiments where nickel and sulphur are present in excess, or in the (D/C) experiments where sulphur concentrations in the melts are low. Whether CH_4 occurs in the melts is not known at present but it seems unlikely given that the experiments were carried out under low pressure (French 1966; Karzharvin and Vendillo 1970) and that an obvious source of hydrogen (as opposed to H_2O) in any of the melt components is lacking. It would therefore appear that CO_2 and smaller quantities of CO are the most likely gases in the melt.

The question then arises; how might any of the above species influence the volatility of the PGE ? Reactions between CO_2 and the PGE are not known (Cotton and Wilkinson 1980). Organometallic PGE compounds with methyl (CH_3) groups are known but can only be prepared in solutions in the presence of very strong reducing agents such as pure alkali metals (Cotton and Wilkinson 1980; Greenwood and Earnshaw 1984; Crabtree 1988). Gas phase reactions between the PGE and CH_4 are not known to produce any volatile products. In contrast to both CH_4 and CO_2, CO can form volatile compounds with the PGE and reactions forming carbonyls or related species do seem to offer the most likely explanation for the experimental observations thus far.

If carbonyls or carbonyl-like compounds are the non-polar species involved in the transport of the noble metals, the presence of characteristic carbonyl absorption bands (1600-1750 cm^{-1} for bridging carbonyl groups and 1950-2100 cm^{-1} for terminal carbonyl groups) recorded from an infrared (IR) spectrum of the toluene fraction would provide very strong evidence for such a mechanism. The experiments outlined in section 6.5 were therefore repeated using inactive Pt and Ir and the toluene fraction was analysed by an IR spectrometer. The sample

matrix and the order of the traps was the same as that outlined in experiment 2 on Table 6.10. The Pt and Ir were added to separate sample mixtures and separate reactions were carried out for the two metals in order to determine any differences in their behaviour.

6.6.2. Infrared Analysis Of The Toluene.

In an attempt to minimize any delays between sample preparation and IR analysis, the samples were analysed using a JASCO 5000 FT/IR spectrometer in the Department of Chemistry of the University of the Witwatersrand. Under this arrangement, samples were prepared and within 10-20 minutes (the time taken for transport between the radiochemistry lab at Schonland Centre and the Chemistry Department, and to get the IR cell ready) could be loaded into the spectrometer, ready for analysis. The spectra of the toluene containing Pt and the toluene containing Ir, run against a reference cell containing pure toluene are shown in Figure 6.19.

Figure 6.19(a) shows Pt toluene sample 23 minutes after sample preparation. The spectrum reveals the presence of absorption bands between 920 and 1150 cm^{-1}. Uncertain baseline corrections with the pure toluene reference give the appearance of negative peaks either side of this region. Small peaks at 2890, 2974 and 3622 cm^{-1} are also present.

The spectrum recorded from the Ir toluene sample 25 minutes after preparation (Figure 6.19(b)) shows the presence of very small peaks at 1720 and 2050 cm^{-1} which were not present in the spectrum from the Pt toluene sample. These peaks might indicate the presence some kind of Ir carbonyl species in the toluene but if so, the carbonyl compound (or compounds) is not very abundant. Very strong absorption bands between 920 and 1150 cm^{-1}, a complex multiplet of positive and negative absorptions between 2890 and 3015 cm^{-1} and a small peak at 3626 cm^{-1} are also evident.

The toluene used for in the traps was not distilled, nor was it as fresh as the toluene which was used in the reference cell. When the blank trap toluene was run against the clean toluene in the reference cell, strong absorptions were found between 920 and 1150 cm^{-1}, between 2876 and 3018 cm^{-1} and at 3625 cm^{-1}. The spectrum of the trap toluene is shown in Figure 6.20. This indicates that many of the absorptions noted in the Pt and Ir sample spectra were related to species

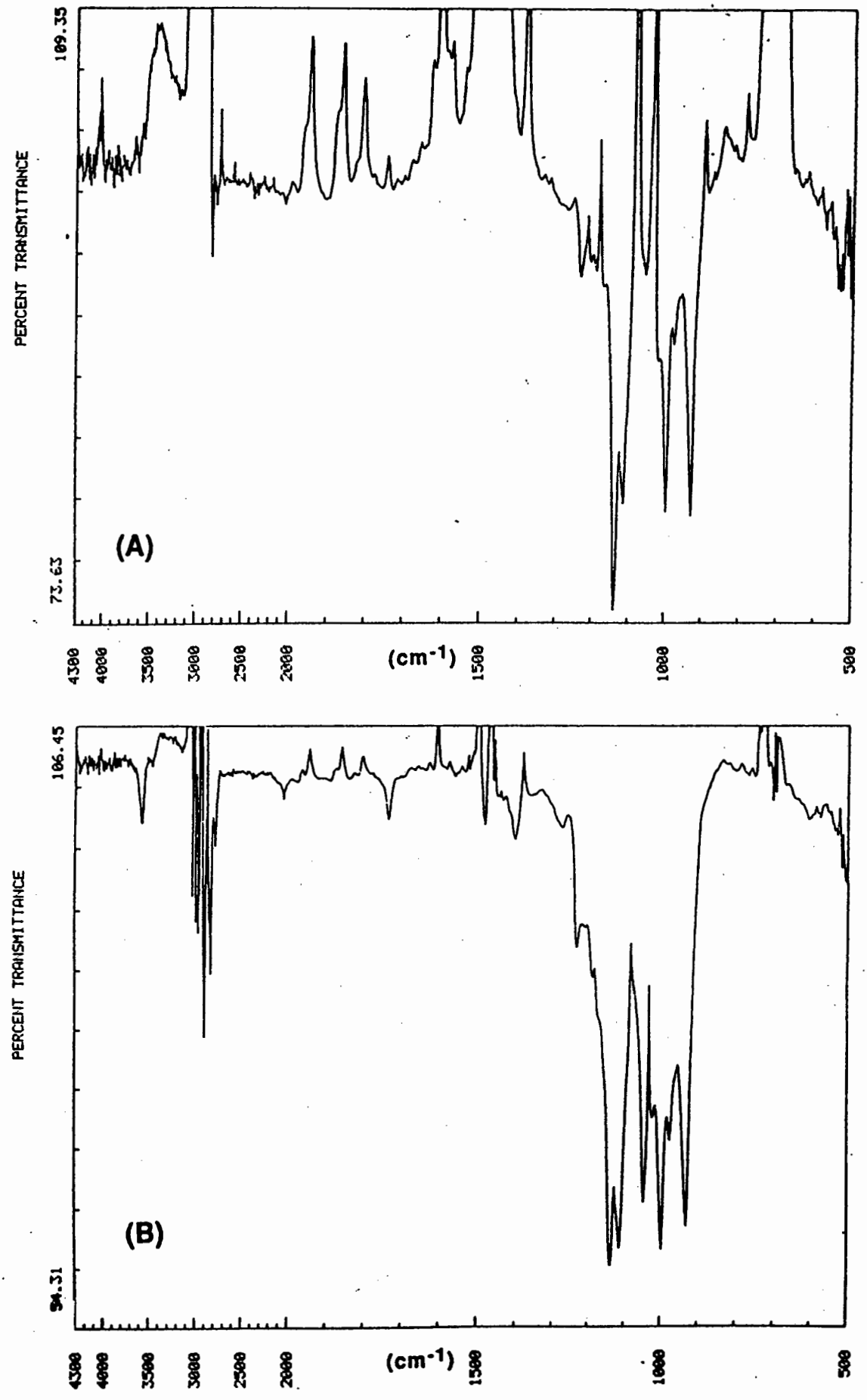

Figure 6.19: FT/IR spectra recorded from (a) the "Pt" toluene fraction; and (b) the "Ir" toluene fraction, 25 minutes after sample preparation.

present in the trap toluene itself. The only peaks in the Ir toluene sample apparently not present in the trap toluene are those at 500, 1428, 1740, and 2050 cm^{-1}.

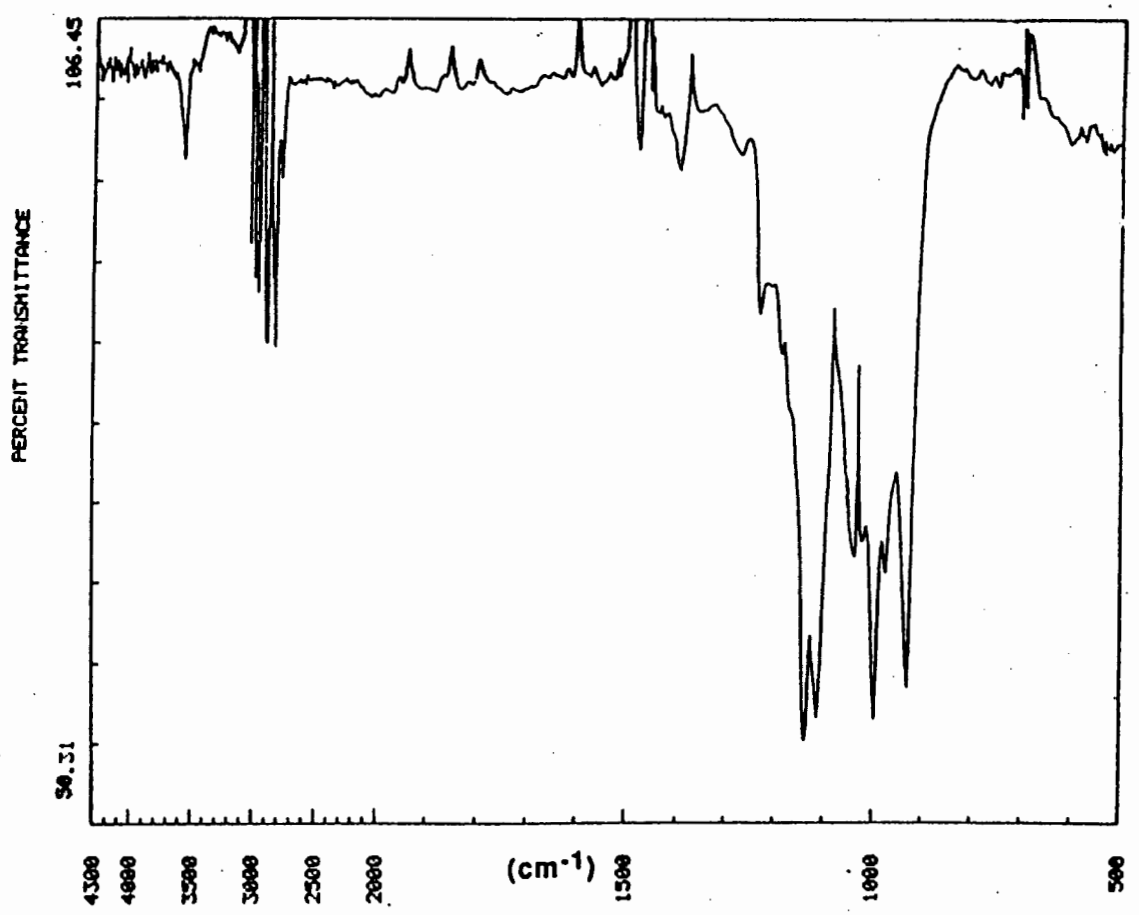

Figure 6.20 : FT/IR spectra recorded from the trapping toluene run against a reference cell of distilled toluene.

The obvious question is; what could be causing this absorption in the toluene? The peak at 3625 cm^{-1} is suggestive of an aryl or aromatic alcohol. The structure between 2870 and 3020 cm^{-1} may be due to a shift to lower energies in C-H bond vibration on the aromatic ring due to substitution of other functional groups on the ring (van der Mass 1972; Smith 1979) Substitution of aromatic rings by other groups in the 1:3 or 1:3:5 poistions can cause absorptions between 900 and 1100 cm^{-1} but much stronger absorptions between 700 and 800 cm^{-1} would also be expected (Grassell and Ritchely 1975). If the species were carboxylic acids, very strong absorption between 1220 and 1300 cm^{-1} should be present. Benzoate compounds may be ruled out for similar reasons. Aromatic ortho ketones have characteristic absorptions between 1610 and 1655 cm^{-1}, which are not observed.

The only likely species with strong absorptions in the 920 to 1150 cm region, with a lack of peaks at higher frequencies, is an ether, perhaps with the oxygen atom serving as the bridge between two aromatic rings. From the complicated nature of the spectrum, it seems possible that a complex mixture of species, perhaps alcohols and ethers, may be present in the trap toluene.

If the small, anomalous peaks at 1720 and 2050 cm^{-1} in the Ir toluene sample do represent the presence of carbonyl species and if their concentrations are relatively low, this could indicate that either; (1) carbonyls are present but are a relatively minor species; or (2) carbonyls were initially present in larger amounts but were unstable and have broken down to other species due to oxidation. Although the samples were sealed and protected from light during transport to the spectrometer, decanting of the toluene from the trap into the sample vial was carried out in air, and this certainly offers the possibility of oxidation.

A means by which the second possibility could be tested was to try to record a spectra as quickly as possible, in the hope of seeing a greater concentration of carbonyl species, and then to observe the variation in the intensity of the 1720 and 2050 cm^{-1} peaks with time. In order to minimize oxidation prior to analysis, the entire toluene trap was removed from the distillation train and the inlet and outlet pipes were sealed from the air with vacuum grease. The trap was then packed in ice, to try to slow down any carbonyl decomposition, and driven to the Chemistry Department to minimize the delay before measurement. Only once the sample reached the spectrometer, was the trap opened and the toluene extracted. IR spectra from the Ir sample recorded 8 minutes, 12 minutes and 30 minutes after the end of sample preparation are shown in Figure 6.21.

The spectrum recorded 8 minutes after sample preparation (Figure 6.21a) shows the presence of sharp peaks at 1723 and 2058 cm^{-1} which are visibly more intense than those seen in the spectrum recorded after 25 minutes. With time, these peaks decrease in intensity until after 40 minutes, the peak at 2050 cm^{-1} can no longer be resolved from the background and only a very small 1724 cm^{-1} peak remains. A similar experiment was carried out with the "Pt" sample. No carbonyl peaks could be resolved from the background even with the use of a more rapid measurement.

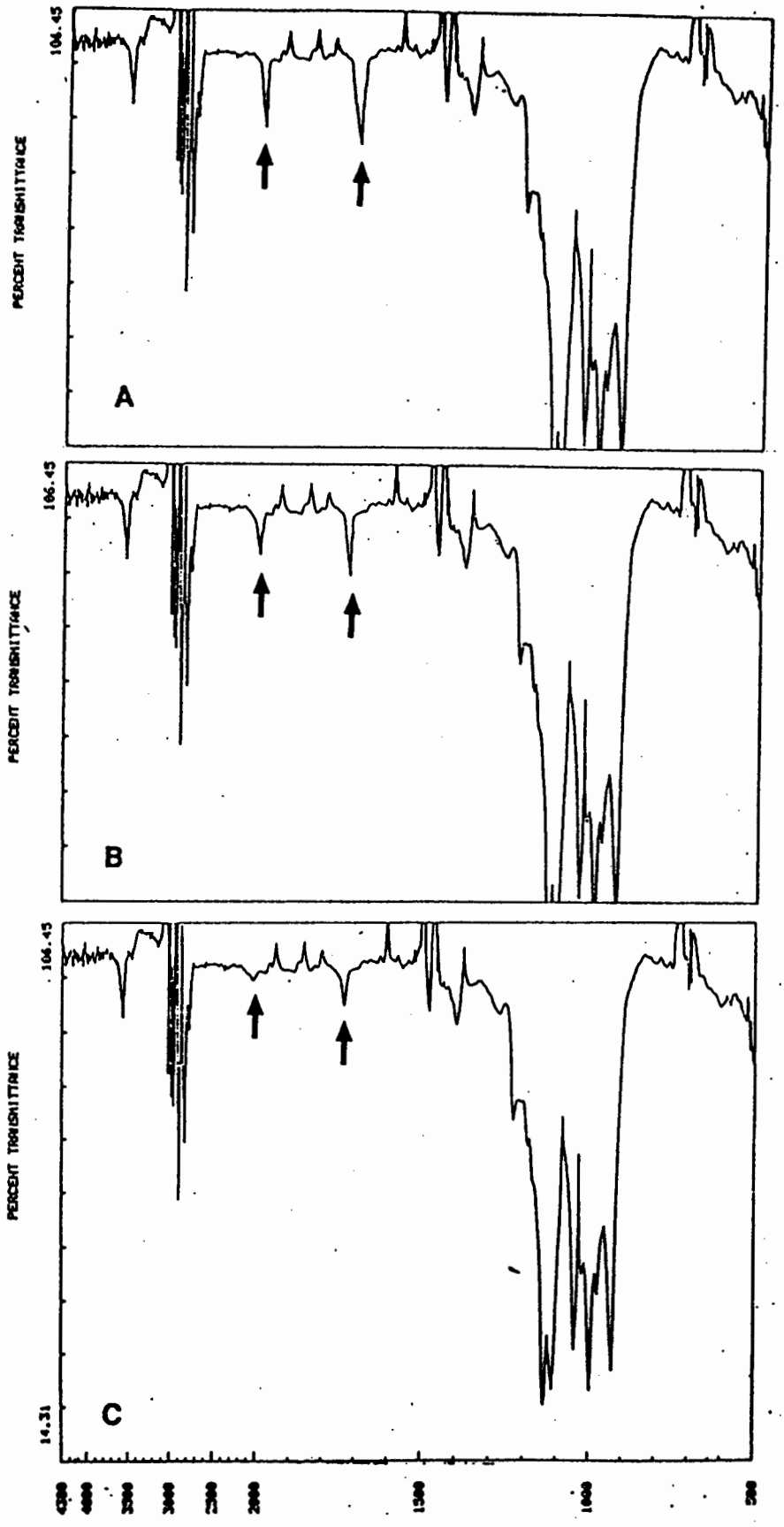

Figure 6.21 : FT/IR spectra recorded from the "Ir" toluene fraction after (a) 8 minutes; (b) 12 minutes; and (c) after 30 minutes. All of the spectra are shown to the same scale. Peaks at 1724 and 2050 wave numbers are indicated with small arrows and are seen to decrease in intensity with time.

The variation of the intensity of the 1723 and 2058 cm^{-1} peaks with time contrasts sharply with the constant nature of the other absorptions and strongly indicates that the two sets of peaks are not related. The constant absorptions between 920 and 1150, between 2870 and 3020 and at 3625 cm^{-1} arise from relatively stable species, while the peaks at 1723 and 2058 cm^{-1} are produced by species which are much more reactive.

The possibility that some Ir carbonyl species are present in the toluene fraction after the trapping of Ir but that these species are very unstable and break down within a matter of minutes is entirely compatible with these observations. Pt carbonyls are generally much less stable than most Ir carbonyls (Tripathi et al. 1976; Pruchnik 1990) and it is likely that, if any were originally present, they might have decomposed prior to measurement.

In summary then, the IR spectra recorded from the Ir toluene sample which was measured within a few minutes of sample preparation reveals peaks which are suggestive that a carbonyl complex (or complexes) perhaps containing both terminal and bridging carbonyl groups may be present in the toluene. The species is/are unstable and the peaks in the carbonyl region decrease in intensity with time, eventually merging into the background approximately 40 minutes after the end of sample preparation. This observation argues for the generation of volatile Ir carbonyl compounds as a mechanism for transporting Ir from the fire-assay melt to the toluene trap No clear evidence for carbonyl absorptions was found within the Pt toluene sample but the general instability of many Pt carbonyls may play a significant role in this.

6.7. Discussion.

6.7.1. Processes Occurring During Fusion Of The Sample With Carbon.

CO_2 and traces of CO were detected in the gases exsolved from the cooling SA, WA and WP4A melts to which carbon had been added. The presence of free carbon in some of the solid products in the SA(C/S) experiments implies that incomplete reaction of carbon may have taken place in the SA(C/S) melt. In contrast, the absence of carbon in the solid products from the WA(C/S) melt (see section 6.3.1) suggests that all of the carbon originally present in the melt had reacted to form gas and that conditions may have been more favourable for the oxidation of all of the carbon.

At high temperatures, several metal oxides can be reduced by carbon to the metal and either CO or CO_2, depending on the reaction temperature and the oxide in question (Alcock 1976). Ellingham plots of free energy of reaction versus temperature, shown in Greenwood and Earnshaw (1984 p. 327), indicate that the only major oxides in the silicate melt which might be reduced to a metal form are FeO and Fe_2O_3. Trace element oxides in the rock such as Cu_2O, SnO, HgO, PbO, NiO and ZnO may also be reduced by the action of carbon at 1000°C.

$NiCO_3$ dissociates to NiO and Ni at moderate temperatures (400-500°C) and might be a possible oxidising agent but above 500°C NiO rapidly reacts with S to form the very stable Ni sulphides which comprise the final assay button. Thermodynamic calculations predict that NiO will be converted to Ni sulphides (NiS and Ni_3S_2) at temperatures 150-200°C below the temperature at which NiO reduction by carbon becomes thermodynamically favourable. In addition, $NiCO_3$ is present in both the SA and WA sample matrices, one of which has carbon in the products while the other does not. For these reasons, $NiCO_3$ does not appear a likely oxidising agent for carbon.

In this respect, the presence of Fe (without accompanying Ni and S) as tiny spheroidal particles or droplets on the walls of the assay crucible (see section 6.3.6) is significant. The reduction of FeO to Fe at 1 atmosphere, would imply that fO_2 conditions as low as 10^{-15} or 10^{-16} atmospheres of oxygen (Sato and Valenza 1980) may have prevailed in some of the SA(C/S) and WA(C/S) melts. Lee (1991) notes that as the temperature is increased, reactions between Fe oxides, carbon and CO during steelmaking generally follow the sequence shown below:

$3\,Fe_2O_3 + CO = 2\,Fe_3O_4 + CO_2$	<400°C
$Fe_2O_3 + CO = 2\,FeO + CO_2$	
$Fe_3O_4 + CO = 3\,FeO + CO_2$	
$Fe_2O_3 + C = 2\,FeO + CO$	400-600°C
$FeO + CO = Fe + CO_2$	600-800°C
$FeO + C = Fe + CO$	800-1000°C
$2\,FeO + C = 2\,Fe + CO_2$	800-1000°C

If the reduction of metal oxides, and particularly iron oxides, is responsible for the generation of CO in all of the melts then this has very serious implications for melts generated from sample mixtures which contain different amounts of these reducible oxides. A particular case in point is the composition of the SA and the WA sample mixtures. As noted previously, the SA sample mixture is extremely silica rich and contains only 10% of the amount of iron oxides and other reducible components normally present in a basic igneous rock (10-15 weight% FeO and Fe_2O_3). SiO_2 cannot be reduced by carbon unless temperatures in excess of 1600ºC are used so that once the supply of reducible oxides has been exhausted, unreacted carbon may remain in the melt. On the other hand, the analysis of Wits-1 in Table 5.2 shows that this material has close to 12 weight % total Fe. The WA sample matrix therefore has the potential to oxidise much more carbon than the SA matrix and this may explain the absence of carbon in the NiS buttons and slags produced from the WA sample matrix.

The strongly bound carbon which is present on the surfaces of the small spheroids in the SA(C/S) experiments appears to be intimately mixed with the sulphide. I believe that this reflects a coating or adsorption of tiny particles of unreacted carbon on the surface of the sulphide as the droplet which formed the spheroid descended through the silicate melt. The carbon coating may then act as an impermeable armour or membrane around the sulphide droplet which prevents the droplet mixing with the larger volume of carbon-free sulphide melt. After crystallization of the sulphide, the carbon-coated droplets retain their forms and are preserved as apparently "immiscible" sulphide spheroids within the sulphide button. This process is summarized in Figure 6.22.

As the sulphide melt cools, the physical instabilities created in the melt by the carbon-coated spheroids may act as foci for the exsolution of any carbonaceous gases trapped in the sulphide as it descends and collects. If the exsolving gases cannot escape upwards through the slag they may expand and force their way through the sulphide forming complex gas channels. The largest spheroids, which are the focus of the greatest gas activity ultimately serve as junctions between the developing gas channels. The increasing pressure as the gases exsolve may ultimately force apart the sulphide to form numerous fragments.

Carbon filled gas channels, small spheroids and fragmentation of the sulphide button were not observed in the WA(C/S) experiments and this is readily

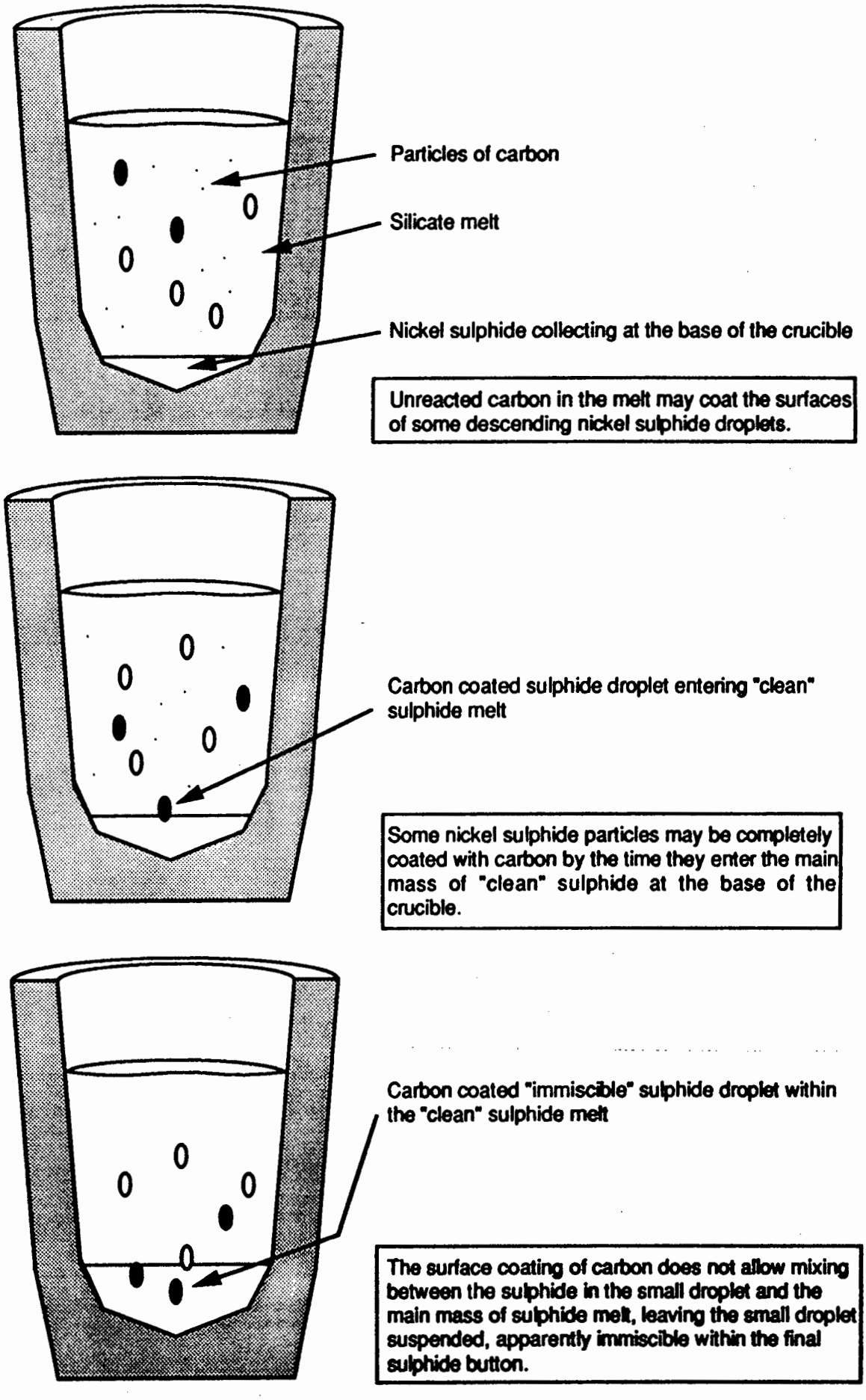

Figure 6.22: Schematic representation of the formation of immiscible carbon coated spheroids within the larger mass of nickel sulphide.

explained in terms of the above model. Firstly, the greater amount of reducible oxides present in the WA sample matrix suggests that all of the carbon initially present in the mixture may have been converted to gas, via the reduction of Fe oxides, leaving little or no free carbon to coat the sulphide droplets and form small spheroids.

Secondly, a detailed examination of the melting behaviour of the WA and SA silicate slags was made by increasing the temperature of the furnace in 10ºC steps and observing when melting took place. This indicated that the WA slag began melting at 760ºC and was completely molten by 790ºC. In contrast, the SA slag only began melting at 815ºC and was completely molten by 850ºC. Millerite (NiS) and heazlewoodite (Ni_3S_2) are important constituents of the final sulphide button (Robért et al. 1971; Lindsay 1989). If the release of any gases dissolved in the sulphide melt coincides with the crystallization of these major phases at 797ºC and 790ºC respectively, then the SA slag above the sulphide will already be solid. Any gases exsolved from the sulphide between 800 and 790ºC could be trapped beneath the slag, increasing the pressure to the point where fragmentation of the button may take place. In contrast, if gases are released between 800ºC and 790ºC in the WA(C/S) experiment, the slag is still molten and the gases may be able to escape through it, causing little or no damage to the button.

XRD spectra of carbon removed from the gas channels and of the graphite which was originally added are shown in Figure 6.23. The channel carbon spectrum shows a broad peak which is less intense relative to background and which has shifted by ~2º from the graphite peak angle. This suggests that the carbon in the gas channels may be more amorphous than the graphite. McDonald et al. (1991b) suggested that the frothy carbon present in bubbles at the sulphide-slag interface (see Figure 6.1) might reflect the decomposition of CO via the reaction

$$2CO_{(g)} = C_{(coke)} + CO_{2(g)} \qquad \text{...equation (6.1)}$$

This reaction could also explain the frothy carbon present in the gas channels. The forward reaction is favoured under high pressure (Marsh and Kuo 1989), which is implied by the the intensely pockmarked surfaces of the gas channels and by the overall level of fragmentation in the buttons, and by falling temperature (the forward reaction has a negative Gibbs free energy (ΔG) below 700ºC). There is some evidence to suggest that conversion of CO is promoted by

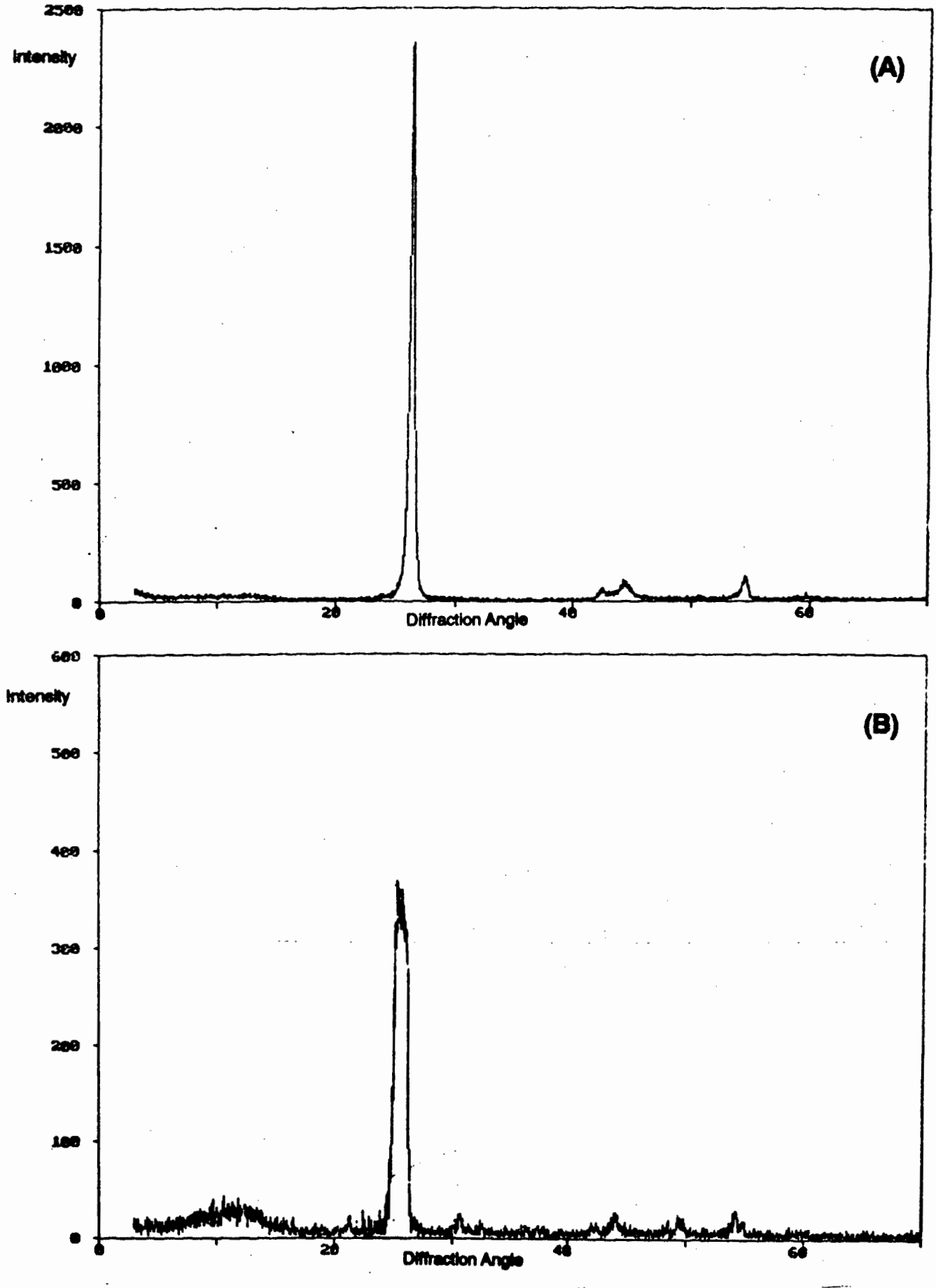

Figure 6.23 : X-ray diffraction spectrum of (a) specpure graphite; and (b) carbon extracted from the gas channels in a SA(C/S) button.

the presence of Ni (Anderson et al. 1977) and the formation of coke (amorphous carbon) from CO on catalysts is frequently linked to the presence of sulphur (Delahay and Duprez 1989).

The combination of these circumstances could drive equation (6.1) to the right, causing any CO exsolving from the sulphide mass to react, precipitating amorphous, frothy carbon on the walls of the channels. This process would explain the close association observed between the small spheroids and the frothy carbon with in the gas channels (see Figures 6.5 and 6.7). The accumulation of carbon-coated spheroids and the formation of gas channels is summarized in Figure 6.24.

6.7.2. A Model For The Removal Of The PGE And Au Into The Volatile Phase.

The most important observation is that the presence of carbon in the melt produces losses of the PGE from the melt to the vapour phase. Based on the conclusions of sections 6.4, 6.5 and 6.6, a reaction between the PGE and CO in the melt to produce volatile metal carbonyls (or related species) is considered as the most likely mechanism to explain all of the experimental observations. If we assume that carbonylation reactions are taking place, a number of additional points must also be considered before a complete model for the behaviour of the PGE and carbon in fire-assay melts can be constructed.

(1) What are the significant differences between the sulphide-rich and sulphide-free melts ?

(2) What is the nature of the reaction ?

(3) Why do the losses of the PGE decrease when >300 mg of carbon was employed in the SA(C/S) experiments whereas the WA(C/S) experiments define a smooth curve ? The reversal coincides with the first presence of gas channels and/or small spheroids; these features related ?

Taking point (1) first, the results of the (C/S) and (D/C) experiments indicate that losses of the noble metals to the volatile phase are greater in the absence of a sulphide melt. It was noted in section 6.2 that the typical values for $D_{sulphide/silicate}$ in the normal (N) fire-assay melt were between 33 and 47 for the PGE. The losses of the PGE in the (D/C) experiments suggest values for

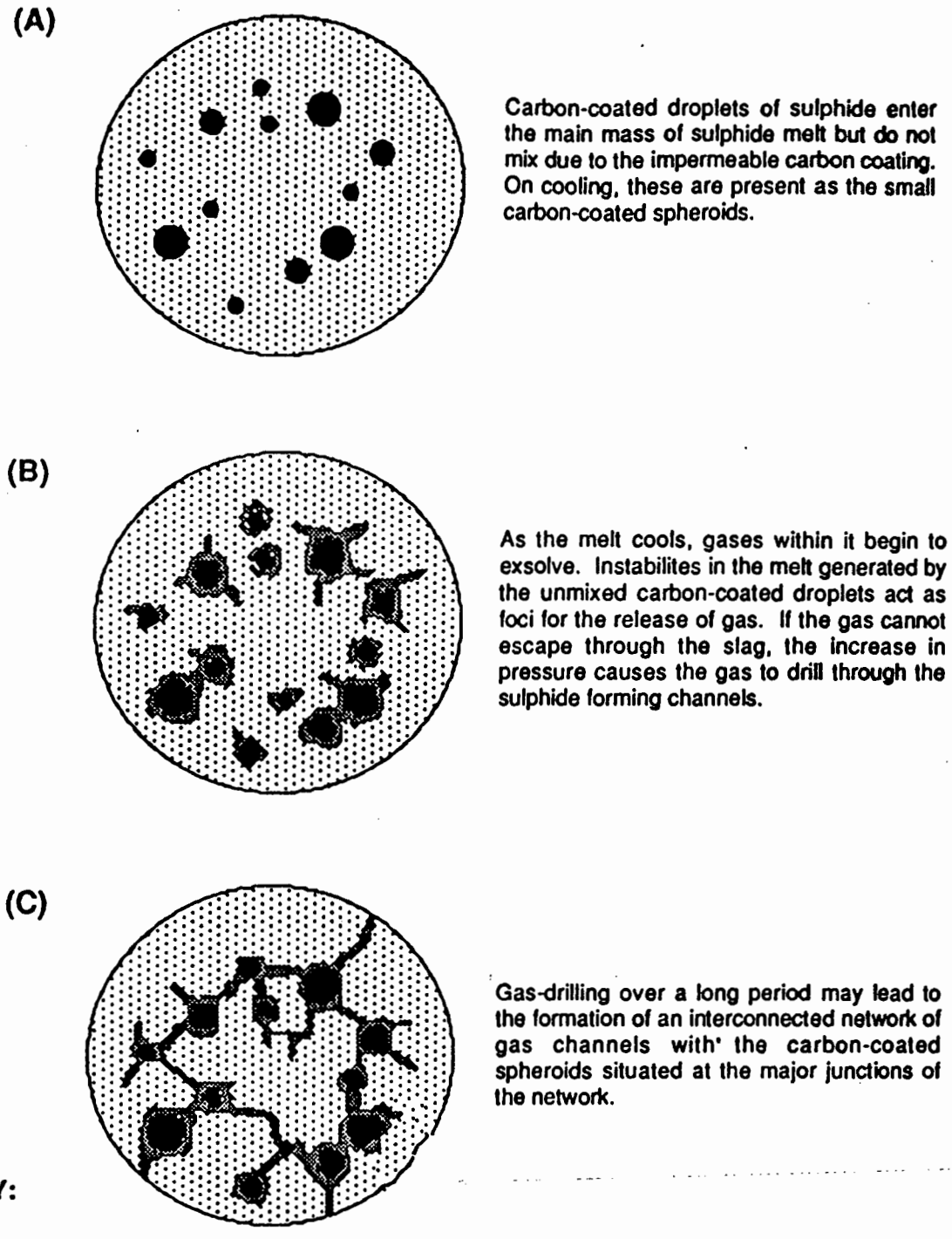

Figure 6.24: Schematic representation of the development of gas channels and ultimately a network of channels in SA(C/S) nickel sulphide buttons. The diameter of the button in this diagram is ~25mm.

$D_{vapour/silicate}$ may vary between 1.5 and 33. This suggests that sulphide collection is a slightly stronger process than removal as volatile species and that the presence or absence of immiscible sulphide will exert a strong control on the amount of PGE which might be released from the melt in this manner.

Taking point (2) now. Section 6.2 included a brief description of the model porposed by Lindsay (1989), that the PGE in silicate melts might be present in the form of electrochemically neutral, polymetallic clusters of >100 PGE atoms which suffered only physical interactions with the melt. The submicroscopic clusters would have very high surface energies which might be stabilized by the physical adsorption of chalcogenide melt components (S, As, Sb or Te) on their surfaces (Lindsay 1989). Considering the macroscopic scale, this model predicts that the PGE would act as tiny, discrete particles suspended within, but not chemically bonded to, the silicate melt.

Lindsay (1989) proposed that a physical coating of chalcogenides on a PGE cluster is the mechanism by which the cluster is physically incorporated first onto the surface and then subsequently into the bulk of a descending sulphide droplet. As discussed in section 2.5.2, carbonylation reactions are promoted by the presence of sulphur and chalcogenides. McDonald et al. (1991b) noted a possible analogy between the form of the proposed metal clusters and the reaction conditions employed in many of the earliest high temperature carbonyl syntheses. These authors speculated that, if clusters did exist, carbonylation reactions with them would be favoured by the fact that the metals were present in an extremely finely divided form.

This feature alone might allow the possibility of carbonylation reactions, producing volatile species. The chemical literature indicates that carbonylation of PGE metals prepared in the form of a black or as finely ground powder, only takes place under very high pressures of CO (10-30 MPa CO, eg. Mond et al. 1910; Hieber 1970; Greenwood and Earnshaw 1984). The clusters proposed by Lindsay (1989) might be as small as 5 nm in diameter, several orders of magnitude smaller than the finest PGE powders (particles <8 μm across). A situation closer to that observed in the carbonylation of PGE solutions (see section 2.5.2) may prevail in the melt environment and it could be this extremely fine degree of division which allows the reaction to proceed at low pressures.

For illustration, let us imagine a reaction between CO fluxing freely through the melt and a PGE cluster either floating free in the melt or temporarily exposed on the surface of a sulphide droplet (see Figure 6.22). Before the cluster is assimilated into the main mass of sulphide (and therefore isolated from the carbonaceous gas phase), CO may displace the chalcogenide species from the surfaces of the cluster by forming strong σ and π bonds to the metals. The π bonds allow a "back bonding" interaction which allows a drift of electrons from filled electron orbitals on the metal to empty electron orbitals on the carbon atom. The π bonds remain very close to neutrality (Cotton and Wilkinson 1980), thus reaction with CO can fulfil the same function as physical adsorption of chalcogenides (ie lowering the surface energy whilst keeping the whole cluster electrochemically neutral). However bonding between the metals and CO involves a *chemical* interaction which is much stronger than the postulated physical adsorption of chalcogenides.

The formation of many metal-CO bonds over the surface of the cluster and the resultant movement of charge out onto the carbon atoms may eventually weaken the intermetallic bonds within the bulk of the cluster causing it to break up into several smaller fragments. This process exposes more metal faces to attack by CO until smaller, more volatile species akin to known carbonyl compounds are formed. This is shown schematically in Figure 6.25. In the (D/C) experiments, the suggested reaction process is similar but the PGE clusters are not collected by sulphide and act as very finely divided particles dispersed throughout the silicate melt.

Turning to point (3), it is my opinion that the reversal seen in the % loss curves and the appearance of small spheroids in the SA(C/S) melt <u>are</u> related. Furthermore, the differences in the pattern of PGE losses between SA(C/S) and WA(C/S) melts might be explained in terms of the presence or absence of unreacted carbon in the melt (see section 6.7.1). Research on the properties of finely divided PGE catalysts has shown that the presence of carbon on the catalyst surfaces has a very serious effect on the ability of the PGE catalyst to complex with CO (Coughlin et al. 1982; J.G. Webb pers. comm. 1989). Carbon can be very strongly adsorbed on metal catalyst surfaces (Greenwood and Earnshaw 1984; Delahay and Duprez 1989) and once present it requires very strong heating or a prolonged reaction with hydrogen in order to remove it. Considering again the example of a PGE cluster which has been physically adsorbed and temporarily

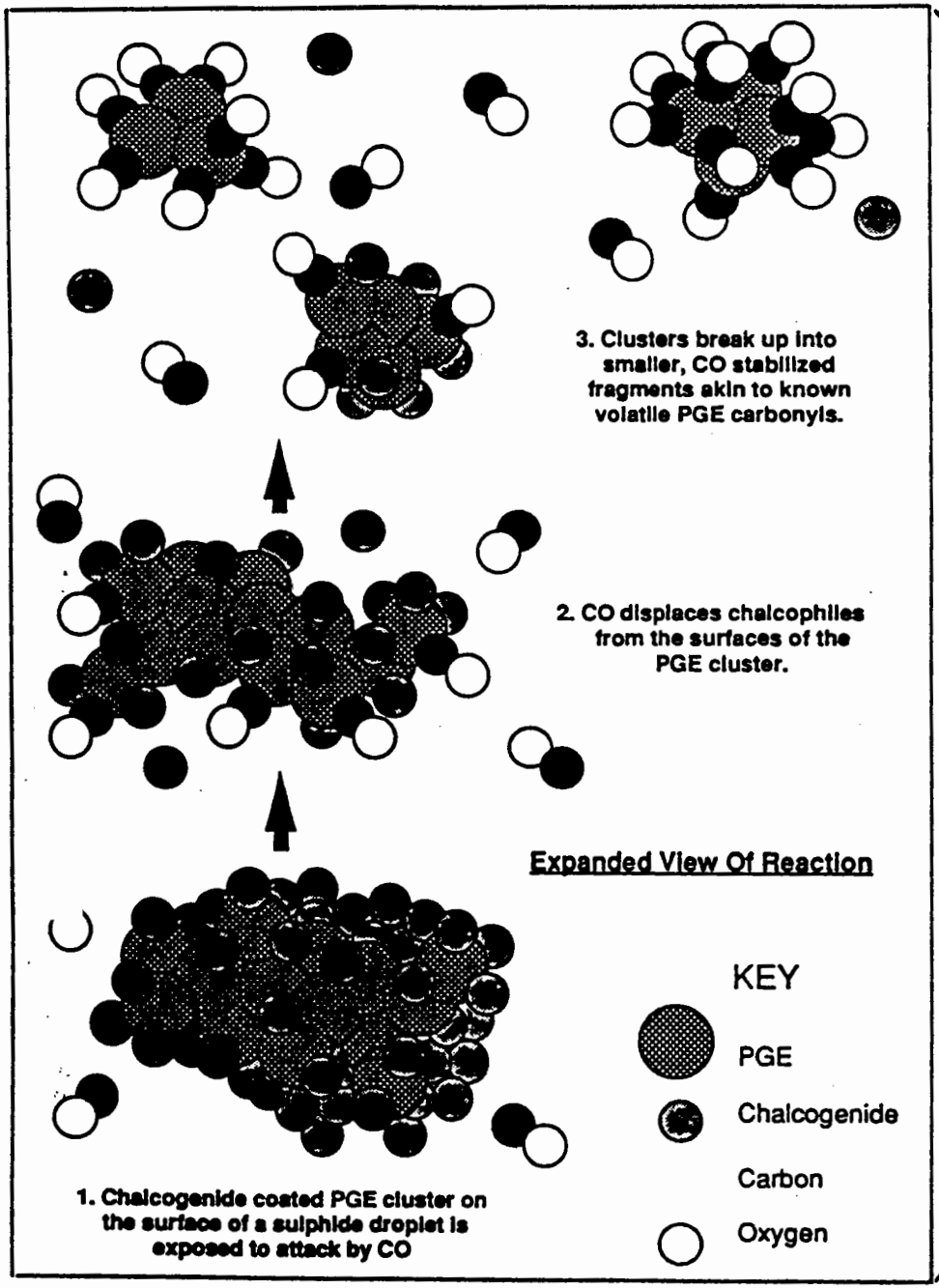

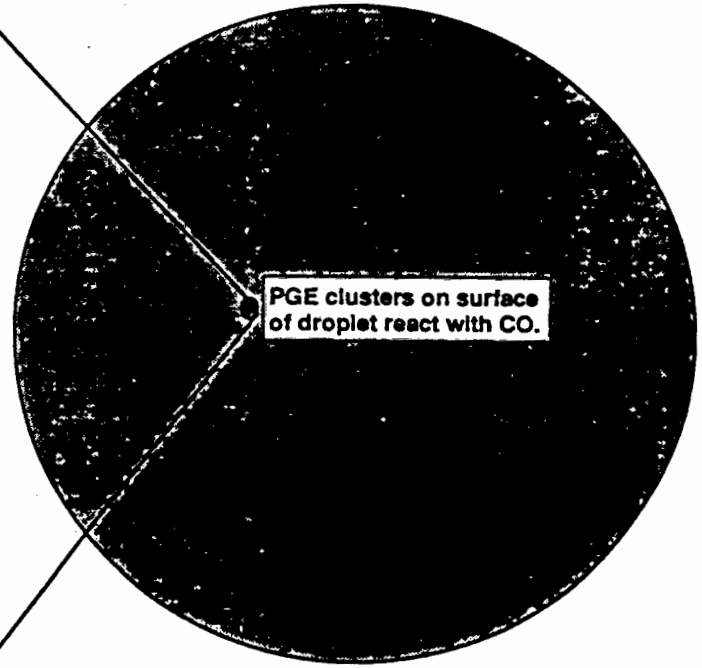

Nickel sulphide droplet descending through a melt containing a CO rich vapour phase.

Figure 6.25: Schematic representation of the possible reaction between CO and noble metal clusters on the surfaces of sulphide droplets. (after McDonald et al. 1991b)

exposed on the surface of a sulphide droplet, then this has analogies with a PGE particle on a catalyst surface.

If the surface of the droplet and the exposed cluster become coated with microscopic particles of carbon from the silicate melt, it may be much more difficult for CO to react on the surface of the PGE cluster. A coating of unreacted carbon on the surface of the cluster may then act as an armour against carbonylation, preventing or reducing any losses of the metals as volatile species and making it more likely that they will be incorporated into the sulphide button. This process is shown schematically in Figure 6.26.

This model predicts that the coating of sulphide droplets with carbon will have two related effects, namely the formation of small spheroids in the sulphide melt and the inhibition of carbonylation reactions with the PGE. It is suggested that SA(C/S) melts containing > 300 mg of carbon do not contain enough reducible oxides to convert all of the carbon to gas and some free carbon may be present to coat the sulphide droplets. In the absence of free carbon, as appears to be the case in the WA(C/S) melt, where a complete reaction between carbon and the metal oxides is believed to have taken place, neither of these effects will be observed.

6.8. Conclusions.

The experimental data presented in this chapter indicate that when carbon is present in fire-assay melts the PGE may be lost from the melt to the volatile phase. The volatilization process takes place even in the presence of NiS, which acts as a very efficient collector of the PGE in conventional fire-assay. Losses were found to greatly increase when NiS was not present, indicating that large amounts of PGE might be mobilized from sulphide-poor melts.

Radiotracer experiments indicate that the volatile PGE species generated from the carbon-bearing melts can be preferentially trapped in organic solvents. IR analysis of the solvent indicates the presence of weak carbonyl peaks. It is proposed that CO may be generated during the fire-assay process and that this may complex with PGE in the melt, forming volatile carbonyl species which are then released along with the other gases (CO and CO_2). The possible application of this model to the generation of volatile PGE species in real igneous melts is discussed in the next chapter.

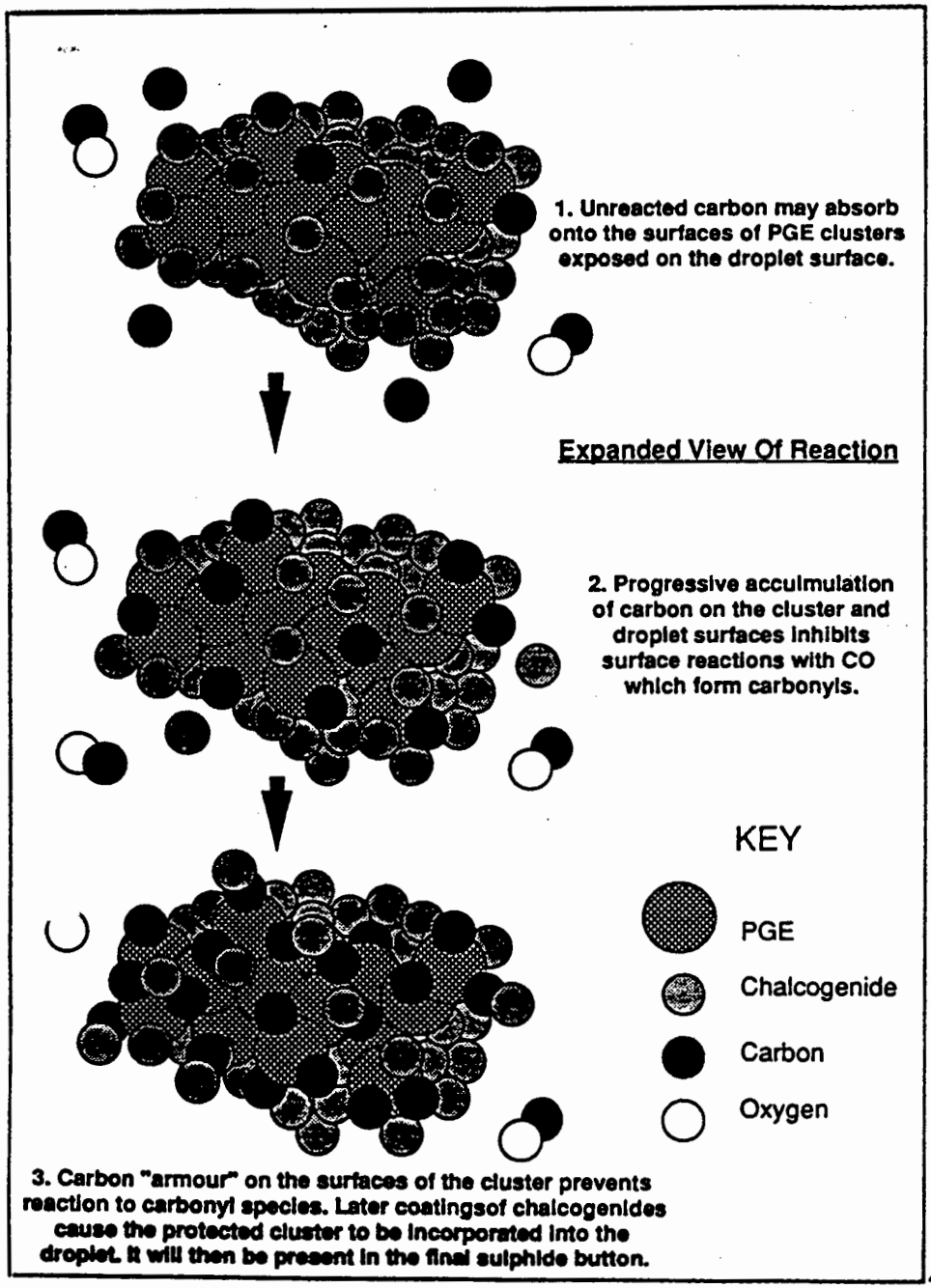

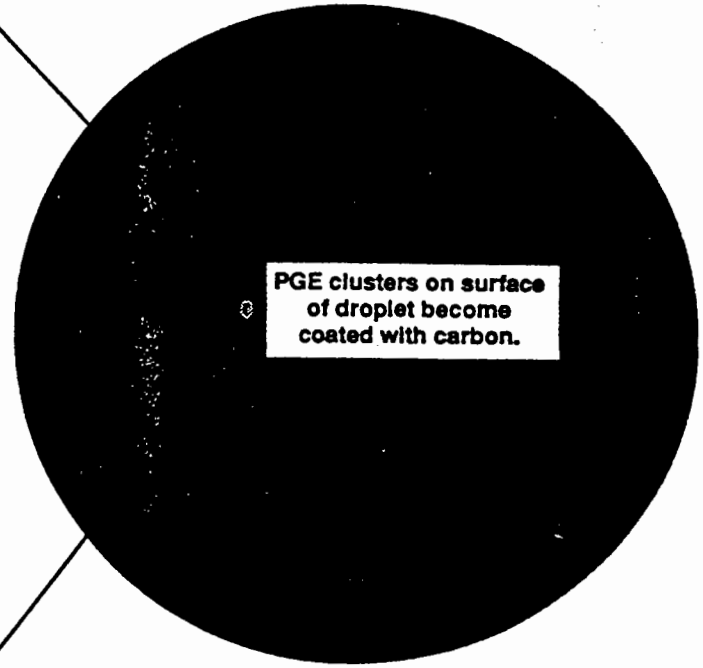

Nickel sulphide droplet descending through a melt containing a CO rich vapour phase and unreacted carbon.

Figure 6.26 : Schematic representation of "carbon armouring" of noble metal clusters when unreacted carbon is present in the melt. This effect may deactivate the cluster with respect to carbonylation reactions.

Chapter 7

Discussion Of The Possible Role Of Reactions Between Carbonaceous Volatiles And The PGE In Natural Igneous Melts.

7.1. Introduction.

The experimental data presented in chapter 6 indicate that the PGE may be converted to volatile species (apparently carbonyls or related compounds) at atmospheric pressure, when carbon is allowed to react with the melt at low pressures. Fractionation of the PGE via the carbonylation reactions at atmospheric pressure inferred in chapter 6 follows the order Ir > Rh ~ Os > Ru ~ Pt > Pd. The purpose of this chapter is to evaluate whether the possible presence of CO in igneous melts under various conditions might have led to transport of the PGE from the melt into the vapour or the fluid phase.

7.2. The C-H-O System In Melts At High Pressures And Temperatures.

In the system C-H-O, CO and H_2 are generally only important species at high temperatures (>750ºC) and low pressures (0.1-1 MPa) (French 1966; Marsh and Kuo 1989). Even at very high temperatures (> 1200ºC), the activity of CO in melts decreases sharply as pressure rises (Karzhavin and Vendillo 1970). If large amounts of water are present in the system, CO reacts via the Water-Gas-Shift reaction shown in equation (7.1):

$$CO + H_2O = CO_2 + H_2 \qquad \text{...equation (7.1)}$$

Karzhavin and Vendillo (1970) calculated the various proportions of CO, CO_2, H_2, H_2O and CH_4 which might be in equilibrium with graphite under temperatures of 227 to 1227ºC and pressures of 0.1-500 MPa. The results of their reaction equations predicted that even at moderate pressures (>1 MPa) and high temperatures (>1000ºC), almost all of the CO and H_2 will react via equation (7.2):

$$4CO + 8H_2 = 2H_2O + CO_2 + 3CH_4 \qquad \text{...equation (7.2)}$$

In addition, the oxygen fugacities (fO_2) of most basic magmas and of the mantle are believed to be quite oxidised, lying close to the quartz-fayalite-magnetite (QFM) buffer (Ryabchikov et al. 1981; Mathez 1988a; Wood and Virgo 1989). Under these conditions, the dominant fluid phase components, over a wide range of pressures and temperatures, are CO_2 and H_2O. On both pressure and fO_2 grounds, it would therefore appear unlikely that CO will have much of a role to play under the pressures encountered in hypabyssal intrusions (pressure 50-100 MPa), layered mafic complexes (200-500 MPa) or in the mantle (>500 MPa), unless extremely reducing conditions (close to the iron-wüstite (IW) buffer) prevailed locally and the system was water-poor. In this section, two different rocks which might meet these criteria are examined and their PGE geochemistry is discussed with regards to the transport of the PGE via suggested carbonylation reactions with CO.

For both of the rocks under study, major element compositions were determined by XRF spectrometry at the University of Cape Town using the methodology of Norrish and Hutton (1969) and Le Roex and Dick (1981). INAA for a limited number of trace elements was carried out at Schonland Centre using the procedure outlined in Figure 5.1. The details of noble metals analysis for each group of samples are discussed in the relevant section.

7.2.1. Iron-Rich Dunites From The Bushveld Complex.

Segregations of Fe-rich pegmatoidal ultramafic rocks occur throughout the Critical Zone of Bushveld Complex (Wagner 1929; Cameron and Desborough 1964). They take the form of sheets or pipes, often with a pinched and swollen appearance, which cut across the magmatic stratigraphy (Viljoen and Scoon 1985). Wagner (1929) believed them to be intrusive Fe-rich magmas but most recent authors (Cameron and Desborough 1964; Schiffries 1982; Viljoen and Scoon 1985) believe the pegmatoids formed by the metasomatism or replacement of the earlier anorthosites and norites by a Fe-rich intercumulus melt or fluid. Four large pipes in the eastern Bushveld (Driekop, Mooihoek, Onverwacht and Twyfelaar) had very high concentrations of PGE and were among the earliest Pt deposits in the Bushveld to be exploited (Wagner 1929). Aspects of the PGE mineralization in these pipes are discussed by Stumpfl (1961) and Tarkian and Stumpfl (1975).

Mathez et al. (1989) attempted to model the earliest graphite saturated fluid phases which they expected to exsolve from the Stillwater and Bushveld magmas. Indications that Cl (as HCl) might have been an important component of the

intercumulus fluid in these intrusions comes from high concentrations of Cl in intercumulus apatite (Boudreau et al. 1986) and graphite (Ballhaus and Stumpfl 1985) and Cl-rich fluid inclusions (Ballhaus and Stumpfl 1986). Furthermore, Viljoen et al. (1986) suggested that the presence of graphite and native Cu in intercumulus veins and pipes was evidence of reducing conditions. The thermodynamic calculations performed by Mathez et al. (1989) indicated that, in the system C-H-O-Cl, the earliest fluids might be H_2O-poor mixtures of HCl, CO_2 and CO, which became progressively enriched in H_2O as the fluid temperature fell. This hypothesis is based on rather arbitrary assumptions for the activity of Cl (f_{Cl}) and for the fO_2 of the fluid, both of which are poorly constrained at present. Both of these variables will strongly affect the proportion of CO present in the fluid. However, if the assumptions made by Mathez et al. (1989) are reasonable, their modelling suggests that CO might be an important fluid phase at high pressures (300-400 MPa) under conditions of high f_{Cl} and low fO_2.

Schiffries (1982) proposed that the Pt mineralization at Driekop was formed via the transport and precipitation of PGE chloride complexes during Fe-rich metasomatism. Alternatively, Stumpfl and Rucklidge (1982) and McDonald et al. (1991b) suggested that an association between carbon and PGE in the pipes was not coincidental and that the PGE may have been transported as an organometallic compound (possibly a carbonyl). In order to examine the proposition of PGE transport in the fluid phase and possibly distinguish between the two models, five samples of Fe-rich dunite from the Driekop, Onverwacht and Mooihoek pipes were analysed for their noble metal concentrations. A non-mineralized dunite from the outer margin of the Mooihoek pipe was also analysed as a measure of the PGE background outside the mineralized zone. The mineralized samples were donated from the Wagner Collection at the University of Cape Town and represent material collected from underground mining operations during the 1920's. The marginal dunite (MD-1) was a surface sample collected by the author in 1991. Brief descriptions of the samples in hand specimen are shown at the foot of Table 7.1.

XRF and INAA data for the dunite samples is shown in Table 7.1. All of the samples were analysed for the noble metals using the method outlined in section 4.6 and the results are summarized in Table 7.2. For the mineralized samples, the results represent the mean of three 10g aliquots. These samples produced large volumes of PGE sulphides which had to be filtered after dissolution of the NiS

button and this sometimes led to problems during the folding and packing of the filter papers for irradiation. Larger masses of sample would have made this problem worse. Two 50g aliquots of sample material were employed for the analysis of MD-1. The high PGE concentrations and the sporadic nature of the mineralization (Wagner 1929; Tarkian and Stumpfl 1975) impaired the precision of the analysis in comparison to the analysis of Wits-1 (see Table 5.4). The average COV for Ir was 12%, while the COV for Os, Ru and Pd was 20-24%. Pt and Au were the least homogeneous metals with COVs of 28% and 35% respectively.

Table 7.1 : Summary of major and trace element data for Bushveld Fe-rich dunites. Major elements were analysed by XRF or gravimetric methods and are expressed in oxide weight%. Total Fe is shown as Fe_2O_3. Trace elements were analysed by INAA and are expressed in parts per million. Sample descriptions are given in the footnotes to this table.

	D-731	D-672	D-434	D-661	D-723	MD-1
SiO_2	38.07	34.43	30.50	39.08	36.57	43.43
TiO_2	4.09	2.36	2.93	5.08	1.64	0.36
Al_2O_3	4.23	1.68	0.58	1.50	1.72	1.08
Fe_2O_3*	31.67	37.03	40.83	26.61	32.67	26.02
MnO	0.55	0.67	0.49	0.36	0.44	0.53
MgO	18.61	14.24	20.06	13.86	19.11	24.17
CaO	7.66	5.87	2.89	10.75	7.10	1.92
Na_2O	0.22	0.08	0.30	0.12	0.13	0.03
K_2O	1.46	0.24	0.05	n.d.	n.d.	n.d.
P_2O_5	0.06	0.09	0.01	0.01	0.02	0.30
H_2O	1.86	1.39	0.40	0.90	0.96	0.51
L.O.I.	0.59	1.08	0.21	0.14	0.43	0.20
Total	99.11	100.16	99.35	98.41	101.02	98.53
Cr	2670	780	651	906	456	402
Ni	106	123	91	178	154	292
Co	92	103	84	113	70	162
La	1.3	2.1	1.7	1.1	1.8	7.2
Ba	49	52	31	27	23	40
Sc	6.2	4.5	2.5	3.1	3.9	5.2
As	98	84	71	45	56	17
Sb	24	31	25	11	19	10

D-731 : coarse, pegmatoidal dunite from Mooihoek, contains large phlogopite plates and brecciated chromite grains.
D-672 : coarse, pegmatoidal dunite from Onverwacht, granular texture with visible sulphide/alloy grains between the olivines.
D-434 : medium grained dunite from Onverwacht, granular texture with small segregations of amphibole and tiny sulphide grains.
D-661 : medium grained dunite from Onverwacht, granular texture with small grains of chromite.
D-723 : medium grained dunite from Driekop, granular texture with small patches of amphibole surrounding the olivines.
MD-1 : coarse to medium grained dunite from Mooihoek, slightly serpentinized, granular texture with small sulphide crystals enclosed within olivine grains.

Table 7.2. Summary of noble metal concentrations in Bushveld dunites. Concentrations are expressed in parts per billion. "n.d" indicates not detected and "n.d.a." indicates no data available for this element at present.

	Concentration Present						
	Os	Ir	Ru	Rh	Pt	Pd	Au
D-731†	1170	885	890	n.d.a.	101000	5770	2300
D-672†	900	1150	1530	n.d.a.	145000	12300	4700
D-434	59	87	214	n.d.a.	10800	1820	380
D-661	80	140	367	n.d.a.	11400	4400	600
D-723	3.5	4.1	15	n.d.a.	362	78.8	15.1
MD-1	n.d.	0.63	2.1	n.d.a.	8.0	9.3	2.2

† indicates a coarse grained pegmatoidal sample

Table 7.2 clearly shows that the pegmatoidal samples (D-731 and D-672) contain the highest concentrations of PGE, offering support to suggestions that fluids were responsible for transporting the metals into the pipe. A summary of inter-noble metal ratios is shown in Table 7.3.

Table 7.3 : Summary of inter-noble metal ratios for Bushveld dunites. Data from Table 7.2.

	Os/Ir	Ru/Ir	Pt/Ir	Pt/Pd	Pd/Ir	Pt/Au	Au/Ir
D-731	1.32	1.01	114.2	17.5	6.53	43.89	2.60
D-672	0.78	1.32	126.1	11.8	10.7	30.85	4.09
D-434	0.67	2.45	123.6	5.93	20.8	28.42	4.35
D-661	0.57	2.62	81.4	2.59	31.4	19.14	4.26
D-723	0.85	3.75	88.3	4.60	19.2	23.97	3.68
MD-1	n.a.	3.33	12.7	0.86	14.8	3.64	3.49

Chondrite normalized PGE patterns for the dunite samples are shown in Figure 7.1. Figure 7.1 and Table 7.3 show that Pt is strongly enriched relative to all of the other metals in the pipes when compared with the marginal dunite MD-1. The Os/Ir and Au/Ir ratios do not change much between the interior and the margin of the pipe but Ir is enriched over Pd and Ru in the pegmatoidal samples. The experiments carried out in chapter 6 indicated that Ir, Rh and Os should be more volatile than Ru, Pt and Pd if carbonylation reactions took place within the system. Thus there might be some support for this process when Os and Ir are compared with Ru and Pd, but not when they are compared with Pt, the most strongly enriched metal. This observation rather argues against the model

proposed by McDonald et al. (1991b; Appendix 5) which suggested carbonylation might be the primary mechanism by which the PGE were transported into the pipes.

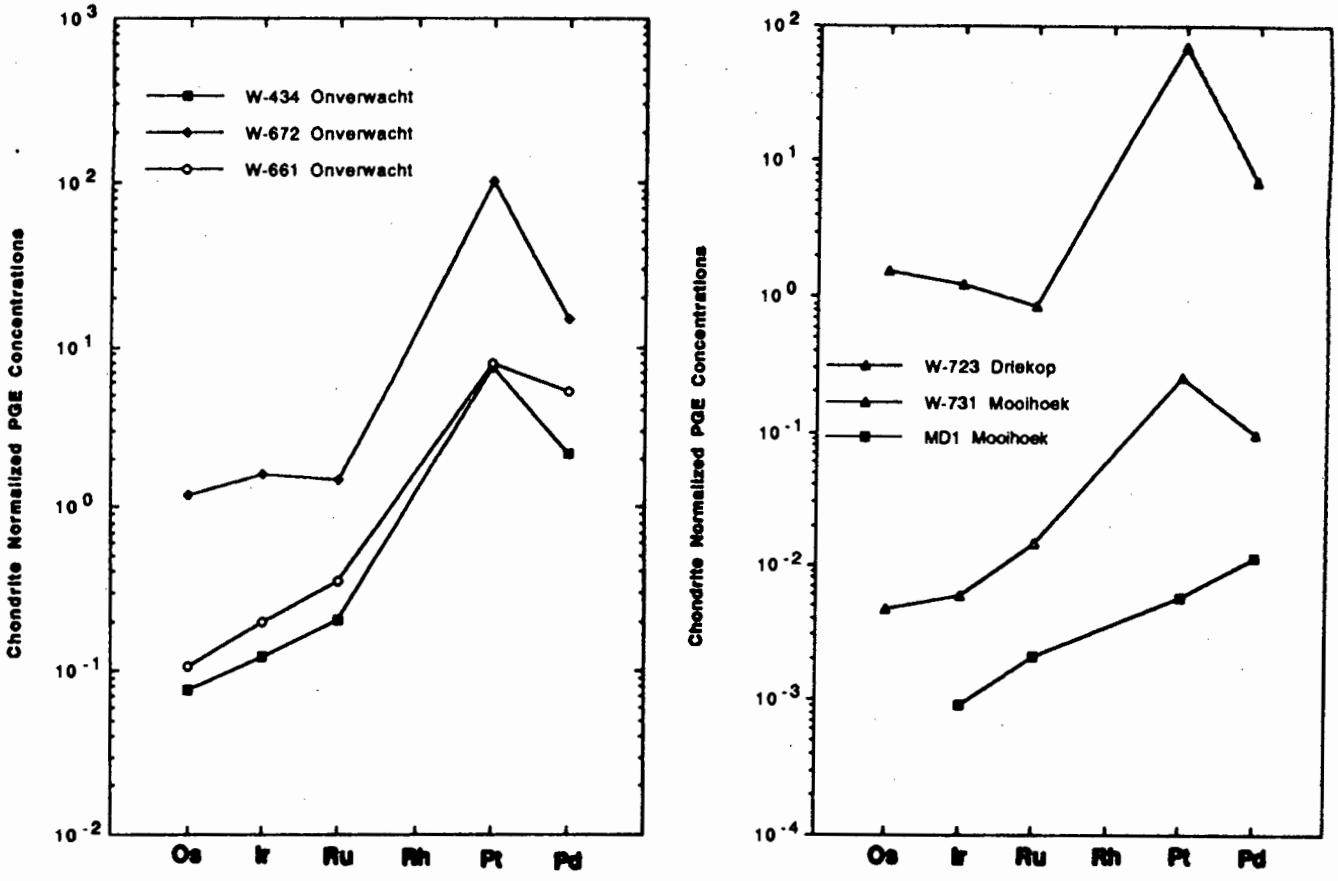

Figure 7.1. Chondrite normalized PGE patterns for Bushveld Dunites. Normalization values in ppb from Tredoux et al. (1989); Os (761); Ir (710); Ru (1071); Rh (201); Pt (1430); Pd (836).

The strong enrichment in Pt relative to all of the other metals is consistent with the model proposed by Schiffries (1982), in which the greater stability of the $Pt(Cl)_6^{2-}$ complex relative to other PGE chlorides was suggested to have acted to preferentially transport or fractionate Pt from the other PGE. However, modelling of the transport of PGE chlorides in hydrothermal solutions (eg Wood 1987; Mountain and Wood 1988; Sassani and Shock 1990) predicts that Pd species may be much more mobile than Ir and Os species. Au is also believed to be much more mobile in Cl-rich solutions than Os and Ir (Mountain and Wood 1988). Therefore the enrichment of Os and Ir relative to Pd in the pegmatoidal rocks and the lack of variation in the Au/Ir ratio between MD-1 and the pegmatoids implies that, either

Ir and Os are just as mobile, or more mobile, in Cl-rich fluids than Pd and Au, or that an additional transport process may be involved.

On the basis of the strong Pt fractionation and enrichment, the Schiffries (1982) model PGE transport as chloride species must be considered as a serious possibility. Carbonylation processes, if they operated at all, probably played a very minor role. It should be stressed that these conclusions are tentative and more analyses (preferably with Rh data) than were performed in this preliminary study, will probably be required before a better understanding of these PGE-enriched pipes can be reached.

7.2.2. Carbonate-Rich Segregations In Kimberlites.

Kimberlites are deeply-derived alkaline magmas which are rich in CO_2 and incompatible elements, and which sometimes contain elemental carbon in the form of diamond or graphite (Dawson 1980; Mitchell 1986). Mitchell (1986) presents a comprehensive review of many aspects of kimberlite geology; some of these points are contained in chapter 8 but for the purposes of this chapter we shall only be concerned with carbonaceous fluids in kimberlites. These fluids tend to be oxidised and dominated by CO_2 (Clement 1982; Mitchell 1986; Spriggs 1988). However, carbon in the form of diamond or graphite can react with (and be resorbed by) the kimberlitic melt during its passage to the surface (Wagner 1914; Wilson 1982; Meyer 1985) and may sometimes help to buffer the fO_2 towards more reduced conditions. The possibility of resorption taking place appears to be related to the speed of kimberlite emplacement and how quickly the melt cools i.e., if the melt cools slowly the chances of resorption are greatly increased (Meyer 1985).

Resorption processes may be important in large hypabyssal kimberlites, particularly sills, which appear to have crystallized slowly under moderate pressures (20-100 MPa). This may have created locally very reducing conditions, such as those described by Tompkins and Haggerty (1985), under which CH_4 and possibly CO might be important minor components of the CO_2-dominated fluid phase. PGE carbonyl compounds tend to be stable in CO-CO_2 mixtures (Hieber and Bader 1928; Hieber 1970; Pruchnik 1990). Therefore, if any CO exsolving from the kimberlite was able to react with PGE in the melt, the PGE might have been transported into the fluid phase and subsequently concentrated with the fluid when it crystallized.

Dawson and Hawthorne (1973) reported CO_2-rich fluid segregations and diapirs in the Benfontein kimberlite sill. This sill crystallized under a pressure of no greater than 50 MPa (Dawson and Hawthorne 1973) and the segregations had clearly migrated from the region of their formation and had invaded other partially consolidated layers of the sill. Such migrated segregation structures are controversial; they might represent (a) immiscible liquids (Mitchell 1984); (b) gas condensates in vesicles i.e. truly migrated amygdales (Clement 1982); or (c) vesicles which have been breached and subsequently filled with CO_2-rich fluid (Donaldson and Reid 1982). If either suggestion (b) or (c) is correct, the segregations will contain a sample of the crystallized fluid (M.B. Kirkley pers. comm. 1993).

In order to examine whether a concentration of PGE into the carbonate diapirs might have taken place in the Benfontein sill, a layer in which the diapirs comprise ~65% of the rock, and a carbonate-free olivine cumulate layer were analysed for their noble metal concentrations using the procedure outlined in Appendix 4. The olivine-rich sample was also analysed for major and trace elements by XRF and INAA (the results are shown as the "Benfontein" sample in Table 8.2 of chapter 8) and was analysed for noble metals using the "normal" fire-assay flux, while the carbonate-rich layer required the use of the "high-carbonate" flux mixture. The results are shown in Table 7.4 and in both cases, represent the average of two 100g duplicates. Typical COVs for all of the metals was comparable with values obtained for the analysis of Wits-1 (see Table 5.4).

Table 7.4 : Noble metal concentrations in kimberlite samples from Benfontein. Data is expressed in parts per billion. "n.d." indicates not detected. "n.d.a." indicates no data available for that element at present.

	Concentration Present						
	Os	Ir	Ru	Rh	Pt	Pd	Au
Bfntn-18	2.3	1.8	3.6	n.d.a.	4.8	3.5	0.84
Bfntn-carb	n.d.	0.36	1.1	n.d.a.	n.d.	n.d.	0.24

The data in Table 7.4 clearly shows that the carbonate-rich layer has much lower PGE and Au concentrations than the olivine-rich layer. This result does not appear to offer any support for carbonylation reactions, as outlined in chapter 6, operating in the fluid phase of the Benfontein hypabyssal kimberlite.

In the light of the negative results from both the dunites and the kimberlites, the suggestion of McDonald et al. (1991b) that PGE carbonyls may be important species in basic melts at moderate to high pressures and under reducing conditions, is not supported and must be viewed with caution.

7.3. The C-H-O System In Melts At Low Pressures And High Temperatures.

At low pressures and high temperatures, equation (7.2) favours the production of CO and H_2 over H_2O, CO_2 and CH_4 (Karzhavin and Vendillo 1970; Kuo and Marsh 1989) and the equilibrium at 0.1 MPa and 1227ºC is dominated by these two gases. As pressure falls, carbon-bearing melts tend to become self-reducing (Sato and Valenza 1980; Goodrich and Bird 1985) as reactions producing CO and H_2 become thermodynamically favourable.

The (D/C) experiments carried out in chapter 6 probably allow a closer comparison with melts containing a carbonaceous volatile phase which have erupted as lavas and which chill and degas at surface pressures, than with high pressure rocks. Hawaiian-type magmatism, where the eruptive style is quite gentle and magmas tend to degas close to or at the surface (Hall 1987), offers a good example of this phenomenon. Although CO_2 and H_2O are by far the most important volatile species emitted by Hawaiian basalts, CO has been detected in gases from Kilauea and from crushed basalts from which gases have been liberated under vacuum (Shepherd 1938; Graeber et al. 1979; Hall 1987). There are also other examples of volcanoes which emit high concentrations of reduced volatile species such as CO, CH_4 and hydrocarbons (Konnerup-Madsen et al. 1979; Byers et al. 1983). Karzhavin and Vendillo (1970) proposed that a variety of simple hydrocarbons (such as C_2H_4 and C_2H_6) might be synthesized via Fischer-Tropsch reactions between CO and H_2 under low pressures or from CH_4 at greater pressures, possibly employing transition metals as catalysts.

CO-rich gases may be formed from reactions with carbon already present in the melt in response to changes in pressure or from the addition of carbon to a melt at low pressure. Taking the first case, in a magma chamber at 1km depth (pressure ~30 MPa) the C-H-O equilibrium under reducing conditions suggests a gas phase dominated by CH_4, CO_2, H_2O and hydrocarbons. However, if the magma in the chamber is erupted and the pressure suddenly lowered to 0.1 MPa without a rapid fall in temperature (eg. if the hot melt were to pond in the centre of a large lava

lake), the equilibrium of equation (7.2) above, may shift dramatically towards the left, with increasing concentrations of CO and H_2 being exsolved and emitted from the melt (French 1966; Karzhavin and Vendillo 1970).

In the second case, and in a manner similar to the addition of carbon to the fire-assay charges, the lava might assimilate carbonaceous material from shallow sediments as it intrudes through them to the surface (Goodrich and Bird 1985), or even from the surface over which it flows. The incorporation of tree trunks (eg. MacCulloch's Tree in the Hebridean province of Scotland; MacCulloch 1819) or other plant material from the inter-lava horizons (Bailey and Anderson 1925; Graeber et al. 1979), by the lava would almost certainly introduce carbon into the melt. The C-H-O equilibrium predicts the generation of concentrations of significant concentrations of CO at magmatic temperatures and atmospheric pressure, which would rapidly flux through the melt and be emitted from the lava. This has been observed from lava flows on Hawaii which have pyrolized vegetation underneath them as they flowed (Graeber et al. 1979).

Under these conditions, and in the absence of an immiscible sulphide phase, it might be possible to effect a large transport of PGE into any aerosols emitted from the erupted lava. Reaction times extending over weeks or months as the lava cools from its eruption temperature (~1250ºC) to the solidus, continually pyrolyzing any incorporated carbonaceous material as it does so, might also increase the amount of PGE removed from the melt.

Removal of the PGE from the melt itself is really only half of the problem however. A mechanism to transport the metals from the source and disperse them over long distances must also be found in order to explain the observations of Koeberl (1989). While the formation of carbonyl-like species might provide a strong initial push by removing the PGE from the melt, transporting the metals much further than the immediate environment of the degassing vent or lava poses more of a problem. Due to their susceptibility to oxidation, pure carbonyls are not very stable in air and will tend to break down rapidly to the metal and CO or CO_2 (Hieber 1970; Greenwood and Earnshaw 1984; Pruchnik 1990). This makes it rather unlikely that pure carbonyls would allow transport of the PGE in air over the long distances (>1000km) implied by Koeberl (1989).

However, if carbonyls can react with some other species in the aerosol or in the melt (eg. halides or sulphur-bearing gases) to form a volatile, air-stable, derivative compound, then transport over greater distances (perhaps even 100's of km) may be possible before the species breaks down and the PGE metals are precipitated onto dust or ash particles in the aerosol. It is interesting to note that many gaseous Os, Ir, Ru and Rh carbonyl derivatives (halides, carbides, etc) are stable in air (see section 2.5.2) and could potentially remain in a volcanic aerosol for an extended period of time before being deposited.

7.3.1. Hawaiian And Antarctic Aerosols.

The most extensive studies to data of noble metal enrichment in the aerosols emitted from lavas have been made in Hawaii and in Antarctica and any working hypothesis must be examined against these observations. It should be stressed however that all of the aerosols which were studied were from basalts erupted within the main volcanic caldera (Mt. Erebus) or from spattered basalt close to lava fountains (Hawaii) which had not interacted with surface material. Therefore these observations only serve as a test of the first scenario in section 7.3, i.e. that carbonyl species might be produced in a melt whose C-H-O volatiles undergo self-reduction in response to a rapid fall in pressure.

Olmez et al. (1986) reported that Ir was 2.5 to 10 times more volatile than Au in Hawaiian aerosols. Finnegan et al. (1990) measured elemental concentrations in Hawaiian aerosols on particulate filters and found that Ir, Os and Re were among the 8 most volatile elements of the 41 which were analysed. In the case of Re and Os, only Se and S were more volatile. The order of volatility between the precious metals appeared to be Au < Ir < Os < Re and it was found that 1-12% of the Ir in the melt had been mobilized into the volatile phase.

Meeker et al. (1992) found that large amounts of Au in the aerosols from Mount Erebus in Antarctica were deposited within a few km of the vent, suggesting that Au species could be rapidly precipitated back to the metal when released into the air. Finnegan et al. (1990) found that Ir was present as both gas and particulates during their measurements. When charcoal filters for trapping gas were used in conjunction with the particulate filters, Finnegan et al. (1990) noted that up to 60% of the volatile Ir could be collected on the charcoal filters. The early stages of the eruption is the point where air is first admixed into the eruption column (Fisher

and Schmincke 1984) and it may have had a stronger influence on Au species than Ir species in the aerosol.

The remarkably high volatility of Ir, Os and Re, determined by Finnegan et al. (1990), relative to the base metals, rather argues against transport of the PGE as halide species (Wood 1987). The order of volatility among the precious metals is more comparable with the volatilities of the metals as oxides rather than as carbonyl species. OsO_4 and Re_2O_7 are more volatile than IrO_3, but Au does not form stable oxide species. The (D) and (D/C) experiments (see section 6.2.3.) carried out in chapter 6 indicated that Os was only more volatile than Ir in highly oxidised melts where there was some evidence to suggest that Os did form a volatile oxide. The Hawaiian basalts are much less oxidised than the (D) fire-assay melt but the formation of some precious metal oxides may still be possible, with any partially stable Au species breaking down very rapidly.

Alternatively, experiments have shown that Au can also be lost from fire-assay melts which have reacted with carbon in a similar manner to the PGE (McDonald et al. 1991b) and that Au showed a similar pattern of behaviour to Pd (McDonald and de Wit 1992). Au does not form carbonyl compounds easily and the few Au carbonyl species which are known are all unstable (even more so than Pt or Pd species) and react (oxidise) quickly back to the metal (Cotton and Wilkinson 1980; Pruchnik 1990). The rapid oxidation of Au carbonyl compounds followed by Au precipitation might be another explanation for the contrast in volatility between Au and the other metals outlined above.

Apart from the possibly rapid precipitation of Au from the aerosol, the present observations from Hawaii and Antarctica do not lend strong support for emission of the PGE involving carbonyl-like species from melts whose volatiles which might have undergone self-reduction. However, it is my opinion that the addition of external carbon to an erupted melt (via assimilation) offers a closer simulation of the conditions operating in the (D) and (D/C) experiments in chapter 6. Therefore much more revealing experiment would be a similar analysis to that carried out by Graeber et al. (1979) on the gases from a lava which has assimilated and pyrolized surface vegetation. Until this is carried out, the possibility that the PGE may be lost from basalts as volatile carbonyl compounds, cannot be ruled out.

7.3.2. Speculations On Volatile Ir From Basalts At The K/T Boundary.

An important area of current debate with regards volatile PGE species is whether aerosols emitted from the Deccan plateau basalts at 65 Ma could have supplied enough PGE to account for the PGE anomaly at the Cretaceous-Tertiary (K/T) boundary (see Olmez et al. 1986; Officer et al.1987; Strong et al. 1987; Finnegan et al. 1990 and Officer 1993 for a discussion). Although the release of volatile PGE species from basalts which have reacted with carbon low pressures, has yet to be proved, I believe that some speculations relevant to this debate can be made.

Finnegan et al. (1990) calculated that if the original Ir concentration of the Deccan basalts was 0.1ppb, just under 50% of the Ir needed to be mobilized to account for the 1.3×10^8 kg of Ir estimated by Alvarez et al. (1982) and Kyte et al. (1985) to have been deposited at the boundary. If the Ir concentration of the basalts was much lower, 0.02-0.006ppb (Murali et al. 1988), then 85-95% of the Ir would need to be mobilized. Based on observations from Hawaii which indicated that only up to 12% of the Ir could be mobilized from the melt, Finnegan et al. (1990) concluded that it appeared unlikely that the Deccan basalts could supply enough Ir to meet the estimated flux at the K/T boundary.

I feel that this conclusion may be premature. Firstly, the Ir mass estimate is based on the Ir abundances at the most PGE-enriched K/T sites, which Kyte et al. (1985) assumed were the most pristine. Kyte et al. (1985) did not consider the possibility that local sedimentation conditions might cause the preferential enrichment of PGE in certain areas and not others (Schmitz 1985; Schmitz et al. 1988). For example, Ekdale and Bromley (1984) and Tredoux et al. (1989b) report sites which show no Ir anomaly at all. Because the estimate made by Kyte et al. (1985) is biased towards the most PGE-enriched sites, it must serve as an upper limit for the mass of Ir deposited at the K/T boundary. Therefore the estimated quantities of Ir mobilized from the Deccan basalts by Finnegan et al. (1990) may also be overestimates.

Secondly, the Deccan basalts are continental flood basalts (Mahoney 1988) and had a much greater opportunity to interact with carbon in the near-surface and surface environment than the basalts studied in Hawaii. If this process produced losses of volatile PGE species comparable with the (D/C) experiments in section 6.4, then a high degree of Ir volatilization may be attainable. As a result of this, the present noble metal concentrations of the Deccan basalts should be extremely

low. Very low Ir concentrations, barely above detection limits, have been reported for Deccan lavas by Rocchia et al. (1988) and Murali et al. (1988).

It is interesting to note that strong evidence for a large meteorite impact in the northern hemisphere at time of the K/T boundary has recently been presented (Kring and Boynton 1992; Sharpton et al. 1992; Koeberl 1993) and PGE patterns at K/T sites in the northern hemisphere tend to be only slightly fractionated relative to chondrite (Kyte et al. 1980; Kyte et al. 1985; Tredoux et al. 1989b). In contrast to this, K/T sites in the southern hemisphere show fractionated PGE patterns which resemble basaltic patterns (Tredoux et al. 1989b). The latter authors speculated that the PGE signature in southern hemisphere may have been dominated by a local volcanic PGE source rather than an impact signature. The possibility that the Deccan basalts might have been a major source of volatile PGE, which entered the sedimentary environment in the southern hemisphere at the time of the K/T boundary, would be enhanced if clear proof of PGE enrichment in aerosols, produced from basalts contaminated with carbon, could be found.

7.4. Summary.

Thermodynamic calculations indicate that CO is not a significant fluid species at moderate to high pressures in magmas. Even considering favourable circumstances (low fO_2 and H_2O-poor fluids), no clear evidence was found for the fractionation of PGE (as predicted by the experiments in chapter 6) in Bushveld dunite pipes which are believed to have formed via the infiltration of HCl, CO and Fe-rich intercumulus fluids. Carbonate segregations, which might represent migrated fluids, in the Benfontein kimberlite are depleted in PGE relative to olivine-rich layers. This suggests that CO_2-rich fluids which formed during kimberlite crystallization do not carry elevated concentrations of PGE.

The experiments carried out in chapter 6 perhaps offer a closer analogy with basalts which have assimilated carbon and have degassed at atmospheric pressure. CO may be an important gas phase species under these conditions. The data obtained thus far from studies of volatile PGE in aerosols does not strongly support the model proposed in section 6.7, but neither do these studies rule the model out. If high concentrations of PGE in aerosols emitted from basalts contaminated with carbon can be found, it could reopen the debate on the role of the Deccan basalts as a source of (at least some of the) PGE at the K/T boundary.

Chapter 8

The Geochemical Behaviour Of The PGE In Southern African And Brazilian Kimberlites.

8.1. Introduction

Kimberlites are relatively rare igneous rocks which are produced during continental intraplate alkaline magmatism (Mitchell 1986). Kimberlites are frequently emplaced within or on the margins of ancient cratons and are economically important because they carry a wide variety of upper-mantle-derived xenoliths, including diamonds. Kimberlites are apparently derived from deeper levels of the mantle than most other magmas (Mitchell 1986; Hall 1987) and the fragments they incorporate during their passage to the surface provide a direct sample of the lithospheric mantle beneath the cratons. Figure 8.1 illustrates the idealized kimberlite magmatic system proposed by Mitchell (1986) showing the relationships between effusive rocks, diatremes and hypabyssal sills and dykes.

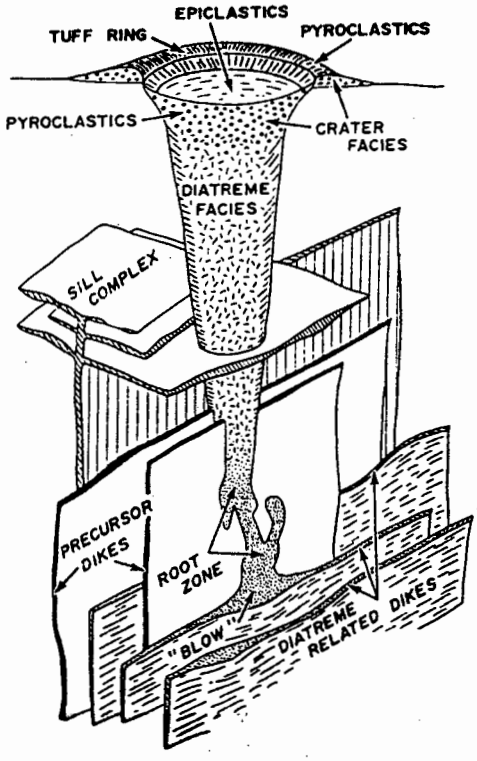

Figure 8.1 : Idealized view of a kimberlite intrusion, from Mitchell (1986).

Mitchell (1986) proposed that kimberlite diatremes form by a number of hydrovolcanic explosions 1-2 km below the surface as the rising magma interacts with groundwater. Burnham (1985) and Clement and Reid (1989) prefer a model of explosive brecciation generated by the release of volatiles (initially present in the melt) via retrograde boiling 0.5-1 km beneath the surface. Hydrovolcanic explosions are suggested to be only a minor component of diatreme formation.

Studies of PGE concentrations in kimberlites are very rare in the geochemical literature (Barnes et al. 1985). Results from Siberian kimberlites (Kaminskiy et al. 1974) do not compare at all with partial analyses of South African and Indian kimberlites (Paul et al. 1979; Tredoux 1990). The only consistent feature to emerge from these three studies was that there appeared to be a fractionation between Ir and Pd and Au during kimberlite genesis (Crocket 1981). Apart from this very general fractionation, the restricted nature of the database up to this time has precluded more detailed modelling of the geochemical behaviour of the PGE in kimberlitic melts with any degree of confidence. However, the recent refinement by McDonald et al. (1993) (see appendix 4), of an analytical procedure for the PGE based on nickel sulphide fire-assay and neutron activation analysis which offers improved limits of detection (see Table 4.7), has allowed an expansion of the present database for the PGE in kimberlites.

This chapter will offer a very brief overview of kimberlites, focusing mainly on the known differences between kimberlite types, the controversy over kimberlite source regions, the possible nature of the lithosphere beneath cratons and the role that PGE geochemistry can play in providing us with additional information on these questions. For a more comprehensive review of general kimberlite geology, the reader is referred to the studies of Dawson (1967a; b), Nixon (1973), Mitchell (1986), Dawson (1989) and Mitchell (1989).

Smith (1983) observed that southern African kimberlites can be divided isotopically into two distinct groups. These groups are broadly equivalent to the "basaltic" (Group I) and "micaceous" (Group II) kimberlites of Wagner (1914) and Dawson (1967a). In a later study, Smith et al. (1985) indicated that the two groups could also be distinguished, although less clearly, in terms of their major and trace element chemistries. Smith et al. (1985) also suggested that Group I kimberlites could be further divided into two subgroups (IA and IB), corresponding to those kimberlites emplaced into the Kaapvaal craton and those

which were emplaced outside the boundaries of the craton. On the basis of major and trace element chemistry of off-craton kimberlites, Spriggs (1988) has expressed doubts over the IA and IB subgrouping.

Isotopically, Group II kimberlites have higher $^{87}Sr/^{86}Sr$ ratios and lower $^{143}Nd/^{144}Nd$ and $^{206}Pb/^{204}Pb$ ratios than Group I kimberlites (see Figure 8.2), indicating that the sources of Group II kimberlites are characterized by time averaged LREE enrichment and elevated Rb/Sr and Pb/U ratios relative to the sources of Group I kimberlites. Smith (1983) and Hawkesworth et al. (1983) concluded that the source region for Group II kimberlites experienced an ancient metasomatic enrichment event (with a minimum age of at least 1.4 to 1.0 Ga) which had not affected the source regions for the Group I kimberlites.

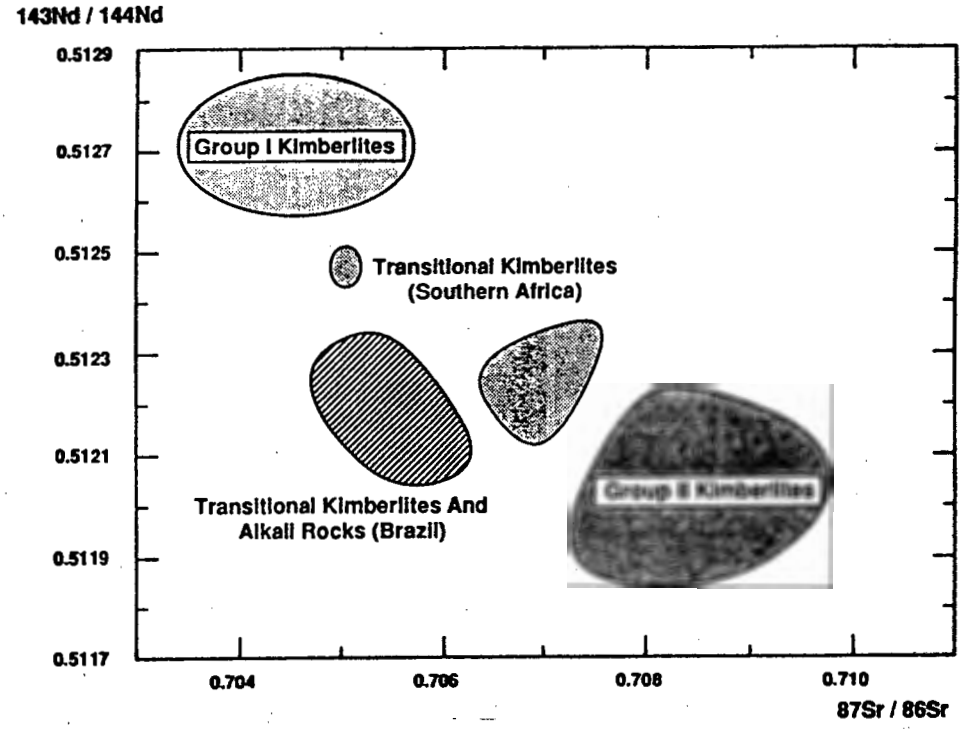

Figure 8.2.: Sr and Nd isotope plot showing the fields for Group I, Group II and transitional kimberlites (after Smith 1983; Skinner et al. 1993 and Bizzi et al. 1993b)

Recently, kimberlites which show signatures isotopically *transitional* between Groups I and II have been discovered bordering the margins of the Kaapvaal craton and the Sao Francisco craton in Brazil (Clark et al. 1990; Skinner et al. 1993; Bizzi et al. 1993a; b). In addition, one kimberlite (Lace) from the interior of the Kaapvaal craton has also been shown to have less radiogenic Sr and more radiogenic Nd than typical Group II rocks, suggesting that transitional kimberlites

are not always restricted to the craton margins (Skinner et al. 1993). Clark et al. (1990) suggested that the transitional kimberlites represent some mixing or contamination between the Group I and Group II source regions.

The nature and the positions of the kimberlite source regions relative to one another is still highly controversial. The first models proposed by Smith (1983) and Smith et al. (1985) suggested that Group I kimberlites have their source within the asthenosphere and Group II kimberlites originate within a region of the lithospheric mantle which has suffered an ancient enrichment event. Alternative models suggested by Le Roex (1987) and Spriggs (1988) proposed that both kimberlite groups originate within the asthenosphere, and that the differences can be explained in terms of melting processes or interaction with the lithosphere. Models which place both Group I and Group II source regions within the lithosphere have also been proposed (Skinner 1989; Smith et al. 1992; Skinner et al. 1993).

Tredoux (1990) expressed the belief that PGE geochemistry has the potential to provide important information on mantle processes which are not reflected in lithophile element geochemistry. In particular, Groves et al. (1987) and Tredoux et al. (1989) have suggested that the lower lithosphere may contain elevated concentrations of the PGE which might be reflected in kimberlites generated in or which pass through this region. With this in mind, it was hoped that an investigation of PGE concentrations in kimberlitic and alkalic rocks might be able to shed new light on some of the uncertainties over kimberlite source regions outlined in the previous paragraph.

During the course of this thesis, 32 samples of hypabyssal kimberlite, hypabyssal melilitite and effusive alkali basalt were analysed for the noble metals. Twenty four samples were taken from the interior, the margin and from outwith the southern African Kaapvaal craton, while the remaining samples came from the margin of the Brazilian Sao Francisco craton. Both cratons have geological histories which extend into the Archean (> 2.5 Ga) (Almeida 1977; De Wit et al 1992; L. Bizzi unpubl. data) In carrying out PGE and Au analyses on this suite of samples, it was hoped to provide some information on the following:

(1) To check the existing PGE data obtained for southern African kimberlites by Paul et al. (1979) and Tredoux (1990). This would confirm or deny the apparently

lower PGE concentrations seen in these samples compared with Siberian kimberlites and whether any significance can be drawn from this.

(2) Whether differences in terms of PGE concentrations are observed between Group I and Group II kimberlites, similar to those seen for isotopes and lithophile elements.

(3) If differences do exist, whether they provide any additional information on kimberlite source regions.

(4) Whether there are significant differences in terms of PGE concentrations between kimberlites emplaced into the craton and those emplaced off the craton.

(5) To examine the PGE budget and the nature of the lithosphere beneath the two Archean cratons. Groves et al. (1987) and Tredoux et al. (1989a) have proposed that the lower lithosphere of ancient cratons may contain elevated concentrations of the PGE. Kimberlites originating in or passing through these regions might indicate some evidence for the proposed PGE reservoir.

8.2. Geological Settings Of The Kimberlites And Alkaline Rocks.

8.2.1. Kaapvaal Craton And Western Margins, Southern Africa

The Archean tectonic evolution of the Kaapvaal craton up to its stabilization at 2.6 Ga has recently been reviewed by de Wit et al. (1992) and de Wit and Hart (1993). After cratonization, early-mid Proterozoic sedimentary sequences accumulated on the craton and underwent mild deformation. Along the margins, Proterozoic sediments and volcanics were transported via thrusting onto the craton. Tectonothermal events of the Natal-Namaqua Mobile Belt (NNMB) affected the southern and western margins of the Kaapvaal craton between 2.0 and 1.0 Ga (Tankard et al. 1982). The region of the NNMB around the southwest margin of the Kaapvaal craton formed by a combination of plate convergence and crustal accretion over the period 2.0 to 0.95 Ga. There is evidence for two subduction related events at 2.0 and 1.35 Ga, during which a significant volume of new calc-alkaline crust was created (Moore et al. 1990). Large scale deformation was accompanied by extensive shearing along the western craton margin (Tankard et al. 1982; Hartnady et al. 1985).

Dating of inclusions within some southern African diamonds indicate diamond ages up to 3.2 Ga (Richardson et al. 1984), implying that cool, stable cratonic lithosphere of >150 km thickness had been developed by this time. Kimberlite activity on and around the Kaapvaal craton has probably taken place since 3.0 Ga as alluvial diamonds from a presumably kimberlitic primary source are present in Witwatersrand sediments deposited between 3.0 and 2.7 Ga (Wagner 1914; Wilson 1982). Episodic kimberlite events from the Proterozoic to the late Mesozoic, can be traced from the Kuruman occurrences at 1.6 Ga (Bristow et al. 1986) to the 70Ma Gibeon kimberlites in Namibia (Spriggs 1988).

The locations of the southern African kimberlites and melilitites analysed in this study are shown in Figure 8.3. A summary of the age of intrusion, emplacement environment (on the craton, marginal to the craton and off the craton) and isotopic character for each sample is shown in Table 8.1. In this study I define "marginal kimberlites" as those emplaced within ~100 km of the craton margin

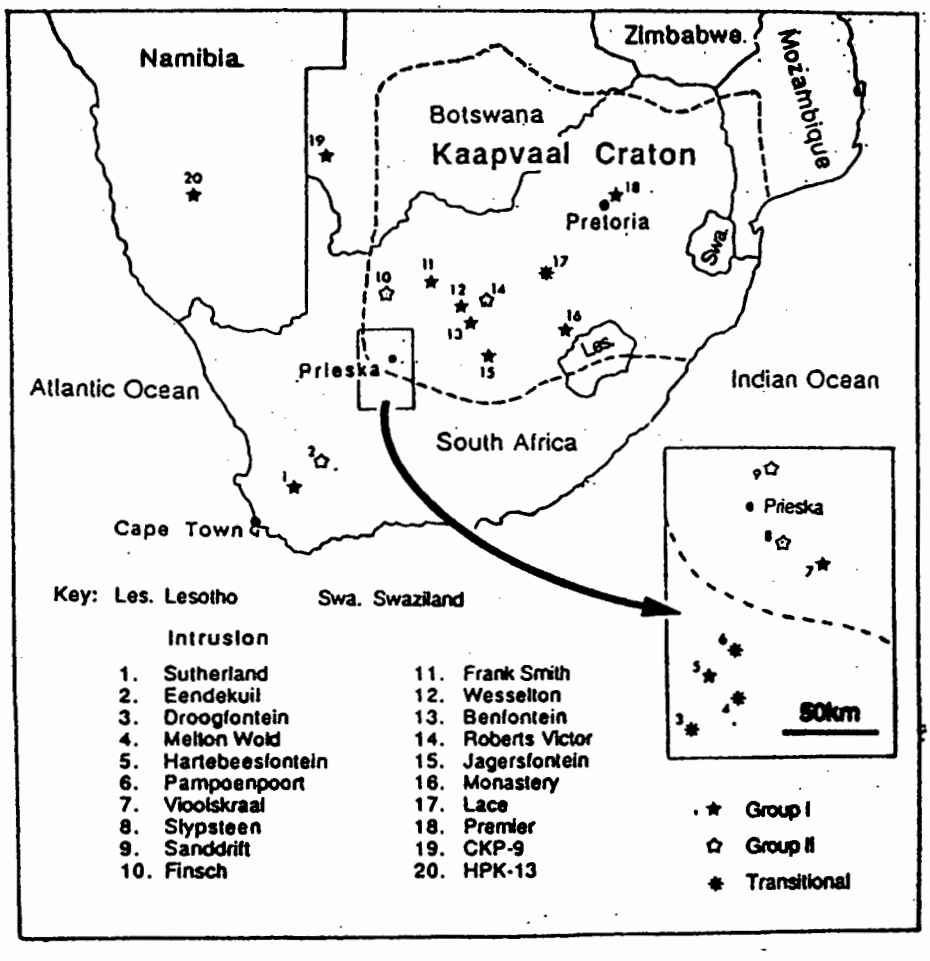

Figure 8.3.: Locations of southern African kimberlites and alkali rocks. The suggested margin of the Kaapvaal craton is shown with a dashed line.

and "off-craton kimberlites" as those emplaced >100 km from the craton margin. Many of the South African samples included in this study have either been described or analysed previously for major elements, selected trace elements and isotopes (Smith 1983; Smith et al. 1985; Shee 1986; Spriggs 1988; Viljoen 1988; Skinner et al. 1993) These sources are acknowledged in Table 8.1 and Appendix 6.

Table 8.1 : Summary of emplacement and isotopic data for southern African and Brazilian kimberlites and alkali rocks. "I/II" indicates transitional with Group I affinities. "II/I" indicates transitional with Group II affinities. Full sample number are shown in Appendix 6.

	Intrusion	Age	Emplacement Environment	Group	Reference
Africa					
	Frank Smith	114 Ma	On-craton	I	B
	Jagersfontein	86 Ma	On-craton	I	B
	Wesselton	86 Ma	On-craton	I	C
	Premier	1180 Ma	On-craton	I	A
	Monastery	83 Ma	On-craton	I	B
	Benfontein	?	On-craton	I	H
	Vioolskraal	?	Craton margin	I	G
	Hartebeesfontein	74 Ma	Craton margin	I	G
	Sutherland 259	75 Ma	Off-craton	I	D
	Sutherland 261	75 Ma	Off-craton	I	D
	Sutherland 266	75 Ma	Off-craton	I	D
	CKP-9	87 Ma	Off-craton	I	B
	HPK-13	70 Ma	Off-craton	I	E
	Finsch	118 Ma	On-craton	II	B
	Roberts Victor	126 Ma	On-craton	II	B
	Sanddrift	118 Ma	Craton margin	II	G
	Slypsteen	?	Craton margin	II	G
	Eendekuil	114 Ma	Off-craton	II	G
	Lace K2	140 Ma	On-craton	II/I	C
	Droogfontein	176 Ma (?)	Craton margin	II/I	G
	Melton Wold	145 Ma	Craton margin	II/I	G
	Pampoenpoort	103 Ma	Craton margin	I/II	G
Brazil					
	Tres Ranchos	95 Ma	Uncertain*	II/I	F
	Limeira	95 Ma	Uncertain*	II/I	F
	Japecanga	109 Ma	Uncertain*	I/II	F
	Pantano	87 Ma	Craton margin	II/I	F
	Pres. Olegario	85 Ma	Craton margin	II/I	F
	Carmo Paranaiba	85 Ma	Craton margin	II/I	F
	Sucesso	118 Ma	Craton margin	II/I	F

* see section 8.2.2.

References:
A: Robinson (1975)
B: Smith et al. (1985)
C: Shee (1986)
D: Viljoen (1988)
E: Spriggs (1988)
F: Bizzi et al. (1993a)
G: Skinner et al. (1993)
H: Dawson and Hawthorne (1973)

8.2.2. Southwestern Sao Francisco Craton, Brazil.

The Sao Francisco craton is a basement granite-gneiss/greenstone terrane which stabilized during the late Archean (2.6-2.7 Ga) (Almeida 1977; Tompkins and Gonzaga 1989). However, the margins of the Sao Francisco craton were subjected to much more widespread and intense tectonothermal metamorphism than that which affected the western margin of the Kaapvaal craton (see section 8.2.1). Basement rocks flanking the southwest margin of the Sao Francisco craton were first affected by the Transamazônican orogenesis (2.1-1.8 Ga) and then very extensively defromed during the 0.80-0.45 Ga Braziliano tectonothermal event (Teixeira 1982). The basement to the west of the craton consists largely of juvenile island-arc type crust of late-Proterozoic age which was progressively accreted against the Sao Francisco craton during the Braziliano event. Crustal development appears to have been largely restricted to arc-accretion and that slivers or smaller blocks of Archean and early-Proterozoic crust played only a limited role in this process (Tompkins and Gonzaga 1989; L.A. Bizzi pers. comm 1992).

The western margins of the Sao Francisco craton are overlain by both Braziliano-age thin-skinned fold and thrust belts and Phanerozoic sediments. Because of the cover rocks and the lack of reliable geochronological data, the current knowledge of the continental crust underlying this section of the Brasilia thrust belt is very limited (Bizzi et al. 1993a). As shown in Figure 8.4, the limits of the craton are not well defined and the western margin is the least well constrained (Tompkins and Gonzaga 1989). The surface geology indicates that late Proterozoic metamorphism affected the Coromandel area and may have extended as far as 46°W (Schobbenhaus and Campos 1984). However, the geophysical studies carried out by Pires (1986) suggest that the craton limits may be extended further to the west, underlying the deformed rocks which were thrust onto the craton.

The ill-defined southwestern margin of the craton was later intruded by kimberlites, carbonatite complexes and alkaline diatremes (Bizzi 1993; Bizzi et al. 1993b). The most important foci of alkaline magmatic activity occured between about 120 and 80 Ma in an area of continental extension (the Alto Paranaiba uplift and the volcanic domains of the Mata da Corda formation). The locations of the kimberlites and alkaline rocks analysed in this study were sampled and made available to the author by Luiz Bizzi of the University of Cape Town. The ages of

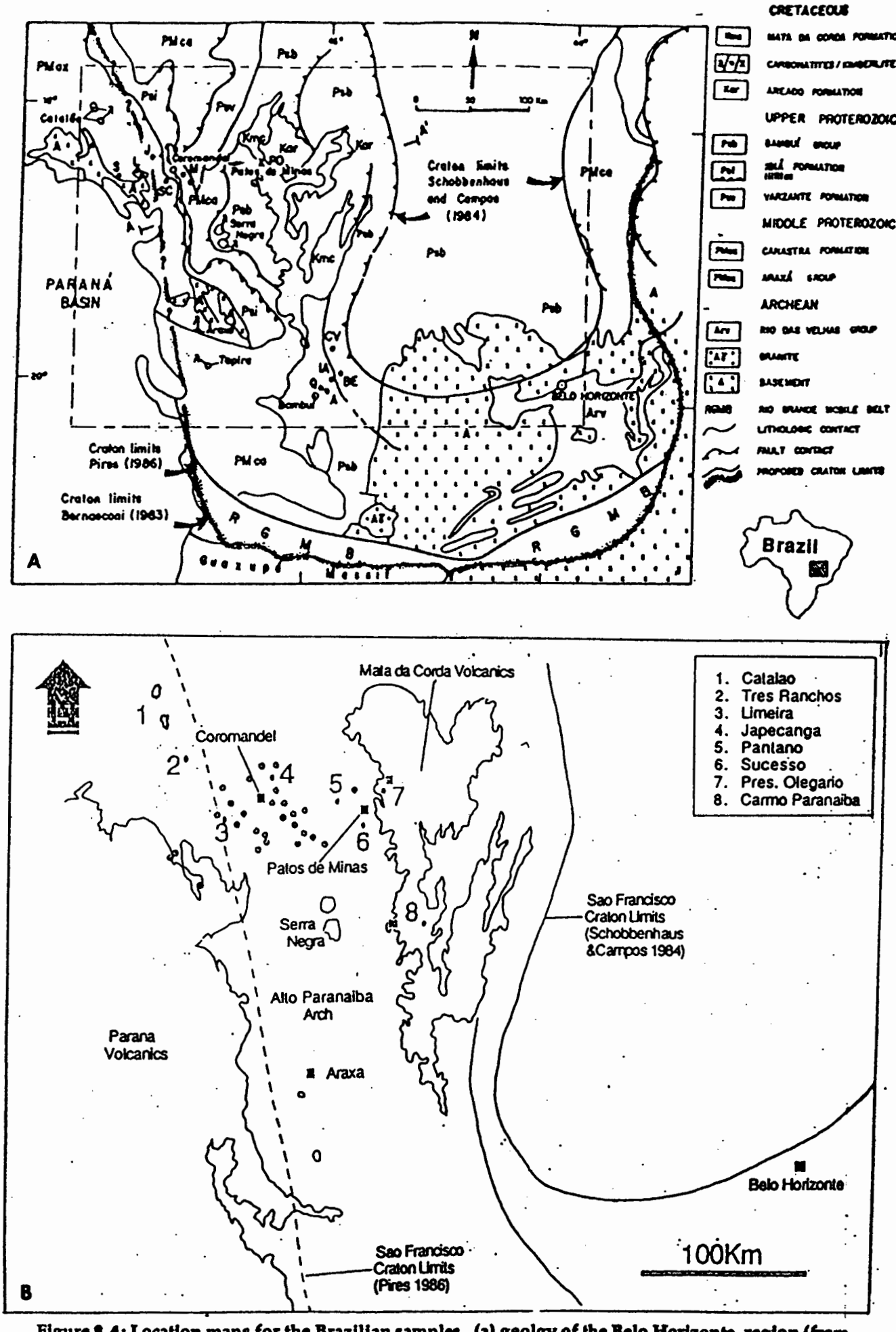

Figure 8.4: Location maps for the Brazilian samples. (a) geolgy of the Belo Horizonte region (from Thompkins and Gonzaga 1989) and (b) inset map showing a more detailed view of the kimberlites and alkali rocks of the Coromandel area (modified after Bizzi et al. 1993). Proposed margins of the Sao Francisco craton are also shown.

the intrusions and lavas are shown in Table 8.1 and the sample locations are illustrated in Figure 8.4.

The kimberlites and alkali rocks under study have been described in detail by Bizzi et al. (1991), Bizzi et al. (1993a), Leonardos et al. (1993) and Meyer et al. (1993). This group of samples represents a number of apparently genuine kimberlites, eg. Tres Ranchos and Limeira, "ambiguous kimberlites" such as the Japecanga and Pântano mica peridotites, and alkali rocks and basalts related to the Mata da Corda volcanics (Bizzi 1993).

Most of the rocks are isotopically transitional between Groups I and II with the exception of Japecanga which shows similarities to Group I kimberlites in terms of U and Pb isotopes (Bizzi et al. 1993a). Bizzi et al. (1993b) proposed that the transitional character of these rocks reflects mixing or contamination of a deeply derived Group I-like melt with enriched lithosphere. From a study of isotopic compositions and the geothermometry and geobarometry of xenolith suites, these authors proposed the pattern of melt source depths shown in Figure 8.5.

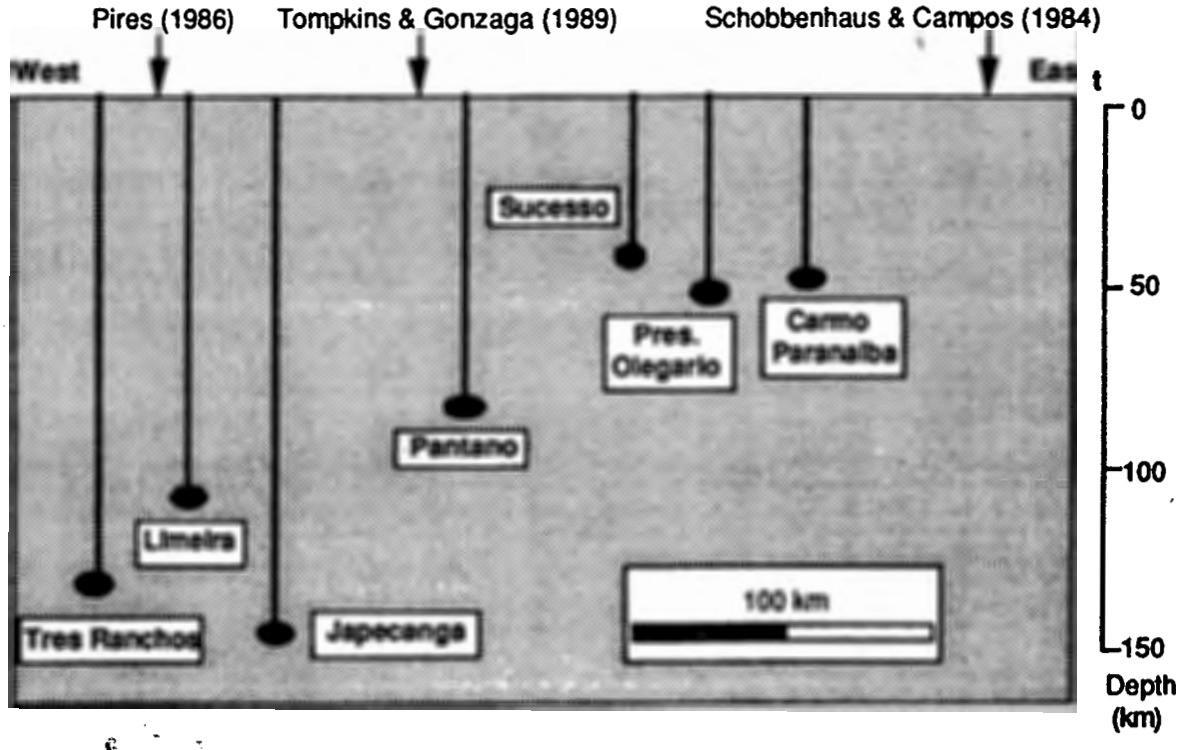

Figure 8.5: Schematic representation of relative the melt generation depths for Brazilian kimberlites and alkali rocks (after Bizzi et al. 1993b). The position of the western craton margin, as suggested by varoius authors, is shown by arrows at the top of the figure.

The uncertainty over the precise location of the western margin of the Sao Francisco craton outlined above, means that the emplacement environment of some of the intrusions is also uncertain (see Figure 8.5). If one accepts the interpretation of Pires (1986), then all of the intrusions with the exception of Tres Ranchos, probably lie on the craton. Tompkins and Gonzaga (1989) modified the craton margins proposed by Pires (1986) to suggest that the craton margin in the Coromandel area lies between Coromandel and Patos de Minas (see Figure 8.4). If this interpretation is correct, then the Tres Ranchos, Limeira and Japecanga intrusions lie off the craton margin. However, if the geophysical evidence cited by Pires (1986) is incorrect and the Brasiliano thrust belt marks the craton boundary (Schobbenhuas and Campos 1984) then none of the intrusions or the lavas may have been emplaced into the craton. I shall return to this topic later, where the role of the PGE as indicators of on-craton and off-craton emplacement environments is discussed.

8.3. Analytical Procedures Employed.

A detailed description of the sample preparation and the analytical procedures employed for noble metals analysis is contained in Appendix 4. X-ray fluorescence (XRF) spectrometry for the determination of major and some trace elements was carried out at the University of Cape Town using the methodology described by Norrish and Hutton (1969) and Le Roex and Dick (1981). Concentrations of rare earth elements (REE) and additional trace elements were determined at Schonland Research Centre by INAA using a similar procedure to that shown in Figure 5.1 and employing the instrumentation and dual detector system described in Appendix 2. A summary of major element and trace element data for all of the samples is shown in Table 8.2.

Noble metal concentrations are summarized in Table 8.3. With the exception of CKP-9, for which very little sample material was available, the noble metal concentrations represent the average of two 100g duplicate analyses. In general, the precision of the duplicate 100g determinations was similar to that obtained for the routine analysis of Wits-1 (see Table 5.4) using 50g of sample. Average COV for Ir and Rh varied between 5 and 10%, while COV for Os, Ru, Pt and Pd were 10-15%. The precision for Au was improved by the use of larger sample masses. In comparison with the high COV obtained for Wits-1 (>40%), the average COV for Au in the kimberlite samples was 22%.

Table 8.2 : Major and trace element concentrations of kimberlites and alkaline rocks. Major elements expressed in weight %, trace elements in parts per million. Major elements, Cu, Zn and Pb analysed by XRF, all other trace elements analysed by INAA.

	Frank Smith	Jagersfontein	Wesselton	Premier Grey	Prem. Pibali	Prem. C. Dyke	Monastery	Benfontein	Vlooiskraal	Hartebeesfntn	Suthrlnd. 259
SiO2	32.64	34.92	24.31	46.73	40.34	8.21	28.24	18.04	28.29	29.29	35.49
TiO2	1.96	1.03	3.19	1.79	1.31	1.68	3.11	5.98	3.26	3.94	3.68
Al2O3	1.89	1.90	3.89	3.92	3.68	0.98	3.69	4.25	3.96	3.95	8.15
Fe2O3*	9.51	8.32	9.77	7.12	6.71	14.04	11.02	20.25	14.86	13.07	13.03
MnO	0.18	0.15	0.19	0.16	0.13	0.40	0.18	0.34	0.3	0.2	0.21
MgO	31.19	34.76	25.12	24.31	19.81	8.62	27.55	23.48	18.93	25.01	16.17
CaO	5.86	3.38	15.89	3.59	10.12	36.07	9.91	11.58	13.79	11.62	15.81
Na2O	0.05	0.16	0.09	0.21	0.32	0.79	0.39	0.14	0.06	0.12	3.35
K2O	0.38	0.52	0.13	0.72	0.18	0.30	2.15	0.79	0.85	1.99	2.31
P2O5	1.32	0.74	1.51	0.16	0.11	1.41	0.75	1.73	1.94	1.11	1.02
H2O	0.79	0.26	8.41	0.81	0.49	0.10	0.28	0.25	1.17	0.76	0.13
L.O.I.	13.58	13.15	5.75	8.92	16.82	27.80	12.78	12.89	12.4	8.93	0.76
Total	99.35	99.09	98.26	98.44	100.02	100.40	100.05	99.72	99.81	99.99	100.13
La	172	86.6	227	28.9	152	206	104	309	283	85	76.3
Ce	293	139	386	51	266	334	162	600	471	134	147
Pr	n d a	n d a	47.2	n.d.a.	n.d.a.	43.2	12.2	70.1	49.2	n d a	n d a
Nd	91	53.9	153	18.7	87.3	129	62.1	249	194	54.2	56.1
Sm	19.2	10.6	33.5	3.8	21.3	28.3	13.2	19.2	46.3	12.8	14.8
Eu	4.5	2.6	8.3	0.99	5.2	6.5	3.45	9.9	11.2	3.4	3.7
Gd	7.32	4.11	11.8	2.8	8.1	14.8	5.4	15.6	14.7	5.8	6.1
Tb	1.4	0.91	2.03	n.d.a.	1.88	2.04	0.87	2.2	2.8	0.99	1.5
Yb	0.72	0.31	1.29	0.71	1.36	1.27	0.62	1.04	2.53	0.94	1.31
Lu	0.14	0.089	0.23	0.15	0.19	0.18	0.12	0.17	0.43	0.15	0.21
Ba	461	357	1430	449	196	548	932	1260	1810	1140	563
Cs	15	17	21	22	n.d.	n.d.	0.94	n.d.	27	24	n.d.
Rb	37	36	70	25	n.d.	n.d.	143	n.d.	24	160	71
Sr	522	313	842	n.d.	840	1230	323	561	1080	275	943
Sc	15	13	23	8.4	22	28	14	36	29	15	27
Co	85	92	56	68	53	63	83	96	69	84	66
Ni	1180	1620	810	798	508	530	838	708	597	850	408
Cr	1380	1680	2160	823	174	89	762	1690	626	799	709
Th	19	11	31	6.6	31	47	13	61	37	13	10
U	3.4	2.8	5.7	1.8	1.8	5.7	1.6	7.9	15	2.9	2.7
Zn	62	53	122	n.d.a.	n.d.a.	55	95	144	160	86	n.d.a.
Cu	48	44	73	n.d.a.	n.d.a.	97	75	79	78	81	n.d.a.
Pb	7.8	n.d.a.	n d a	n.d.a.	n.d.a.	n.d.a.	24	n.d.a.	22	10	n.d.a.
As	0.58	0.25	0.21	0.65	0.54	0.21	0.21	0.28	0.56	0.28	n.d.
Sb	0.32	0.23	0.32	n.d.	0.34	0.38	0.21	0.63	0.57	0.28	n.d.
Ta	10	6.8	25	5.1	15	22	13	32	17	9.6	7.1
Zr	340	326	664	273	385	849	595	1150	1090	280	341
Hf	7.4	4.1	12	4.1	6.9	6.6	12	21	11	7.7	7.2

Table 8.2 (continued).

	Suthrlnd. 261	Suthrlnd. 266	CKP-9	HPK-13	Finsch	Rob. Victor	Sanddrift	Slypsteen	Eendekuil	Lace K-2	Droogfontein
SiO2	33.89	31.55	19.92	27.84	36.98	32.88	35.86	44.27	30.17	38.81	36.07
TiO2	3.21	2.98	3.21	1.55	0.74	0.89	0.71	1.91	2.71	2.46	3.21
Al2O3	7.25	6.93	2.29	2.27	3.10	2.76	2.77	6.26	5.95	2.99	6.69
Fe2O3*	11.42	13.81	14.14	8.17	8.12	7.94	7.53	9.38	10.27	8.14	10.2
MnO	0.21	0.31	0.26	0.16	0.14	0.16	0.18	0.14	0.18	0.12	0.17
MgO	18.88	19.17	25.28	26.73	30.57	30.16	28.75	18.23	11.23	22.44	22.25
CaO	13.69	18.15	15.64	11.73	5.34	7.70	5.32	7.02	17.69	8.22	7.68
Na2O	0.80	3.11	0.22	0.03	0.42	0.19	0.04	0.68	0.08	0.11	0.05
K2O	2.32	1.31	0.19	0.99	3.19	1.90	2.61	3.72	4.33	5.35	2.72
P2O5	0.92	1.78	2.73	0.63	0.57	2.19	0.04	1.09	0.77	0.39	2.03
H2O	0.61	0.12	0.41	n.d.a.	0.45	0.31	1.79	1.66	0.78	0.27	1.49
L.O.I.	6.61	0.87	14.25	16.95	9.43	12.57	14.29	5.49	15.5	10.42	7.34
Total	99.81	100.02	98.54	97.05	99.05	99.65	99.89	99.85	99.93	98.72	99.9
La	75.6	135	297	91.7	51.4	154	83.8	125	190	174	160
Ce	132	253	517	143	88.7	253	165	206	321	310	237
Pr	n.d.a	n d a	n d a	n d a	n.d.a.	23.6	n d a	n d a	n d a	n.d.a.	23.5
Nd	48.6	86.5	170	43.4	36.6	81.9	52.3	78.1	90.4	97.9	83.1
Sm	12.8	21.8	39.4	9.1	6.4	13.1	9.4	14.6	19.1	18.7	16.2
Eu	3.4	5.8	8.9	2.1	1.5	2.7	1.9	3.2	4.2	4.1	3.7
Gd	4.5	8.4	14.6	2.6	3.5	6.1	3.9	5.8	10.3	8.8	8.4
Tb	1.2	2.2	2.7	0.68	n.d.	1.8	n.d.	0.95	1.2	1.1	1.4
Yb	1.21	1.76	1.52	0.37	0.34	1.6	0.43	0.86	1.1	1.2	1.11
Lu	0.18	0.31	0.31	0.11	0.07	0.28	0.09	0.15	0.16	0.18	0.16
Ba	671	580	968	2080	1610	4880	914	1370	876	1390	3350
Cs	6.3	9.6	16	28	25	21	25	16	43	54	28
Rb	90	44	41	81	156	78	106	167	199	216	118
Sr	374	1750	1990	1910	341	894	309	840	1660	1580	1110
Sc	23	27	22	14	15	28	16	19	15	22	17
Co	66	69	81	71	82	72	86	63	60	77	72
Ni	728	598	820	1070	1400	1300	1810	1100	650	1180	823
Cr	784	753	515	1400	1860	1480	1700	1260	495	1600	887
Th	10	21	36	11	5.9	26	9	17	27	24	20
U	1.9	3.8	9.2	2.3	3.9	3.9	n.d.	3.7	3.1	5.1	4.8
Zn	n.d.a.	n.d.a.	104	n.d.a.	59	63	55	86	77	n.d.a.	85
Cu	n.d.a.	n.d.a.	78	n.d.a.	34	29	12	54	29	n.d.a.	81
Pb	n.d.a.	n.d.a.	17	n.d.a.	n.d.a.	n.d.a.	2	23	23	n.d.a.	24
As	0.62	0.78	1.9	1.2	0.19	0.32	0.66	0.39	0.88	2.9	0.27
Sb	0.27	n.d.	0.67	0.51	0.14	0.33	n.d.	n.d.	0.53	0.86	0.31
Ta	7.1	8.6	19	17	2.5	5.9	4	4.6	8.2	7.1	11
Zr	305	498	784	2410	n.d.	824	n.d.	375	178	360	577
Hf	6.2	7.1	13	44	3.3	12	4.8	7.2	5.1	9.1	11

Table 8.2 (continued).

	Melton Wold	Pampoenpoort	Tres Ranchos	Limeira	Japecanga	Pantano	Pres. Olegario	Carmo Paran.	Sucesso GREEN	Sucesso RED
SiO2	35.24	29.27	34.47	29.74	34.71	32.27	37.74	37.69	36.52	43.74
TiO2	0.93	1.98	1.25	2.41	2.22	4.78	6.14	5.19	7.24	3.78
Al2O3	2.39	2.22	2.57	1.85	0.89	2.49	5.02	5.51	4.66	7.41
Fe2O3*	8.61	10.11	9.82	10.98	12.74	14.06	14.41	14.05	14.73	11.67
MnO	0.15	0.18	0.24	0.22	0.19	0.24	0.21	0.34	0.21	0.17
MgO	32.01	30.77	31.62	29.88	30.51	24.09	16.35	13.19	15.66	9.19
CaO	4.92	9.33	4.63	10.84	2.63	10.95	10.29	11.84	9.03	11.11
Na2O	0.02	0.06	0.09	0.02	0.02	0.11	0.44	0.46	0.95	1.35
K2O	1.63	1.08	0.93	1.05	0.25	2.42	1.74	0.92	2.81	3.53
P2O5	0.36	0.84	1.21	2.57	0.19	0.93	0.41	0.84	1.44	0.93
H2O	0.09	0.71	1.07	0.69	2.56	1.54	1.84	1.98	1.69	2.67
L.O.I.	13.43	12.37	11.64	9.04	12.82	5.09	3.73	4.45	4.34	3.86
Total	99.78	99.92	99.33	99.25	99.7	98.96	98.32	96.45	99.27	99.41
La	114	121	429	291	68.1	274	202	224	197	192
Ce	164	197	614	480	117	435	364	366	366	360
Pr	17.2	n d a	59.5	49.1	14.9	42.1	46.8	44.1	38.6	39.1
Nd	57.6	63.5	191	194	45.2	160	156	156	150	154
Sm	9.8	13.9	28.7	35.6	7.9	26.9	26	25.7	23.8	23.6
Eu	2.3	3.3	6.3	8.5	1.9	6.5	6.6	6.5	6.9	6.7
Gd	6.9	7.2	11.8	15.4	3.3	12.3	12.2	11.9	10.9	10.8
Tb	0.47	0.97	1.8	2.4	0.62	1.6	1.7	1.9	1.9	1.9
Yb	0.54	0.44	1.01	1.44	0.47	1.09	1.18	1.29	1.51	1.44
Lu	0.11	0.11	0.19	0.22	0.16	0.17	0.18	0.21	0.21	0.22
Ba	2410	723	2730	2150	590	2580	6540	17600	3120	2980
Cs	15	15	18	17	12	23	68	49	168	121
Rb	117	49.5	72	100	20	162	203	91	176	55
Sr	455	417	1490	2160	191	1830	1870	1960	1850	1260
Sc	10	13	15	20	12	24	25	28	23	20
Co	91	89	90	82	115	89	75	70	76	53
Ni	1560	1390	1550	1200	990	900	530	480	560	524
Cr	1651	1320	1840	1230	1280	1080	582	332	624	589
Th	17	15	41	23	9	26	25	20	19	18
U	3.5	3.6	7.7	5.4	7.4	5.9	5.6	5.7	3.4	3.2
Zn	65	73	75	79	68	88	103	106	128	103
Cu	53	42	37	53	11	124	122	129	92	55
Pb	5	10	13	8.2	6	8.4	11	8.9	12	9
As	0.24	0.16	2.1	1.8	0.5	1.1	1.2	1.6	1.5	1.8
Sb	0.22	0.24	0.82	0.99	0.24	0.92	0.72	1.1	0.87	0.95
Ta	7.5	8.1	11	10	19	16	15	11	12	11
Zr	n.d.	334	413	632	766	842	803	652	1130	503
Hf	1.9	5.5	6.5	12	16	17	16	15	26	22

Table 8.3 : Noble metal concentrations in kimberlites and alkali rocks. All concentrations in parts per billion. "n.d.a." inidcates no data avaliable for that element at present.

		Concentration Present						
Sample	**Group**	**Os**	**Ir**	**Ru**	**Rh**	**Pt**	**Pd**	**Au**
Frank Smith	K I (c)	3.3	2.9	5.4	0.81	5.7	2.8	0.65
Jagersfontein	K I (c)	2.3	2.0	3.6	n.d.a.	3.2	2.4	0.85
Wesselton	K I (c)	2.1	1.3	2.7	0.74	4.6	3.4	2.3
Premier Grey	K I (c)	0.85	0.79	2.7	0.70	4.1	3.3	0.48
Premier Piball	K I (c)	0.76	0.71	2.1	0.66	3.6	2.5	0.64
Premier C.Dyke	K I (c)	0.68	0.47	1.0	0.46	3.0	1.6	0.44
Monastery	K I (c)	2.0	1.6	2.8	n.d.a.	5.5	4.1	0.69
Benfontein	K I (c)	2.3	1.8	3.6	n.d.a.	4.8	3.5	0.84
Vioolskraal	K I (m)	0.91	0.67	1.9	0.52	3.4	2.0	0.41
Hartebeesfontein	K I (m)	0.84	0.63	2.3	0.60	2.9	2.1	0.57
Sutherland 259	M I (oc)	0.38	0.64	1.9	0.64	10.4	7.5	0.23
Sutherland 261	M I (oc)	0.44	0.68	2.6	0.58	11.4	7.1	0.33
Sutherland 266	M I (oc)	0.52	0.71	3.3	0.84	11.1	7.3	0.22
CKP-9	K I (oc)	1.1	1.2	1.5	0.93	22.9	13.3	6.4
HPK-13	K I (oc)	0.99	1.3	2.3	0.78	15.4	9.4	4.3
Finsch	K II (c)	1.4	1.2	2.5	n.d.a.	4.9	6.5	1.9
Roberts Victor	K II (c)	1.7	1.3	2.3	n.d.a.	6.4	0.92	1.6
Sanddrift	K II (m)	1.2	1.1	2.1	0.54	5.2	5.1	1.2
Slypsteen	K II (m)	0.84	0.64	1.9	n.d.a.	5.9	3.8	1.3
Eendekuil	K II (oc)	0.48	0.71	1.8	0.75	12.6	8.7	2.0
Lace K-2	K T (c)	1.8	1.6	3.0	1.15	11.2	6.8	3.7
Droogfontein	K T (m)	1.3	1.5	4.0	1.49	10.6	6.3	2.9
Melton Wold	K T (m)	1.5	1.1	3.4	n.d.a.	8.0	5.4	1.8
Pampoenpoort	K T (m)	2.1	1.8	4.1	1.35	4.3	2.9	0.80
Tres Ranchos	K T (??)	1.3	2.3	4.5	1.10	14.1	9.9	0.24
Limeira	K T (??)	1.7	1.8	4.6	1.20	11.7	8.8	2.1
Japecanga	P T (??)	0.59	0.55	1.6	0.36	2.6	1.4	0.33
Pantano	P T (m)	0.99	0.92	2.9	n.d.a.	9.9	6.2	2.4
Pres. Olegario	B T (m)	0.48	0.45	0.54	n.d.a.	8.6	5.7	2.5
Carmo Paranaiba	B T (m)	0.51	0.41	0.62	n.d.a.	8.5	6.9	0.55
Sucesso (Green)	B T (m)	0.26	0.28	0.66	0.30	7.4	5.3	2.7
Sucesso (Red)	B T (m)	0.30	0.37	1.1	0.35	7.1	5.2	0.25
Chondrite		761	710	1071	201	1430	836	218

Key to Group column:
K = kimberlite; P = peridotite/kimberlite?; B = basalt; M = melilitite
I = Group I; II = Group II; T = Transitional
(c) = On the craton; (m) = Marginal; (oc) = Off the craton; (??) = Uncertain (see text)

The concentrations of PGE and Au obtained in this study indicate that the earlier analyses of South African kimberlites by Paul et al. (1979) and Tredoux (1990) are broadly correct (see Appendix 4 for comparison of data). The agreement was found to be best for Os and Ir, while abundances of Pt, Pd and Au may have been overestimated in the earlier studies. No evidence of very high concentrations of PGE, as was reported from Siberian kimberlites by Kaminskiy et al. (1974), was found in either the Brazilian or southern African samples. The consistency of the Brazilian and southern African data suggest that kimberlites are typically characterised by PGE concentrations of <20 ppb and that the Siberian data must be viewed with extreme caution until the data can be confirmed by additional analyses.

8.4. Platinum-Group Element Geochemistry

Inter-noble metal ratios for all of the samples are shown in Table 8.4. Chondrite normalized PGE patterns where the samples are distinguished in terms of isotopic grouping and/or emplacement environment, are shown in Figures 8.6 to 8.10. The normalization uses the chondrite data suggested by Tredoux et al. (1989a) and groups the PGE in order of increasing melting point (Naldrett 1979). The selected groupings of samples are summarized as follows:

(a) On-craton and marginal Group I kimberlites from southern Africa
(b) Off-craton Group I kimberlites from southern Africa
(c) Group II kimberlites from southern Africa
(d) Transitional kimberlites from Southern Africa
(e) Transitional kimberlites from Brazil

The most important noble metal characteristics of each of these groupings will be briefly described with the aim of presenting a summary of the main similarities or differences between them. As noted in section 2.2, the PGE are commonly divided into two geochemically similar groups [Os, Ir, Ru] and [Rh, Pt, Pd]. Tredoux et al. (1986) developed the terms HTPGE (high temperature PGE) and LTPGE (low temperature PGE) to refer to these two groups respectively. The same terminology will be adopted in this section, where appropriate.

Table 8.4 : Summary of inter-noble metal ratios. Group column notation is the same as Table 8.3.

Sample	Group	Os/Ir	Ru/Os	Ru/Ir	Rh/Ir	Pt/Ir	Pd/Ir	Au/Ir
Frank Smith	K I (c)	1.14	1.64	1.86	0.27	1.96	0.96	0.22
Jagersfontein	K I (c)	1.15	1.56	1.80	-	1.78	1.20	0.43
Wesselton	K I (c)	1.61	1.29	2.08	0.57	3.54	2.61	1.77
Premier Grey	K I (c)	1.08	3.17	3.41	0.89	5.19	4.18	0.98
Premier Piball	K I (c)	1.07	2.76	2.95	0.93	5.07	3.52	0.90
Premier C. Dyke	K I (c)	1.45	1.47	2.13	0.98	6.38	3.40	0.94
Monastery	K I (c)	1.25	1.4	1.75	-	3.43	2.56	0.43
Benfontein	K I (c)	1.28	1.56	2.00	-	2.67	1.94	0.47
Vioolskraal	K I (m)	1.36	2.09	2.83	0.78	5.07	2.98	0.61
Hartebeesfontein	K I (m)	1.33	2.73	3.65	0.95	4.60	3.33	0.90
Sutherland 259	M I (oc)	0.59	5.00	2.97	1.00	16.25	11.71	0.36
Sutherland 261	M I (oc)	0.65	5.91	3.82	0.86	16.76	10.44	0.48
Sutherland 266	M I (oc)	0.73	6.35	4.64	1.18	15.63	10.23	0.31
CKP-9	K I (oc)	0.91	1.36	1.25	0.78	19.08	11.08	5.33
HPK-13	K I (oc)	0.76	2.32	1.77	0.60	11.85	7.23	3.31
Finsch	K II (c)	1.17	1.78	2.08	-	4.08	5.41	1.58
Roberts Victor	K II (c)	1.31	1.35	1.77	-	4.92	0.71	1.23
Sanddrift	K II (m)	1.09	1.75	1.91	0.49	4.72	4.63	1.09
Slypsteen	K II (m)	1.31	2.26	2.96	-	9.22	5.94	2.03
Eendekuil	K II (oc)	0.67	3.75	2.53	1.04	17.75	12.25	2.81
Lace K-2	K T (c)	1.13	1.67	1.88	0.69	7.00	4.25	1.97
Droogfontein	K T (m)	1.20	2.22	2.67	0.99	7.07	4.20	1.93
Melton Wold	K T (m)	1.36	2.27	3.09	-	7.27	4.90	1.63
Pampoenpoort	K T (m)	1.17	1.95	2.27	0.75	2.39	1.61	0.44
Tres Ranchos	K T (??)	0.56	3.46	1.95	0.48	6.13	4.30	0.10
Limeira	K T (??)	0.94	2.71	2.55	0.66	6.50	4.89	1.17
Japecanga	P T (??)	1.07	2.71	2.91	0.65	4.73	2.54	0.60
Pantano	P T (m)	1.08	2.93	3.15	-	10.76	6.74	2.61
Pres. Olegario	BT (m)	1.07	1.13	1.20	-	19.11	12.67	5.55
Carmo Paranaiba	B T (m)	1.24	1.22	1.51	-	20.73	16.83	1.34
Sucesso (Green)	B T (m)	0.93	2.54	2.35	1.07	26.43	18.93	9.64
Sucesso (Red)	B T (m)	0.81	3.67	2.97	0.94	19.19	14.05	0.68
Chondrite		1.07	1.41	1.51	0.28	2.01	1.17	0.31

8.4.1. On-Craton And Marginal Group I Kimberlites, Southern Africa.

Figure 8.6 shows the chondrite normalized PGE patterns obtained from Group I kimberlites from within the boundaries of the Kaapvaal craton and from the southwest craton margin at Prieska. The most consistent feature of the patterns is that a negative Ir anomaly is present in every case. Those samples for which Rh data is available show consistently positive Rh anomalies accompanied by slight to pronounced negative Pt anomalies. Pd/Ir ratios range from pseudo-chondritic (0.96) to slightly fractionated (4.18) relative to chondrite. An examination of the Ru/Ir, Ru/Os, Rh/Ir and Pd/Ir ratios suggests that two subgroups might be

present. The first subgroup shows a relatively flat overall pattern with small Ir, Rh and Pt anomalies. Examples of this subgroup are Wesselton and Frank Smith. The second subgroup has lower concentrations of Os and Ir relative to the other PGE. Examples of the second subgroup are Premier and Vioolskraal.

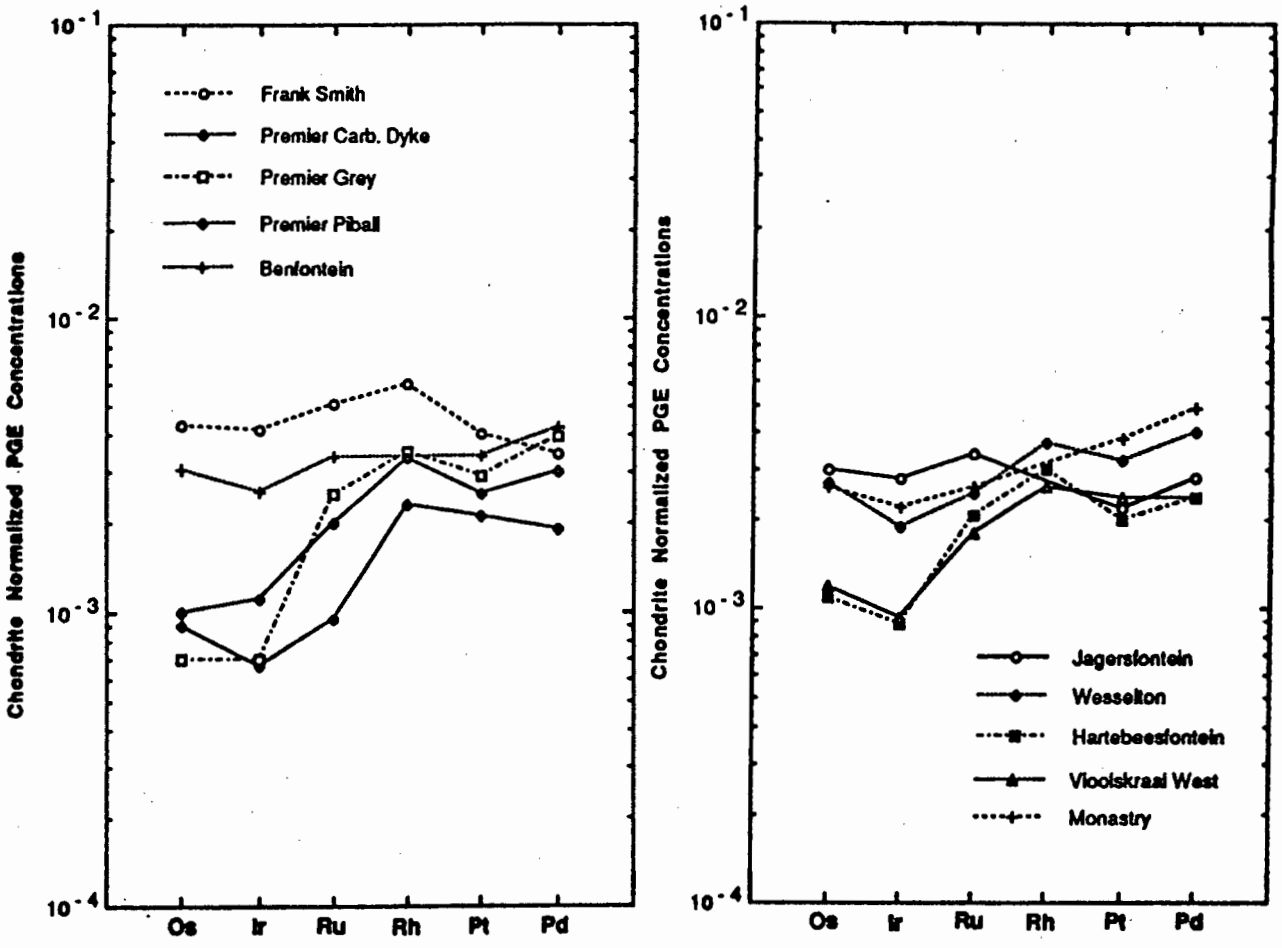

Figure 8.6: Chondrite normalized PGE patterns from on-craton and marginal Group I kimberlites. All data from Table 8.3. Normalization values from Tredoux et al. (1989a).

The data from the Premier kimberlite is striking in that a very similar pattern and group of inter-PGE ratios are evident from several different bodies of the Premier intrusion. These bodies vary considerably in terms of composition (see Table 8.2), volume and their relative emplacement (Robinson 1975) but the PGE patterns indicate similar trends with the only variable being the relative concentrations of PGE. These patterns indicate that the PGE signature has not been influenced by either the emplacement history or by the degree of differentiation, implying that the PGE may be hosted by a common phase (or phases) in each of the Premier intrusions. The earliest intrusion, the Grey

kimberlite, contains most of this phase (or phases) while the very late stage carbonate dyke contains the least.

It is also notable that the PGE ratios and patterns from the Premier kimberlite closely match those shown by the Hartebeesfontien and Vioolskraal kimberlites. A similar pattern is seen in bodies which differ by 1.1 Ga. This implies that age does not affect the PGE signature, nor are there significant differences in terms of PGE and Au between Group I kimberlites on the craton and those close to the margins. These points are discussed in greater detail later.

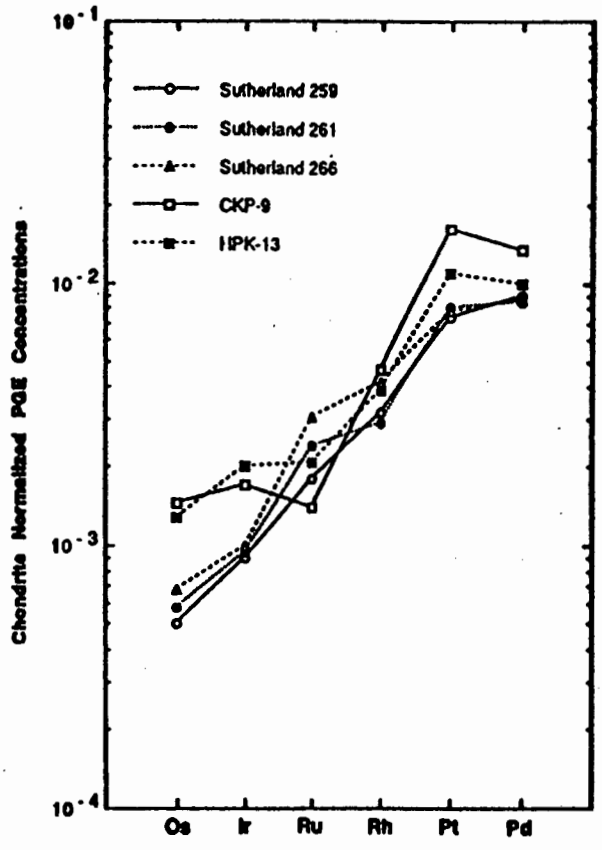

Figure 8.7: Chondrite normalized PGE patterns from off-craton Group I kimberlites and melilitites. All data from Table 8.3.

8.4.2. Off-Craton Group I Kimberlites And Melilitites, Southern Africa.

Chondrite normalized PGE patterns from kimberlites and alkali rocks, showing Group I isotopic signatures and situated well off the craton are shown in Figure 8.7. The patterns are fractionated, with pronounced positive slopes and a strong enrichment in Pt and Pd compared to Group I kimberlites from the on-craton and craton margin environments. The patterns from the three Sutherland melilitites are very similar in character with strong LTPGE fractionation (Pt/Ir >15, Pd/Ir >10) and no Ir anomaly. The kimberlites (CKP-9 and HPK-13) show higher Os

and Ir contents than the melilitites with small positive Ir anomalies and high Pt/Ir (>11) and Pd/Ir (>15) ratios. The available Rh data indicate that the patterns for both the melilitites and the kimberlites are almost linear between Ru and Pt. Pt anomalies are strongly positive, in contrast to the negative anomalies observed in Group I kimberlites on the craton and at the craton margins.

8.4.3. Group II Kimberlites, Southern Africa.

PGE patterns from Group II kimberlites are shown in Figure 8.8. Rocks from the on-craton, craton margin and off-craton environments are represented in this small dataset. With the exception of the very low Pd concentration at Roberts Victor, which may be related to weathering or alteration, the patterns shown by the marginal and the on-craton kimberlites are generally consistent. There is a slight to moderate LTPGE fractionation shown by the Pt/Ir ratio (4 to 9), which is just slightly higher than that shown by the on-craton Group I kimberlites. A negative Ir anomaly is seen in all of the samples with the exception of Eendekuil and the absolute concentrations of the HTPGE show a systematic increase as the point of melting moves from the margin further onto the craton (see Figure 8.3).

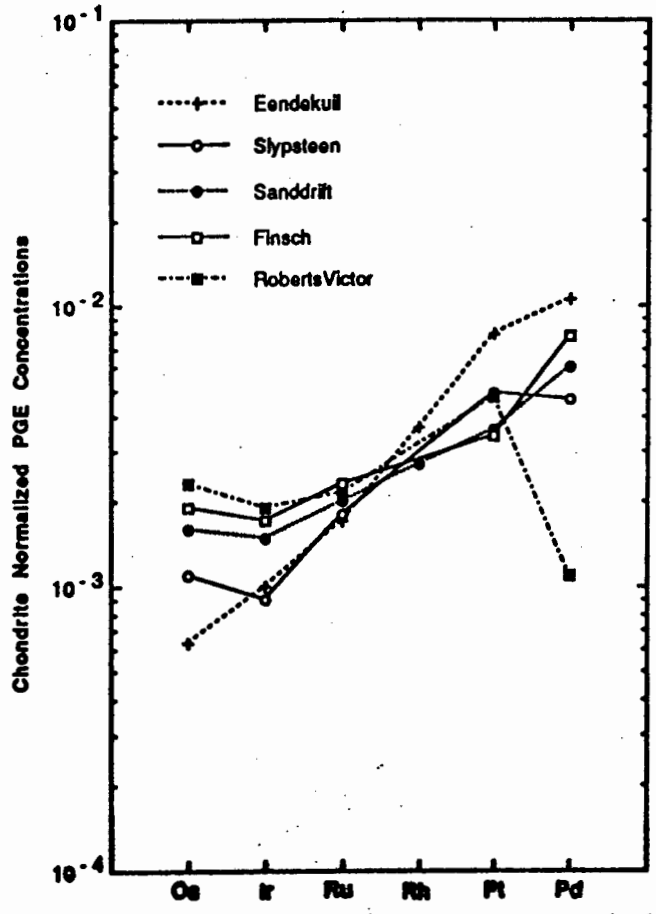

Figure 8.8: Chondrite normalized PGE patterns from on-craton, marginal and off-craton Group II kimberlites. All data from Table 8.3.

The off-craton kimberlite at Eendekuil displays a considerably more fractionated pattern and a higher Pt/Ir ratio (~17) than the other Group II samples. The Eendekuil pattern is essentially linear between Os and Pt, with no Ir anomaly, and generally resembles the patterns displayed by the off-craton Group I rocks.

8.4.4. Transitional Kimberlites, Southern Africa.

Figure 8.9 shows the normalized PGE patterns from isotopically transitional kimberlites on the margin and in the centre of the Kaapvaal craton. Small, negative Ir anomalies are a consistent feature in all of the samples. Excluding Pampoenpoort for the moment, Pt and Pd concentrations and Pt/Ir and Pd/Ir ratios, are higher than on-craton Group I or Group II kimberlites. In the samples for which Rh data is available, pronounced to slightly positive Rh anomalies are shown.

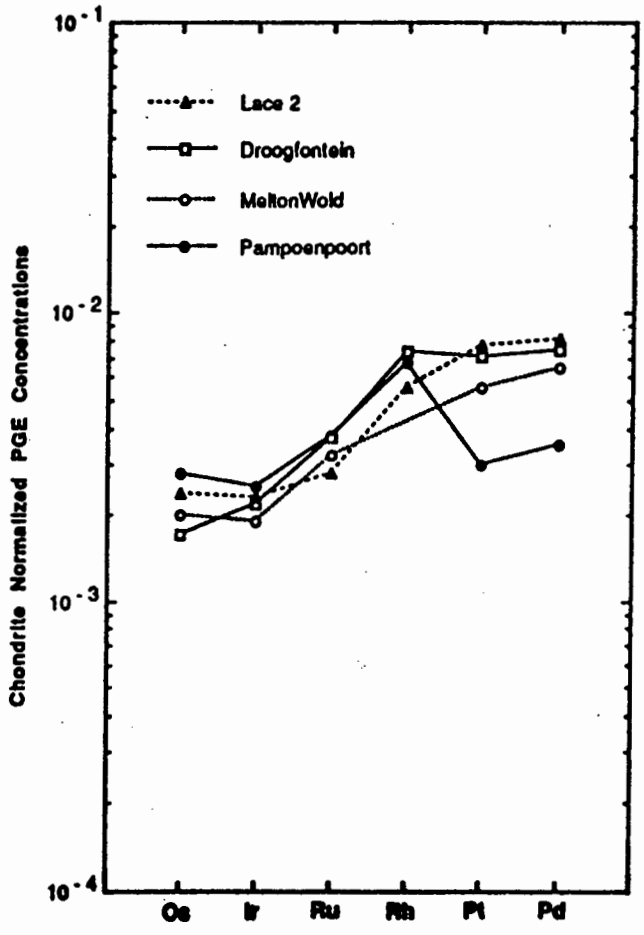

Figure 8.9: Chondrite normalized PGE patterns from southern African transitional kimberlites. Data from Table 8.3.

Unlike the other rocks, which are transitional between Groups I and II, the Pampoenpoort kimberlite has an isotopic composition only slightly removed

from typical Group I kimberlites (Skinner et al. 1993). Pampoenpoort shows a PGE pattern with a pronounced positive Rh anomaly with accompanying negative Ir and Pt anomalies and a set of inter-PGE ratios very similar to those seen in Group I kimberlites from marginal and on-craton environments (see Figure 8.6 and Table 8.4).

A notable feature amongst this group is the close fit between the PGE patterns from Droogfontein, Lace and Pampoenpoort in terms of Os, Ir, Ru and Rh (see the appropriate inter-PGE ratios in Table 8.4). While Pampoenpoort is strongly depleted in Pt and Pd, Droogfontein and Lace are enriched in these elements. The possible significance of this feature is discussed in a later section.

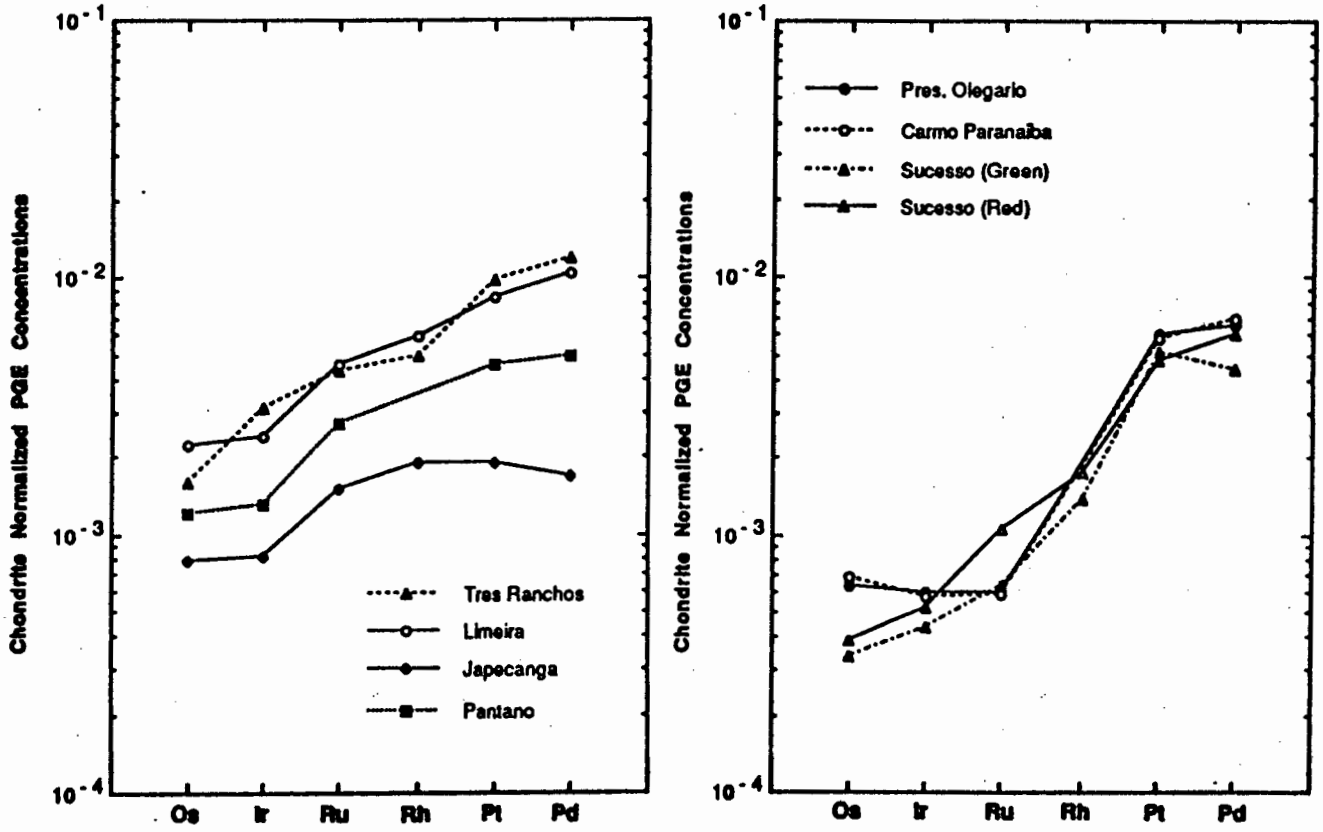

Figure 8.10: Chondrite normalized PGE patterns from Brazilian transitional kimberlites and alkali rocks. Data from Table 8.3.

8.4.5. Transitional Kimberlites And Alkali Rocks, Brazil.

Figure 8.10 shows the normalized PGE patterns obtained from the Brazilian samples. In terms of PGE patterns and of Pt/Ir and Pd/Ir ratios, the rocks show a continuum from the "ambiguous" kimberlite at Japecanga, which is the most

primitive and least fractionated relative to chondrite, to the alkali basalt from Sucesso, which is the most fractionated. This continuum is caused by the fact that the kimberlites and peridotites generally have similar or slightly higher abundances of Pt and Pd to the alkali basalts but contain significantly more HTPGE. This has the effect of flattening the overall PGE pattern.

The alkali basalts show a very consistent series of PGE patterns and in terms of Pt/Ir ratios (>19), are the most fractionated rocks in this study. The two samples from the Sucesso locality come from the centre (green) and the oxidised top (red) of the same lava flow. The red sample shows slightly higher concentrations of HTPGE than the green sample but the positively sloping, linear patterns are very similar. This feature may reflect secondary enrichment of the immobile HTPGE during weathering (Naldrett 1981). The basalts from Presidente Olegario and Carmo Paranaiba are pseudo-chondritic in terms of HTPGE (see Figure 8.9 and the relevant Os/Ir, Ru/Ir and Ru/Os ratios in Table 8.4) but the overall patterns are highly fractionated.

The Tres Ranchos and Limeira kimberlites display moderately fractionated PGE patterns with Pt/Ir ratios of ~6. The kimberlites have higher absolute concentrations of PGE than any of the other rocks. A small negative Ir anomaly is shown by the Limeira sample while Tres Ranchos displays a slightly positive Ir anomaly. The PGE pattern for the peridotite at Pantano is similar to that shown by the Limeira kimberlite, with a more pronounced negative Ir anomaly.

The "ambiguous" kimberlite sample from Japecanga displays a PGE pattern which is very different from the fractionation seen in the other rocks. As noted previously, it shows the most primitive pattern relative to chondrite, of all the Brazilian samples. In the Japecanga sample, Os and Ir are slightly depleted relative to the other PGE, and both the overall pattern and the inter-noble metal ratios, particularly Pd/Ir and Au/Ir, resemble those seen in on-craton Group I kimberlites from southern Africa.

8.5. Differences In Terms Of PGE And Au Between The Groups.

8.5.1. On-Craton And Marginal Kimberlites Versus Off-Craton Kimberlites.

In the descriptions of the PGE signatures of Group I, Group II and Transitional kimberlites, it was noted that although slightly higher absolute abundances of the

PGE were present in the cratonic kimberlites relative to the marginal kimberlites, ratios and pattern shapes were very consistent. Comparisons between Premier and Hartebeesfontein for Group I, Finsch and Sanddrift for Group II and Lace and Drrogfontein for the transitionals, show this clearly. On this basis I conclude that there do not appear to be significant differences in terms of PGE signatures between on-craton and craton margin kimberlites within the same group (I,II or transitional) and I will consider them as a coherent unit in this section. However, inter-noble metal ratios and PGE patterns indicate that there are significant differences between the on-craton/marginal kimberlites and kimberlites emplaced off the craton.

The most consistent feature of all of the kimberlites and peridotites emplaced into the craton and into the craton margins, is the presence of a negative Ir anomaly. This feature is present throughout Group I, Group II and transitional kimberlites emplaced on or near the craton, but is not present in the off-craton kimberlites and melilitites, nor in the Sucesso basalts. An examination of all of the on-craton and marginal kimberlites from southern Africa revealed that the HTPGE show very strong inter-metal correlations.

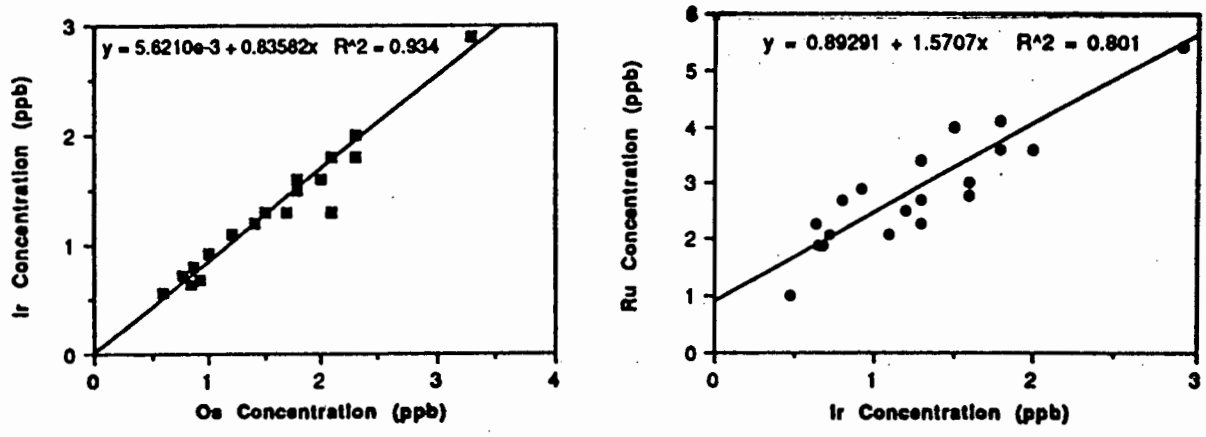

Figure 8.11 : Plots of Os, Ir and Ru in on-craton and marginal kimberlites from southern Africa.

Plots of Ir vs. Os and Ru vs. Ir are shown in Figure 8.11. R^2 correlation coefficients are 0.934 and 0.801 respectively which strongly suggests that Os, Ir and Ru have a restricted behaviour during the generation and emplacement of kimberlites from source regions which show considerable differences in lithophile element signatures. This restricted behaviour preserves the V-like

pattern between Os, Ir and Ru. It follows that whatever is causing the HTPGE signature is either present in both Group I and Group II source regions or is sampled by both types of kimberlite during ascent. The apparent association between the HTPGE signature and an on-craton/craton margin emplacement environment, indicated by the data, suggests that the cause of the HTPGE signature may reside within the cratonic lithosphere.

Kimberlite melts emplaced into the craton or its margin are not strongly fractionated in terms of Pt/Ir and Pd/Ir ratios, relative to chondrite. In contrast to this, all of the kimberlites and melilitites emplaced off the craton generally show much more fractionated PGE patterns which are linear in terms of HTPGE or even show small positive Ir anomalies.

A fundamental observation is that there appear to be large differences in terms of PGE, between melts which are identical in terms of Sr, Nd and Pb isotopes, emplaced into the craton or its margin and those emplaced well away from the craton. A model for this is developed in section 8.7.

8.5.2. Group I, Group II And Transitional Kimberlites.

Examination of the inter-noble metal ratios in Table 8.4 and the patterns in Figures 8.6 and 8.8 indicate that in contrast to the lithophile elements and radiogenic isotopes, Group I and Group II kimberlites do not show greatly differing PGE signatures. In terms of Os, Ir, Ru and Rh, the rocks are almost identical but Group II kimberlites and Group II-like transitional kimberlites appear to be slightly more enriched in Pt, Pd and Au than Group I kimberlites.

Pt/Ir ratios do not show any significant differences between Group I and Group II. However, if one ignores for the moment, the anomalously low Pd content of the Roberts Victor sample (which is not observed in any of the other samples), Pd/Ir ratios offer some hint of separation. Pd/Ir ratios for the on-craton Group I kimberlites cluster between 1 and 4 with a mean of 2.67, while for similar Group II rocks, the ratio is > 4, with an a mean of 5.32. A similar relationship may prevail in the off-craton kimberlites but as a comparison can only be made with a single Group II kimberlite (Eendekuil), the present data do not allow a definite conclusion to be made at this time.

The Au/Ir ratio offers a slightly clearer separation. With the exception of Wesselton, on-craton Group I kimberlites show Au/Ir ratios of < 1. Similar Group II kimberlites show Au/Ir ratios > 1. The opposite trend (Au/Ir ratio for Group I > Au/Ir for Group II) may be present in the off-craton kimberlites but for the reasons outlined above, more data will be required to confirm this.

Transitional kimberlites such as Japecanga and Pampoenpoort, which are isotopically similar to Group I, show PGE patterns and ratios almost identical to Group I kimberlites, while the other transitional kimberlites which are more similar to Group II, show PGE patterns and ratios more consistent with Group II kimberlites. For Lace, Droogfontein and Melton Wold, Pt/Ir, Pd/Ir and Au/Ir ratios indicate a clear separation of these rocks from Group I kimberlites.

Examination of the PGE patterns shown by the Droogfontein, Lace and Pampoenpoort kimberlites (see Figure 8.9) suggests that the differences between the patterns might be explained by the presence of a fractionated PGE signature (with high Pt/Ir and Pd/Ir ratios) at Droogfontein and Lace which has been added to a Group I-like PGE pattern such as that shown by the Pampoenpoort kimberlite. The possible significance of this feature for kimberlite is discussed in sections 8.6.2 and 8.7.

8.5.3. Kimberlites And Alkali Basalts.

The principal difference between the Brazilian alkali basalts and the kimberlites/peridotites is the highly fractionated PGE patterns and ratios of the former relative to the latter. The kimberlites and peridotites have higher HTPGE concentrations and a very characteristic HTPGE signature with a negative Ir anomaly which is not shown by any of the basalts. If the melt generation profile shown in Figure 8.5 is correct, then this implies that the source of the distinctive HTPGE signature may be restricted to a relatively deep level of the lithospheric mantle which is frequently sampled by kimberlite magmatism but incorporated only rarely by alkali basalts which are derived from more shallow melting events. This possibility of HTPGE-enriched zones related to depth has important implications for the PGE budget of the lithosphere and is discussed in greater detail in section 8.7.

8.6. The Nature Of The PGE Signatures For Different Groups.

Having established the main differences in terms of PGE and Au between the separate kimberlite and other rock groups, the discussion will now focus on the PGE signatures themselves and what they indicate about the generation of the melts.

8.6.1. Slightly Fractionated PGE Signatures (On-Craton Group I Kimberlites).

The PGE patterns observed from on-craton and marginal Group I kimberlites are not strongly fractionated relative to chondrite. Although two subgroups may exist within the dataset, the overall degree of LTPGE/HTPGE fractionation is not very high (Pd/Ir between 1 and 4) and the subgroups overlap in terms of Ru, Rh, Pt and Pd. Figure 8.12 compares PGE patterns from MORB and asthenospheric OIB with Group I kimberlites. The patterns are different and indicate that Group I kimberlites appear to be considerably less fractionated than either MORB or OIB.

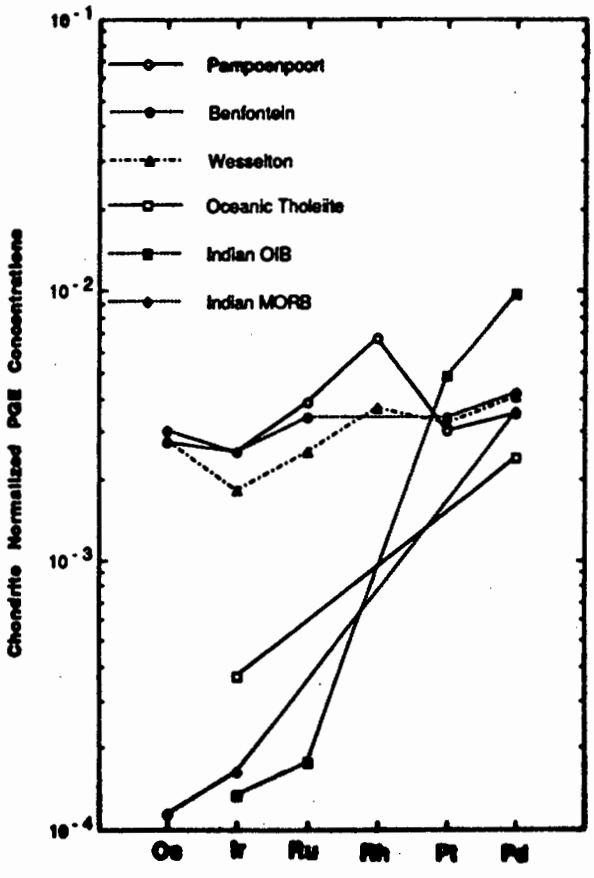

Figure 8.12 : Chondrite normalized PGE patterns showing the comparison between MORB, OIB and some on-craton Group I kimberlites. Indian Ocean MORB data from Hertogen et al. (1980) and Ocean Drilling Program (Leg 115) Tholeiite and OIB data from Jackson et al. (1990).

The characteristic positive Rh and negative Ir and Pt anomalies seen in all of the on-craton Group I kimberlite samples bear a close resemblance to material from

the 3.5 Ga Ni-rich Bon Accord (BA) body studied by de wit and Tredoux (1988) and Tredoux et al. (1989a). These authors defined two groups of BA samples; Group A from the centre of the body and Group B from the margin of the body. Group A contained more Ni-rich and metallic phases than Group B and it was speculated that the margin had undergone a much larger degree of oxidation than the centre (Tredoux et al. 1989a).

Table 8.5: Summary of PGE and Au concentrations in Bon Accord (BA) rocks analysed by Tredoux et al. (1989a) and a comparison between inter-noble metal ratios for BA, on-craton Group I kimberlites and the Japecanga mica peridotite. All concentrations expressed in parts per billion. Group column abbreviations are the same as shown in Table 8.3.

		Concentration Present						
Sample	**Group**	**Os**	**Ir**	**Ru**	**Rh**	**Pt**	**Pd**	**Au**
R 4.5	BA (A)	488	651	1556	478	2166	1852	170
BA 83.B	BA (A)	1114	932	1830	515	1764	1537	250
BA 83.1	BA (A)	550	730	1314	n.d.a	1794	1793	n.d.a
DBS-3	BA (A)	584	501	1771	493	1478	1845	190
BA 84.3	BA (A)	441	380	1722	426	1694	1533	340
L 4.5	BA (A)	278	384	1123	n.d.a	n.d.a	1561	120
BA 84.1	BA (B)	108	150	684	221	1321	896	180
BA 84.2	BA (B)	73	72	617	225	1078	833	210
D 4.5	BA (B)	66	97	849	242	1583	461	200

Sample	**Group**	**Os/Ir**	**Ru/Os**	**Ru/Ir**	**Rh/Ir**	**Pt/Ir**	**Pd/Ir**	**Au/Ir**
R 4.5	BA (A)	0.75	3.19	2.39	0.73	3.33	2.81	0.26
BA 83.B	BA (A)	1.19	1.64	1.96	0.55	1.89	1.65	0.27
BA 83.1	BA (A)	0.75	2.39	1.80	-	2.45	2.46	-
DBS-3	BA (A)	1.16	3.03	3.53	0.98	2.95	3.68	0.38
BA 84.3	BA (A)	1.16	3.91	4.53	1.12	4.46	4.04	0.89
L 4.5	BA (A)	0.72	4.04	2.93	-	-	4.07	0.31
BA 84.1	BA (B)	0.72	6.34	4.56	1.47	8.81	5.98	1.20
BA 84.2	BA (B)	1.01	8.43	8.57	3.12	14.97	11.61	2.92
D 4.5	BA (B)	0.67	12.96	8.75	2.49	16.32	4.74	2.06
Frank Smith	K I (c)	1.14	1.64	1.86	0.27	1.96	0.96	0.22
Jagersfontein	K I (c)	1.15	1.56	1.80	-	1.78	1.20	0.43
Wesselton	K I (c)	1.61	1.29	2.08	0.57	3.54	2.61	1.77
Premier Grey	K I (c)	1.08	3.17	3.41	0.89	5.19	4.18	0.98
Premier Piball	K I (c)	1.07	2.76	2.95	0.93	5.07	3.52	0.90
Premier C. Dyke	K I (c)	1.45	1.47	2.13	0.98	6.38	3.40	0.94
Monastery	K I (c)	1.25	1.4	1.75	-	3.43	2.56	0.43
Benfontein	K I (c)	1.28	1.56	2.00	-	2.67	1.94	0.47
Vioolskraal	K I (m)	1.36	2.09	2.83	0.78	5.07	2.98	0.61
Hartebeesfontein	K I (m)	1.33	2.73	3.65	0.95	4.60	3.33	0.90
Pampoenpoort	K T (m)	1.17	1.95	2.27	0.75	2.39	1.61	0.44
Japecanga	P T (??)	1.07	2.71	2.91	0.65	4.73	2.54	0.60

A summary of BA data and a comparison of the inter-noble metal ratios between the kimberlites and the BA rocks is shown in Table 8.5 and PGE patterns are

shown in Figure 8.13. Table 8.5 indicates that all of the BA rocks are highly enriched in PGE relative to the kimberlites but the ratios obtained from the on-craton Group I kimberlites completely overlap with the range of ratios observed in BA Group A. BA Group B is depleted in Os and Ir relative to the other PGE and shows higher Ru/Os, Ru/Ir, Pd/Ir and Au/Ir ratios than any of the kimberlite samples. Figure 8.13 also illustrates the similarity in terms of pattern shape between BA Group A and the kimberlites.

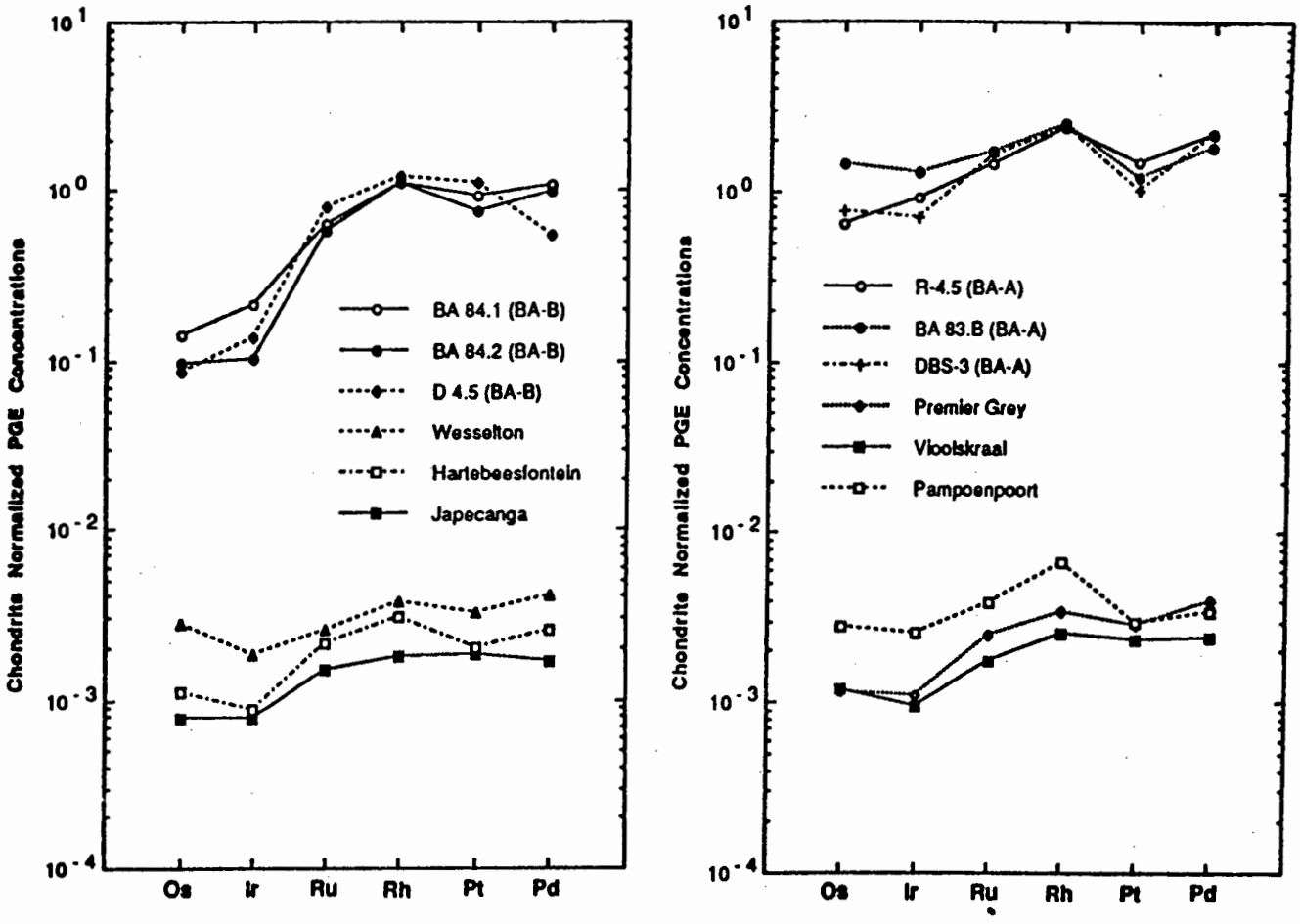

Figure 8.13 : Chondrite normalized PGE patterns showing the comparison between Bon Accord rocks and Group I kimberlites. Data from Tables 8.3 and 8.5.

Tredoux et al. (1989a) suggested that the fractionation in terms of Os and Ir between Groups A and B took place at temperatures in excess of 2300°C and these authors interpreted this as evidence that BA had a deep mantle (>1000 km depth) origin. De Wit and Tredoux (1988) and Tredoux et al. (1989a) proposed that BA was emplaced into the peridotitic portion of 3.5 Ga oceanic lithosphere via deep mantle upwelling. The oceanic lithosphere was subsequently stacked and thickened to form the earliest proto-continents (de Wit et al. 1987b; de Wit et al. 1992) and it was proposed that, as shown in Figure 8.14, pods of BA-like material

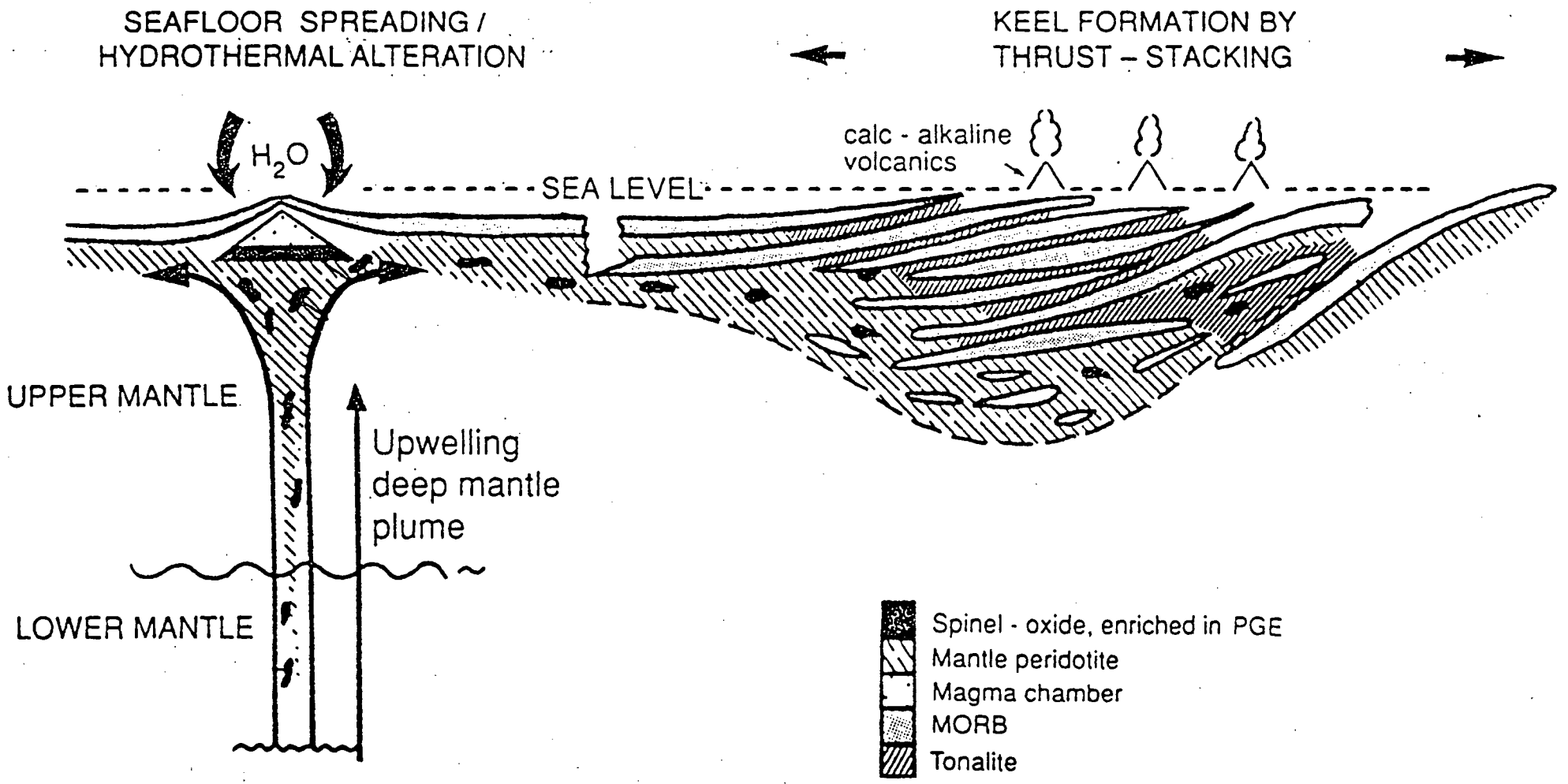

Figure 8.14: Model for the formation of Bon Accord (BA)-like material and its incorporation into the earliest continental lithosphere (from Tredoux et al. 1990). Ni and PGE-rich metallic pods are broughtupwards from the core-mantle boundary in mantle plumes. The pods are incorporated into early oceanic and then subsequently continental lithosphere.

might form a PGE store in the keels of the continental lithosphere which could be sampled by later magmatism (Tredoux et al. 1989a).

Although Figure 8.13 indicates that the absolute concentrations of the PGE are lower by factors of 300-500 in the kimberlites relative to BA, the similarities in terms of ratios and PGE patterns between the two rock types are striking. I suggest that sampling of PGE from the lithospheric keels as suggested by Tredoux et al. (1989a) could have taken place and that the PGE signature of the on-craton and marginal Group I kimberlites is dominated by tiny xenocrysts of almost pristine BA-like material which has been physically incorporated into the melt. The fact that the BA-like signature is replicated in three separate phases of the Premier intrusion (see section 8.4.1) is strong evidence for this process of physical incorporation.

The BA-like, negative Pt anomaly seen in the kimberlites is not greatly disturbed, even at relatively low concentrations of Pt and Pd, by any LTPGE enrichment (cf. the off-craton Group I kimberlites, MORB and OIB; see Figures 8.7 and 8.12). This would imply that the LTPGE concentrations of the on-craton Group I kimberlitic melt itself must have been very low (<2 ppb). The generation of a PGE-poor melt may therefore be a characteristic of the on-craton Group I source region or a consequence of the melting processes taking place. Furthermore, I would like to suggest that in an analogous fashion to diamonds (Gurney 1991), the BA xenocrysts are "passengers" carried upwards by the kimberlite "bus" and that the characteristic BA-like PGE pattern and inter-PGE ratios are preserved but the PGE concentrations are heavily diluted by a larger volume of PGE-poor melt.

Tredoux et al. (1989a) proposed that BA-like material was only incorporated into oceanic and subsequently continental lithosphere during the high heat flow environment developed during the Archean and implied that the material should be absent from later rocks. If this suggestion is correct, the presence a BA-like signature in kimberlites such as Hartebeesfontein and Pampoenpoort which lie outside the craton margin defined by Skinner et al. (1993) on the basis of surface geology, implies that Archean rocks containing BA-like material could exist at depth. BA-like PGE signatures may therefore be good indicators for the presence of Archean rocks at depth, although not necessarily diamonds, as both the Hartebeesfontein and Pampoenpoort kimberlites are barren of diamonds.

If Archean rocks do exist outside the margins of the craton, what is the nature of these rocks ? A scenario similar to that outlined for the Sao Francisco craton, where the margin of the craton might extend underneath Proterozoic and younger cover rocks, is not consistent with shear wave studies which suggest that the wester margin of the Kaapvaal craton is almost vertical around the proposed margin (M.J. de Wit pers. comm. 1993). Could a fragment or a detached block of Archean material have been accreted against the edge of the Kaapvaal craton during the Natal-Namaqua event and still be present at depth ? Further geophysical and isotopic studies will need to be made in the Preiska region before this possibility can be confirmed.

8.6.2. Intermediate PGE Signatures (Transitional And Group II Kimberlites).

8.6.2.1. Brazilian Samples.

It was noted in section 8.4.5 that the kimberlites and alkali basalts from Brazil appear to show a continuum of Pt/Ir and Pd/Ir ratios. These ratios are highest in the basalts and lowest in the kimberlites and peridotites, particularly the sample from Japecanga which most closely resembles the on-craton Group I kimberlites from southern Africa. The lowering of the ratios and the overall flattening of the PGE pattern appears to be related to the sampling of a greater amount of a HTPGE by the kimberlites in comparison to the basalts.

On the basis of xenolith studies and Sr, Nd and Pb isotope systematics, Bizzi et al. (1993b) suggested that Japecanga was a deeply derived melt similar to southern African Group I kimberlites. Table 8.6 and Figure 8.13 indicate that the inter-noble metal ratios and PGE pattern observed at Japecanga resembles BA. In view of the similarity with Japecanga in terms of Os/Ir, Ru/Os and Ru/Ir ratios (see Table 8.4), it was decided to investigate whether the HTPGE signature in the Tres Ranchos, Limeira and Pantano rocks might also come from BA-like material.

The method chosen to test this hypothesis was to assume that the Japecanga sample, like Group I kimberlites, represents a sample of a volumetrically small, BA-like contaminating phase and that this phase is physically assimilated into a kimberlitic or basaltic melt which has an initially fractionated pattern, similar to that seen at Sucesso. This approach assumes that any mixing relationship follows a $y = mx+c$ type of curve where y represents the final PGE concentration in the contaminated rock, c represents the PGE concentration in the fractionated melt

and m represents differing amounts of contamination by a Japecanga or BA-like component (x).

Table 8.6.: Comparison between the data obtained for Brazilian kimberlites and alkali rocks and simulated PGE concentrations based on contamination of a LTPGE fractionated melt (Sucesso) with BA-like material (Japecanga).

	Concentration Present					
	Os	Ir	Ru	Rh	Pt	Pd
Sucesso (SUC) fractionated melt	0.26	0.28	0.66	0.30	7.4	5.3
Japecanga (JAP) contaminant	0.59	0.55	1.6	0.36	2.6	1.4
Tres Ranchos Real Data	1.3	2.3	4.5	1.10	14.1	9.9
Simulation (SUC + 2.6 JAP)	1.79	1.71	4.82	1.24	14.16	8.94
Limeira Real Data	1.7	1.8	4.6	1.20	11.7	8.8
Simulation (SUC + 2.5 JAP)	1.73	1.66	4.66	1.20	13.9	8.80
Pantano Real Data	0.99	0.92	2.9	n.d.a.	9.9	6.2
Simulation (SUC + 1.1 JAP)	0.91	0.92	2.42	-	10.26	6.84
Pres. Olegario Real Data	0.48	0.45	0.54	n.d.a.	8.6	5.7
Simulation (SUC+ 0.4 JAP)	0.49	0.50	1.30	-	8.44	5.86

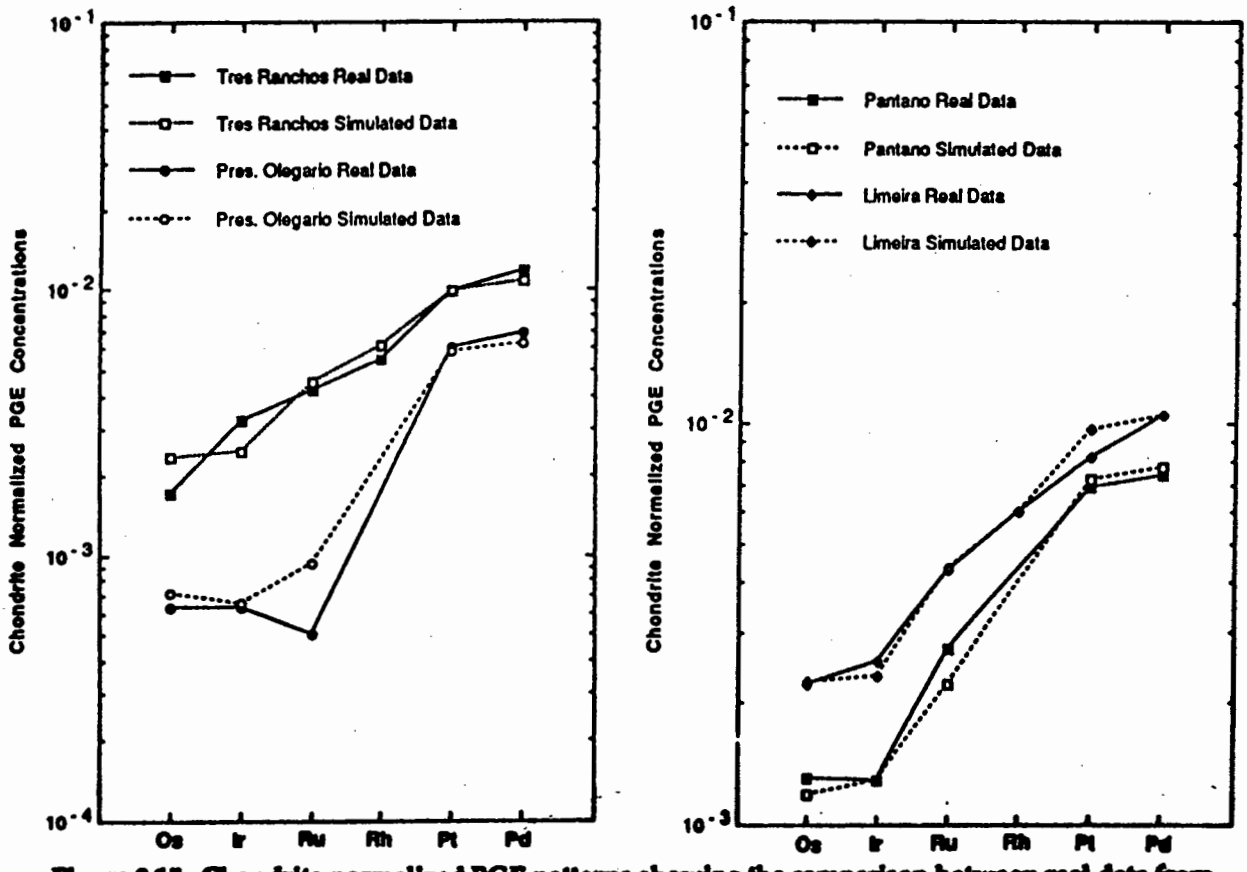

Figure 8.15: Chondrite normalized PGE patterns showing the comparison between real data from the Brazilian rocks and simulations calculated from Sucesso:Japecanga mixing and contamination. All data from Table 8.6.

It was found that this approach was able to simulate the PGE concentrations of all of the Brazilian rocks fairly well. The model Sucesso:Japecanga mixtures which show the best fit with the observed PGE concentrations at Tres Ranchos, Limeira, Pantano and Presidente Olegario are summarized in Table 8.6. Chondrite normalized PGE patterns of the model data and the real data are shown in Figure 8.15. The generally close fit which is observed between the two suggests that a PGE contamination process similar to that outlined above may have taken place during the generation of the Brazilian rocks.

8.6.2.2. Transitional Kimberlites On The Kaapvaal Craton.

Like the Brazilian rocks, transitional kimberlites on the Kaapvaal craton show slightly higher Pt/Ir, Pd/Ir and Au/Ir ratios than similar Group I kimberlites. A fractionated (LTPGE enriched) signature superimposed on a Group I-like pattern was suggested to explain the different PGE patterns observed in the Droogfontein, Lace and Pampoenpoort kimberlites (see section 8.5.2) and an analogous simulation to that performed for the Brazilian samples was investigated for the Kaapvaal transitional kimberlites.

Although only Ir and Pd data are available, the PGE composition of the Sucesso basalt is comparable with data from Karoo basalts (Crocket 1981). Therefore I have made the assumption that the Sucesso composition can be taken as representative of a PGE fractionated melt on the Kaapvaal craton. This assumption means that the model for the Kaapvaal is less well constrained than that for Brazil. Despite this, table 8.7 and Figure 8.16 indicate that the Droogfontein and Lace PGE patterns can be reasonably well simulated by contaminating a Sucesso-type signature with variable amounts of a Pampoenpoort-like (Group I) signature.

The success of this simulation appears to indicate that the Kaapvaal transitional kimberlites may have formed via a contamination process similar to that modelled for Brazil. However, the present dataset is small and PGE data from a greater number of Kaapvaal transitional kimberlites will be needed before a more definite conclusion can be drawn.

Table 8.7.: Comparison between the data obtained for southern African transitional kimberlites and simulated PGE concentrations based on contamination of a LTPGE fractionated melt (Sucesso) with BA-like material (Pampoenpoort).

	Concentration Present					
	Os	Ir	Ru	Rh	Pt	Pd
Sucesso (SUC) fractionated melt	0.26	0.28	0.66	0.30	7.4	5.3
Pampoenpoort (PAM) contaminant	2.1	1.8	4.1	1.35	4.3	2.9
Lace K 2 Real Data	1.8	1.6	3.0	1.15	11.2	6.8
Simulation (SUC + 0.65 PAM)	1.62	1.45	3.32	1.18	10.20	7.18
Droogfontein Real Data	1.3	1.5	4.0	1.49	10.6	6.3
Simulation (SUC + 0.70 PAM)	1.72	1.54	3.53	1.25	10.41	7.33

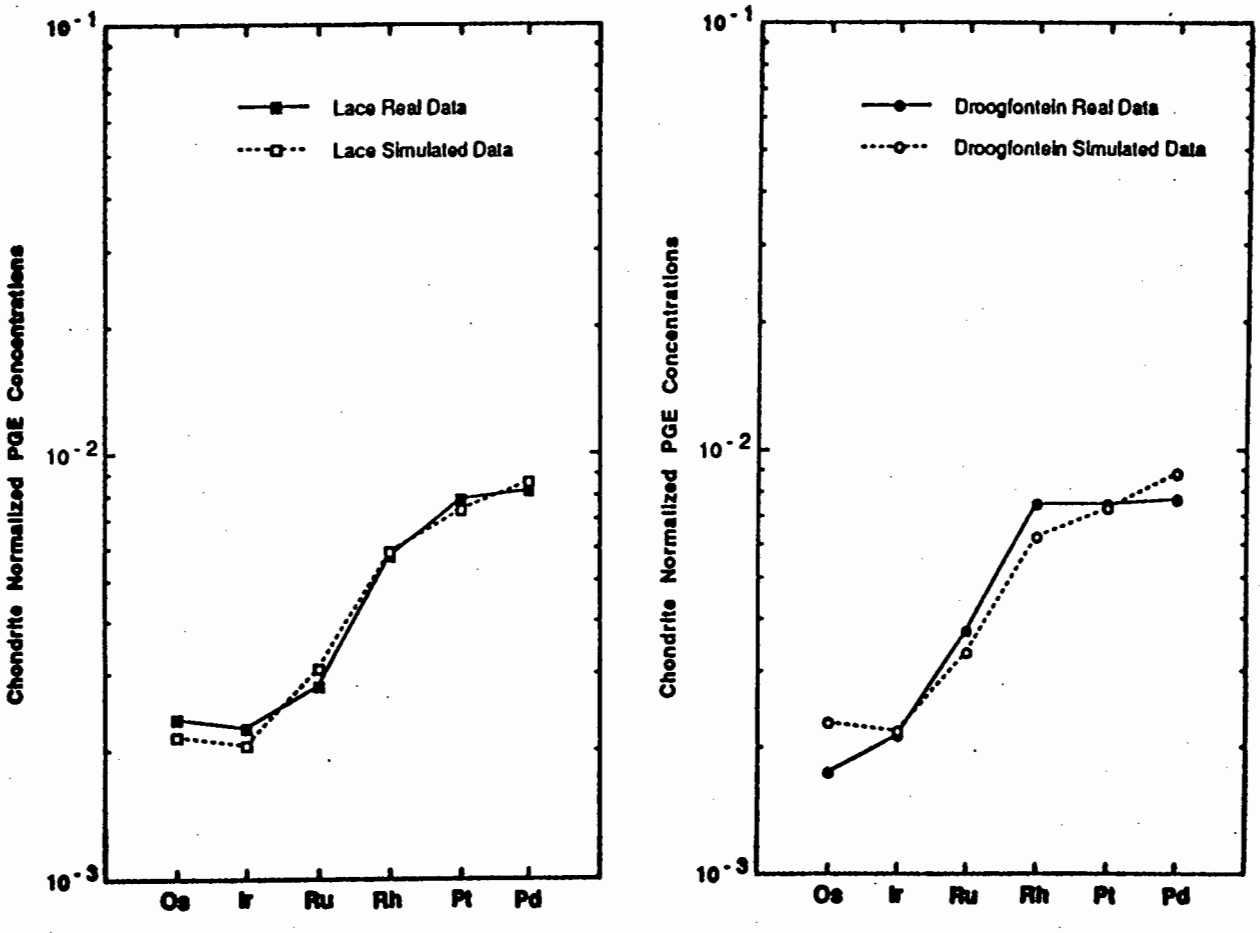

Figure 8.16: Chondrite normalized PGE patterns showing the comparison between real data from southern African transitional kimberlites rocks and simulations calculated from Sucesso::Pampoenpoort mixing and contamination. All data from Table 8.7.

8.6.2.3. On-Craton And Marginal Group II Kimberlites.

On the basis of the strong overlap in terms of the HTPGE and the higher Pd/Ir and Au/Ir ratios seen in Group II kimberlites relative to Group I, I would tentatively suggest that mixing between a contaminant with a BA-like PGE signature and a PGE-fractionated melt may have taken place during the generation of Group II kimberlites. The LTPGE concentrations in Group II kimberlites are less than seen in the Sucesso basalt which means that a $y = mx + c$ simulation using Sucesso as the c component will always produce LTPGE concentrations higher than actually observed in the rocks.

A number of hypothetical PGE-fractionated melts with lower LTPGE contents than the Sucesso basalt and Pd/Ir ratios ranging between 6 and 10 have been used in simulations. Although it has been possible to achieve some reasonable fits with the Sanddrift and Finsch data, this approach is extremely arbitrary and very poorly constrained. While it is considered possible that contamination of a PGE fractionated melt could have taken place during the generation of Group II kimberlites, at present this cannot be well modelled due to the very large uncertainties associated with the composition of any PGE-fractionated melt.

8.6.3. Highly Fractionated PGE Patterns (Alkali Basalts And Off-Craton Rocks).

The alkali basalts, melilitites and off-craton kimberlites all show fractionated PGE patterns similar to MORB and OIB (see Figure 8.12). HTPGE contents of these rocks are for the most part significantly lower than kimberlites from the cratonic environment and a BA-like HTPGE signature with a negative Ir anomaly is not observed in these rocks. This group of samples most likely represent PGE fractionated melts which have not incorporated any BA-like material either from their source region or during ascent.

The source regions of these melts which gave rise to such fractionated patterns remain a point of debate. Off-craton Group I kimberlites and melilitites are suggested to have an asthenospheric source (Smith et al. 1985; Viljoen 1988; Spriggs 1988) and represent melts of fertile mantle. Enriched lithospheric mantle has been proposed as a source for the Brazilian alkali basalts (Bizzi et al. 1993a) and the Group II kimberlite at Eendekuil (K.S. Viljoen pers comm. 1992). Fractionated PGE patterns are also shown by the southern African Karoo basalts (Crocket 1981; Barnes et al. 1985), which are believed to have been derived from enriched lithosphere (Hawkesworth et al. 1985).

It would appear likely that small volumes of melting in the asthenospheric mantle or enriched lithosphere can produce fractionated PGE patterns. However, the most important feature of all of these rocks is that melts appear to have ascended through lithosphere which did not contain any BA-type material. In the case of the off-craton kimberlites and melilitites, this is probably related to the lack of BA-bearing Archean lithosphere outside the area of the craton. While for the shallow derived alkali basalts, it could reflect the deep-seated location of BA material within the lithospheric keel (Tredoux et al. 1989a). For either of these reasons, contamination did not take place during ascent and the melts retained a highly fractionated PGE signature.

8.7. A Model For The Generation Of PGE Signatures In Kimberlites.

In section 8.6, three groups of kimberlites were recognised in terms of their PGE signatures and the possible source of these signatures were discussed. In this section, I will attempt to use these signatures to place some constraints on the sources of kimberlite and other alkaline melts and how these melts might interact with the lithosphere.

The signatures from on-craton Group I kimberlites and Group I-like transitional kimberlites have been interpreted as the contamination of a PGE-poor melt with variable amounts of BA-like material (see section 8.6.1). Off-craton Group I rocks show highly fractionated (LTPGE enriched) patterns apparently without a contribution from BA contamination (see section 8.6.3). On-craton Group II and Group II-like transitional kimberlites are also suggested to be fractionated, LTPGE enriched melts, but which have suffered BA contamination (see section 8.6.2).

This complex set of signatures does not fit well with the models proposed by Le Roex (1987), Spriggs (1988) and Ringwood et al. (1992). These authors have suggested that all kimberlites are derived from the asthenosphere and are similar to the melts which formed ocean island basalts (OIB). Plume-derived melts of the asthenospheric mantle, such as OIB, always give rise to fractionated PGE patterns, often with strong LTPGE enrichment (see Figure 8.12) and while presence of fractionated PGE signatures implied in some of the Group II and Group II-like transitional kimberlites resemble OIB patterns, the on-craton Group I kimberlites do not.

The consistency of the PGE patterns from on-craton Group I kimberlites over a wide range of ages (see Table 8.1) suggests that PGE-poor melts must have been available in order to generate these kimberlites for at least 1.1 Ga (the age of the Premier kimberlite). The apparently PGE-poor nature of the melt may reflect either magmatic processes which operated to remove PGE from the melt during ascent, or a PGE-depleted source region which releases very little PGE into the liquid when subjected to melting. If we assume that kimberlite generation produces an initially fractionated, LTPGE enriched melt, then this can satisfy the most of the signatures seen but it would require the on-craton Group I kimberlites to have somehow lost PGE prior to emplacement. Hamlyn and Keays (1986) suggested that if an immiscible sulphide settles out during ascent of a melt, this would deplete the silicate fraction in PGE and base metals. Relics of apparently primary immiscible sulphides were observed in some kimberlites (Mitchell and Clarke 1976; C.B. Smith pers. comm. 1993) but these are very rare. Furthermore, if sulphide was retained in the mantle during kimberlite genesis, why did this only occur with on-craton Group I kimberlites and not any of the others ?

Alternatively, if the on-craton Group I kimberlites indicate generation from a PGE-poor source region, then it seems highly unlikely that the source of these kimberlites was the asthenospheric mantle as convection will cause a continual mixing of any PGE-poor region with the much larger volume of fertile mantle. If a distinctive PGE-poor source region has been in existence since at least 1.1 Ga, then the only way to preserve such a deeply located trace element signature over that period of time is to isolate it from the convecting asthenospheric mantle. This might take place in the lithosphere (Smith 1983; Skinner et al. 1993) or in very old slabs of subducted ocean crust which have been proposed by Ringwood (1989) and Ringwood et al. (1992) to lie along the 650km discontinuity.

This brings us back to the principal controversy discussed in section 8.1; do kimberlites originate in the lithosphere or from greater depths (perhaps even the transition zone). The Ringwood et al. (1992) model shown in Figure 8.17 has provoked considerable debate and I shall consider it first. Ringwood et al. (1992) predict that both kimberlites (Group I, Group II and transitionals) and OIB form in response to refertilization of mantle harzburgites via melting of the garnetite slab by a rising convection current. If the proto-kimberlite melts arising from the melting of the refertilized harzburgite were initially PGE-poor then those melts

which formed the Group II kimberlites, the transitional kimberlites and the off-craton Group I kimberlites/melilitites must have acquired LTPGE during ascent.

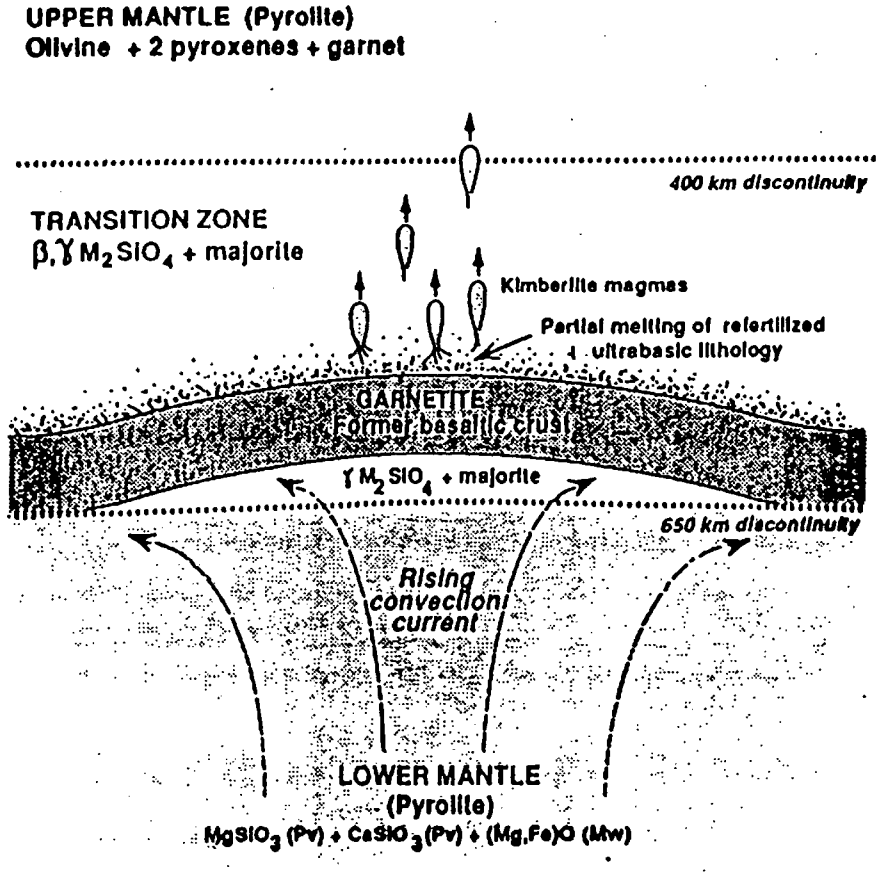

Figure 8.17 : A model for the generation of kimberlite magmas (from Ringwood et al. 1992). Elevated temperatures arising from the convection current cause small degrees of partial melting of the garnetite and refertilized ultrabasic lithology, producing kimberlite magmas.

Models which propose to generate kimberlites in the asthenosphere or transition zone envisage that transitional and Group II kimberlites acquire their distinctive isotopic and trace element characteristics by more extensive contamination by enriched lithosphere than is the case for Group I kimberlites and OIB (eg. Spriggs 1988; Bizzi et al. 1993a). If assimilation of the lithospheric mantle also introduces LTPGE into the melt then this might explain the PGE signatures of the Group II and the transitional kimberlites. However, the Sr, Nd and Pb isotopic signatures of the off-craton kimberlites and melilitites and OIB indicate that they have not suffered much interaction with enriched lithopshere yet they have higher LTPGE concentrations than any of the other rocks.

In the Ringwood et al. (1992) model, the main difference between cratonic kimberlites and OIB is that OIB melted in the Upper Mantle and mixed with

magmas were highly enriched in PGE; (Sharpe et al. 1982; Davies and Tredoux 1985) might therefore leave significant volumes of the cratonic keels depleted in PGE. It is my belief that kimberlite melts generated in these PGE-poor regions would also be PGE-poor and any BA-like material physically assimilated from the more pristine (unmelted) keel during ascent would dominate the final PGE pattern.

The PGE patterns observed in the off-craton Group I kimberlites and melilitites are compatible with the melting of an undepleted source. This source is suggested to be lithospheric mantle outside the cratonic keel which was not affected by Bushveld-type melting events; either because melting was largely confined to the keel or that the source material for the kimberlites is of a younger age than the ancient melting event. The source material was also unaffected by any ancient metasomatism, possibly for similar reasons (ie. it may be of a younger age).

Smith (1983), Smith et al. (1985) and Hawkesworth et al. (1985) have presented Sr, Nd and Pb isotopic evidence to suggest that Group II kimberlites are derived from enriched lithosphere. A similar origin is also suggested for the Group II-like transitional kimberlites (Bizzi et al. 1993b). This study has shown that the PGE patterns from the transitional kimberlites (and possibly the Group II kimberlites as well) can be modelled as contamination of a LTPGE-fractionated melt of similar composition to lithospherically derived alkali basalts.

The proposed model for the generation of Group II and transitional kimberlites involves the melting of a lithospheric source region which has either not suffered PGE depletion or has been subsequently PGE enriched, possibly by the metasomatic event envisaged by Smith (1983) and Hawkesworth et al. (1983). If the H_2O-rich, small-volume metasomatic melts proposed by Hawkesworth et al. (1985) also contained high concentrations of F and Cl, they might have transported Pt and Pd (Mountain and Wood 1988; Sassini and Shock 1990) which could enrich the metasomatised region in these elements. However, either of the above explanations for the source region character can explain the subsequent generation of a LTPGE-fractionated kimberlite melt and, at present, it would not be prudent to exclude either mechanism.

With the exception of the off-craton kimberlite at Eendekuil, the melts which separated from this source region were contaminated by BA-like material during ascent, giving rise to a characteristic PGE pattern. It would appear that on the basis of the above discussion, the PGE signatures of all of the kimberlites, melilitites and basalts in this study can be generated by interactions within the lithosphere alone and that an asthenospheric melt is not specifically required.

Highly simplified models showing the proposed structures of the of the Sao Francisco and Kaapvaal cratons in terms of PGE are shown in Figures 8.18 and 8.19. The PGE patterns expected for different lithospheric environments and kimberlite groupings are also summarized. The precise relationship between regions of the lithosphere which are PGE-depleted and those which are undepleted or metasomatized is unclear. The PGE depleted regions are shown as large isolated pods on the figures but this may not be the case and they may actually be much more continuous on a horizontal or a vertical scale.

I believe that the presence of BA-like signature in the most westerly kimberlites in the Coromandel area indicates that Archean material exists at depth and that the western margin of the Sao Francisco craton extends at least as far west as the Tres Ranchos kimberlite (see Figures 8.4 and 8.5). This is in agreement with the geophysical studies of Pires (1986). The western margin of the Kaapvaal craton does not appear to dip under any younger rocks, as appears to be the case for the Sao Francisco craton (M.J. de Wit pers comm 1993). Therefore the presence of BA-like signatures in Group I and transitional kimberlites just outside the margin may indicate the presence of a fragment of (non-Kaapvaal ?) Archean material at depth which has been wedged along the side of the craton.

The only way to provide conclusive proof of the proposed model for PGE signatures in kimberlites would be to perform conventional PGE analysis combined with a detailed Re-Os isotope study on a large number of kimberlite samples. To date, only two kimberlites have been analysed for Os isotopes by Walker et al. (1989). Both samples were from on-craton kimberlites, a Group I kimberlite from Letseng le Terae in Swaziland and a Group II kimberlite from Bellsbank. The data obtained from these samples led Walker et al. (1989) to conclude that the Group I kimberlite had been generated from material with a chondritic Re/Os ratio and that the Group II kimberlite had been generated from material which had suffered Re depletion, perhaps in an ancient melting event.

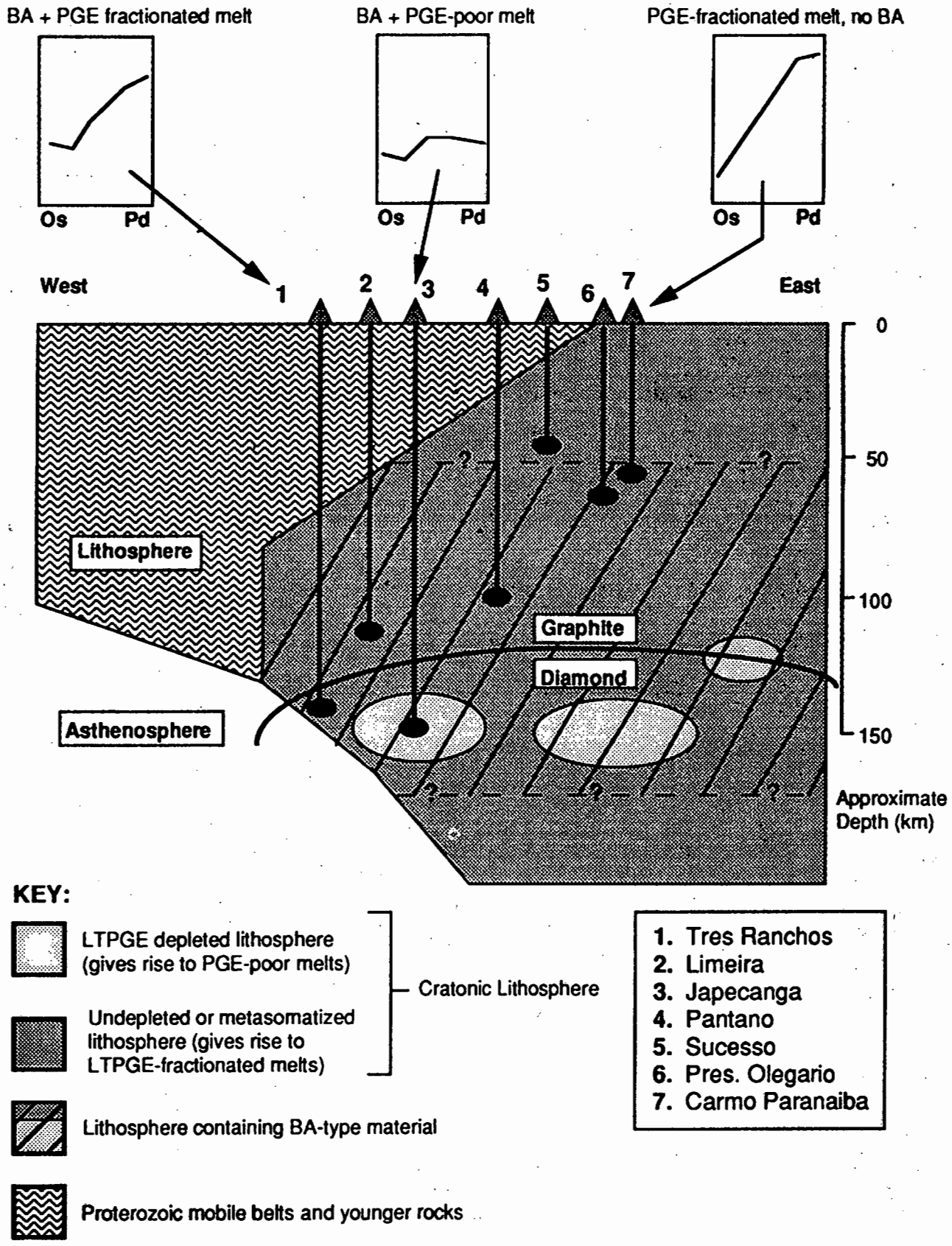

Figure 8.18: Simplified section through the western margin of the Sao Francisco craton showing the major PGE reservoirs and the PGE patterns which are likely to to be generated via the mixing or contamination mechanism outlined in the text. The limits of the area of cratonic lithosphere which contains Bon Accord-like material are not well constrained and are shown with question marks.

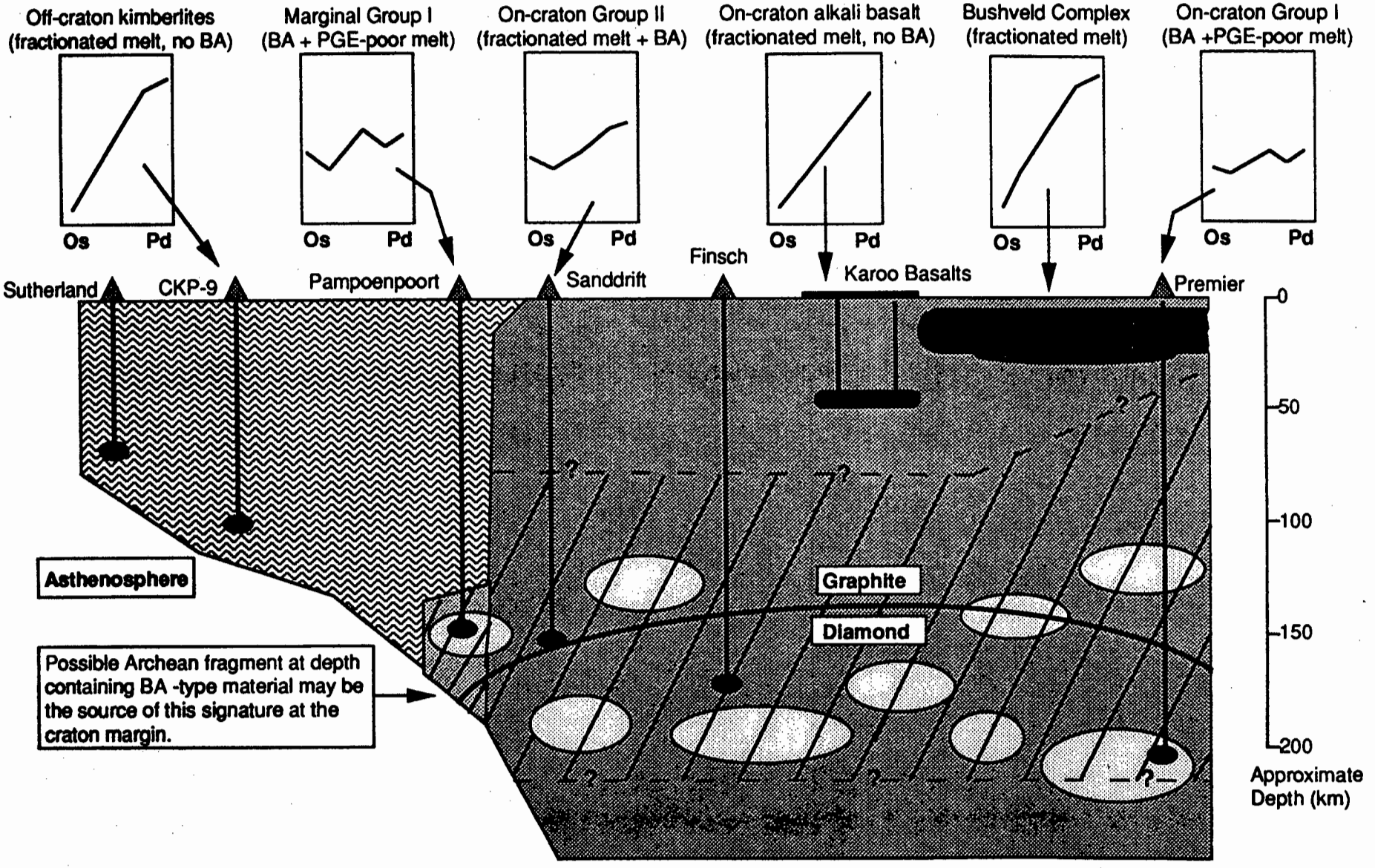

Figure 8.19: Simplifed section through the Kaapvaal craton showing major the major PGE reservoirs and the PGE patterns likely to be generated via the contamination mechanism outlined in the the text. Symbols for PGE reservoirs are the same as shown in Figure 8.18. The limits of the region containing BA-like material are poorly constrained and are shown with question marks.

These conclusions appear to be in direct contrast to the model which I have proposed above, however some clarification is necessary. The procedure employed for Os extraction by Walker et al. (1989) involved digestion of the kimberlite powder using a combination of acids, whereas more recent methods have relied on NiS fire-assay as an initial extraction step (Martin 1989; Pegram and Allegre 1992; Hauri and Hart 1993). Walker et al. (1989) comment specifically on problems with refractory phases (notably spinels) using a digestion procedure. If, as outlined earlier, a sizeable fraction of the PGE in kimberlites are in the form of alloys or sulphides in BA xenocrysts (possibly themselves located within spinels) then these might not be effectively recovered by an acid dissolution (see section 2.3.2) causing errors in the final analysis (Riesberg et al. 1991).

In addition, it is not known how closely the geochemical behaviour of Re, particularly during melting, matches that of Rh, Pt or Pd (ie. Re depletion may not necessarily indicate LTPGE depletion). The geochemical behaviour of Re in magmatic or metasomatic fluids is even less well constrained that that for the PGE so it is not known whether they can even occur in the same fluids (eg if a depleted area were metasomatized with a fluid containing Pt and Pd, would that fluid also contain Re ?). The isotope data reported by Walker et al. (1989) provide a useful first step but until a much wider suite of kimberlite samples is analysed for Os isotopes using NiS fire-assay extraction techniques, any conclusions must be tinged with caution. Future combined studies of PGE elemental concentrations and isotopes will no doubt provide a much more coherent picture than has been possible thus far using either approach alone.

8.8. Summary.

The analyses presented in this study indicate that the concentrations of the PGE and Au in kimberlites are comparable with the concentrations in other ultramafic rocks (generally <20ppb). Important differences in terms of PGE patterns and inter-noble metal ratios were observed between on-craton and off-craton kimberlites, and between kimberlites and alkali basalts.

Considerable overlap was observed in the signatures of Group I, Group II and transitional kimberlites and separation of these groups via their PGE signatures is very much less clear than the separation shown by the lithophile elements and Sr, Nd and Pb isotopes. However, it would appear that Group II and most

transitional kimberlites contain more LTPGE and Au and show more fractionated PGE patterns than Group I kimberlites.

The PGE signature of on-craton and craton-margin Group I kimberlites resembles that seen in the Bon Accord (BA) Ni-rich body described by Tredoux et al. (1989). These authors proposed that Ni-rich pods similar to BA were incorporated into the keels of the Earth's earliest continents, forming a PGE store which could be sampled by later magmatism. It is proposed that the PGE signature of Group I kimberlites developed via the contamination of a PGE-poor kimberlitic melt with xenocrysts of BA-like material. The apparently PGE-poor nature of the Group I melt, its consistent recurrence in kimberlites over a period of more than 1.1 Ga, and the restriction of the PGE-poor signature to the vicinity of the craton suggests that it cannot have arisen via a generalized melting of the convecting asthenosphere or of refertilized material on the 650 km discontinuity. A lithospheric origin is therefore suggested for the on-craton Group I and all other kimberlites.

Alkali basalts generated within the craton and kimberlites from off-craton environments show strongly fractionated PGE signatures with no evidence for contamination by BA-like material. Tredoux et al. (1989) proposed that BA-like material is restricted to the craton, and more specifically to the deep cratonic keels. Kimberlites which are emplaced off the craton, through Proterozoic or younger crust, do not encounter any BA-like material and are not contaminated. Similarly, the shallow depth of alkali basalt generation (<100km) may not be deep enough to sample the BA-rich portions of the lithospheric keel and therefore no contamination is evident in the final PGE pattern.

It is suggested that the PGE signatures of on-craton and craton-margin Group II and transitional kimberlites can be developed by the contamination of a LTPGE-fractionated melt with xenocrysts of BA-like material. The LTPGE-fractionated melt may have arisen from the melting of lithosphere which had not undergone previous melting and PGE depletion, or from lithosphere which had been metasomatically enriched in the LTPGE.

It is proposed that distinct PGE-bearing reservoirs exist within the ancient continental lithosphere. These are shown schematically in Figures 8.18 and 8.19. Interactions (melting or contamination) between these reservoirs during alkaline

magmatism can give rise to the variety of PGE signatures observed in this study. However, future Os isotope studies will almost certainly be required in order to test this hypothesis adequately.

Chapter 9

Summary Of Main Conclusions.

The principle conclusions reached in this thesis can be summarized as follows:

(1) There is probably no unique system of inter-metal discrimination which can be applied to the PGE as a variety of physical or chemical properties can influence the behaviour of the individual metals. Classification schemes such as those of Barnes et al. (1985) and Tredoux et al. (1986) are only based on a physical property and while this might serve in one chemical environment, it might be completely inappropriate for another environment. In attempting to understand a PGE distribution, all of the possible factors which might influence the PGE behaviour must be evaluated.

(2) The NiS fire-assay and NAA (NiS-NAA) procedure outlined in Chapter 4 and Appendix 4 offers low limits of detection (≤ 2.5 ppb) for all of the PGE. Coprecipitation was not employed in this study and extreme care must be taken by the analyst during dissolution of the NiS button in order to reach the correct end point. If the dissolution is too short, Te may be present in the residue. Activation of Te produces ^{123m}Te which may interfere with the Pt analysis. If the dissolution carries on too long, there may be losses of Pt and Pd as chlorides dissolved in the HCl.

(3) Multiple analyses of a potential komatiite standard (Wits-1) using the NiS-NAA procedure indicated better COVs than the analysis of SARM-7. This suggests that Wits-1 may be more homogeneous in terms of PGE than SARM-7. Data obtained by NiS fire-assay and NAA show a good agreement with data obtained fire-assay and ICP-MS. The three sets of Au data show little agreement which suggests that Au may be very inhomogeneously distributed throughout the rock and that Wits-1 is a much better standard for the PGE than for Au.

(4) The presence of carbon in fire-assay melts generates losses of the PGE to the volatile phase. Losses of the PGE are always greater in the absence of a sulphide melt and losses of the metals follow the trend, Ir > Rh ~ Os > Ru ~ Pt > Pd.

(5) Radiotracer experiments indicated that the volatile PGE species were more soluble in an non-polar organic solvent (toluene) than in polar media. Infrared analysis of the toluene fraction suggested that metastable PGE carbonyls were present and may have been the species involved in transporting the PGE from the melt to the volatile phase.

(6) C-H-O fluids at high pressures do not contain significant quantities of CO unless low fugacities of oxygen and water are present in the melt. No clear evidence was found for the transport and fractionation of the PGE via the proposed carbonylation reactions in Bushveld dunites of hypabyssal kimberlites which might have been influenced by a CO-bearing fluid.

(7) A closer analogy between the fire-assay experiments and real rocks might be the degassing, at atmospheric pressure, of a lava flow which either contained CO initially or assimilated carbon from sub-surface sediments or from the surface over which it flowed. Literature data from aerosols in Hawaii and Antarctica do not confirm or deny the proposed model and analyses of aerosols from basalts contaminated with carbon will be required before any definite conclusions can be drawn.

(8) The PGE signatures of kimberlites show significant differences between on-craton and off-craton kimberlites. Kimberlites emplaced into the craton are believed to sample and dilute xenocrysts of material with a similar PGE signature to the Bon Accord (BA) Ni-rich pods which were proposed by Tredoux et al. (1989a) as a major PGE store in the lithospheric keels of cratons. Off-craton kimberlites do not pass through the cratonic keel and show no evidence for contamination by this material.

(9) In contrast to the their lithophile element and isotopic signatures, Group I, transitional and Group II kimberlites do not show very different PGE patterns. In terms of Os, Ir, Ru and Rh, the groups are identical but the transitional and Group II rocks are slightly enriched in Pt, Pd and Au relative to Group I.

(10) The PGE signatures seen in transitional kimberlites from Brazil and South Africa can be modelled as contamination of a melt with a fractionated (LTPGE enriched) PGE signature, by BA-like material. A similar relationship may hold for Group II kimberlites but this cannot be proven at present.

(11) A model for the PGE signatures in kimberlites is proposed where different PGE reservoirs might exist in the subcontinental lithospheric mantle. The manner in which these reservoirs interact can produce all of the signatures observed.

References.

Abel, E.W. and Stone, F.G.A., (1969): The chemistry of transition metal carbonyls: structural considerations. Quart. Rev. Chem. Soc. **23**, 325-

Abel, E.W. and Stone, F.G.A. , (1970): The chemistry of transition metal carbonyls : synthesis and reactivity. Quart. Rev. Chem. Soc. **24**, 498-

Adams, F., and Dams, R., (1970): Applied gamma-ray spectrometry. 2nd edition, Pregamon Press, London, 753pp.

Alcock, C.B., and Hooper, G.W., (1960): Thermodynamics of the gaseous oxides of the platinum-group metals. Proc. Roy. Soc. **A254**, 551-561.

Almeida, F.F.M., (1977): O craton do Sâo Francisco. Revista Brasileira de Geosciências **7**, 364-394.

Alvarez, W., Alvarez, L.W., Asaro, F., and Michel., H.V., (1982): Current status of the impact theory for the terminal Cretaceous extinction. Geol. Soc. America Spec. Paper **190**, 305-315.

Anders, E., Wolf, R., Morgan, J.W., Ebihara, M., Woodrow, A.B., Janssens, M.J., and Hertogen, J., (1988): Radiochemical neutron activation analysis for 36 elements in geological materials. Nuclear Science Series NAS-NS-3117, U.S. Dept. of Comm., Springfield, Virginia, 95pp.

Anderson, S., Landquist, B.I., and Norskov, J.K., (1977): Possible mechanism for the catalytic action of nickel surfaces on the reaction $CO = C + CO_2$. Proc. 7th Intl. Vacuum Congress, Vienna, 815.

Andeweg, A.H., and Watterson, J.I.W., (1980): A large capacity sample changer for fully automated gamma-ray spectroscopy. I.E.E.E. Trans. Nucl. Sci., **NS-27**, 1.

Andeweg, A.H., and Modiba, J., (1990): Liquid nitrogen automatic fill control system. Schonland Res. Centre intl. rept. 90/19, 6pp.

Andeweg, A.H., Fearick, R.W., Watterson, J.I.W., and Hart, R.J., (1990): Dual detector counting system for INAA. (abstract) S. African Inst. Physics Conf., Port Elizabeth, 3-6 July 1990, 67.

Apt, K.E., and Gladney, E.S., (1975): Loss of Os during fusion of geological materials. Anal. Chem. **47**, 1484.

Bailey, E.B, and Anderson, E.M., (1925): The geology of Staffa, Iona and western Mull. Mem. Geol. Sruv. Scotland.

Ballhaus, C.G., and Stumpfl, E.F., (1985): Occurrence and petrological significance of graphite in the upper Critical Zone, western Bushveld Complex, South Africa. Earth Planet. Sci. Lett. **74**, 58-68.

Ballhaus, C.G., and Stumpfl, E.F., (1986): Sulphide and platinum mineralization in the Merensky Reef: evidence from hydrous silicates and fluid inclusions. Contrib. Miner. Petr. **94**, 193-204.

Barnes, R.M., and Diallo, A., (1986): Application of inductively coupled plasma atomic emission spectroscopy to the determination of platinum-group metals, silver, tantalum, thorium and uranium in geological materials with a poly(dithiocarbamate) resin separation. in L.R.P. Butler (ed.) Analytical chemistry in the exploration, mining and processing of materials. Blackwell, Oxford, 3-13.

Barnes, S.-J., Naldrett, A.J., and Gorten, M.P., (1985): The origin of the fractionation of platinum-group elements in terrestrial magmas. Chem. Geol. **53**, 303-323.

Barnes, S.-J., Boyd, R., Korneluissen, A., Nilsson, L.-P., Often, M., Pedersen, R.B., amd Robins, B., (1988): The use of mantle normaliztion and metal ratios in discriminating between the effects of partial melting, crystal fractionation and sulphide segregation on platinum-group elements, gold nickel and copper: examples from Norway. in H.M. Pritchard, P.J. Potts, J.F.W. Bowles and S.J. Cribb (eds.) Geo-platinum 87, Elsevier, London, 113-143.

Barnes, S.J., and Naldrett, A.J., (1985): Geochemistry of the J-M (Howland) Reef of the Stillwater Complex, Minneapolis Adit Area. I. Sulphide chemistry and sulphide-olivine equilibrium. Econ. Geol. **80**, 627-645.

Bartlett, N., Gennis, M., Gibler, D.D., Morrell, B.K., and Zalkin, A., (1973): Crystal structures of [XeF] [RuF_6] and [XeF_5] [RuF_6]. Inorg. Chem. **12**, 1717-1721.

Beamish, F.E., (1966): The analytical chemistry of the noble metals. Pergamon Press, Oxford, 609pp.

Beamish, F.E., and Van Loon, J.C., (1972): Recent advances in the analytical chemistry of the noble metals. Pergamon Press, Oxford, 511pp.

Beamish, F.E., and Van Loon, J.C., (1977): Analysis of noble metals; Overview and selected methods. Academic Press, New York, 327pp.

Berlincourt, L.E., Hummel, H.H., and Skinner, B.J., (1981): Phases and phase relations of the platinum-group elements. in Cabri, L.J., (ed.) Platinum-Group Elements: Mineralogy, Geology, Recovery. Canadian Institute of Mining and Metallurgy Spec. Publ. **23**, 47-64.

Bizzi, L.A., Smith, C.B., De Wit, M.J., Armstrong, R.A., and Meyer, H.O.A., (1993a): Mesozoic kimberlites and related alkalic rocks in the south-western Sao Francisco craton, Brazil: a case for local mantle reservoirs and their interaction. Proc. 5th Intl. Kimberlite Conf., Brasilia (in press).

Bizzi, L.A., Smith, C.B., de Wit, M.J., and Armstrong, R.A., (1993b): "Dupal-type" common source kimberlites, carbonatites, alkalic and flood basalts in Brazil. Earth Planet. Sci. Lett. (submitted).

Blum, J.D., Wasserburg, G.J., Hutcheon, I.D., Beckett, J.R., and Stolper, E.M., (1988): Domestic origin of opaque assemblages in refractory inclusions in meteorites. Nature **331**, 405-409.

Blum, J.D., Wasserburg, G.J., Hutcheon, I.D., Beckett, J.R., and Stolper, E.M., (1989): Diffusion, phase equilibria and partitioning experiments in the Ni-Fe-Ru system. Geochim. Cosmochim. Acta **53**, 483-489.

Borg, G., Tredoux, M., Maiden, K.J., Sellschop, J.P.F., and Wayward, O.F.D., (1988): PGE and Au distribution in rift-related volcanics, sediments and stratabound Cu/Ag ores of middle Proterozoic age in central SWA/Namibia. in H.M. Pritchard, P.J. Potts, J.F.W. Bowles and S.J. Cribb (eds.) Geo-platinum 87, Elsevier, London, 303-317.

Borthwick, A.A., and Naldrett, A.J., (1984): Neutron activation analysis for platinum-group elements and gold in chromitites. Anal. Lett. **17**, 265-275.

Boudreau, A.E., Mathez, E.A., and McCallum, I.S., (1986): Halogen geochemistry of the Stillwater and Bushveld complexes: Evidence for transport of the platinum-group elements by Cl-rich fluids. Jour. Petrol. **27**, 967-986.

Bowen, H.J.M., and Gibbons, D., (1963): Radioactivation analysis. Clarendon Press, Oxford, 295pp.

Bowles, J.F., (1986): The development of the platinum-group minerals in laterites. Econ. Geol. **81**, 1278-1285.

Boyd, R., Grenne, T., and Pedersen, R.B., (1992): Stratiform Pt-Pd-Au mineraliztions in ophiolites - Norwegian and other examples. (abstract) Geol. Soc. Lond. Min. Deposits Studies Group AGM, University of Aberdeen, 6-7th January 1992.

Bristow, J.W., Smith, C.B., Allsop, H.L., Shee, S.R., and Skinner, E.M.W., (1986): Setting, geochronolgy and geochemical charactersitics of 1600Ma kimberlites and related rocks from Kuruman Province, South Africa. (abstract) 3rd Intl. Kimberlite Conf.

Brookins, D.G., (1987): Platinoid metal Eh-pH diagrams (25ºC, 1 bar) in the systems M-O-H-S with geochemical applications. Chem. Geol. **64**, 17-24.

Brown, H., and Goldberg, E.D., (1949): The neutron pile as a tool in quantitative analysis. Science **109**, 347.

Brügmann, G.E., Arndt, N.T., Hofmann, A.W., and Tobschall, H.J., (1987): Noble metal abundances in komatiite suites from Alexo, Ontario and Gorgona Island, Colombia. Geochim. Cosmochim. Acta **51**, 2159-2169.

Burnham, C.W., (1985): Energy release in subvolcanic environments: implications for breccia formation. Econ. Geol. **80**, 1515-1522.

Byers, C.D., Muenow, D.W., and Garcia, M.O., (1983): Volatiles in basalts and andesites from the Galapagos Spreading Centre, 85º to 86º W. Geochim. Cosmochim. Acta. **47**, 1551-1558.

Cabri, L.J., (1972): The mineralogy of the platinum-group elements. Mineral. Sci. Eng. **4**, 3-29.

Campbell, I.H., and Barnes, S.J., (1984): A model for the geochemistry of the platinum-group-elements in magmatic sulphide deposits. Canad. Mineral. **22**, 151-160.

Campbell, I.H., Naldrett, A.J., and Barnes, S.J., (1983): A model for the origin of platinum-rich sulphide horizons in the Bushveld and Stillwater complexes. J. Petrol. **24**, 133-165.

Cameron, E.N., and Desborough, G.A., (1964): Origin of certain magnetite-bearing pegmatites in the eastern part of the Bushveld Complex, South Africa. Econ. Geol. **59**, 197-225.

Chou, C.-L., Shaw, D.M., and Crocket, J.H., (1983): Siderophile trace elements in the Earth's oceanic crust and upper mantle. J. Geophys. Res. **88**, (suppl.) A507-518.

Chyi, L.L., (1982): The distribution of gold and platinum in bituminous coals. Econ. Geol. **77**, 1592-1597.

Clark, T.C., Smith, C.B., and Rickard, D., (1990): Geochemical character of Prieska Province kimberlites and perovskites - some comparisons to cratonic types. (abstract) Geocongress 1990, Geol. Soc. S. Afr., University of Cape Town, 92-95.

Clarke, D.B., and Mitchell, R.H., (1975): Mineralogy and petrology of the kimberlite from Somerset Island, N.W.T., Canada. Phys. Chem. Earth **9**, 123-136.

Clement, C.R., (1982): A comparitive geological study of some major kimberlite pipes in the Northern Cape and Orange Free State. Unpubl. PhD thesis, University of Cape Town.

Clement, C.R., and Skinner, E.M.W., (1979): A textural classification of kimberlite rocks. (ext. abstr.) 2nd Intl. Kimberlite Conf., Cambridge.

Clement, C.R., and Reid, A.M., (1989): The origin of kimberlite pipes: an interpretation based on a synthesis of geological features displayed by southern African occurrences. in Kimberlites and related rocks., Proc. 4th Intl. Kimb. Conf., Geol. Soc. Australia Spec. Publ. **14**, 632-647.

Cotton, F.A., and Wilkinson, G. (1980): Advanced inorganic chemistry; A comprehensive text. Wiley Interscience, Chinchester, 1396pp.

Coughlin, R.W., Kawakami, K., Hasan, A., and Buu, P. (1982): Dynamic activation, deactivation, and coking on Pt and PtRe catalysts for dehydrogenation of methlycyclohexane (MCH). in B. Imelik, C. Naccache, G. Coudurier, H. Praliaud, P. Meriaudeau, P. Gallezot, G.A. Martin, and J.C. Verdine (eds.) Metal-support and metal-additive effects in catalysis. Elsevier, Amsterdam, 307-314.

Crabtree, R.H., (1988): The organometallic chemistry of the transition metals. Wiley Interscience, Toronto, 205pp.

Crocket, J.H., (1969): Platinum metals. in K.H. Wedepohl (ed.) Handbook of Geochemistry, Springer Verlag, Berlin.

Crocket, J.H., (1971): Neutron activation analysis for noble metals in geochemistry. in A.O. Brunfelt and E. Steinnes (eds.) Activation analysis in geochemistry and cosmochemistry. Universiteitsforlaget, Oslo, 339-351.

Crocket, J.H., (1981): Geochemistry of the platinum-group elements. in Cabri, L.J., (ed.) Platinum-Group Elements: Mineralogy, Geology, Recovery. Canadian Institute of Mining and Metallurgy Spec. Publ. **23**, 47-64.

Crocket, J.H., Keays, R.R., and Hsieh, S., (1968): Determination of some precious metals by neutron activation analysis. J. Radioanalyt. Chem. **1**, 487-507.

Crocket, J.H., and Cabri, L.J., (1981): Analytical methods for the noble metals. in Cabri, L.J., (ed.) Platinum-Group Elements: Mineralogy, Geology, Recovery. Canadian Institute of Mining and Metallurgy Spec. Publ. **23**, 71-81

Crocket, J.H., and MacRae, W.E., (1986): Platinum-group element distribution in komatiitic and tholeiitic volcanic rocks from Munro Township, Ontario. Econ. Geol. **81**, 1242-1251.

Crowe, B.M., Finnegan, D.L., Zoller, W.H., and Boynton, W.V., (1987): Trace element geochemistry of volcanic gases and particles from the 1983-84 eruptive episodes of Kilauea volcano. J. Geophys. Res. **92**, 13708-13714.

Cummings, J.B., Parekh, P.P., and Murali, A.V., (1988): A novel approach to the determination of iridium via Ge-coincidence/NaI(Tl)-anticoincidence gamma-ray spectrometry. Nucl. Instrum. Methods in Phys. Res. **A265**, 468-474.

Date, A., Davies, A.E., and Cheung, Y.Y., (1987): The potential of fire assay and inductively coupled plasma source mass spectrometry for the determination of the platinum-group elements in geological materials. Analyst **112**, 1217-1222.

Davidson, R.J., (1990): A pre-burial adsorption model for the genesis of gold in the Witwatersrand. J. S. Afr. Inst. Min. Metall. **90**, 53-57.

Davies, G., and Tredoux, M., (1985): The platinum group element and gold contents of the marginal rocks and sills of the Bushveld Complex. Econ.Geol. **80**, 838-848.

Dawson, J.B., (1967a): A review of the geology of kimberlite. in P.J. Wyllie (ed.) Ultramafic and related rocks. John Wiley & Sons, New York, 241-251.

Dawson, J.B., (1967b): Geochemistry and origin of kimberlite. in P.J. Wyllie (ed.) Ultramafic and related rocks. John Wiley & Sons, New York, 269-278.

Dawson, J.B., and Hawthorne, J.B., (1973): Magmatic sedimentation and carbonatitic differentiation in kimberlitic sills at Benfontein, South Africa. J. Geol. Soc. Lond. **129**, 61-85.

de Bruin, M., (1992): Present and future position of neutron activation analysis. J. Radioanalyt. Nucl. Chem. **160**, 31-40.

Delahay, G., and Duprez, D., (1989): Effect of sulphur on the coking of rhodium in the steam reforming of 1-Methylnaphthalene. Appl. Catal. **53**, 95-105.

de Ment, J., and Drake, H.C., (1949): Rarer Metals. Temple Press, London, 215-261.

de Wet, W.J., Turkstra, J., and Toerien, F.V.S., (1971): Direct determination of the noble metals by activation analysis utilizing high-resolution gamma spectrometry. in Brunfelt, A.O., and Steinnes, E., (eds.) Activation analysis in geochemistry and cosmochemistry. Universiteitsforlaget, Oslo, 371-379.

de Wit, M.J., (1985): Minerals and mining in Antarctica: Science and technology, economics and politics. Clarendon Press, Oxford, 127pp.

de Wit, M.J., Hart, R.A., and Hart, R.J., (1987): The Jamestown Ophiolite Complex, Barberton mountain belt: a section through 3.5 Ga oceanic crust. J. Afr. Earth Sci. **5**, 681-730.

de Wit, M.J., and Tredoux, M. (1988): PGE in the 3.5 Ga Jamestown ophiolite complex, Barberton greenstone belt, with implications for PGE distribution in the simatic lithosphere. in H.M. Pritchard, P.J. Potts, J.F.W. Bowles and S.J. Cribb (eds.) Geo-platinum 87, Elsevier, London, 319-341.

de Wit, M.J., and Kruger, F.J., (1990): The economic potential of the Dufek Complex. in Splettstoesser, J.F., and Dreschhoff, G.A.M., (eds.) Mineral Resources Potential Of Antarctica. Antarctic Research Series **51**, 33-52.

de Wit, M.J., Roering, C.J., Hart, R.J., Armstrong, R.A., de Ronde, C.E.J., Green, R.W.E., Tredoux, M., Peberdy, E., and Hart, R.A., (1992): Formation of an Archean continient. Nature **357**, 553-562.

de Wit, M.J., and Hart, R.A., (1993): Earth's earliest continetal lithosphere, hydrothermal flux and crustal recycling. Lithos (in press).

Donaldson, C.H., and Reid, A.M., (1982): Multiple intrusion of a kimberlitic dyke. Trans. Geol. Soc. S. Africa **85**, 1-12.

Eddy, B.T., Robért, R.V.D., and Russell, G.M., (1991): The analysis of the precious metals: a review. Proc. 4th Intl. Conf. on Appl. Mineral., Pretoria, South Africa, Paper **14**.

Ehmann, W.D., Baedecker, P.A., and McKown, D.M., (1970): Gold and iridium in meteorites and selected rocks. Geochim. Cosmochim. Acta **34**, 493-507.

Erasmus, C.S., Fesq, H.W., Kable, E.J.D., Rasmussen, S.E., and Sellschop, J.P.F., (1977): The NIMROC samples as reference standards for neutron activation analysis. J. Radioanal. Nucl. Chem. **39**, 323-334.

Erasmus, C.S., van Wyk, E., Novak, E., and Ramjee, B., (1982b): The determination of ultra-traces of the platinum-group elements and gold, in borehole cores from the western regions of the Bushveld Complex, by neutron activation analysis after preconcentration by nickel sulphide fire-assay. Mintek Tech. Mem. 10928, Council for Mineral Technology, Randburg, South Africa, 31pp.

Fesq, H.W., and Lee, C.A., (1978): A geochemical investigation of the lower portion of the Bushveld Complex with particular emphasis on the platinum-group elements. NPRU internal report 7815, Wits University, Johannesburg, 13pp.

Finnegan, D.L., Zoller, W., and Mroz, E., (1984): Trace element enrichments in volcanic gases from the 1984 eruption of Mauna Loa volcano. Trans. Am. Geophys. Un. **65**, 1138.

Finnegan, D.L., Miller, T.L., and Zoller, W.H., (1990): Iridium and other trace-metal enrichments from Hawaiian volcanoes. in Sharpton, V.L., and Ward, P.D., (eds.), Global catastrophes in Earth History; An interdisciplinary conference on

impacts, volcanism and mass mortality. Geol. Soc. America Spec. Paper 247, 111-116.

Fisher, R.V., and Schmincke, H-U., (1984): Pyroclastic rocks. Springer-Verlag, Berlin, 472pp.

Fleet, M.E., and Stone, W.E., (1991): Partitioning of platinum-group elements in the Fe-Ni-S system and their fractionation in nature. Geochim. Cosmochim. Acta **55**, 245-253.

Fouché, F.J., (1991): Instrumental neutron activation analysis (NAA) for environmental monitoring: applications for air. Proc. 10th NACA Conf., Durban, 8-12 November 1991, 1-11.

French, B.M., (1966): Some geological implications of equilibrium between graphite and a C-H-O gas phase at high temperatures and pressures. Rev. Geophys. **4**, 223-253.

Friberg, L.T., and Vostal, J.J., (1972): Mercury in the environment. CRC Press, London, 289pp.

Friedlander, G., Kennedy, J.W., and Miller, J.M., (1964): Nuclear And Radiochemistry. (2nd edition) John Wiley, London, 585pp.

Ganapathy, R., (1980): A major meteorite impact on the Earth 65 million years ago: evidence from the Cretaceous-Tertiary boundary clay. Science **209**, 921-923.

Gijbels, R., (1971): Determination of the noble metals by neutron activation analysis. Talanta **18**, 587-601.

Goldschmidt, V.M., (1954): Geochemistry. Oxford Press, London, 730pp.

Goodrich, C.A., and Bird, J.M., (1985): Formation of iron-carbon alloys in basaltic magma at Uivfaq, Disko Island: the role of carbon in mafic magmas. J. Geol. **93**, 475-492.

Graeber, E.J., Modreski, P.J., and Gerlach, T.M., (1979): Compositions of gases collected during the 1977 East Rift eruption, Kilauea, Hawaii. J. Volcanol. Geotherm. Res. **5**, 337-344.

Grassell, J.G., and Ritchley, W.H., (1975): Atlas of spectral data and physical constants for organic compounds. (2nd edition), vol. 1, CRC Press, Cleveland, Ohio, 488pp.

Greenwood, N.N., and Earnshaw, A., (1984): Chemistry of the elements. Pergamon Press, Oxford, 1542pp.

Groves, D.I., Ho, S.E., Rock, N.M.S., Barley, M.E., and Muggeridge M.T., (1987): Archean cratons, diamond and platinum: evidence for coupled long-lived crust-mantle systems. Geology **15**, 801-805.

Guinn, V.P., (1992): Past, present and future of neutron activation analysis. J. Radioanalyt. Nucl. Chem. **160**, 9-19.

Gurney, J.J., (1990): The diamondiferous roots of our wandering continent. Trans. Geol. Soc. S. Afr. **93**, 424-437.

Halban, H. von, Joliot, F., and Kowarski, L., (1939): The number of neutrons liberated in the nuclear fission of uranium. Nature, **143**, 680.

Hall, A., (1987): Igneous Petrology. Longman, Harlow, UK, 328pp.

Hall, G.E.M., and Bonham-Carter, G.F., (1988): Review of methods to determine gold, platinum and palladium in production oriented geochemical laboratories, with application of a statistical procedure to test for bias. J. Geochem. Expl. **30**, 255-286.

Hamlyn, P.R., and Keays, R.R., (1986): Sulfur saturation and second-stage melts: application to the Bushveld platinum metal deposits. Econ. Geol. **81**, 1431-1445.

Hart, S.R., (1988): Heterogeneous mantle domains: signatures, genesis and mixing chronologies. Earth Planet. Sci. Lett. **90**, 273-296.

Hartley, F.R., (1991): The occurence, extraction, properties and uses of the Platinum-Group Elements. in F.R. Hartley (ed.) Chemistry of the Platinum-Group Elements: recent developments. Elsevier, Amsterdam, 624pp.

Hartnady, C., Joubert, P. and Stowe, C., (1985): Proterozoic crustal evolution in southwest Africa. Episodes **8**, 236-243.

Hattori, K., and Hart, S.R., (1991): Osmium isotope ratios of platinum-group minerals associated with ultramafic intrusions: Os isotopic evolution of the oceanic mantle. Earth Planet. Sci. Lett. **107**, 499-514.

Hawkesworth, C.J., Erlank, A.J., Marsh, J.S., Menzies, M.A., and Van Calsteren, P., (1983): Evolution of the continental lithosphere: evidence from volcanics and xenoliths in Southern Africa. in C.J. Hawkeswroth and M.J. Norry (eds.) Continental basalts and mantle xenoliths. Shiva Publishing, London, 111-138.

Hawkesworth, C.J., Fraser, K.J., and Rogers, N.W., (1985): Kimberlites and lamproites: extreme products of mantle enrichment processes. Trans. Geol. Soc. S. Afr. **88**, 439-447.

Hauri, E.H., and Hart, S.R., (1993): Re-Os isotope systematics of HIMU and EMII oceanic island basalts from the south Pacific Ocean. Earth Planet Sci. Lett. **114**, 353-371.

Hertogen, J., and Gijbels, R., (1971): Instrumental neutron activation analysis of rocks with a low-energy photon detector. Anal. Chim. Acta. **56**, 61-82.

Hertogen, J., Janssens, M-J., and Palme H., (1980): Trace elements in ocean ridge basalt glasses: implications for fractionations during mantle evolution and petrogenesis. Geochim. Cosmochim. Acta **44**, 2125-2143.

Hieber, W., (1970): Metal carbonyls, forty years of research. Adv. Organomet. Chem. **8**, 1-28.

Hieber, W., and Bader, G., (1928): Reaktionen und derivate des eisencarbonyls II: neuartige kohlenoxyd-verbindungen von eisenhalogeniden. Ber. Deut. Chem. Ges. **61**, 1717-1722.

Hieber, W., and Bader, G., (1930): Neuartige kohlenoxyduerbindungen von eisenhalogeniden und ihre chemische charakterisierung. Z. Anorg. Allgem. Chem. **190**, 193-204.

Hieber, W., Ries, K., and Bader, G., (1930): Über die raumbeanspruchung des kohlenoxyds in seien metallsalz-verbindungen und in den metallcarbonylen. Z. Anorg. Allgem. Chem. **190**, 215.

Hieber, W., and Fischer, H., (1941): Ruthenium carbonyl. Chem. Abstr. **35**, 5657.

Hinkley, T.K., (1991): Distribution of metals between particulate and gaseous forms in a volcanic plume. Bull. Volcanol. **53**, 395-400.

Hoffman, E.L., Naldrett, A.J., Van Loon, J.C., Hancock, R.G.V., and Manson, A., (1978): The determination of all of the platinum-group elements and gold in rocks and ores by neutron activation analysis after preconcentration by a nickel-sulphide fire-assay technique on large samples. Anal. Chim. Acta **102**, 157-166.

Hunt, C.B., (1977): Metallocenes - the first 25 years. Educ. Chem. **14**, 110-113.

Ionov, D.A., Hoefs, J., Wedepohl, K.H., and Wiechert, U., (1992): Content and isotopic composition of sulphur in ultramafic xenoliths from central Asia. Earth Planet. Sci. Lett. **111**, 269-286.

Jackson, S.E., Fryer, B.J., Gosse, W., Healey, D.C., Longerich, H.P., and Strong, D.F., (1990): Determination of the precious metals in geological materials by inductively coupled plasma-mass spectrometry (ICP-MS) with nickel sulphide fire-assay collection and tellurium coprecipitation. Chem. Geol. **83**, 119-132.

Johnson, B.F.G., (ed.) (1980): Transition metal clusters. Wiley Interscience, Chinchester, 681pp.

Kaminskiy, F.V., Frantsesson, Y.V., and Khvostova, V.P., (1974): First information on platinum-group metals (Pt, Pd, Rh, Ir, Ru, Os) in kimberlitic rocks. Doklady Akad. Nauk SSSR., **219**, 190-193.

Karzhavin, V.K., and Vendillo, V.P., (1970): Thermodynamic equilibrium and conditions for the existence of hydrocarbon gases in a magmatic process. Geochem. Intl. **7**, 797-803.

Kerrich, R., and Fyfe, W.S., (1981): The gold-carbonate association: source of CO_2 and CO_2 fixation reactions in archean lode deposits. Chem. Geol. **33**, 265-294.

Kesson, S.E., and Fitz Gerald, J.D., (1992): Partitioning of MgO, FeO, NiO, MnO and Cr_2O_3 between magnesian silicate perovskite and magnesiowüstite: implications for the origin of inclusions in diamonds and composition of the lower mantle. Earth Planet. Sci. Lett. **111**, 229-240.

Kinloch, E., (1982): Regional trends in the platinum group mineralogy of the Critical Zone of the Bushveld Complex, South Africa. Econ. Geol. **77**, 1328-1347.

Kinloch, E.D., and Peyerl, W., (1990): Platinum-group minerals in various rock types of the Merensky Reef: genetic implications. Econ. Geol. **85**, 537-555.

Koeberl, C., (1989): Iridium enrichment in volcanic dust from blue ice fields, Antarctica, and possible relevance to the K/T boundary event. Earth Planet. Sci. Lett. **92**, 317-322.

Koeberl, C., (1992): A shortcourse introduction to neutron activation analysis. University of the Witwatersrand, 13th February 1992, 32pp.

Koeberl, C., (1993): Chicxulub crater, Yucatan: tektites, impact glasses and the geochemistry of target rocks and breccias. Geology **21**, 211-214.

Konnerup-Madsen, J., Larsen, E., and Rose-Hansen, J., (1979): Hydrocarbon-rich fluid inclusions in minerals from the alkaline Ilimaussaq intrusion, south Greenland. Bull. Mineral. **102**, 642-653.

Kring, D.A., and Boynton, W.V., (1992): Petrogenesis of an augite-bearing melt rock in the Chicxulub structure and its relationship to K/T impact spherules in Haiti. Nature **358**, 141-144.

Krogmann, K., Binder, W., and Hausen, H.D., (1968): Crystal structure of "$Ir(CO)_3Cl$" = $Ir(CO)_{2.93}Cl_{1.07}$. Angew. Chem. **80**, 844-845.

Krugers, J., (1973): Instrumentation in applied nuclear chemistry. Plenum Press, New York, 408pp.

Kucha, H., (1982): Platinum group metals in the Zechstein copper deposits, Poland. Econ.Geol. **77**, 1578-1591.

Kucha, H., (1983): Precious metal bearing shale from the Zechstein copper deposits, Lower Silesia, Poland. Trans.Inst.Min.Metal. **92**, B72-B79.

Kuznetsov, A.P., Kukushkin, Y.N., and Makarov, D.F., (1974): Determination of the platinum metals by fire-assay using nickel sulphide as collector. J. Anal. Chem. SSSR. **29**, 2155.

Kyte, F.T., Zhou, Z., and Wasson, J.T., (1980): Siderophile-enriched sediments from the Cretaceous/Tertiary boundary. Nature **288**, 651-656.

Kyte, F.T., Smit, J., and Wasson, J.T., (1985): Siderophile interelement variations in the Cretaceous-Tertairy boundary sediment from Caravaca, Spain. Earth Planet. Sci. Lett. **73**, 183-195.

Laws, M.J., (1991a): Sample collection (preconcentration of precious metals). (Ext. Abstr.) Symp. on Analytical Techniques for the PGE, Mintek, Randburg, South Africa, 6th September 1991, 1-4.

Laws, M.J., (1991b): Atomic absorption spectroscopy / graphite furnace. (Ext. Abstr.) Symp. on Analytical Techniques for the PGE, Mintek, Randburg, South Africa, 6th September 1991, 5-7.

Lea, D.E., (1934): Combination of proton and neutron. Nature, **133**, 24.

Lee, C.A., and Tredoux, M., (1986): Platinum-group element abundances in the lower and lower critical zones of the eastern Bushveld Complex. Econ. Geol. **81**, 1087-1095.

Lee, C.A., and Parry, S.J., (1988): Platinum-group element geochemistry of the middle group chromitites of the eastern Bushveld Complex. Econ. Geol. **83**, 1127-1139.

Lee, J.D., (1991): Concise inorganic chemistry. 4th Edition, Chapman and Hall, London, 1032pp.

Lenahan, W.C., and Murray-Smith, R. de L., (1986): Assay And Analytical Practice In The South African Mining Industry. Chamber of Mines, Johannesburg, S. Afr. Inst. Min. Metal. monograph **6**, 640pp.

Leonardos, O.H., Ulbrich, M.N.C., and Gaspar, J.C., (1991): The Mata de Corda volcanic rocks. 5th Intl. Kimberlite Conf. Field Guide Book, 65-74.

Le Roex, A.P., (1987): Geochemical correlation between South African kimberlites and South Atlantic hotspots. Nature **324**, 243.

Le Roex, A.P., and Dick, H.J.B., (1981): Petrology and geochemistry of basaltic rocks from the Conrad fracture zone on the America-Antarctic Ridge. Earth Planet. Sci. Lett. **54**, 117-138.

Lindsay, N.M., (1989): The processing and recovery of the platinum group elements. Unpubl. Ph.D. thesis, University of the Witwatersrand.

Livingstone, S.E., (1975): The second and third row elements of group VIII a,b and c. in Baidar, J.C., Emeleus, H.J., Nyholm, R., and Trotman-Dickson, A.F., (eds.) Comprehensive Inorganic Chemistry Pergamon Press, Oxford, 1163-1370.

Mahoney, J.J., (1988): Deccan traps. in MacDougall, J.D., (ed.) Continental flood basalts. Kluwer Academic Publications, Dordrecht, 151-194.

Mallet, R.C., (1986): Wet-chemistry and separation techniques in a minerals and extractative-metallurgical laboratory. in L.R.P. Butler (ed.) Analytical chemistry in the exploration, mining and processing of materials. Blackwell, Oxford, 101-112.

Manchot, W., and Gall, H., (1929): Uber eine bildungsweise des nickelcarbonyls. Ber. Deut. Chem. Ges. **62**, 678-681.

Marsh, H., and Kuo, K., (1989): Kinetics and catalysis of carbon gasification. in Marsh, H., (ed.) Introduction to carbon science. Butterworth, London, 107-151.

Mathez, E.A., (1988a): Vapor associated with mafic magma and controls on its composition. in Whitney, J.A., and Naldrett, A.J., (eds.) Ore Deposition Associated With Magmas Rev. Econ. Geol. **4**, 21-31.

Mathez, E.A., (1988b): Interactions involving fluids in the Stillwater and Bushveld complexes: observations from the rocks. in Whitney, J.A., and Naldrett, A.J., (eds.) Ore Deposition Associated With Magmas Rev. Econ. Geol. **4**, 167-179.

Mathez, E.A., and Peach, C.L., (1988): The geochemistry of the platinum-group elements in mafic and ultramafic rocks. in Whitney, J.A., and Naldrett, A.J., (eds.) Ore Deposition Associated With Magmas Rev. Econ. Geol. **4**, 33-43.

Mathez, E.A., Dietrich, V.J., Holloway, J.R., and Boudreau, A.E., (1989): Carbon distribution in the Stillwater Complex and evolution of vapour during crystallization of Stillwater and Bushveld magmas. J. Petrol. **30**, 153-173.

McCarthy, T.S., (1978): Geochemical studies of selected granitic terrains in South Africa. Unpubl. PhD thesis, University of the Witwatersrand.

MacCulloch, J., (1819): A description of the western isles of Scotland. 2 vols., London 568pp.

McDonald, I., (1991): The analysis of Vaal Triangle aerosols by instrumental neutron activation analysis. Schonland Research Centre Internal Report 91081, 17pp.

McDonald, I., Tredoux, M., de Wit, M.J., and Hart, R.J., (1991a): Investigations into the role of carbon monoxide in magma chambers and possible transport of the PGE as volatile carbonyl complexes. (abstract) 6th Intl. Platinum Symp., Perth, Australia.

McDonald, I., Tredoux, M., Lindsay, N.M., Hart, R.J., and de Wit, M.J., (1991b): Carbon monoxide and the volatile transport of the Platinum-Group Elements

during magmatic processes. Proc. 4th Intl. Conf. on Appl. Mineral., Pretoria, South Africa, Paper 34.

McDonald, I, and de Wit, M.J., (1992): PGE carbonyls: a new model for the development of Pt mineralization in pipe deposits. (abstract) Geol. Soc. Lond. Min. Deposits Studies Group AGM, University of Aberdeen, 6-7th January 1992.

McDonald, I., Hart, R.J., and Tredoux, M., (1993): The analysis of the platinum-group elements in South African kimberlites by nickel sulphide fire-assay and neutron activation analysis. Anal. Chim. Acta (submitted)

Meeker, K.A., Chuan, R.L., Kyle, P.R., and Palais, J.M., (1992): Emission of elemental gold particles from Mount Erebus, Ross Island, Antarctica. Geophys. Res. Lett. **18**, 1405-1408.

Menzies, M.A., and Hawkesworth, C.J., (1987): Upper mantle processes and composition. in Nixon, P.H., (ed.), Mantle xenoliths, John Wiley, Chinchester, 725-738.

Meyer, H.O.A., (1985): Genesis of diamond: a mantle saga. Am. Mineral. **70**, 344-355.

Meyer, H.O.A., Garwood, B.L., and Svisero, D.P., (1991): The Pantano intrusion. 5th Intl. Kimberlite Conf., Field Guide Book, 59-64.

Mingos, D.M.P., and Wales, D.J., (1991): Introduction to cluster chemistry. Prentice Hall International, London, 316pp.

Mitchell, J.W., (1982): State-of-the-art contamination control techniques for ultratrace element analysis. J. Radioanal. Chem. **69**, 47-105.

Mitchell, R.H., (1986): Kimberlites: mineralogy, geochemistry and petrology. Plenum Press, New York, 442pp.

Mitchell, R.H., (1989): Aspects of the petrology of kimberlites and lamproites: some definitions and distinctions. in Kimberlites and related rocks., Proc. 4th Intl. Kimb. Conf., Geol. Soc. Australia Spec. Publ. **14**, 7-44.

Mitchell, R.H., and Clarke, D.B., (1976): Oxide and spinel mineralogy of the Peuyuk kimberlite, Somerset Island, N.W.T., Canada. Contrib. Mineral. Petrol. **56**, 157-172.

Mond, L., Langer, C., and Quinke, F., (1890): Action of carbon monoxide on nickel. J. Chem. Soc. **57**, 749-753.

Mond, L., Hirtz, H., and Cowap, M.D., (1910): Some new metallic carbonyls. J. Chem. Soc. **97**, 798-810.

Moore, J.M., Watkeys, M.K., and Reid, D.L., (1990): The regional setting of the Aggneys and Gamsberg base metal deposits, Namaqualand, South Africa. in P. Spry and T. Bryndzia (eds.) Regional metamorphism of ore deposits. VSP, The Netherlands, 78-95.

Morgan, J.W., Wandless, G.A., Petrie, R.K., and Irving, A.J., (1981): Composition of the earth's upper mantle -1. Siderophile trace elements in ultramafic nodules. Tectonophysics **76**, 47-67.

Morrisey, C.J., (1988): Exploration for platinum: a contemporary viewpoint. in Prichard, H.M., Potts, P.J., Bowles, J.F.W., and Cribb, S.J., (eds.) Geo-platinum 87. Elsevier, London, 57-82.

Mountain, B.W., and Wood, S.A., (1988): Chemical controls on the solubility, transport and deposition of Pt and Pd in hydrothermal solutions: a thermodynamic approach. Econ. Geol. **83**, 492-510.

Mughabghab, S.F., Divadeenam, M., and Holden, N.E., (1981): Neutron Cross Sections Volume 1. Neutron resonance parameters and thermal cross sections. Part A: Z=1-60., Academic Press, New York, 98pp.

Mughabghab, S.F., (1984): Neutron Cross Sections Volume 1. Neutron resonance parameters and thermal cross sections. Part B: Z=61-100., Academic Press, New York, 60pp.

Murali, A.V., Schuraytz, B.C., and Parekh, P.P. (1988): Deccan volvanism and K/T boundary signatures. (abstract) Global catastrophes in Earth history: An

interdisciplinary conference on impacts, volcanism and mass mortality. Lunar and Planetary Institute, Houston, Texas, 128-129.

Murphy, T.J., (1976): The role of the analytical blank in accurate trace analysis. U.S. Nat. Bur. Std. Spec. Publ. **422**, U.S. Govn. Printing Office, Washington D.C., 509-537.

Nadkarni, R.A., and Morrison, G.H., (1974): Determination of the noble metals in geological materials by neutron activation analysis. Anal. Chem. **46**, 223-233.

Naldrett, A.J., (1981): Platinum-group element deposits. in Cabri, L.J., (ed.) Platinum-Group Elements: Mineralogy, Geology, Recovery. Canadian Institute of Mining and Metallurgy Spec. Publ. **23**, 197-232.

Naldrett, A.J., and Campbell, I.H., (1982): Physical and chemical constraints on genetic models for komatiite-related Ni-sulphide deposits. in Arndt, N.T., and Nesbitt, E.G., (eds.) Komatiites. Geogre Allen and Unwin, London, 423-434.

Nicholas, D.J., (1985): The rapid separation and analysis of the primary platinum-group elements, gold and silver: application to geochemistry, mineralogy and the mineral processing environment. (ext. abstr.) 2nd Intl. Symp. on Analytical chemistry in the exploration, mining and processing of materials, Pretoria, South Africa, 15-19 April 1985.

Nixon, P.H., (1973): Perspective. in P.H. Nixon (ed.) Lesotho kimberlites. Lesotho National Development Corporation, Maseru, 300-312.

Norrish, K., and Hutton, J.T., (1969): An accurate X-ray spectrographic method for the analysis of a wide range of geological samples. Geochim. Cosmochim. Acta **33**, 431-453.

Officer, C.B., (1993): Death of the dinosaurs: victims of volcanoes. New Scientist **1861**, 34-38.

Officer, C.B., Hallam, A., Drake, C.L., and Devine, J.D., (1987): Late Cretaceous-Tertiary extinctions. Nature **326**, 143.

Olmez, D., Finnegan, D.L., and Zoller, W.H., (1986): Iridium emissions from Kilauea volcano. J. Geophys. Res. **91** (B1), 653-663.

Palmer, R., and Watterson, J.I.W., (1971): The recovery of noble metals for analysis. A radiotracer investigation of losses. N.I.M. Report 1185, Council for Mineral Technology, Randburg, South Africa, 11pp.

Parry, S.J., Asif, M., and Sinclair, I.W., (1988): Radiochemical fire-assay for the determination of the platinum-group elements. J. Radioanal. Nucl. Chem. **123**, 593-606.

Paul, D.K., Crocket, J.H., and Nixon, P.H., (1979): Abundance of palladium, iridium and gold in kimberlites and associated nodules. in Boyd, FR., and Meyer, H.O.A., (eds.) Kimberlites, diatremes, and diamonds: their geology, petrology and geochemistry. Proc. 2nd Intl. Kimberlite Conf. 272-279.

Peach, C.L., Mathez, E.A., and Keays, R.R., (1990): Sulphide melt-silicate melt distribution coefficients for noble metals and other chalcophile metals as deduced from MORB: implications for partial melting. Geochim. Cosmochim. Acta **54**, 3379-3389.

Pegram, W.J., and Allégre, C.J., (1992): Osmium isotopic compositions from oceanic basalts. Earth Planet. Sci. Lett. **111**, 59-68.

Perlman, I., (1981): Measurement and techniques. in S. Amiel (ed.) Nondestructive activation analysis. Elsevier, Amsterdam, 9-24.

Pernicka, E., and Wasson, J.T., (1987): Ru, Re, Os, Pt and Au in meteorites. Geochim. Cosmochim. Acta **51**, 1717-1726.

Perry, B.J., van Loon, J.C., and Barefoot, R.R., (1992): A dry-chlorination/ICP-MS analytical method for PGE and gold in rocks. (abstract) 3rd Intl. Symp. on Analytical chemistry in the exploration, mining and processing of materials. Sandton, South Africa, 2-7 August 1992.

Peyerl, W., (1982): The influence of the Driekop dunite pipe on the platinum-group mineralogy of the UG-2 chromitite in its vicinity. Econ. Geol. **77**, 1432-1438.

Pillay, A.E., Watterson, J.I.W., and Andeweg, A.H., (1990): A pool type irradiation facility for a ^{252}Cf neutron source. Int. J. Radiat. Appl. Instrum. Part E, **4**, 209-216.

Pires, F.R.M., (1986): The southern limits of the Sâo Francisco craton. Acad. Brasileira Genc. Anais., **58**, 139-145.

Pouchert, C.J., (1981): The Aldrich library of infrared spectra. 3rd Edition, Aldrich Chemical Co., Milwaukee, USA, 1868pp.

Pruchnik, F.P., (1990): Organometallic chemistry of the transition metals. Plenum Press, New York, 757pp.

Reus, U., and Westmeier, W., (1983): Catalog of gamma rays from radioactive decay, part 2. Atom. Data Nucl. Data Tables **29**, 193-406.

Richardson, S.H., Gurney, J.J., Erlank, A.J., and Harris, J.W., (1984): Origin of diamonds in old enriched mantle. Nature **310**, 198-202.

Riesberg, L.C., Allégre, C.L., and Luck, J.M., (1991): The Re-Os isotope systematics of the Ronda ultramafic complex of southern Spain. Earth Planet. Sci. Lett. **105**, 196-213.

Ringwood, A.E., (1989): Constitution and evolution of the mantle. in Kimberlites and related rocks, Proc. 4th Intl. Kimb. Conf., Geol. Soc. Australia Spec. Publ. **14**, 457-485.

Ringwood, A.E., Kesson, S.E., Hibberson, W., and Ware, N., (1992): Origin of kimberlites and related magmas. Earth Planet. Sci. Lett. **113**, 521-538.

Robért, R.V.D., van Wyk, E., and Palmer, R., (1971): Concentration of the noble metals by a fire-assay technique using nickel sulphide as the collector. N.I.M. Report 1371, Council for Mineral Technology, Randburg, South Africa, 14pp.

Robinson, D.N., (1975): Magnetite-serpentine-calicte dykes at Premier Mine and aspects fo their relationship to kimberlite and carbonatite of alkalic carbonatite complexes. Phys. Chem. Earth **9**, 61-70.

Robson, G.G. (1985): Platinum 1985. Johnson Matthey Plc., London, 71pp.

Rocchia, R., Boclet, D., Courtillot, V., and Jaeger, J.J., (1988): A search for iridium in the Deccan traps and inter-traps. Geophys. Res. Lett. **15**, 812-815.

Ross, J.R., and Keays, R.R., (1979): Precious metals in volcanic-type nickel sulphide deposits in Western Australia. Part I: relationship with the composition of the ore and their host rocks. Can. Mineral. **17**, 417-435.

Rowe, J.J., and Simon, F.O., (1971): Determination of platinum and palladium in geological materials by neutron activation analysis after fire-assay preconcentration. Talanta **18**, 121-125.

Ryabchikov, I.E., Green, D.H., Wall, V.J., and Brey, G.P., (1981): The oxidation state of carbon in the reduced velocity zone. Geochem. Intl. **18**, 221-232.

Sassani, D.C., and Shock, E.L., (1990): Speciation and solubility of palladium in aqueous magmatic-hydrothermal solutions. Geology **18**, 925-928.

Sato, M., and Valenza, M., (1980): Oxygen fugacities of the layered series of the Skaergaard intrusion, East Greenland. Am. J. Sci. **280**, 134-158.

Saxby, J.D., (1969a): Metal-organic chemistry of the geochemical cycle. Rev. Pure Appl. Chem. **19**, 131-150.

Schiffries, C.M., (1982): The petrogenesis of a platiniferous dunite pipe in the Bushveld Complex: infiltration metasomatism by a chloride solution. Econ. Geol. **77**, 1439-1453.

Schmitz, B., (1985): Metal precipitation in the Cretaceous-Tertiary boundary at Stevns Klint, Denmark. Geochim. Cosmochim. Acta **49**, 2361-2370.

Schmitz, B., Andersson, P., and Dahl, J., (1988): Iridium, sulphur isotopes and rare earth elements in the Cretaceous-Tertiary boundary clay at Stevns Klint, Denmark. Geochim. Cosmochim. Acta **52**, 229-236.

Schobbenhaus, C., and Campos, D. de A., (1984): A evolucâo da platforma Sul-Americana no Brasil e suas principas concentraçôes minerais. in C.

Schobbenhaus, D. de A. Campos, D. Dereze, and H.E. Asmus (eds.) Geologicol do Brasil. Departamento Nacional de Produçâo Mineral., Brasilia, 9-53.

Schoeller, W.R., and Powell, A.R., (1955): The analysis of mineral and ores of the the rarer elements. Charles Griffen & Co., London, 325-394.

Scott, E.R.D., Wasson, J.T., and Buchwald, V.F, (1973): The chemical classification of iron meteorites-VII. A reinvestigation of irons with Ge concentrations between 25 and 80 ppm. Geochim. Cosmochim. Acta **37**, 1957-1983.

Sharpe, M.R., (1982): Noble metals in the marginal rocks of the Bushveld Complex. Econ. Geol. **77**, 1286-1295.

Sharpton, V.L., Dalrymple, G.B., Marin, L.E., Ryder, G., Schuraytz, B.C., and Urrutia-Fucugauchi, J., (1992): New links between the Chicxulub impact structure and the Cretaceous-Tertiary boundary. Nature **359**, 819-821.

Shazali, I., (1988): Determination of precious metals in ores and rocks by reactor neutron activation analysis after preconcentration by fire assay. Unpubl. PhD thesis, University of Antwerp.

Shazali, I., Van't Dack, L., and Gijbels, R., (1987): Determination of precious metals in ores and rocks by thermal neutron activation/γ-spectrometry after preconcentration by nickel sulphide. Anal. Chim. Acta **196**, 49-58.

Shee, S.R., (1986): The petrogenesis of the Wesselton mine kimberlites, Kimberley, South Africa. Unpubl. PhD thesis, University of Cape Town.

Shepherd, E.S., (1938): The gases in rocks and some related problems. Am. Jour. Sci. **35**, 311-351.

Skinner, E.M.W., (1989): Contrasting Group I and Group II kimberlite petrology: towards a genetic model for kimberlites. in Kimberlites and related rocks, Proc. 4th Intl. Kimb. Symp., Geol. Soc. Australia Spec. Publ. **14**, 528-544.

Skinner, E.M.W., Smith, C.B., Viljoen, K.S., and Clark, T.C., (1993): The petrology, tectonic setting and emplcement ages of kimberlites in the south

western border region of the Kaapvaal craton, Prieska area, South Africa. Proc. 5th Intl. Kimberlite Conf., Brasilia, (in press).

Smith, A.L., (1979): Applied infrared spectroscopy. Chemical Analysis **54**, John Wiley, New York, 322pp.

Smith, C.B., (1983): Pb,Sr and Nd isotopic evidence for sources of southern African Cretaceous kimberlites. Nature **304**, 51-54.

Smith, C.B., Gurney, J.J., Skinner, E.M.W., Clement, C.R., and Ebrahim, N., (1985): Geochemical character of southern African kimberlites: a new approach based on isotopic constraints. Trans. Geol. Soc. S. Afr. **88**, 267-280.

Smith, C.B., Schulze, D.J., Viljoen, K.S., and Barton, E.S., (1992): The origins of the subcalcic megacryst suite in kimberlite: implications for the origins of kimberlite and the constitution of the deep subcontinental lithosphere. Proc. 24th Geocongress, Geol. Soc. S. Africa, Bloemfontein, 379-381.

Spriggs, A.J., (1988): An isotopic and geochemical study of kimberlite and associated alkaline rocks from Namibia. Unpubl. PhD thesis, University of Leeds.

Steele, T.W., Levin, J., and Copelowitz, I., (1975): The preparation and certification of a precious metal ore. N.I.M. report 1696, Council for Mineral Technology, Randburg, South Africa, 50pp.

Steger, H.F., (1983): Certified reference materials. CANMET report 83-3E, Can. Cent. Miner. Energy. Technol., Ottowa, Ontario, 35pp.

Stockman, H.W., (1983): Neutron activation determination of noble metals in rocks: a rapid radiochemical separation based on tellurium coprecipitation. J. Radioanalyt. Chem. **78**, 307-317.

Stolper, E., and Holloway, J.R., (1988): Experimental determination of the solubility of carbon dioxide in molten basalt at low pressure. Earth Planet. Sci. Lett. **87**, 397-408.

Strong, C.P., Brooks, R.R., Wilson, S.M., Reeves, R.D., Orth, C.J., Mao, X.Y., Qunitana, L.R., and Anders, E., (1987): A new Cretaceous-Tertiary boundary site at

Flaxbourne River, New Zealand: biostratigraphy and geochemistry. Geochim. Cosmochim. Acta **51**, 2769-2777.

Stumpf, E.F., (1961): Some new platinoid-rich minerals identified with the electron microanalyser. Min. Mag. **32**, 833-847.

Stumpfl, E.F., and Tarkian, M., (1976): Platinum genesis: New mineralogical evidence. Econ. Geol. **71**, 1451-1460.

Stumpfl, E.F., and Rucklidge, J.C., (1982): The platiniferous dunite pipes of the eastern Bushveld Complex. Econ.Geol. **77**, 1419-1431.

Stumpfl, E.F., and Ballhaus, C.G., (1986): Stratiform platinum depostis: New data and concepts. Fortschr. Miner. **64**, 205-214.

Sun, S-S., (1982): Chemical composition and origin of the earth's primitive mantle. Geochim. Cosmochim. Acta **46**, 179-192.

Tankard, A.J., Jackson, M.P.A., Erikson, K.A., Hobday, D.K., Hunter, D.R., and Minter, W.E.L., (1982): Crustal evolution of southern Africa: 3.8 billion years of earth history. Springer-Verlag, New York, 523pp.

Tarkian, M., and Stumpfl, E.F., (1975): Platinum mineralogy of the Driekop pipe, South Africa. Mineral. Deposit. **10**, 71-85.

Teixeira, W., (1982): Geochronology of the southern part of the Sâo Francisco craton. Revista Brasileira de Geociências, **12**, 268-277.

Tompkins, L.A., and Haggerty, S.E., (1985): Groundmass oxide minerals in the Koidu kimberlite dykes, Sierra Leone, West Africa. Contrib. Mineral. Petrol. **91**, 245-263.

Tompkins, L.A., and Gonzaga, G.M., (1989): Diamonds in Brazil and a proposed model for the origin and distribution of diamonds in the Coromandel region, Minas Gerais, Brazil. Econ. Geol. **84**, 591-602.

Tredoux, M., (1990): The platinum group elements: Nuclear methods for their analysis and their behaviour in terrestrial rocks and meteorites. Unpubl. PhD. thesis, University of the Witwatersrand.

Tredoux, M., Davies, G., Lindsay, N.M., and Sellschop, J.F.P., (1986): The influence of temperature on the geochemistry of the platinum-group elements and gold. Extd. Abstr. Geocongress '86, Geol. Soc. S. Afr. Conf., Johannesburg.

Tredoux, M., De Wit, M.J., Hart, R.J., Armstrong, R.A., Lindsay, N.M., and Sellschop, J.P.F., (1989a): Platinum-group elements in a 3.5Ga nickel-iron occurrence: possible evidence of a deep mantle origin. J. Geophys. Res. **94**, 795-813.

Tredoux, M., de Wit, M.J., Hart, R.J., Armstrong, R.A., Lindsay, N.M., Verhagen, B.T., and Sellschop, J.P.F., (1989b): Chemostratigraphy across the Cretaceous-Tertiary boundary and a critical assessment of the iridium anomaly. J. Geol. **97**, 585-605.

Tredoux, M., de Wit, M.J., and Hart, R.J., (1990): The enrichment of the platinum-group elements in the cratonic lithosphere: implications for exploration, tectonic studies and the Cretaceous-Tertiary boundary. (ext. abstr.) 15th Colloquium of African Geology, Nancy, 10-13 Sept. 1990.

Tredoux, M., Lindsay, N.M., and McDonald, I., (1991): Cluster chemistry and its relevance to the behaviouir of the PGE in magmatic systems. (abstract) 6th Intl. Platinum Symp., Perth, Australia.

Tripathi, S.C., Srivastava, S.C., Mani, R.P., and Shrimal, A.K., (1975): Advances in platinum metal carbonyls and their substituted derivatives I. Ruthenium and Osmium carbonyls. Inorganica Chim. Acta **15**, 249-290.

Tripathi, S.C., Srivastava, S.C., Mani, R.P., and Shrimal, A.K., (1976): Advances in platinum metal carbonyls and their substituted derivatives II. Rhodium, iridium, platinum and palladium carbonyls. Inorganica Chim. Acta **17**, 257-290.

Turkstra, J., Pretorius, P.J., and De Wet, W.J., (1970): Non destructive determination of platinum metals in ores, matte and lead assay beads by reactor

activation analysis and high resolution gamma spectroscopy. Anal. Chem. **42**, 835-841.

van der Flier-Keller, E., (1991): Platinum-group elements in Tulameen coal, British Columbia, Canada. Econ. Geol. **86**, 387-395.

van der Maas, J.H., (1972): Basic infrared spectroscopy. Heyden and Son Ltd, London, 109pp.

van Loon, J.C., (1984): Accurate determination of the noble metals I. Sample decomposition and methods of separation. Trends in Anal. Chem. **3**, 24-29.

van Loon, J.C., (1985): Accurate determination of the noble metals II. Determination methods. Trends in Anal. Chem. **4**, 24-29.

van Wyk, E., and Dixon, K., (1983): The recovery of the platinum-group elements and gold by the lead collection step of the fire-assay procedure. Report M88, Council for Mineral Technology, Randburg, South Africa, 18pp.

Viljoen, K.S., (1988): Petrology of the Sutherland Commonage melilitite inrusives. Unpubl. MSc. thesis, University of Cape Town.

Viljoen, M.J., and Viljoen, R.P., (1969b): The geology and geochemistry of the lower ultramafic unit of the Onverwacht Group and a proposed new class of igneous rock. Sp. Publ. Geol. Soc. S. Afr. **2**, 55-85.

Viljoen, M.J., and Scoon, R.N., (1985): The distribution and main geologic features of discordant bodies of iron-rich ultramfic pegmatite in the Bushveld Complex. Econ. Geol. **80**, 1109-1128.

Viljoen, M.J., Theron, J., Underwood, B., Walters, B.M., Weaver, J., and Peyerl, W., (1986): The Amandebult section of Rustenburg Platinum Mines Limited, with reference to the Merensky Reef. in Anhaeusser, C.R., and Maske, S., (eds), Mineral Deposits Of Southern Africa, 2 vols., Geol. Soc. South Africa, 1041-1060.

Vincent, E.A., and Smales, A.A., (1956): The determination of palladium and gold in igneous rocks by radioactivation analysis. Geochim. Cosmochim. Acta **9**, 154-160.

Wagner, P.A., (1914): The diamond fields of southern Africa. The Transvaal Leader, Johannesburg, 355pp.

Wagner, P.A., (1929): The platinum deposits and mines of South Africa. Edinburgh, Oliver and Boyd, 326pp.

Walker, P.J., Carlson, R.W., Shirey, S.B., and Boyd, F.R., (1989): Os, Sr, Nd and Pb isotope systematics of southern African peridotite xenoliths: implications for the evolution of the subcontinental mantle. Geochim. Cosmochim. Acta **53**, 1583-1595.

Watterson, J.I.W., (1975): INAA in the classification of granites from the Bushveld Complex. Unpubl. PhD thesis, University of the Witwatersrand.

Watterson and McDonald (1991): Neutron activation analysis (NAA) for the precious metals. (ext abstract) Symp. on Analytical Techniques for the PGE, Mintek, Randburg, South Africa, 6th September 1991, 21-25.

Wedepohl, K.H., (ed.) (1978): Handbook of geochemistry, 5 vols.,. Springer-Verlag, Berlin.

Westland, A.D., (1981): Inorganic chemistry of the platinum-group elements. in Cabri, L.J., (ed.) Platinum-Group Elements: Mineralogy, Geology, Recovery. Canadian Institiute of Mining and Metallurgy Spec. Publ. **23**, 5-18.

Wilson, A.N., (1982): Diamonds: from birth to eternity. Gemological Institute of America, Santa Monica, 450pp.

Wood, B.J., and Virgo, D., (1989): Upper mantle oxidation state: ferric iron contents of lherzolite spinels by ^{57}Fe Mössbauer spectroscopy and resultant oxygen fugacities. Geochim. Cosmochim. Acta **53**, 1277-1291.

Wood, S.A., (1987): Thermodynamic calculations of the volatility of the platinum-group elements (PGE): the PGE content of fluids at magmatic temperatures. Geochim. Cosmochim. Acta **51**, 3041-3050.

Wood, S.A., (1991): Experimental determination of the hydrolysis constants of Pt^{2+} and Pd^{2+} at 25ºC from the stability of Pt and Pd in aqueous hydroxide solutions. Geochim. Cosmochim. Acta **55**, 1759-1767.

Zoller, W.H., Parrington, J.R., and Phelam-Korta, J.M., (1983): Iridium enrichment in airbourne particles from Kilauea volcano, January 1983. Science **222**, 1118-1121.

Appendix 1

Technical Information On The SAFARI-1 Reactor.

A1.1 Introduction.

SAFARI-1 is a 20MW Oak Ridge type research reactor situated at Pelindaba, the headquarters of the Atomic Energy Corporation (AEC) of South Africa. The reactor site is approximately 60km from Schonland Research Centre and this meant that samples could be conveniently taken to and from the reactor by road. IAEA safety regulations regarding the packaging of irradiated samples and anticipated dose levels during transport were strictly adhered to. Reactor site monitoring was performed by AEC Health Physics department and their approval had to be obtained before any samples were allowed off the site. Separate monitoring was carried out by Schonland Centre staff when the samples reached the laboratory and the activity of each batch of samples was carefully logged.

The SAFARI-1 reactor was originally designed to run at 20MW using highly enriched uranium (90% ^{235}U) as fuel. Due to the imposition of a ban on the sale of nuclear materials and equipment to South Africa by the United States government in the late 1979, power output was dropped to conserve the existing fuel stocks. Presently SAFARI-1 runs at 5MW using locally produced fuel which has been enriched to between 40 and 45% ^{235}U (D. Robertson pers. comm. 1992). All of the irradiations which took place during this thesis were performed under the 5MW power rating.

A schematic plan view of the SAFARI-1 core configuration is shown in Figure A1.1. Twenty nine fuel channels are presently available and fuel rods are inserted into the core via a drive mechanism housed beneath the reactor. Shielding around the core margins is achieved by numerous Al, Be and Pb shielding elements and the outer pressure vessel is stainless steel. As is shown in Figure A1.2., several meters of water and concrete form the biological shield beyond the limits of the pressure vessel. A diagram of the SAFARI-1 reactor neutron spectrum is shown in Figure 3.1 of Chapter 3.

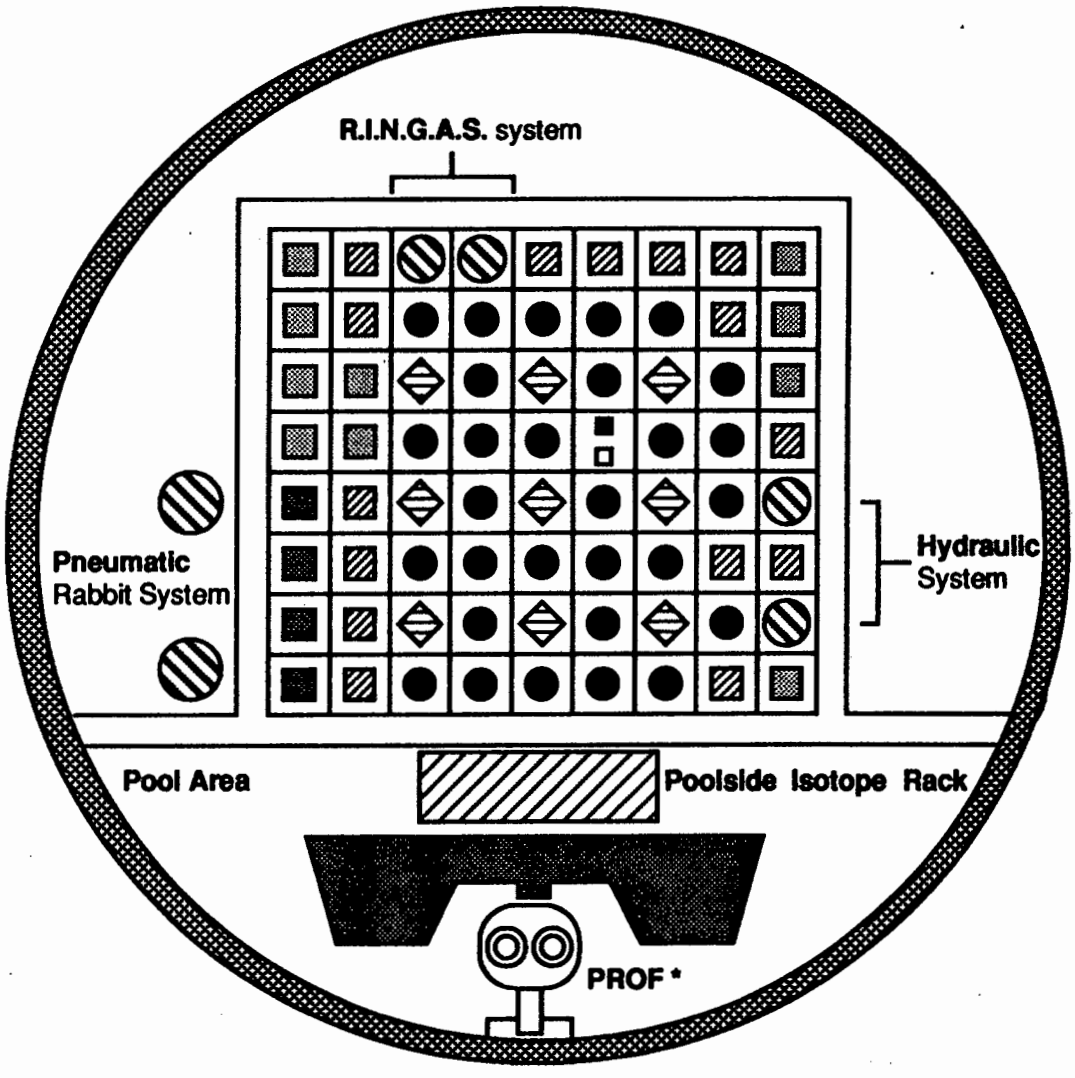

Key:

- Fuel Element
- Control Rod
- Fast Flux Position
- Lead Shielding
- Beryllium Shielding
- Aluminium Shielding
- Irradiation Tubes

PROF * = Poolside Rotating Facility

Figure A1.1.: Schematic plan view of the SAFARI-1 core configuration showing "in-core" irradiation positions and the Poolside Rotating Facility (courtesy P. Louw (AEC))

A1.2. Neutron Activation In The SAFARI-1 Reactor.

SAFARI-1 has five irradiation positions available for neutron activation and the relative positions of these are shown in Figures A1.1 and A1.2. Details of each of these are summarized in Table A1.1. Irradiation of PGE materials was carried out in the Poolside Rotating Facility (PROF) and the Pneumatic Facility. INAA of untereated silicate rocks for the analysis of other trace elements requires higher neutron fluxes and both the Pneumatic Facility and the Poolside Isotope Rack (PIR) were used for this work. These three facilities are described in detail in the following sections.

Table A1.1.: Summary of the neutron irradiation positions available in SAFARI-1

Irradiation Facility	Neutron Flux ($n.cm^{-2}.sec^{-1}$)	Maximum T_{irr}§	Loading And Unloading	Cadmium Ratio*	Number Of Samples
PROF	2.6×10^{12}	24 hours	Manually	35	30-200
Pneumatic	4.9×10^{12}	12 hours	Pneumatic air line	65	9-28
PIR	1.5×10^{13}	12-14 days	Manually	7-15	5-120
Hydraulic	1.0×10^{13}	3 hours	Hydraulic tube	10	5-15
RINGAS†	1.2×10^{13}	120 seconds	Pneumatic air line	15	1-100

§ irradiation time

* defined as $\frac{\Sigma(\text{thermal + epithermal flux})}{(\text{epithermal flux})}$

† Routine Instrumental Neutron and Gamma Analysis System

A1.2.1. The Poolside Rotating Facility (PROF).

The PROF rig comprises two main sections; a balanced trolley on wheels which can be used to move the samples closer to or further from the core face, and a front "head" section. The "head" of the rig consists of two rotating, high-purity Al drums and two drive motors. One of the drums is lined with Cd to provide a dominantly epithermal neutron flux Samples irradiated in the PROF were packed into custom built polythene racks which could accomodate vials for both samples and monitors. One of these racks and is shown in Figure A1.3. Two racks were stacked on top of one another in a cylindrical 500ml plastic irradiation

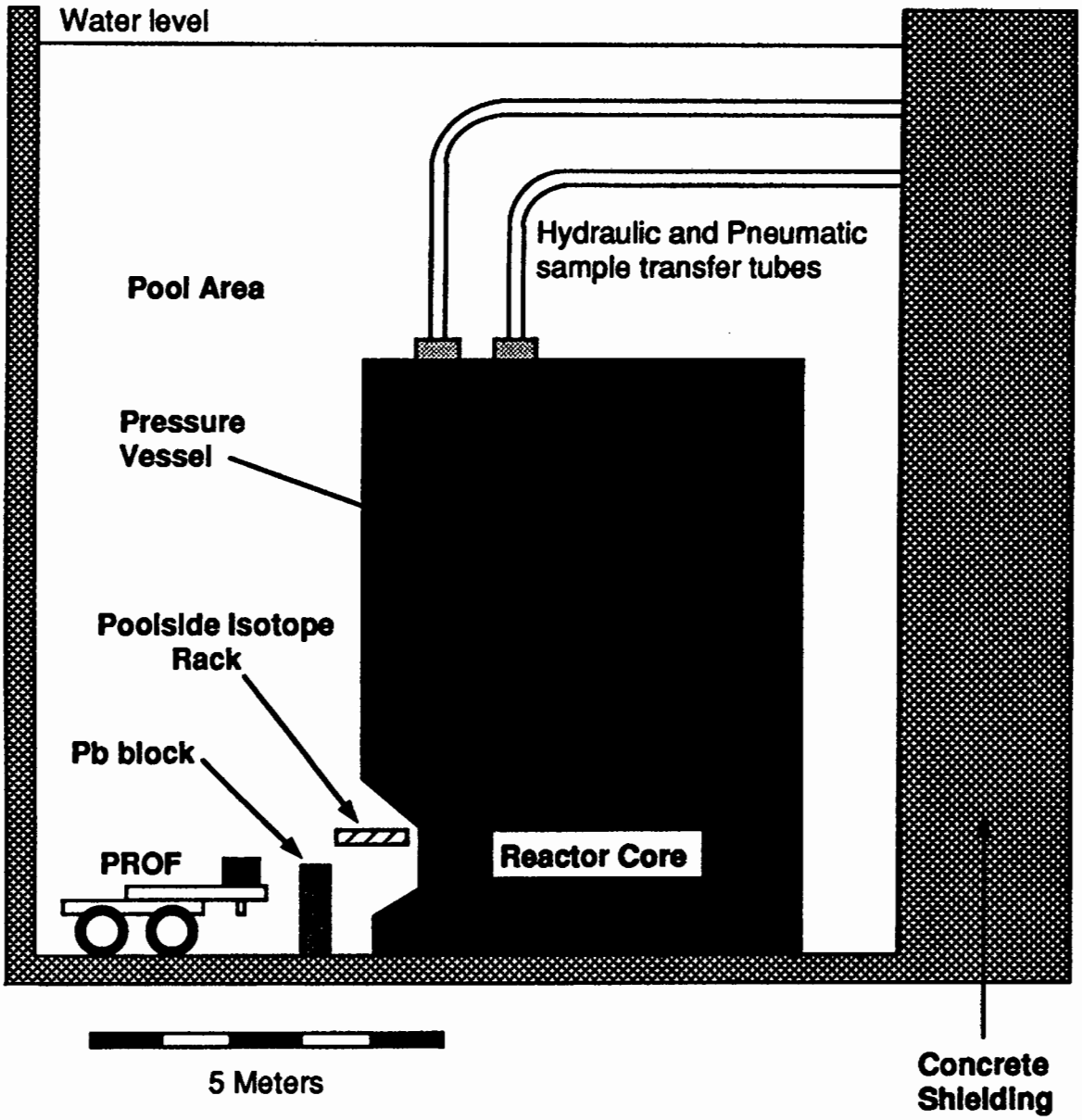

Figure A1.2.: Side view of SAFARI-1 showing pool area irradiation positions. Courtesy P. Louw and A. Faanhof (AEC)

container, which was then loaded into the non-Cd drum on the front end of the PROF. The rig was then moved forward into position behind the lead wall (28.8 centimeters from the core face) and the drums were rotated at about 5 revolutions per minute throughout the irradiation period. Thus ensures a very even distribution of neutron flux over the whole container (Fouché 1991) Irradiations of between 1 and 24 hours are available in the PROF. At the end of the irradation, the rig is moved back from the core face and the plastic sample container is removed in a hot cell using remote handling gear. For PGE irradiations of between 12 and 24 hours, samples typically have to cool for between 6 and 8 hours before they are ready to be transported by road.

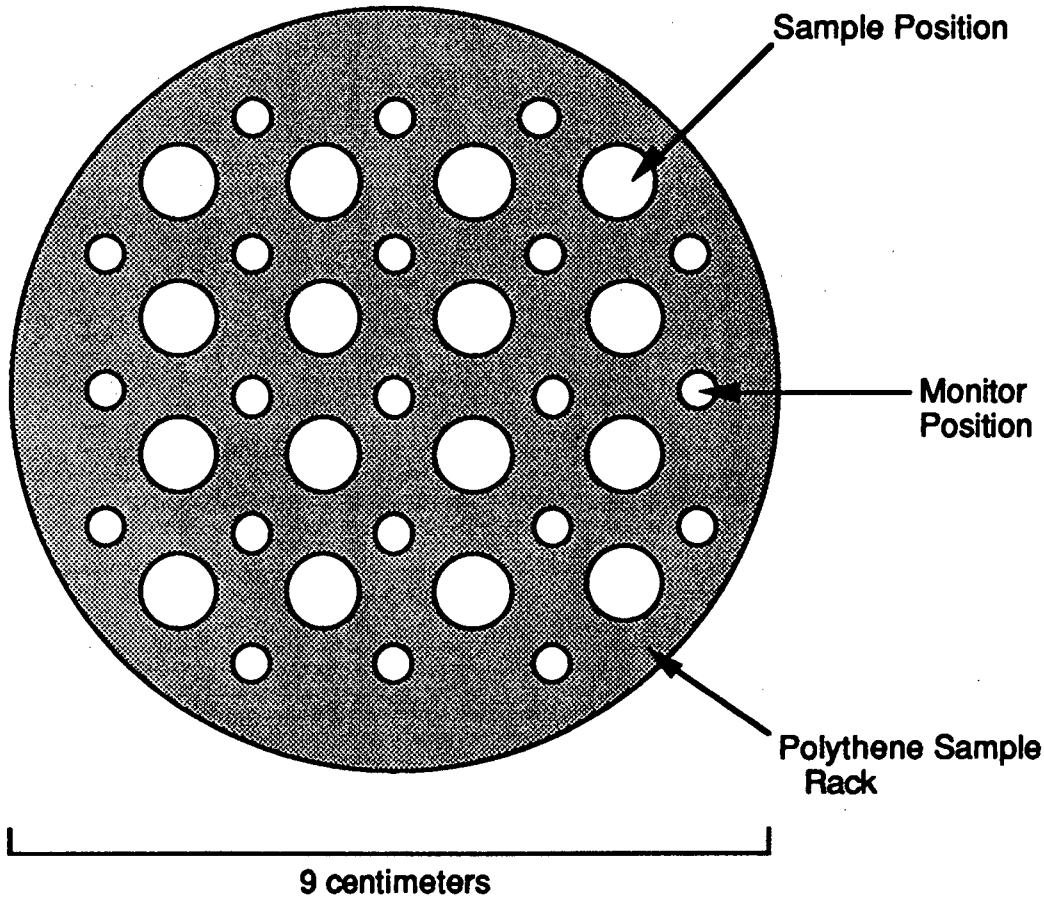

Figure A1.3.: Diagram of sample rack for PROF irradiation

A1.2.2. The Pneumatic Facility.

As Figure A1.1. shows, the Pneumatic Facility is located on the edge of the SAFARI-1 core. Samples are packed into high purity polythene containers called "rabbits". The rabbit consists of male and female sections which are screwed

tightly together to form a seal. The male section of the rabbit contains the samples and the female section contains foam or plastic padding to enusre that the samples move as little as possible as the rabbit is transfered in and out of the core along Al sample tubes by strong blasts of compressed air. The rabbit is sent into the core with considerable force and a combination of air braking and a spring are used to ensure that the rabbit is not damaged as it goes into position. The male section of a typical rabbit and the arrangment of samples within it are shown in Figure A1.4.

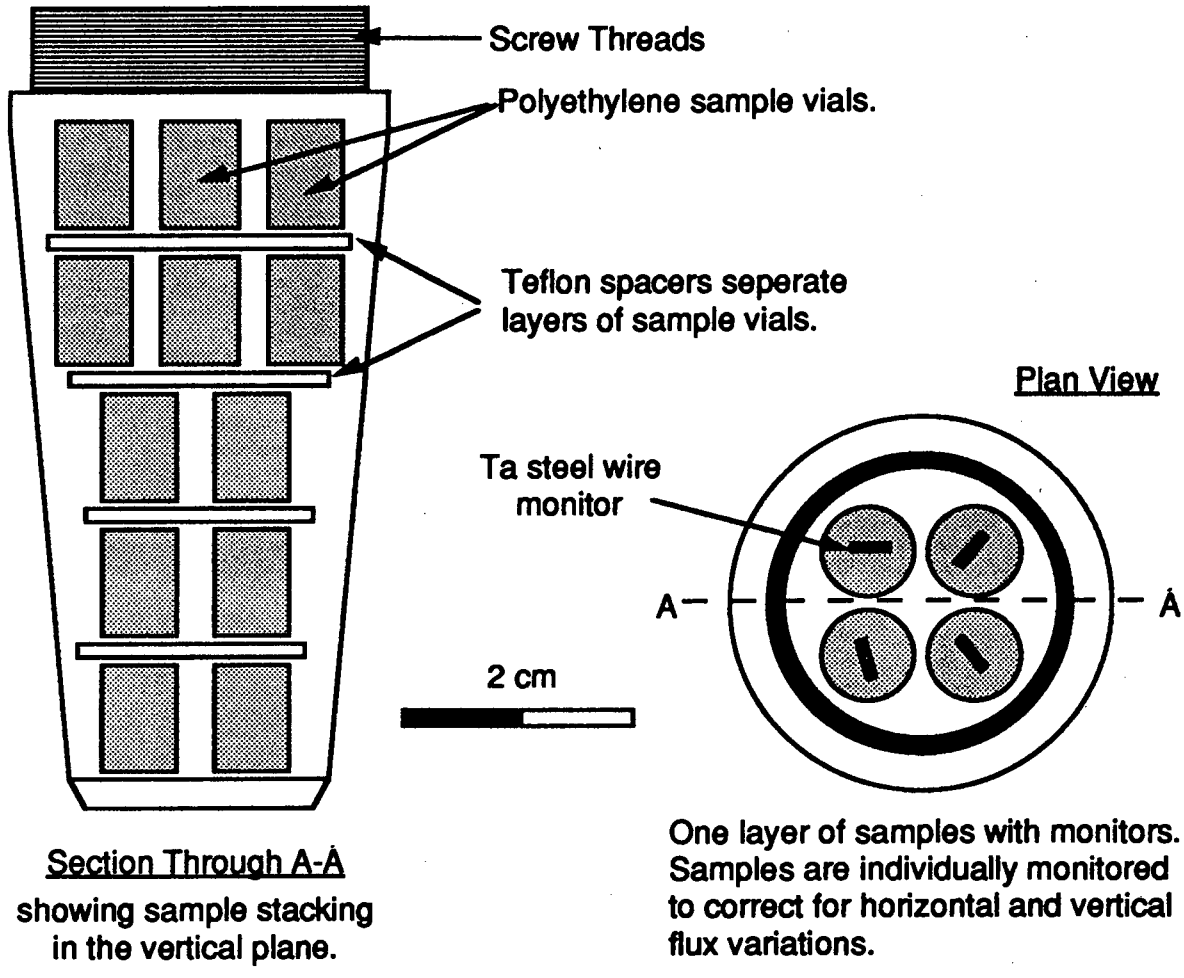

Figure A1.4.: Packing of samples inside the male section of a Pneumatic rabbit.

Unlike the PROF, samples are not rotated during irradiation and both horizontal and vertical flux variations have to be corrected for on an individual sample basis. Although the Pneumatic Facility is located very close to the core, the

intervening Be shield elements seriously reduce the avaliable flux. The line of Pb shielding prevents excessive gamma-ray heating of the plastic rabbit and allows more lengthy irradiations. Irradiation periods of between 10 seconds and 12 hours can be utilized in this facility. At the end of the irradiation period, the sample is driven back out of the core by compressed air into a shielded storage area where it is allowed to cool before being packed. For PGE concentrates on filter papers, cooling times of 8 to 10 hours are usually required before the samples are released for transport but for rock samples, cooling times of up to 2 days may be needed.

A1.2.3. The Poolside Isotope Rack.

The Poolside Isotope Rack (PIR) stretches across the front face of the core and extends backwards into the pool area. The rack swings in and out of position on metal hinges. It offers the twin advantages of a high overall neutron flux and a neutron energy spectrum which has a large component of epithermal neutrons. The rack has 24 holes or sockets for irradiation cans. The sockets are arranged in three rows; A, B and C. The A row is closest to the core face and receives the highest flux. Neutron flux falls by about 26% from A row to C row and the Cd ratio also changes, rising from 7.6 in the centre of A row to 14.6 in the centre of C row.

The front of the rack is only about 10 centimeters from the core face and considerable heating of the samples is experienced. Plastic vials cannot be used in this facility and samples must therefore be sealed in silica glass capsules. Five sample capsules with individual Ta wire flux monitors are packed into sealed metal irradiation cans which are then fitted into the sockets of the rack. For a dominantly thermal irradiation, Al cans are used. If the user wishes to make use of the large epithermal neutron component, samples can also be sealed inside Cd cans. As the samples are sealed inside silica glass there is no danger of the capsules melting or splitting during the irradiation and very long irradiation times (up to two weeks) can be employed when using the PIR. Loading and unloading of the samples is carried out in a hot cell by remote handling gear but samples usually have to be left to cool for 2 or 3 days after the end of the irradiation before they are ready for road transport.

Appendix 2

Detector Systems Employed During NAA.

A2.1. Introduction.

All nuclear detection measurements are based on detection of the interaction of the emitted radiations with the detector crystal. The detection methods are generally based on excitation or ionisation of atoms within the detector via the passage of electrons (Adams and Dams 1970). A gamma-ray quantum striking a scintillator crystal (also called a phosphor) such as NaI doped with Tl, coverts its energy into luminescent emission. The emitted photons are collected on a photosensitive cathode which causes the cathode to eject photoelectrons which can then be accelerated and collected in a photomultiplier to produce a signal. In contrast, gamma-ray quanta striking a semiconductor such as a crystal of Ge cause valence band electrons within the semiconductor to be excited into the conduction band. This interaction directly produces pulses of charge which represent each interaction. In the energy range from 10 eV to 5 MeV, electromagnetic radiations (including gamma-rays) give rise to energetic electrons by one of three separate processes (Bowen and Gibbons 1963; Adams and Dams 1970; Koeberl 1992):

(1) *The photoelectric effect* - in which the gamma photon donates all of its energy to a bound electron which in turn uses part of the energy to overcome its binding energy to the nucleus and absorbs the rest as kinetic energy. Photoelectrons may be ejected from any electron orbital energy level but in practice absorption by the outermost shells is negligible. The probability of the photoelectric effect occurring is approximately proportional to the fourth power of the atomic number of the absorbing species and inversely proportional to the cube of the gamma-ray energy. Thus it occurs most noticeably with heavy elements and with low energy (<500 keV) gamma-rays.

(2) *The Compton effect* - in which the gamma photon is deflected by the orbital electrons. Provided the gamma energy appreciably exceeds the electron binding energy, both photon and electron are scattered as if the electron had originally

been free and at rest and an elastic collision had taken place. This is shown in Figure A2.1. The energies of the scattered electrons cover a wide range and are dependant on the angle of incidence of collision (θ) with the gamma photon. The probability of the Compton effect occurring is proportional to the atomic number of the absorber and is inversely proportional to the gamma energy. In general, the Compton effect is much less important than the photoelectric effect for incoming gamma-rays below 500 keV, but predominates above about 1000 keV.

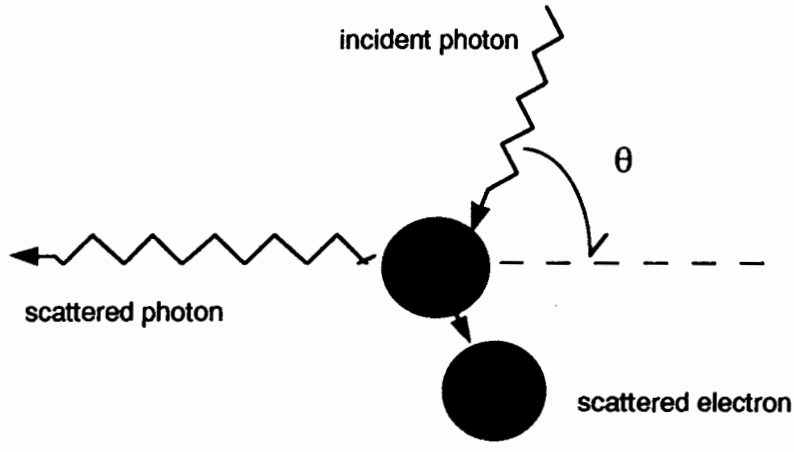

Figure A2.1.: Compton scattering of gamma-photon and electron.

(3) *Pair production* - in which the gamma-ray photon interacts with the Coulomb field surrounding a nucleus or an electron, and then disappears with the creation of an electron-positron pair as shown in Figure A2.2.

This effect can only occur with gamma radiation of energy greater than the energy of the particles themselves ($2mc^2$ = 1.024 MeV), but thereafter the effect increases with energy. The newly created electron moves off on its own trajectory while the newly created positron annihilates with the nearest electron and produces two 0.512 MeV gamma rays which may undergo their own Compton or photoelectric interactions. A similar annihilation effect is produced during the emission of positrons by some radioiosotopes such as ^{24}Al and ^{94}Tc.

In gamma-ray spectrometry, the only interactions of importance are those in which the gamma ray photon loses all of its energy. This eliminates electrons produced via the Compton effect which results from the partial absorption of the electromagnetic radiation. The Compton effect and the very broad range of energies of the recoil electrons it produces are more of a hindrance than an advantage in gamma-ray spectrometry (Adams and Dams 1970), in that they

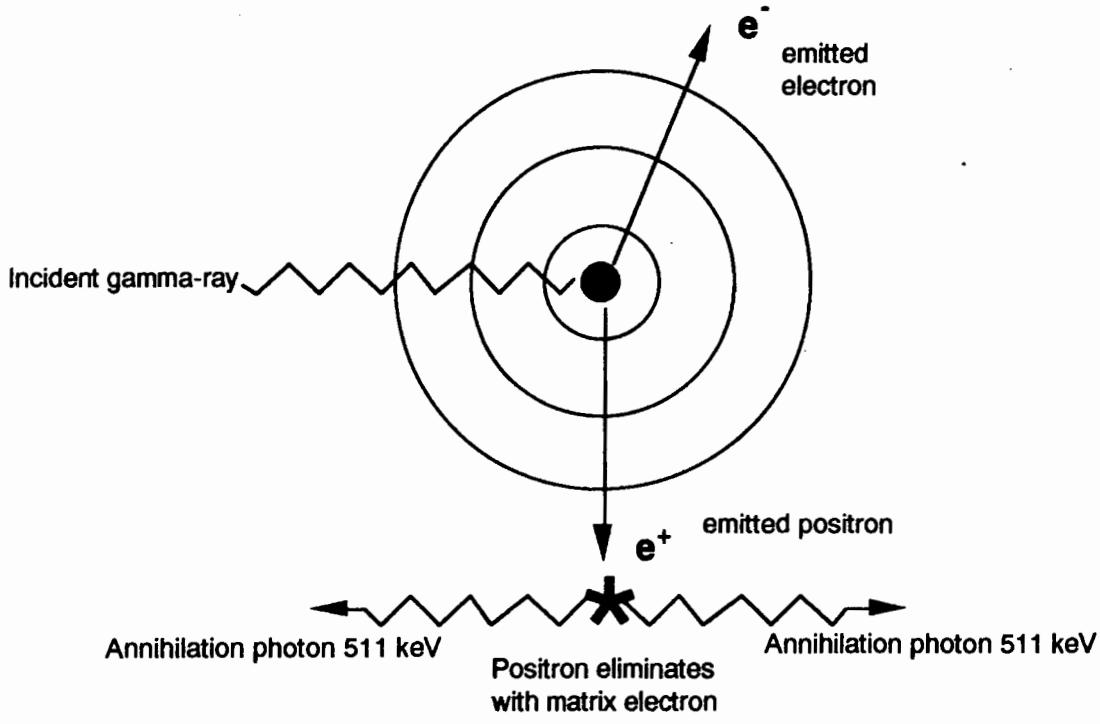

Figure A2.2.: Gamma-ray interaction with matter resulting in pair production. The positron produced by the first collision will encounter and annihilate with a matrix electron to produce two 511 keV gamma photons.

contribute to the background in the final energy spectrum. A large variety of anti-Compton shielding devices are now available to help reduce this unwanted contribution to a minimum.

With the proper choice of detector material and coupled signal processing electronics, the number of electrons produced in the detector by each event (and hence the energy of the event) and the occurrence of each event in time can be measured. For example, in Ge crystals, a 1000 keV gamma-ray will promote about $3x10^5$ electrons into the conduction band. Each separate pulse of charge can then be converted into a digital format by an analogue to digital converter (ADC) unit and combined to give an energy spectrum which is the sum of the radiation sources in the sample.

A2.2. Detectors.

A variety of materials have been used as detectors in NAA. During the late 1950's and early 1960's measurements were performed using sodium iodide (NaI) crystals, containing ~0.1% Tl as an active impurity. These NaI(Tl) scintillation detectors were highly sensitive to incoming gamma-rays but had very poor gamma-ray energy resolution, measured as the full width at half maximum (FWHM) in keV of the 1332 keV line of ^{60}Co (Perlman 1981; Guinn 1992). They can be successfully employed in radiochemical procedures where separations have been used to obtain relatively pure final products but they are generally not suitable for multielement NAA (Koeberl 1992).

The problem of detector resolution was solved in 1960 with the advent of the lithium-drifted germanium semiconductor [Ge(Li)] detector (Guinn 1992). Ge(Li) detectors offered energy resolutions of 2-3 keV at 1332 keV, about 20-30 times better than NaI(Tl) crystals, which largely solved the problem of overlapping peaks in the resulting gamma spectrum (Perlman 1981; Guinn 1992). The main disadvantage with Ge(Li) detectors was their poor detection efficiency as compared with conventional 7.62 cm x 7.62 cm NaI(Tl) detectors. An additional problem was the need to constantly keep a Ge(Li) detector at the temperature of liquid nitrogen (77K), firstly to minimize the high levels of electronic noise associated with the drifted crystal, and secondly, to stop the Li atoms moving out of the drifted layer and incapacitating the semiconductor crystal.

Advances in crystal growing techniques have allowed the growth of Ge crystals with very low impurity levels ($<10^{10}$ impurity atoms cm^{-3}). This material is known as hyperpure or high purity Ge (HPGe) and does not need charge compensation by Li drifting. Large crystals are now commercially available which offer high efficiencies (50-60% of 7.62 x 7.62 NaI(Tl)) and resolutions of 1.8-1.6 keV at 1332 keV (Koeberl 1992). HPGe detectors also require cooling to 77K during measurements but offer the advantage that they can be cycled up to room temperature without damage when not in use.

A variation on the conventional coaxial design, is the planar detector, which incorporates a flat HPGe cylinder with a small active volume. Planar detectors, also called Low Energy Photon Detectors (LEPD's) are used for the measurement of low energy gamma-rays (10-200 keV) and offer excellent energy resolution in

an area of the spectrum where peaks are often poorly resolved on coaxial HPGe and Ge(Li) detectors (Hertogen and Gijbels 1971; Shazali 1988; Koeberl 1992).

Portable coaxial and planar Ge detectors with small, cylindrical dewars which can maintain liquid nitrogen temperatures for between 8 and 24 hours are also available. When connected to a portable analyser system, the detector can be taken to the irradiation site or the source of radiation, rather than the samples being transported back to the laboratory. This is particularly important for the analysis of species with short half lives when the laboratory is not situated close to the reactor.

A2.3. Signal Processing Electronics.

A2.3.1. Signal Amplification.

The pulses of charge in the detector crystal are collected and amplified by a field effect transistor (FET) in a preamplifier unit. The FET operates under a high voltage bias (2000-4000 volts) and is kept at liquid nitrogen temperatures to minimise external electronic noise and to avoid signal distortion. Modern preamplifiers incorporate shutdown protection circuits to protect the FET from damage if the liquid nitrogen supply should become exhausted and the detector begins to warm up while bias is still being applied.

The output from the preamplifier is a fast rising (~ 50 ns) voltage signal which then exponentially decays with a decay time constant of ~ 50 μs. The output voltage is proportional to the number of electrons flowing through the detector crystal and hence to the energy of the incident gamma-ray. This signal is then processed by a spectroscopy amplifier. This unit performs pulse shaping and baseline corrections to produce a "clean" signal which can be read by the proceeding digital electronics. The output from the spectroscopy amplifier is a near gaussian pulse with an amplitude proportional to the input signal from the preamplifier.

Problems can arise in the spectroscopy amplifier if two pulses arrive very close to one another. This can lead to what is known as "pulse pileup", a superimposition of peaks to produce a summed single gaussian peak which is representative of neither of the input signals. The problem of pileup can be addressed in two ways; the first is to use very short peak shaping times (2-6 μs)

which reduces the chances of pileup but degrades the quality of the output signal. The second solution is the use of pileup rejection circuits. These detect the initial pileup and direct the combined pulse to circuits in the ADC which cause the pulse to be rejected by the digital electronics so that the pileup signal is not recorded by the ADC.

Recently very fast amplifiers, called Gated Integrators, have been developed. These save on peak shaping time by cutting off the second half of the gaussian peak after detection of the peak maximum. This produces shorter peak shaping times without degradation of the signal quality and allows the spectroscopy amplifier to cope with the high rates of signal input associated with highly active samples.

A2.3.2. Signal Conversion.

The output gaussian pulse from the spectroscopy amplifier is then fed into the analogue to digital converter where the analogue voltage is converted into a digital signal which can be stored as a single event in the memory of an analyser. Two types of conversion are available in modern ADCs. Conversion of the signal in Wilkinson ADCs is performed by allowing a capacitor to be charged to the voltage of the input pulse. The capacitor is then discharged at a constant rate and the length of discharge time is monitored by a very fast (50-100 MHz) internal clock.

While the capacitor is discharging, which may take several microseconds, the ADC cannot process any other incoming signals and these are rejected by the electronics. Periods such as this where the analyser is "busy" with one signal and cannot deal with another is known as the analyser "dead-time". Modern ADCs automatically record the number of dead-time rejected signals and use this to compute a dead-time correction which is then applied to the final spectrum.

In order to get around the constraint of discharge times (and therefore dead-times) being related to input voltages, the use of successive approximation ADCs has become more common. These ADC's function by voltage comparison over a resistor chain. This is a uniform process which produces a fixed signal conversion time, usually on the order of only 1-2 μs. Signal processing via a successive approximation ADC therefore substantially reduces the busy time of the electronics and means that the system can deal with higher count rates.

The converted events are stored in the memory of multi-channel analyser (MCA). Each event is assigned to an individual channel which is related to the input voltage and hence the energy of the incident gamma-ray. Modern MCA memories contain 4096 or 8192 channels, which are normally calibrated to span an energy range of about 50-2000 keV. Each gamma-ray which strikes the detector is amplified, converted and stored in the MCA in the manner of a histogram until the full spectrum is complete. Many gamma-ray interactions of the same energy will yield events in the same channel, producing a peak in the resulting spectrum. Once a spectra has been recorded by the MCA, it is usually saved onto the free memory of a computer where it can be processed. The MCA memory is then erased prior to the acquiry of the next spectrum.

A2.4. Data Processing.

The evaluation of a gamma-ray spectra involves several steps; viz, locating peaks in the spectrum, determining peak energies and areas, and the calculation of statistical errors associated with each peak (Koeberl 1992). A large number of programs exist for analysing gamma-ray spectra. Many of these have been published in the literature or presented at conferences (Yule 1981).

Limitations in detector resolution and some electronic noise cause each gamma-ray peak to spread over more than one channel. This spread will ideally form a pseudo- gaussian peak, defined by three or more channels, in the spectrum. Once a peak has been detected by the analysis program's algorithms, the channel containing the centre of the peak is determined and compared with the energy:channel calibration on the MCA to calculate the peak energy (Yule 1981). This value is then compared with a library of radionuclides and peak energies and all species of that energy, plus or minus 2-3 keV, are noted as possible sources of that peak. The library used for peak determination in this thesis was GENLONG.TUB which is a modified version of Yule (1981).

Peak areas can be calculated in two ways; by a direct integration of the measured data, or by the fitting of an appropriate function to the data. The former procedure involves adding together the raw data from the peak and subtracting the underlying background continuum. The most commonly used peak integration routines, incorporating both total peak area (TPA) and partial peak area (PPA) methods, have been reviewed and evaluated by Hertogen et al. (1974).

In fitting methods, a mathematical function, usually a gaussian or modified gaussian, is fitted to the observed data and this is then used to calculate the peak area. These methods have been reviewed by Kokta (1973).

The selection of one or the other technique usually depends on the specific requirements of the experiment. Where peaks are well separated, both methods give similar results. Where peaks overlap onto one another, it is very important to have programs which can resolve the individual peak shapes and in these cases, fitting algorithms generally provide the more accurate results (R.W. Fearick pers. comm. 1991; Koeberl 1992)

The above steps are repeated for each peak in the spectrum. This produces a computer print-out of peak energies, potential radionuclides, peak areas and associated errors. The analyst can then select the desired analytical peaks and process them as outlined in Chapter 3.

A2.5. Gamma Detection Systems Used At Schonland Centre.

All the NAA work undertaken during this thesis was performed with a dual counting system comprising an Ortec 8501-1220-S coaxial Ge(Li) detector opposite an Ortec GLP 25300/13 planar HPGe LEPD. This counting configuration has been previously described by Andeweg et al. (1990) and is summarized in Figures A2.3. and A2.4.. The detectors were connected to separate stepper motors so that sample : detector distances could be varied independently (Andeweg and Modiba 1989). The specifications for the two detectors are as follows:

	Coaxial Ge(Li)	**Planar Ge LEPD**
Detector Volume	86.2 cm^3	6.5 cm^3
Absorbing Layers	1.3 mm Al	0.25 mm Be
	0.7 mm inactive Ge	
Operating Bias	2000 volts	1500 volts
Resolution	1.71 keV at 1333 keV	0.536 keV at 122 keV
	0.87 keV at 122 keV	0.288 keV at 5.9 keV
Efficiency (rel. to NaI(Tl))	16.6 %	3.35 %
Peak:Compton Ratio (^{60}Co)	49.6 : 1	

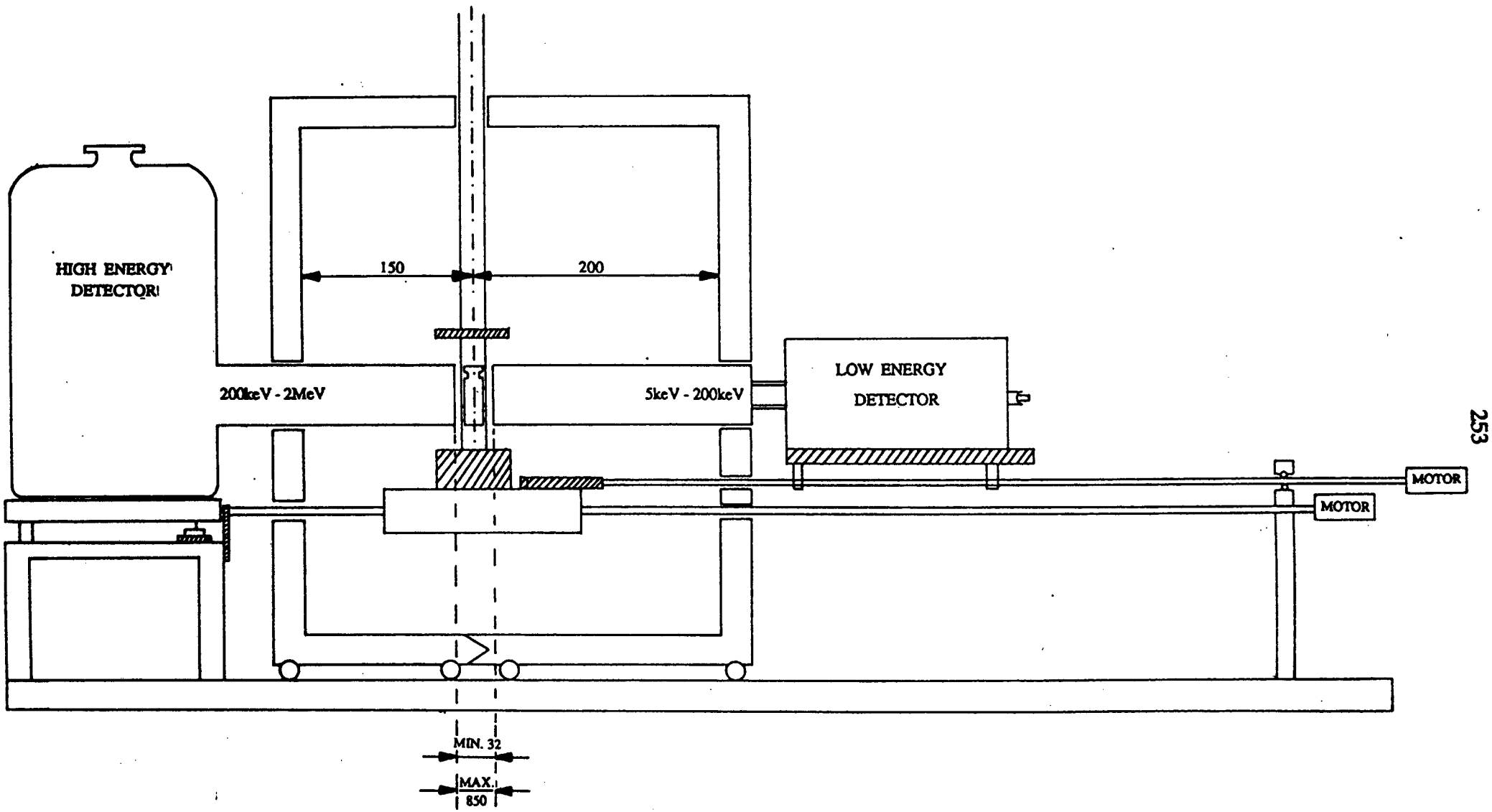

Figure A2.3.: Side view of NAA dual counting system configuration. From Andeweg et al. (1990).

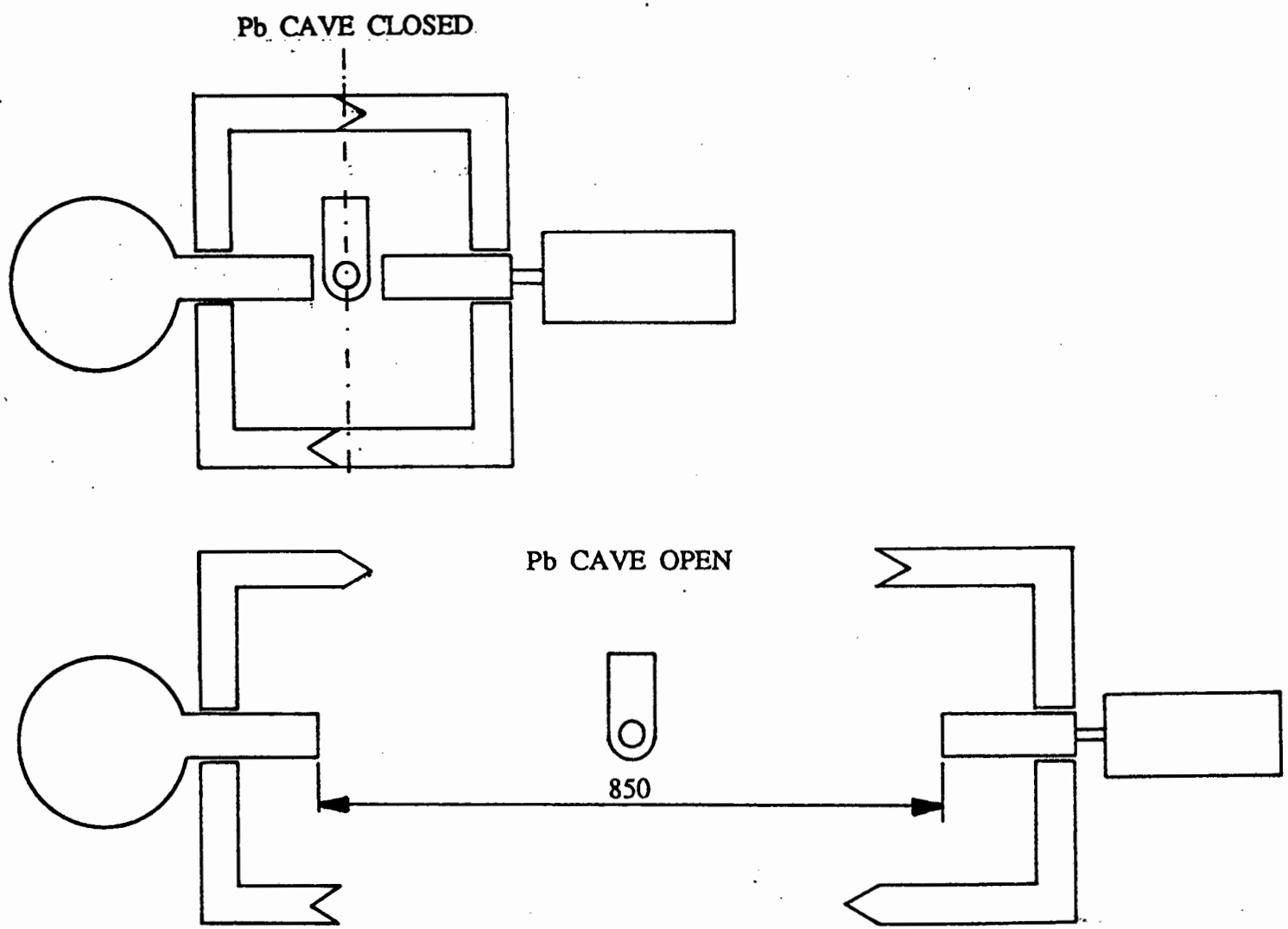

Figure A2.4: Plan view of NAA dual counting system configuration. From Andeweg et al. (1990).

Both detectors were surrounded by Pb shields to minimize any contribution from natural background radioactivity. In addition, the Pb was lined with Cd and Cu to minimize interference from secondary X-rays caused by gamma-ray quanta striking the Pb. Samples were placed into 5cm long polyethylene counting vials. The vials were then loaded into a large capacity sample changer located 180 meters away from the counting station in order to avoid high background activity near the detectors during counting. The sample changer is a fully automated design and has been described in detail by Andeweg and Watterson (1980). Samples were then automatically transferred via a pneumatic air line to the counting position.

The Ge(Li) detector is a fixed design and is supplied with liquid nitrogen from a 30 litre capacity dewar. The LEPD is a portable design with a small 1.2 litre dewar which is refilled automatically every 8 hours (Andeweg and Modiba 1990). When not required for dual system counting, this detector can be removed from its brackets on the counting bench and used as a portable detector for short lived isotope work at the SAFARI-1 reactor. When detached from the automatic refill system, the dewar capacity on the LEPD will allow the detector to remain at 77K for 24 hours before the liquid nitrogen supply is exhausted.

The Ge(Li) detector and the LEPD were connected respectively to Canberra 2010 and Ortec 673 spectroscopy amplifiers. Each amplifier was wired to a Nuclear Data 584 Successive Approximation ADC and the ADCs connected to the parallel ports of a Nuclear Data #455 4096 channel micro-MCA. Energy calibrations for the Ge(Li) detector and LEPD were 0.5 keV per channel and 0.2 keV per channel respectively. The automated sample changer and data acquisition from the MCA were controlled via in-house driver programs running under Microsoft OS/2 on an IBM-PC (R.W. Fearick pers. comm. 1991). Gamma-ray spectra were processed in batch mode on the same computer using a modified version of the HEVESY program (Yule 1968; R.W. Fearick pers. comm. 1991). A simplified circuit diagram of the equipment is shown in Figure A2.5.

During the analysis of short-lived radioisotopes at the reactor site, the LEPD was connected to a portable Tracor Northern TN7200 analyser. This unit was operated using 2048 channels, with an energy calibration of 0.1 keV per channel. Spectra recorded on the analyser were saved on floppy disk before being returned to Schonland Centre for conversion and processing in the same manner as above.

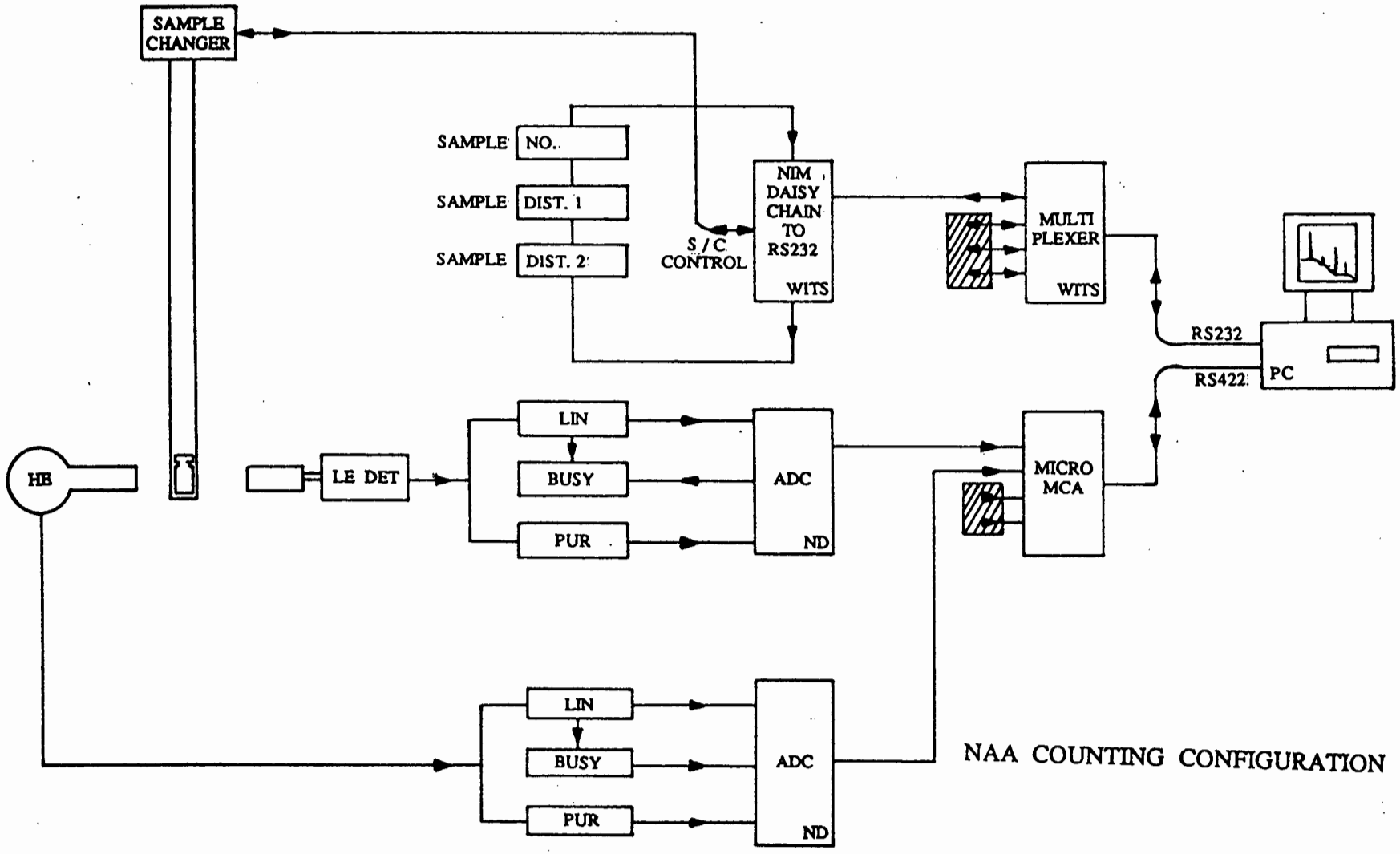

Figure A2.5.: Simplified circuit diagram of the detector systems and the automated sample changer. From Andeweg et al. (1990).

Appendix 3: Neutron Activation Analysis (NAA) For The Precious Metals.

J.I.W. Watterson and I. McDonald

(extended abstract) Symposium On Analytical Technique For Platinum-Group Metals. 4th ICAM, MINTEK, Randburg, 6th September 1991

Neutron Activation Analysis (NAA) for the Precious Metals

by

J.I.W. Watterson† and I. McDonald†*

†Schonland Research Centre for Nuclear Sciences
University of the Witwatersrand
Johannesburg
*Department of Geology, University of Cape Town

1. Introduction

In spite of modern advances in analytical chemistry, neutron activation analysis continues to occupy a special position. This is because it has certain unique characteristics that set it apart from other analytical methods. When the instrumental method is used there is essentially no sample preparation, and hence no reagent blank. In addition the results are independent of the chemical characteristics of the material that is analysed. In this case, the method does not depend on the solubility of different components of the material, or of mineral effects (as in x-ray fluorescence). The instrumental method is thus robust. Once the gamma-ray lines of interest have been identified and found to be free of interferences, the errors in determination are often dominated by the purely statistical errors in the determination of the peak area, and these can be accurately predicted from the Poisson distribution. This independence of methods of extraction and of the chemical form of the analyte, means that instrumental NAA can give highly accurate results, when it is applicable, and can be considered as a referee method in cases where other methods fail to agree.

There are several different forms of NAA depending on the type of neutron source that is used and whether or not the method is purely instrumental. In reactor neutron activation analysis, the value of the neutron flux is high (say 10^{13} n.cm^{-2}.s^{-1}) and the sample size is small (typically 500mg to 1 gram). Where neutron sources are used, the neutron flux would be of the order of 10^{6} n.cm^{-2}.s^{-1} or possibly 10^{7} n.cm^{-2}.s^{-1}, that is at least a million times less. Using accelerators, neutron fluxes somewhat higher than this can be achieved.

Interestingly, large samples can be analysed effectively using sources of these latter types, and the sample size can be as high as a kilogram. This could have important future applications in the analysis of the precious metals including the potential for on-line analysis.

2. Theoretical sensitivities

The theoretical sensitivity depends on the nuclear parameters of the isotopes, i.e. isotopic abundances, cross sections, half lives and gamma-ray intensities, as well as irradiation, decay and counting times. Table 1 shows the theoretical sensitivities of selected reactions with the precious metals under two sets of conditions. In the first set, the irradiation and counting times are 10 minutes each and the decay time is 2 minutes. In the second set the irradiation time is 10 hours, the decay time two days and the counting time is one hour. The sensitivities are quoted in gamma-ray disintegrations per microgram of element for the most intense gamma-ray line in each case. These two choices are respectively appropriate to the use of short lived activities at the reactor site and the use of long-lived activities at a location that could be remote from the reactor. Practical sensitivities will depend on the levels of the other elements in the sample and are more difficult to predict.

The theoretical sensitivities calculated in this way cover cover three orders of magnitude, from gold, the most sensitive, to platinum, the least sensitive. The great sensitivity of gold makes neutron activation a particularly powerful analytical technique for this element. The purely instrumental reactor based technique can be used to determine gold down to levels of a few

parts in 10^9 in small rock samples on the one hand and on the other it offers the possibility of using laboratory-based neutron sources to determine gold at the levels of a part in 10^6, i.e. at levels of interest in mining, using large samples.

Table 1
Nuclear data and theoretical sensitivities for NAA of the precious metals

Reaction	Half-life of product	Principal Gamma-ray energy (keV)	Sensitivity for flux $\phi = 10^{13}$ n.cm^{-2}.s^{-1} gamma-ray disintegrations per µg	
			t_i = 10 mins t_d = 2 mins t_c = 10 mins	t_i = 10 hours t_d = 2 days t_c = 1 hour
$^{197}Au(n,\gamma)^{198}Au$	2.7d	411.8	$3.1x10^6$	$6.2x10^8$
$^{107}Ag(n,\gamma)^{109}Ag$	2.42min	633.0	$1.9x10^6$	-
$^{109}Ag(n,\gamma)^{110m}Ag$	253d	658.0	$1.3x10^3$	$4.7x10^5$
$^{109}Ag(n,\gamma)^{110}Ag$	24s	658.0	$1.2x10^5$	-
$^{96}Ru(n,\gamma)^{97}Ru$	2.88d	215	$7.8x10^2$	$1.7x10^5$
$^{102}Ru(n,\gamma)^{103}Ru$	38.9d	497	$1.6x10^3$	$5.4x10^5$
$^{104}Ru(n,\gamma)^{105}Ru$	4.44h	726	$3.7x10^4$	$3.6x10^3$
$^{103}Rh(n,\gamma)^{104m}Rh$	43s	560	$1.6x10^6$	-
$^{103}Rh(n,\gamma)^{104}Rh$	4.41min	52	$5.3x10^7$	-
$^{102}Pd(n,\gamma)^{103}Pd$	17d	362	$2.8x10^{-1}$	$9.1x10^1$
$^{108}Pd(n,\gamma)^{109}Pd$	13.6h	88	$4.5x10^4$	$1.1x10^6$
$^{184}Os(n,\gamma)^{185}Os$	93.6d	646	$4.4x10^2$	$1.6x10^5$
$^{190}Os(n,\gamma)^{191}Os$	15d	129	$5.2x10^3$	$1.7x10^6$
$^{192}Os(n,\gamma)^{193}Os$	31.5h	460	$2.2x10^3$	$2.5x10^5$
$^{191}Ir(n,\gamma)^{192}Ir$	1.42min	58	$1.4x10^5$	-
$^{191}Ir(n,\gamma)^{192}Ir$	74.2d	316	$3.6x10^5$	$8.4x10^7$
$^{193}Ir(n,\gamma)^{194}Ir$	17.4h	328	$9.9x10^5$	$3.6x10^7$
$^{190}Pt(n,\gamma)^{191}Pt$	3d	539.0	$5.3x10^1$	$1.1x10^4$
$^{196}Pt(n,\gamma)^{197}Pt$	18h	77	$4.3x10^3$	$2.0x10^5$
$^{196}Pt(n,\gamma)^{197}Pt$	78min	346	$2.4x10^3$	-
$^{198}Pt(n,\gamma)^{199}Pt$	30min	543.0	$1.3x10^5$	-
$^{198}Pt(n,\gamma)^{199}Pt$ ^{199}Pt β^- ^{199}Au	3.15d	158.4	$2.7x10^3$	$6.1x10^5$

3. Neutron source activation for gold in large samples

The fact that gold occurs in discrete particles in the Witwatersrand makes it extremely difficult to obtain representative samples. This so-called nugget effect makes the assessment and control of the mining and reduction of the ore problematic and a method that could increase the sample size by several orders of magnitude should have profound effects.

Work with large (500g) samples and a ^{252}Cf neutron source[1] has shown a limit of detection (LOD) of 12ppb of gold with an irradiation time of 17 hours, a decay time of 3d and a counting time of 24 hours. It would be possible to increase the neutron flux using a larger source, or an accelerator, by two to three orders of magnitude, resulting in similar limits of detection with an irradiation time of two hours and counting times of 15 minutes. This would produce a method

that could be developed to replace fire-assay for the routine determination of gold, and also at the same time to revolutionise sampling. Ultimately this method could be fully automated.

Figure 1 shows a calibration curve obtained using 500g samples of ore under the above experimental conditions. Although more points are necessary, there is evidence that the instrumental method yields a linear calibration curve over the range from less than 1 ppm to 12 ppm, with no sample preparation other than crushing and, in this case, grinding.

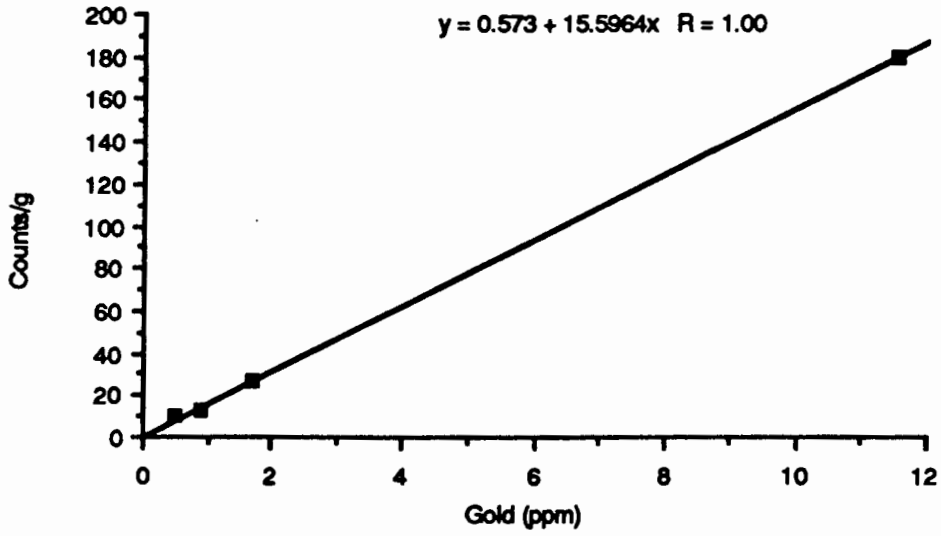

Figure 1 Calibration curve for gold in gold ore. The sample size was 500g and the ore was analysed as received, i.e. with no sample treatment.

Further work is at present under way to investigate the establishment of a method that could replace the method of fire assay with lead collection as the routine method for the assay of gold. The most important aspect of this investigation is the neutron source.

4. The rapid determination of gold by fast neutron activation

In addition to its unique sensitivity for thermal neutrons, gold also has an isomeric state with a particularly large cross-section for 1 MeV neutrons[2]. In this case the gold undergoes the following reaction: $^{197}Au(n,n'\gamma)^{197m}Au$. The isomeric state ^{197m}Au decays with a half-life of 7.8s and emits a 279 keV gamma-ray.

With a suitable high intensity neutron source[3] this reaction can be used for the rapid determination of gold in reasonably large samples and there is the possibility of using this reaction for ore sorting[4]. Both of these methods have the potential for use in on-line analysis.

5. Determination of the PGE at ultra-trace levels

In the case of the platinum group elements (PGE) the NAA method using a reactor is capable of very high sensitivities when combined with the nickel sulphide extraction method. This method has been reported by Hoffman et al[5] and by Davies and Tredoux[6], and recently developed further by McDonald[7]. The following data on this method are taken from the last of these references.

In this procedure some 50g of the sample are mixed with 35g of nickel carbonate together with sulphur, soda ash, borax and pure silica. This is then fired at 1000°C for 75 minutes. After cooling, the NiS button is removed and dissolved in 37% HCl. The release of H_2S, during the dissolution of the NiS, maintains a reducing environment in the solution and inhibits the

dissolution of the PGE sulphides and Au. The solutions are filtered through 0.45μm filter paper and the insoluble PGE sulphides are trapped on the paper.

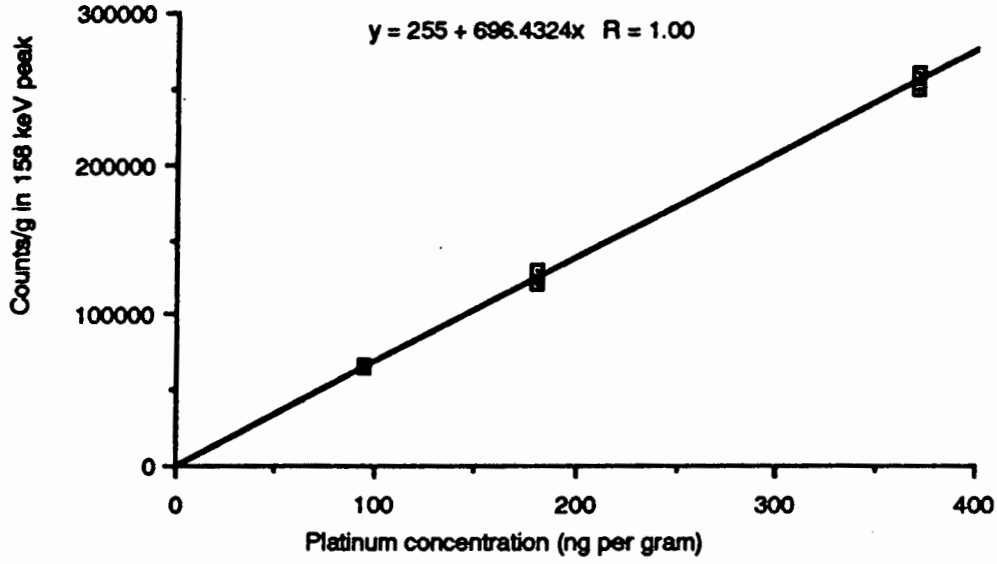

Figure 2 Calibration curve for platinum in SARM 7 using NAA with the NiS extraction method.

One particular advantage of this procedure is that there is no further chemical processing, as is necessary for example in the case of ICP-MS, where the filter paper and the residue must be dissolved. In the NAA procedure, the filter papers are folded, packed into polyethylene vials and irradiated after drying.

Following a 12 hour irradiation, three gamma-ray spectra are accumulated for each sample, after decay times of six hours, six days and 17 days respectively. A dual detector system is used, comprising a normal 60 cm^3 Ge(Li) detector opposite to a planar low energy photon detector (LEPD).

Figure 2 shows a typical calibration curve obtained using this method with three different solid dilutions of the reference material SARM 7.

This method has great sensitivity and the detection limits, calculated as two standard deviations of the background under the peak, are given in Table 2.

Table 2
Calculated limits of detection for NAA of the precious metals using NiS extraction

	Ru	Rh	Pd	Os	Ir	Pt	Au
Limit of detection (ng per gram)	1.0	no data	0.8	0.2	0.005	3.5	0.001

The practical sensitivity is limited by the blank values for the PGE in the reagents, particularly the nickel carbonate. These blank values proved to be below the detection limit, except in the case of the two most sensitive elements, Ir and Au, where blank values of 0.9 and 0.6 ng per gram were found.

This method has a sensitivity that makes it applicable to the determination of the PGE and gold at the levels present in many different rock types including basalts, tholeiites and komatiites and is particularly useful in geochemical studies.

6. Determination of the PGE by NAA with a neutron source

The instrumental method using reactor irradiation has limits of detection that are far higher and in its usual form it suffers from the problem that very small sample sizes (<1g) are used. With these small sizes, the sampling problem for the precious metals in geological samples is so severe that the results can be meaningless.

By using a large sample with an isotopic or accelerator neutron source it is possible to achieve limits of detection in the region of 1 ppm for platinum, 100 ng per gram for rhodium and 10 ng per gram for iridium. This aspect of neutron activation of the precious metals remains to be thoroughly investigated[1].

7. Conclusion

Neutron activation analysis offers a number of different methods for the determination of the precious elements. The instrumental reactor method is particularly sensitive for the determination of gold at levels down to a few ng per gram in geological materials.

When reactor NAA is combined with NiS collection it is theoretically possible to determine gold and iridium at levels of a few parts in 10^{12}, platinum at the level of a few parts in 10^{9} and the other precious metals (except for silver) at levels between these extremes. In practice the blank values limit the sensitivity. This method has many applications in geochemistry and cosmochemistry.

The use of isotopic or accelerator based neutron sources with appropriate irradiation facilities allows the analysis of large samples and offers a method that can be used to overcome the considerable sampling problems associated with the determination of the precious metals in rocks and ores.

Finally there is great potential for the use of NAA with an isotopic or an accelerator source for the on-line analysis of certain elements such as gold, iridium and rhodium.

---

1 M. Lycoudi and J.I.W Watterson, Isotope source neutron activation analysis as an alternative to fire-assay for the determination of gold and the platinum group elements. (In preparation)

2 J.I.W. Watterson, A.E. Pillay, J.P.F. Sellschop and A.H. Andeweg, Ion beams for the production of neutrons and their use in selective activation analysis., Nucl. Instrum and Meth. B35, pp349-357 (1988)

3 J.I.W. Watterson, A.E. Pillay and P. Nailand, Selective activation analysis with ion-beam-tailored neutron spectra – a comparison between the reactions $^{7}Li(p,n)^{7}Be$ and $^{9}Be(p,n)^{9}B$., Nucl. Instrum and Meth. B45, pp75-80 (1990)

4 J.I.W. Watterson, A theoretical study of the sorting of Witwatersrand ore., University of the Witwatersrand, Johannesburg, Schonland Research Centre for Nuclear Science, Report SRCNS 86/03 (1986)

5 E.L. Hoffman, A.J. Naldrett, J.C. van Loon, R.G.V. Hancock and A. Mason, The determination of all the platinum group elements and gold in rocks and ores by neutron activation analysis after preconcentration by a nickel sulphide fire-assay technique on large samples., Anal Chim Acta, 102, pp157-166 (1978)

6 G. Davies and M. Tredoux, The platinum group element and gold content of marginal rocks and sills of the Bushveld Complex., Econ. Geol., 80, pp838-848 (1985)

7 I. McDonald, The analysis of the platinum group elements in South African kimberlites by nickel sulphide fire-assay and neutron activation analysis., University of the Witwatersrand, Johannesburg, Schonland Research Centre for Nuclear Science, Report April 1991.

Appendix 4: The Analysis Of The Platinum-Group Elements In South African Kimberlites By Nickel Sulphide Fire-Assay And Neutron Activation Analysis.

I. McDonald, R.J. Hart, and M.Tredoux

Analytica Chimica Acta (Under Review)

The Analysis Of The Platinum-Group Elements In South African Kimberlites By Nickel Sulphide Fire-Assay And Neutron Activation Analysis.

I. McDonald*[1,2], R.J. Hart[2,3], M. Tredoux[1]

1. Department of Geology, University of Cape Town, Rondebosch 7700, South Africa
2. Schonland Research Centre, University of the Witwatersrand, P.O. Wits 2050, South Africa
3. Seconded from the Geological Survey of South Africa, Private bag X112, Pretoria 0001, South Africa

SUMMARY

Ten kimberlites from various localities in South Africa have been analysed for all of the platinum-group elements (PGE) and gold using a nickel sulphide fire-assay preconcentration followed by neutron activation analysis (NAA). The analytical procedure used in this study suggests solutions to the potential problems of incomplete melting of the kimberlite samples during fire-assay, and mimimising losses of Pt, Pd and Au during subsequent dissolution of the assay button. Furthermore, this improved procedure offers lower limits of detection than previous methods which combined fire-assay and NAA. The concentrations of PGE determined in this study of South African kimberlites are compared with previous partial analyses from the literature, indicating that earlier analyses may have seriously overestimated the concentrations of some PGE in kimberlites.

Keywords: Platinum-group elements, kimberlite, neutron activation analysis, fire-assay.

Although kimberlites are not of economic interest with respect to the PGE, they can potentially provide useful information on the nature of PGE carriers in the Earth's mantle [1]. For example, some authors have suggested that temperature and the degree of partial melting might play a major role in the fractionation of the PGE relative to one another during the extraction of many basic magmas from the mantle [2,3]. As kimberlites are formed by very small degrees of partial melting [4], it was thought that PGE data from kimberlites might help to indicate whether the generation of low partial melt magmas was

subject to similar controls. Analyses for the platinum-group elements (PGE) in kimberlites are rare in the geochemical literature. Published results from Siberian kimberlites [5] do not compare well with partial analyses obtained from southern african kimberlites [6,7] and it is generally agreed that the present database cannot be used to model the behaviour of the PGE in kimberlite melts with any degree of confidence[1,4].

In the earliest study of PGE abundances in southern african kimberlites [6], the analyses were carried out by Radiochemical Neutron Activation Analysis (RNAA). Only two PGE (Pd and Ir), along with Au, were detected in this study. RNAA also suffers from the fact that radiological health considerations place a severe constraint on the amount of material which can be irradiated during RNAA procedures [8]. At most, only a few grams of material can be taken for analysis and the extremely heterogeneous distribution of the PGE in most rocks, the so-called "nugget effect" [9], means that this small amount of sample may not be truly representative of the bulk material, making reproducibility of results very difficult.

Since the early 1980's, the combined use of nickel sulphide fire-assay preconcentration on large samples, first with neutron activation, and now more recently with inductively coupled plasma mass spectrometry (ICP-MS), has proved to be the favoured technique for low level analysis of all of the PGE [10,11]. Laborious and intricate RNAA procedures have largely been superseded, leading to a more prolific output of high quality data for all six PGE than was possible before. Nickel sulphide fire-assay, followed by NAA, was used in a study of four South African kimberlites and showed that in addition to Ir, Pd and Au, Os and Pt could also be detected in some samples [7].

The established limits of detection for nickel sulphide fire-assay and NAA procedures [9,12,13] are comparable with the range of PGE concentrations obtained from previous studies of kimberlites [6,7]. In the light is of this, we wished to develop a routine

analytical procedure based on NAA which could be used to obtain high quality, reproducible data for all six PGE in kimberlites. Firstly, in order to check the existing analyses from South Africa, and secondly, to establish a technique which could be used to expand the presently sparse database for PGE in these rocks. Ten samples of kimberlite, from a number of localities in South Africa were selected for this study. The locations of the kimberlite intrusions are shown in Figure 1.

EXPERIMENTAL METHOD

The analysis comprises four steps. These are; (1) preparing and crushing of the sample; (2) preconcentration by nickel sulphide fire-assay; (3) acid dissolution of the assay button to leave a PGE sulphide residue which can be filtered; and (4) irradiation and gamma spectrometric analysis of the residue.

In order to account for the possibility that the samples might contain very low levels of PGE, we designed an analysis procedure which we felt would optimise the collection and subsequent detection of the PGE. While normal aliquots (i.e. 50g) of sample material would be treated during the fire-assay stage, two assay buttons would be combined during the dissolution and filtering, leading to double the normal amount of PGE residue on the filter paper prior to irradiation. After activation, the analytical peaks from the residue, shown in Table 1, should then be more easily resolved from background noise during gamma counting. Final concentrations obtained from the kimberlites could then just be divided by two to correct for the differing amounts of material processed for the kimberlites, compared with the standards.

Apparatus

The nickel sulphide fire assay was carried out a Keegor Fuzion 42kW electric furnace. A thermocouple circuit stabilized temperatures within 20ºC of the set temperature. All filtrations were performed with a Sartorius SM 16307 (glass frit) filtration unit using

Sartorius 11306 cellulose nitrate filter papers. The filter papers had a diameter of 4.7 cm and a pore size of 0.45μm.

Irradiations were performed in the Poolside Rotating and the Pneumatic facilities of the SAFARI-1 reactor, operated by the Atomic Energy Coporation of South Africa. Thermal neutron fluxes in thse facilities were 3 x 10^{12} n.cm^{-2}.sec^{-1} and 7.5 x 10^{12} n.cm^{-2}.sec^{-1} respectively. Counting was performed on a dual detector system comprising a coaxial Ge(Li) detector opposite a planar Ge Low Energy Photon Detector (LEPD). The coaxial detector had a FWHM of 1.71 keV at 1332 keV and the planar detector had FWHM of 300 eV at 5.9 keV and 545 eV at 122 keV. The detectors were connected respectively through Canberra 2010 and Ortec 673 spectroscopy amplifiers to Nuclear Data 584 analogue to digital converters and a Nuclear Data 4096 channel micro multichannel analyser. Gamma energy calibrations for the two detectors were 0.5 keV per channel and 0.2 keV per channel respectively. Spectra were processed on an IBM-PC using a modified version of the HEVESY program [14]. A short irradiation for ^{104m}Rh was carried out at the reactor site. The gamma spectra were collected on a portable Ge LEPD with the same resolutions as noted above, connected to a Tracor Northern TN 7200 multichannel analyser, using 2048 channels and calibrated for 0.1 keV per channel.

Reagents

During fire-assay, the following reagents were used: finely ground, anhydrous, extra pure sodium carbonate (Merck 6398); fused, GR grade di-sodium tetraborate decahydrate (borax) (Merck 6308); GR grade nickel carbonate (Labchem 6710); extra pure, 250 mesh silica powder (Halpro Chem.); ground, sublimed sulphur (Merck 7982). During the dissolution step, assay butttons were dissolved in extra pure, fuming 37% hydrochloric acid (Merck 314).

Sample Preparation And Crushing

Fresh rock samples were obtained from drill core or from surface outcrops. Visible xenolithic fragments were cut out using a diamond saw and the samples were broken into large fragments with a hammer before being crushed to small chips in a jaw crusher. The chips were sorted under a microscope to remove any smaller xenoliths and the separated fraction was then crushed to minus 100 mesh between agate rings in a swing mill. It has been suggested that Pt, Pd and Au, which are malleable enough, could "smear" onto the agate during crushing, generating a source of possible contamination in subsequent samples. Therefore, as a precaution, after the crushing of each sample was completed and prior to the next sample being treated, barren quartz was crushed between the rings for several minutes to remove any traces of Au or PGE which might have been left by the previous crushing. The quartz was then discarded. In reality, the consistently low levels of Pt, Pd and Au which were found in these samples suggest that any cross contamination of kimberlite samples via the crushing step is likely to be negligible but we consider it wise to include a cleaning step with any unknown material. After crushing, the sample powders were sealed in screw-top bottles and homogenized on a shaker for one hour each, prior to aliquots being removed for fire-assay.

The standards employed were solid dilutions of the certified noble metal standard SARM7 [15] with extra pure silica powder. SARM7, diluted ten, twenty and forty times with silica formed a range of concentrations which was compatible with the range expected in the kimberlite samples. The standards were homogenized on a shaker for 3 hours each prior to fire assay. A silicified komatiite sample, Wits-1, was used as an internal PGE standard and extra pure silica powder was used for the determination of reagent blanks.

Nickel Sulphide Fire-Assay

The fire-assay procedure used is a modified version of several previously published procedures[9,12-14,17]. Samples are combined with a flux and melted at 1000°C in an

assay crucible. During melting of this mixture, nickel sulphide is generated. The PGE are quantitatively extracted from the silicate into the dense, immiscible sulphide phase as it descends through the melt and are present in the final assay button at the base of the crucible.

Experience has shown that some rock types do not fuse properly under the conditions employed by the above authors. In the case of some recently analysed peridotites (>30% MgO and <40% SiO_2), a layer of green crystals is sometimes found to be present just above the nickel sulphide button. X-ray diffraction analysis indicates that this layer is composed of recrystallized forsteritic olivine (Mg_2SiO_4). In addition, samples with high levels of carbonate (>15% CO_2 and <25% SiO_2) do not form a stable melt at all with the flux components: the highly basic mixture strongly attacks the walls of the clay assay crucible and any sulphide button which forms is generally unstable, disintegrating in air over a period of a few days to leave unconsolidated sulphide flakes. A similar disintegration was noted by Shazali [18] when the ratio of carbonate to borax in the charge approached 1:1. For both peridotities, and samples rich in carbonate , it was clear that melting of the sample, and therefore extraction of the PGE into the sulphide, was irregular and probably incomplete.

Kimberlites are peridotitic rocks which may carry variable levels of carbonate[4,19] and we found that both of the above problems arose during fire-assay of some of our kimberlite samples when the original flux mixture and conditions were employed. It was therefore decided to investigate whether the addition of extra acidic components to the flux mixture might neutralize any excess basicity and stabilize the melt.

Irradiated platinum metals were used as tracers to test the recovery of PGE into the sulphide phase during the firing of the internal standard Wits-1 with the conventional flux mixture. The results are shown in Table 2. Losses of PGE and Au to the slag in Wits-1

using the unmodified flux mixture vary between 2 and 5%, with gold showing more serious losses than the PGE. Both of these features are in accord with previous studies [12,20].

We discovered that the addition of a small amount of silica was sufficient to completely melt any olivine in the peridotite samples. High carbonate samples such as limestones or carbonatites are more unpredictable can require the addition of both silica and additional borax to form a stable melt. The recommended "peridotitic" and "high carbonate" flux mixtures are shown in Table 3. Inactive "peridotitic" dunite (RZ4A) and an inactive "high carbonate" carbonatite (C.S.) were spiked with irradiated PGE tracers and treated with the modified and the unmodified flux mixtures. These experiments indicated that serious losses were encountered with the "peridotitic" sample and the unmodified flux, while no button could be formed from the "high carbonate" sample without the use of the modified flux. As Table 2 shows, the use of the modified flux mixtures for the "peridotitic" and "high carbonate" samples, resulted in similar slag losses (2-5%) to those encountered using Wits-1 and the unmodified flux mixture.

It should be stressed however, that the flux mixtures shown in Table 3 are at best, guidelines, and that a detailed examination of the slag after firing is the only way to ensure that complete melting has indeed occurred. In the case of extremely high carbonate samples (>25% CO_2) the analyst should be prepared for the possibility of repeated firings with progressively higher amounts of additional silica and borax.in order to achieve complete melting of the sample and the formation of a stable assay button.

A carbonatite from the Premier mine (10.Prem-243) required the use of the "high carbonate" flux but, in general, the other samples in this study had peridotitic compositions with only small amounts of carbonate and most of the fire-assays were

performed using the "peridotitc" mixture. One analysis of Roberts Victor kimberlite material (8 RoVic-112) was carried out using the unmodified mixture for comparison.

Acid Dissolution And Filtering

After fire-assay, the buttons were removed from the crucibles. Each was weighed and described before being wrapped in a plastic bag and cracked with a hammer. All of the sulphide chips were carefully emptied into a marked beaker and 500 ml of 37% HCl was then added. Dissolution of the nickel sulphide typically takes 4 to 8 hours on a hotplate. The hydrogen sulphide (H_2S) gas generated during the reaction maintains a reducing environment within the solution and this inhibits dissolution of any PGE sulphides [10,20]. These only dissolve under oxidising conditions in HCl solutions and they are etched out of the dissolving nickel sulphide to form a layer of tiny particles on the base of the beaker.

In previously published procedures [9,12-14,17] the hot solutions are allowed to stand for several hours after hydrogen sulphide emissions have ceased. There is considerable debate as to whether losses of PGE and Au can occur at this stage [10,14,20,21]. Previous tracer studies [22] and preliminary tracer work undertaken by us appears to indicate that there are no major losses of PGE and Au to the solution while a reducing environment is maintained, but if the solutions are allowed to stand for 12 hours after evolution of H_2S has ceased, 10-18% of the Au and 3-8% of the Pd may be dissolved in the HCl. Coprecipitation with Te has been used to correct for these losses [11,14,18] but this introduces Te into the final residue which, after activation, strongly interferes with the 158 keV peak of ^{199}Au [14,18]. The less senstive 208 keV peak of ^{199}Au therefore has to be used and this has the effect of raising the limit of detection for Pt by about a factor of three.

As we sought the lowest possible limits of detection, the disadvantage caused by the Te interference on Pt [14] was deemed to outweigh the advantages which could be obtained from Te coprecipitation and it was not used in this study. Instead we adopted the rigourous approach that the hot solutions should be left to stand for as little time as possible after H_2S evolution has ceased. Therefore, immediately after dissolution was complete, the beakers were removed from the hotplate and cooled quickly with damp towels to minimise any potential attack by the hot HCl. In this manner, any losses of Pt, Pd and Au were kept to an absolute minimum and the 158 keV peak of ^{199}Au could be employed.

After cooling, the solutions were filtered under vacuum through micropore filter papers, trapping the PGE sulphide particles as a thin, grey layer. As noted above, for the kimberlite samples, two assay buttons were dissolved seperately and the contents of the two beakers were combined onto one filter paper to yield twice the normal amount of noble metals. The filter papers were then folded into a triangular shape to regulate sample geometry as much as possible, and then packed into polythene vials and dried in a desiccator for several days before irradiation.

Irradiation And Counting Procedures

Batches of 16 to 24 samples, comprising unknowns, standards and blanks, were packed into custom built polythene racks, along with an equal number of Ta steel wire flux monitors. These were then sealed inside a plastic irradiation container. The container was irradiated for 12 hours in the Poolside Rotating Facility (PROF) of the SAFARI-1 reactor.

The samples were allowed to decay for six hours after the end of the irradiation, cleaned with double distilled water, and then counted for one hour each to determine the ^{109}Pd activity. Additional counts were performed: one of two hours per sample, after six days

for ^{198}Au and ^{199}Au, and another of three hours per sample after 20 days for ^{103}Ru, ^{192}Ir and ^{191}Os.

For the determination of ^{104m}Rh, samples were individually re-irradiated for 2 minutes in the Pneumatic facility of SAFARI-1. The samples were allowed to decay for 1 minute and then counted for 2 minutes on a portable planar Ge LEPD. Spectra were temporarliy downloaded onto floppy disk before being returned to Schonland Centre for processing.

The peak areas of the gamma rays shown in Table 1, corrected for neutron flux, decay time and counting time, were calculated and tabulated. The values from the standards and blanks were used in the preparation of calibration curves for each batch of samples. The fitted regression curves were generally good but most of the curves showed slight negative intercepts with the concentration axis, indicating the presence of small quantities of noble metals in the reagents used for the pre-irradiation chemistry. This was confirmed by analysis of the blanks and is discussed in the next section. Peak areas obtained from the samples were compared with calibration curves and the concentrations calculated. A correction for the differing masses (and any reagent blank) between the samples and the standards was also applied to this calculation.

RESULTS AND DISCUSSION

The calculated limits of detection for the combined fire-assay and NAA method, defined as the smallest concentration which gives a net peak area of twice the standard deviation of the estimated background beneath the peak of interest, and the values from blank determinations, are shown in Table 4. The limits of detection obtained in this study offer a modest improvement on those obtained in earlier procedures [9,12,14]. Ir, Rh and Au, the most sensitive elements for NAA, gave quantifiable blanks. For the other elements, the reagent blank was beneath the limit of detection. Detection of Ir, Rh and Au will therefore be strongly constrained by the reagent blank, as sample contributions much

smaller than the reagent blank will be very difficult to resolve. The level of reagent blank therefore offers a better representation of the practical limit of detection for Ir, Rh and Au by the fire-assay and NAA procedure.

The absolute concentrations of the PGE and Au in South African kimberlites are quite low, generally < 10$\mu g.kg^{-1}$, as indicated by Table 5. Despite the low concentrations, the agreement between duplicate analyses is generally good. The Roberts Victor samples run with different flux mixtures also show a reasonable agreement for Os, Ir and Au, although slightly less Ru, Rh, Pt and Pd appear to have been collected by (8.Rovic-112-3), which employed the unmodified flux mixture. This suggests that complete melting and collection may not have taken place in this sample. Comparison with previous data [6,7] shows a generally good agreement for Os and Ir but suggests that abundances of Pt, Pd and Au may have been seriously overestimated in the earlier studies.

The low concentration of Pt in most of the samples appears to confirm our decision not to employ Te coprecipitation during the dissolution step. It is extremely doubtful whether the use of the less sensitive 208 keV peak of ^{199}Au would have allowed the detection of Pt in most of the samples. The view expressed by Shazali et al. [14] that a coprecipitation step is essential clearly does not apply to all cases, especially those where very low levels of Pt are anticipated.

SUMMARY

The analyses presented in this study form one of only a limited number of determinations of PGE abundances in kimberlitic rocks, and even with its small size, makes a significant contribution to a presently very sparse database. The results show that the combined nickel sulphide fire-assay and NAA procedure, without the use of Te coprecipitation, is sufficiently sensitive to determine the concentrations of all six PGE and Au in South African kimberlites with an acceptable degree of precision.

The authors would like to thank Anglo American Research Laboratory who kindly made sample material available for this study. K.S. Viljoen and C.B. Smith are thanked for additional samples and for their keen interest and many helpful discussions. Analytical costs were met by the Geological Survey of South Africa through an operating grant to R.J. Hart and by an FRD grant to Marian Tredoux. Iain McDonald acknowledges financial support via a J.W. Jagger scholarship from the University of Cape Town.

REFERENCES

1. J.H. Crocket, (1981), in L.J. Cabri, (ed.), Platinum-Group Elements: Mineralogy, Geology And Recovery, Can. Inst. Min. Metall. Spec. Vol. 23, (1981), 47.

2. M. Tredoux, G. Davies, N.M. Lindsay, and J.P.F.Sellschop, Geocongress '86, University of the Witwatersrand, (extended abstracts), (1986), 625.

3. D.C. Peck, and R.R. Keays, Can. Mineral., 28, (1990), 553.

4. R.H. Mitchell, Kimberlites, Plenum Press, New York, 1986

5. F.V., Kaminskiy, Y.V., Frantesson, and V.P., Khvostova, Doklady Akad. Nauk SSSR., 219, (1974), 190-193.

6. D.K. Paul, J.H. Crocket, and P.H. Nixon, in F.R. Boyd and H.O.A. Meyer, (eds.), Kimberlites, Diatremes And Diamonds: Their Geology, Petrology And Geochemistry., American Geophysical Union, Washington D.C.,(1979), 272.

7. M. Tredoux, unpubl. PhD thesis, University of the Witwatersrand, 1989

8. J.H. Crocket, and L.J. Cabri, in L.J. Cabri, (ed.), Platinum-Group Elements: Mineralogy, Geology And Recovery, Can. Inst. Min. Metall. Spec. Vol. 23, (1981), 71

9. C.S. Erasmus, N.I.M. Tech. Memo. 10928, (1982).

10. W.C. LENAHAN, and R. de L. MURRAY-SMITH, S. Afr. Inst. Min. and Metall. monograph M6, 1986.

11. S.E. Jackson, B.J. Fryer, W. Gosse, D.C. Healey, H.P. Longerich, and D.F. Strong, Chem. Geol., 83, (1990), 119.

12. E.L. Hoffman, A.J. Naldrett, J.C. van Loon, R.G.V. Hancock, and A.Manson, Anal. Chim. Acta, 102, (1978), 157.

13. R.V.D. Robért, E. Van Wyk, and R.Palmer, N.I.M. Report 1371, 1971.

14. I. Shazali, L. Van't Dack, and R. Gijbels, Anal. Chim. Acta, 196, (1987), 49

15. H.P. YULE, U.S. NBS Spec. Publ. 312, (1968), 115.

16. T.W. Steele, J. Levin, and I. Copelowitz, N.I.M. Report 1696, (1975).

17. G. Davies, and M. Tredoux, Econ. Geol., 80, (1985), 838.

18. I. Shazali, unpubl. PhD thesis, University of Antwerp, 1988.

19. A. Hall, Igneous petrology, Longman, Harlow, 1987.

20. S. Kallman, and C. Maul, Talanta, 30, (1983), 21.

21. A.P. Kuznetsov, Yu N. Kukushin, and D. Makarov, Zh. Anal. Khim., 29, (1974), 2155.

22. R. Palmer, and J.I.W. Watterson, N.I.M. Report 1185, (1971)

Table 1: Summary of PGE and Au Nuclear Data

Induced Nuclear Reaction	% Isotopic Abundance Of Target Isotope	Target Cross Section (barn)	Half Life Of Product Radioisotope	γ-Ray Used (keV)
$^{103}Rh\ (n,\gamma)\ ^{104m}Rh$	100 %	800	4.41 minutes	52
$^{108}Pd\ (n,\gamma)\ ^{109}Pd$	26.7 %	12	13.5 hours	88
$^{198}Pt\ (n,\beta\gamma)\ ^{199}Au$	7.2 %	4	3.15 days	158
$^{190}Os\ (n,\gamma)\ ^{191}Os$	26.4 %	3.9	14.6 days	129
$^{102}Ru\ (n,\gamma)\ ^{103}Ru$	31.5 %	1.4	38.9 days	497
$^{191}Ir\ (n,\gamma)\ ^{192}Ir$	38.5 %	750	74.2 days	317
$^{197}Au\ (n,\gamma)\ ^{198}Au$	100 %	98.8	2.70 days	412

Table 2: **Recovery of PGE into the nickel sulphide phase during fire-assays carried out on Wits-1, dunite R4A, and carbonatite C.S. with the unmodified and the modified fire-assay flux mixtures.**

Sample/Flux	% Activity Present						
	Os	**Ir**	**Ru**	**Rh**	**Pt**	**Pd**	**Au**
Wits1/Unmod.							
Loss To Slag	2.5	2.1	n d a	n d a	2.9	2.4	5.9
NiS Recovery	97.5	97.9	n d a	n d a	97.1	97.6	94.1
R4A/Unmod.							
Loss To Slag	12.6	8.0	n d a	n d a	9.6	12.3	8.6
NiS Recovery	87.4	92.0	n d a	n d a	90.4	87.7	91.4
C.S./Unmod.†							
Loss To Slag	n d a	n d a	n d a	n d a	n d a	n d a	n d a
NiS Recovery	n d a	n d a	n d a	n d a	n d a	n d a	n d a
R4A/Perid.							
Loss To Slag	2.9	1.9	n d a	n d a	2.8	2.6	5.0
NiS Recovery	97.1	98.1	n d a	n d a	97.2	97.4	95.0
C.S./HiCarb							
Loss To Slag	4.0	2.8	n d a	n d a	4.1	2.9	4.6
NiS Recovery	96.0	97.2	n d a	n d a	95.9	97.1	95.4

Unmod. = Conventional flux mixture, e.g. [9,16]
Perid. = "Peridotitic" flux mixture
HiCarb = "High Carbonate" flux mixture
† no data due to unstable melt.

Table 3: **Summary of reagents used in the modified and unmodified fire-assay mixtures. All masses expressed in grams.**

	Peridotite	High Carbonate	Unmodified
Sample composition requirements	<40% SiO_2 >30% MgO	<25% SiO_2 >15% CO_2	
Sample Material	50	50	50
Sodium Carbonate	30	30	30
Borax	60	70	60
Sulphur	12.5	12.5	12.5
Nickel Carbonate	35	35	35
Silica	10	20	zero

Table 4: **Calculated detection limits and reagent blanks for the NiS fire-assay and NAA procedure (see text for more information). "b d l" indicates beneath limit of detection. All values expressed in $\mu g.kg^{-1}$.**

	Os	Ir	Ru	Rh	Pt	Pd	Au
Calc. Limit Of Detection	0.2	0.005	1.0	0.35	2.5	0.8	0.001
Blank (1)	b d l	0.21	b d l	b d l	b d l	b d l	0.45
Blank (2)	b d l	0.30	b d l	0.41	b d l	b d l	0.67

Table 5: Summary Of PGE and Au concentrations in the South African kimberlites analysed in this study compared with values from the literature. Values expressed in $\mu g.kg^{-1}$. "b d l" indicates beneath limit of detection, and "n d a" indicates no data available for that element at present.

	Concentration Present						
Sample	**Os**	**Ir**	**Ru**	**Rh**	**Pt**	**Pd**	**Au**
1.Endkl-2-1	0.53	0.76	1.8	0.70	11.4	5.4	1.1
1.Endkl-2-2	0.75	0.70	1.9	0.74	13.8	4.7	0.92
2.Drftn-9-1	1.1	1.6	4.1	1.7	7.8	3.0	3.7
2.Drftn-9-2	1.5	1.6	4.3	1.8	8.3	3.2	3.0
3.Hrtbs-16-1	0.85	0.65	2.3	0.60	b d l	0.81	0.58
3.Hrtbs-16-2	0.50	0.60	1.7	n d a	b d l	b d l	0.55
4.Pampn-6-1	1.9	2.2	4.5	1.4	3.8	2.9	0.75
4.Pampn-6-2	2.3	1.8	6.0	1.5	4.0	2.3	0.85
5 Snddft-25-1	2.8	2.3	4.9	0.92	5.7	4.8	1.4
5 Snddft-25-2	2.4	2.3	5.8	n d a	4.1	4.7	1.0
6 Fnsch-445-1	1.6	1.2	2.1	n d a	4.5	6.7	1.8
6 Fnsch-445-1	1.4	1.2	2.6	n d a	4.9	8.0	2.1
7 Wesltn-422-1	2.3	1.4	2.7	n d a	4.9	2.9	2.1
7 Wesltn-422-2	1.8	1.2	2.0	n d a	4.7	4.4	2.6
8 RoVic-112-1	1.9	1.3	2.5	0.65	6.1	0.91	1.3
8 RoVic-112-2	1.6	1.3	1.9	n d a	5.6	0.96	2.2
8 RoVic-112-3	2.0	1.4	1.7	0.46	4.0	b d l	1.6
9 Jagftn-46-1	2.5	2.0	4.0	0.82	b d l	2.3	0.91
9 Jagftn-46-2	2.2	2.0	3.8	n d a	b d l	2.4	0.79
10 Prem-243-1	0.89	0.54	0.95	0.44	3.6	1.5	0.81
10 Prem-243-2	0.47	0.42	0.66	n d a	2.8	b d l	0.67
Jagersfontein†	n d a	2.6	n d a	n d a	n d a	8.9	10
Wesselton†	n d a	2.8	n d a	n d a	n d a	18	16
Wesselton*	2.5	1.5	b d l	n d a	b d l	21	3.1
Finsch*	b d l	1.6	b d l	n d a	22.0	b d l	3.7

† Data from Paul et al. [6]
* Data from Tredoux [7]

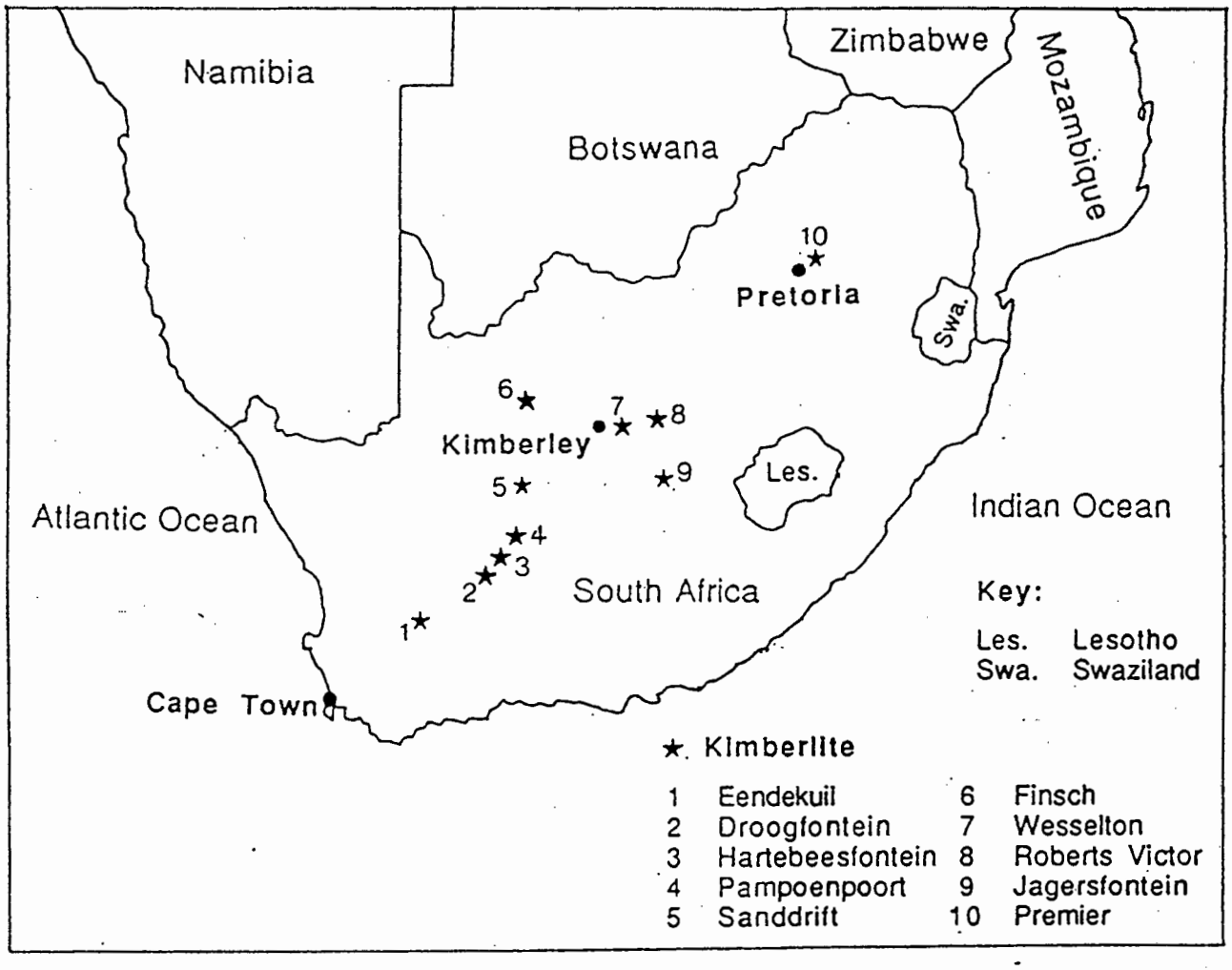

Figure 1

Map of southern Africa showing the locations of the kimberlites analysed in this study.

Appendix 5: Carbon Monoxide And The Volatile Transport Of The Platinum-Group Elements During Magmatic Processes.

I. McDonald, M. Tredoux, N.M. Lindsay, R.J., Hart, and M.J. de Wit

Proceedings 4th ICAM, CSIR, Pretoria, 2-4th September 1991

CARBON MONOXIDE AND THE VOLATILE TRANSPORT OF THE PLATINUM GROUP ELEMENTS DURING MAGMATIC PROCESSES

Iain McDonald[1,2], Marian Tredoux[1], Nicholas M. Lindsay[3]
Rodger J. Hart[2,4] and Maarten J. de Wit[1]

1. Department of Geology, University of Cape Town, Rondebosch, 7700 South Africa

2. Schonland Research Centre, University of the Witwatersrand, P.O. Wits, 2050 South Africa

3. Pedro de Valdivia 295, Santiago, Chile

4. Seconded from the Geological Survey of South Africa, P.Bag X112, Pretoria, 0001 South Africa

Experiments carried out on carbon-spiked and normal nickel sulphide-fire-assays of standard powder SARM-7 indicate that extensive losses of the platinum-group elements (PGE) and gold occur in the carbon-spiked samples. It is proposed that these losses can be explained by the volatilization of the PGE as PGE carbonyls. Movement of the PGE in a carbon monoxide bearing volatile phase is proposed to explain platinum enrichment in the dunite pipes of the Bushveld Complex.

Introduction

Reactions of carbon monoxide (CO) with the first row transition metals of group VIII of the Periodic Table (Fe, Co, and Ni) have been known for more than a century. Ludwig Mond and his co workers successfully produced and described the properties of many of these carbonyls[1,2], most notable of which was their extreme volatility[2]. Reaction between CO and the elements of the second and third rows of group VIII, i.e. the platinum group elements (PGE), have always been more difficult to promote, and although many of these compounds were prepared and characterized in the first half of this century by the German chemist Walter Hieber and his co workers, the systematics of the reactions between CO and the PGE are still largely speculative. The classical syntheses of these volatile PGE carbonyls involved the passage of CO at moderate temperatures (200 to 400°C) and at high pressures (20 to 300 atm) over finely divided PGE metals, halides or sulphides[3].

Recent studies on the possible composition of volatile phases under magmatic conditions[4,5] and on the form of the PGE contained within the silicate melt[6] suggest certain analogies with many of the classical carbonyl syntheses. It has been proposed[6] that the PGE exist as separate entities, quite distinct from the normal structure of the silicate melt. This form is dominated by polymetallic clusters of PGE atoms. These clusters are thought to be chemically and mineralogically incompatible with the melt structure and as such would be carried as microparticles in suspension by the liquid. We postulate that the fluxing of a CO bearing volatile phase through a silicate liquid containing submicroscopic PGE clusters could convert the PGE into volatile carbonyls. The results of a preliminary test study carried out at atmospheric pressure are presented. The possibility that the PGE could be mobilized in this manner is discussed with reference to PGE enrichment and mineralization in late metasomatic replacement pegmatoids.

Experimental Observations

The passing of CO through nickel sulphide-fire-assay melts allows a very crude comparison with a conventional igneous melt containing sulphide and PGE, and, for both ease of preparation and ease of analysis of products, this was the initial medium of choice. In each case the sample material used was the standard rock powder SARM-7. This has been certified for all six PGE and Au[7]. Details of the assay procedure are given elsewhere[8]. Well homogenized 1:10 dilutions of SARM-7 with pure silica were mixed with the flux components

and deliberately spiked with 0.2 grams of carbon in the form of graphite powder. The diluted SARM-7, along with the other flux components, and any added graphite, were mixed by hand for ten minutes on glazed paper prior to pouring into the assay crucibles. Samples with and without added carbon were prepared and fired together under the same conditions.

During heating at 1000°C, carbon reacts with the restricted volume of oxygen present in the melted powder pile. Most basaltic or alkali basaltic melts at one atmosphere have oxygen fugacities in the region of 10^{-7} to 10^{-9} atmospheres of oxygen[5,9] and these estimates are probably a good first order representation of the oxygen fugacity of molten SARM-7 during the fire assay. Under these conditions, and where carbon was added, we expected a mixed gas phase comprising CO_2 and minor CO to be produced[10]. The exact proportions of these species are not known at present but the presence of graphite in some of the fusion products allow some broad inferences to be drawn. These are discussed later.

Both CO_2 and CO are highly insoluble in silicate melts and, as expected, the carbon-spiked melts bubble vigorously during fusion and on cooling. The presence of CO_2 in the evolved gas is implied by the precipitation of $CaCO_3$ from lime water held over the cooling crucibles. In contrast, the normal samples showed relatively little signs of vigorous outgassing as they cooled.

Examination of the fusion products revealed further differences between the two types of sample. Firstly, several of the carbon-spiked assays produced nickel sulphide buttons with central depressions of their top surfaces. These depressions were invariably coated with a thin, surface layer of black carbon. Furthermore, when we reconstructed the crucible and the glass slag around these anomalous buttons we found that while over the "normal" sulphide rim the slag and the sulphide were in perfect contact, the slag visibly arched over the carbon coated depression leaving a vacant hole. We suggest that gas was trapped in this vacant hole, and that the gas accumulated at quite a late stage and was unable to rise through the melt, as this had probably become too viscous to allow the gas to migrate upwards.

The second major difference became apparent when we examined the gross picture of the gases trapped in the slags produced from both types of sample. These seem to indicate separate patterns of gas evolution for the carbon-spiked and the normal samples during the fusion. These patterns are summarized in Figure 1. In the case of the the carbon-spiked samples we believe that we see two distinct phases of gas production and entrapment. An initial, primary phase which was most evident as the intense bubbling observed on cooling. During this phase, carbonaceous gases generated from

the added graphite rise rapidly upwards through the melt and are either lost to the atmosphere or are trapped, and coalesce as a large single bubble at the the top of the silicate which is capped by a thin skin of chilled slag. The second phase is the gas associated with the carbon coated depression on the sulphide which, as we argue above, would seem to relate to a much later release of gas, possibly even associated with the sulphide.

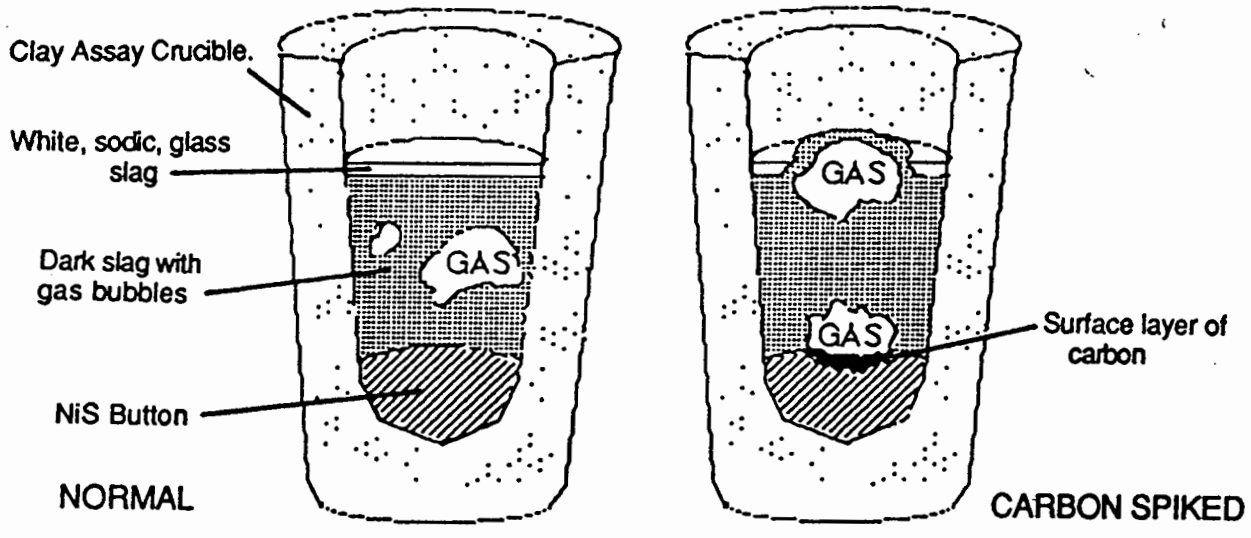

Figure 1: Comparison of gas patterns after assay between normal and carbon-spiked samples.

Slags produced from the normal samples, show a more simple picture. These slags contain several bubbles of gas halfway or just over halfway up the slag, which seem to have risen somewhat through the melt. We suggest that the gas present in these bubbles was produced at a later stage than that which makes up the primary phase in the carbon-spiked samples as these bubbles were clearly trapped separately in the cooling silicate before they could reach the top of the melt and coalesce together into a large single bubble.

While the early gas evolution from the carbon-spiked samples is readily explained by the relative insolubilities of both CO_2 and CO in the melt, the later evolution of gas from the region of the sulphide and the presence of graphite are more problematic. The presence of seemingly unreacted graphite has important implications for the composition of the gas phase. Two explanations can be forwarded to account for the carbon and both indicate a larger fraction of CO present in the volatile phase than the simple fo_2 conditions we inferred above would imply.

1. More graphite was added to the initial mixture than could be transformed into carbonaceous gases at the prevailing fo_2 conditions. A high C/O ratio did not favour the complete oxidation of the carbon to CO_2 and the

fraction of CO in the gas phase would be increased. Unreacted graphite is then physically adsorbed onto the surfaces descending blobs of sulphide and becomes associated with the final button. The graphite is much less dense than the sulphide and floats to the top of the sulphide button.

2. There was complete consumption of the carbon to form CO_2 and CO. The sulphide collected some of these gases as it descended through the melt and they were present in the final button. The presence of carbon on the surface of the button can be explained if CO was present in these sulphide-hosted gases. Graphite can be produced from CO via a disproportionation such as

$$2\ CO_{(g)} = C_{(graphite)} + CO_{2\,(g)} \qquad (1)$$

Nickel and sulphur have been shown to promote reactions of this type and to stabilize carbon in the form of coke (graphite) relative to CO on catalyst surfaces[11,12] and we feel that the hot sulphide button could cause a similar effect during the fire assay. CO contained within the hot sulphide would be released as the button cooled and this would be trapped at the interface between the button and the slag. It could then disproportionate to graphite and CO_2 on the surface of the hot sulphide producing a surface layer of carbon and a small, CO_2 dominated, gas bubble.

Presently we feel that the association of a carbon coated depression with a small gas bubble favours explanation 2. The collection of unreacted graphite could account for the surface carbon layer but not for the accompanying gas bubble. It would appear that in order to generate the gas bubble which we see, CO_2 and CO rather than unreacted carbon alone must be collected into the sulphide melt and then released at a later stage.

We therefore conclude that the addition of carbon to nickel sulphide-fire-assay mixtures produces a carbonaceous gas phase during the fusion. This phase may contain a significant fraction of CO.

Analysis Results

To this point we have analysed all of the solid phases present in the crucibles for their noble metal content. Analyses of the gas phase will be carried out in the near future. Nickel sulphide buttons produced from normal and carbon-spiked samples were analysed by neutron activation analysis (NAA) to yield the concentrations of the six PGE and Au. A summary of these results is presented in Table 1. This shows that in each case where carbon was added to the original powder mixture, less PGE and Au were collected from the silicate melt and transferred into the sulphide button.

Table 1: Summary of analyses from six carbon-spiked and five non-spiked samples of SARM-7 after fire assay at 1000°C. All the concentrations are expressed in ng per gram and all errors are quoted at the one sigma level.

Sample Type	Concentration Present						
	Os	Ir	Ru	Rh	Pt	Pd	Au
Normal Assay 1	6.3	7.5	42.8	24.1	370	150	33
Normal Assay 2	6.0	7.2	40.1	21.3	378	154	30
Normal Assay 3	6.5	7.9	45.3	26.9	379	156	38
Normal Assay 4	5.9	7.1	39.8	21.0	362	153	31
Normal Assay 5	6.9	7.0	41.1	24.9	369	158	30
C-Spiked 1	4.9	6.4	32.1	20.2	352	139	22
C-Spiked 2	5.2	5.7	33.9	17.9	329	131	28
C-Spiked 3	5.4	6.0	36.2	18.4	336	134	24
C-Spiked 4	4.2	6.1	30.7	21.0	340	128	20
C-Spiked 5	5.0	6.1	38.0	18.7	345	136	25
C-Spiked 6	5.6	5.8	29.9	18.3	330	126	21

Element	Average Conc. Normal Assay	Average Conc. Carbon Spiked	% Loss Compared To Normal Assay
Os	6.3 +/- 0.4	5.1 +/- 0.5	19.9 +/- 16.2
Ir	7.3 +/- 0.4	6.0 +/- 0.3	17.9 +/- 10.2
Ru	41.8 +/- 2.3	33.4 +/- 3.2	20.1 +/- 15.1
Rh	23.7 +/- 2.4	19.1 +/- 1.2	19.4 +/- 16.4
Pt	372 +/- 7.0	339 +/- 8.9	8.9 +/- 4.5
Pd	154 +/- 3.1	132 +/- 4.9	14.3 +/- 5.7
Au	32.4 +/- 3.3	23.3 +/- 2.8	28.1 +/- 22.2

We crushed and then performed a second fire-assay on some of the slags from the carbon-spiked samples to check whether any phase trapped in the frozen slag was by some means holding back the missing PGE and Au. Only traces of Ir and Au above blank levels were detected. Carbon separated from the surface of the sulphide was also irradiated and analysed. The results from the analyses of both the slag and the carbon are shown in Table 2. These are clearly not enough to explain the "losses" of the PGE and Au encountered in the carbon-spiked buttons after the fusion.

Table 2: Summary of slag analyses. All concentrations are expressed in ng per gram. n.d. means "not detected" and nda means "no data available" for that element.

Sample	Concentration Present						
	Os	Ir	Ru	Rh	Pt	Pd	Au
Re-assay 1	n.d.	0.1	n.d.	nda	n.d.	n.d.	0.08
Re-assay 2	n.d.	0.2	n.d.	nda	n.d.	n.d.	0.06
Carbon	n.d.	0.01	n.d.	nda	n.d.	n.d.	0.40

In the case of the carbon-spiked samples after fire-assay, we see less PGE and Au in the sulphide button than is the case with the normally prepared samples. This cannot be accounted for by PGE and Au in any of the other solid phases in the crucible. We therefore conclude that these losses are

linked to the addition of carbon and the gas phase it generates during the fusion step. Removal of the PGE and Au as volatile carbonyl species is considered as a possible explanation for these results.

The Form And Potential Reactivity Of The PGE In Silicate Melts

We believe that while most models which attempt to address the magmatic behaviour of the PGE make the assumption that the main chemical control on the final distribution of the PGE is exercised by the availability of any immisible sulphide melt, this perceived association with sulphide is overstated. We suggest that the predominant PGE species is not PGE-S molecules but rather electrochemically neutral, polymetallic clusters of less than 100 PGE atoms. These submicroscopic clusters have high surface energies and are stabilized or "wetted" by the physical adsorption of chalcogenic melt components (S, As, Sb, and Te) on their outer surfaces. Considering the gross scale, the PGE would then act almost as tiny, discrete particles suspended within, but not chemically bonded to, the silicate melt. While some Os, Ir, and Ru might act as nucleation sites for spinels or olivine and be removed from the melt, generally, in the absence of an immisible sulphide liquid which could collect the clusters mechanically, they are not chemically compatible with any of the crystallizing silicate phases and would become progressively enriched in the residual melt.

It was found that the conversion of ruthenium sulphide, (RuS_2), to ruthenium carbonyl was more favoured than a reaction with the metal alone and that the reaction was promoted by the presence of sulphur binding elements, like Cu, Zn, and Pb[13]. It is notable that these three metals are, to varying degrees, also quite incompatible in silicates and would therefore also be concentrated in the residual melt. A carbonylation reaction of this type would be further promoted by having the PGE, sulphur, and chalcophile metals in a very finely divided form, perhaps even on the scale of clusters of atoms. Then, if clusters are the true form of the PGE in melts, these clusters could be subjected to attack by CO exsolving from the melt in a manner analogous to the classical gas/metal or gas/metal sulphide syntheses.

A schematic representation of this type of reaction involving PGE clusters is shown in Figure 2. Chalcogenide species are adsorbed physically on the surfaces of the cluster, and stabilize the cluster by lowering its surface energy and maintaining the neutrality of the metal species. CO displaces the chalcogenides from the surfaces of the cluster and forms strong σ and Π bonds to the PGE[14]. This Π "back bonding" interaction involves a drift of

electrons from the metal electron orbitals to vacant P electron orbitals on the carbon. Magnetic studies have shown that metal-C bonds of this type are very close to neutrality and in this manner, the neutrality of the cluster is maintained[14]. Thus, reaction with CO fulfils the same function as the adsorbed chalcogenides, but allows a stronger, chemical interaction. This interaction in turn, leaves the metal slightly positive. The formation of many metal-C bonds over a cluster's surface, and the resultant movement of charge will weaken the intermetallic bonds within the cluster, causing it to break up into several smaller fragments. These are attacked further until stable, volatile, polymetallic PGE carbonyls are formed. We would like to suggest that the PGE can be transformed from submicroscopic particulate solids into volatile carbonyl species by this reaction mechanism.

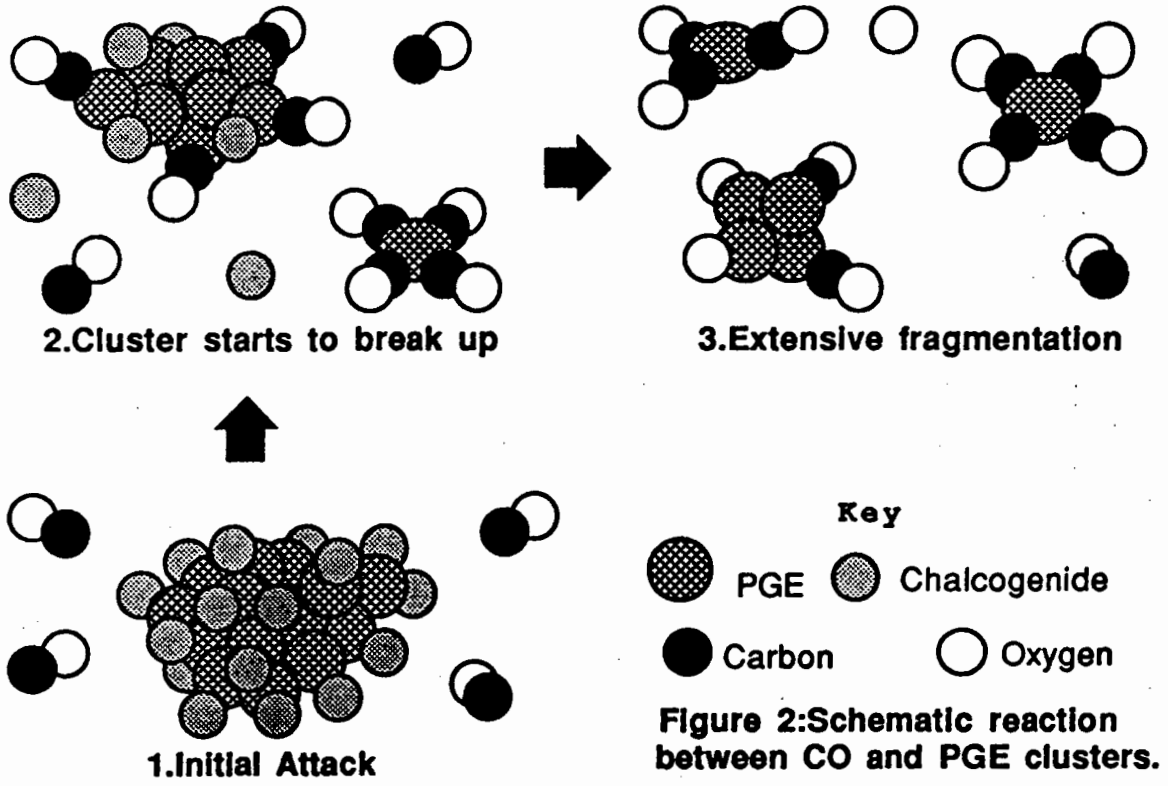

Figure 2:Schematic reaction between CO and PGE clusters.

Volatile Transport Of The PGE Under Magmatic Conditions.

CO and CO_2 are highly insoluble in igneous melts and both will partition into any exsolving volatile fluid. Under the fo_2 conditions typical of many igneous melts at high pressure, the first volatile phase to separate from melts of the Bushveld or Stillwater type might be mixtures of CO_2 and CO with some HCl and small amounts of sulphur species[4]. We believe that the action of CO in this insoluble, volatile phase on similarly insoluble, particulate PGE clusters trapped in the residual, silicate melt could be analogous to

both Hieber's high pressure carbonyl syntheses and our fire-assay experiments and could transform the PGE into volatile species.

A consideration of the possible ways in which residual melts might move in magma chambers is also important here. Sites of structural weakness in the crystal pile, such as faults, could form extensive vertical channelways through which migration of the residual melt and its associated volatiles could occur. Continued lateral migration and accumulation of fluids within these structures over time has been envoked to explain cross-cutting iron-rich pegmatoids in large magma chambers such as the Bushveld Complex[15]. The exsolving volatile fluids, being less dense than the surrounding melt, would migrate easily towards these structural sites, and could be channelled upwards in a very restricted manner through a considerable volume of intercumulus, residual melt, which also contains incompatible PGE clusters

Although CO readily forms carbonyls with metals such as Fe, Co, and Ni, these metals are much more compatible with the silicate and probably do not undergo significant reaction with the insoluble, volatile fluid. The fluid is more likely to undergo interactions with other insoluble components such as the clusters. These structural sites within the crystal pile can then be considered as large flow reactors, where CO bearing volatile fluids enter at the base of the structure and migrate upwards through a restricted, pipe-like, channelway which contains both the residual melt and, we believe, incompatible PGE. The continued passage of CO bearing fluids over time through the channelway could progressively strip the melt of its PGE and effect a considerable mobilzation of the metals into the volatile phase.

Application Of PGE Carbonyls To Replacement Pegmatoids

The iron-rich, dunitic pegmatoid pipes of the Bushveld Complex are believed to be of replacement origin, and brought about by residual, volatile-charged fluids[15]. Of these, the Onverwacht, Mooihoek, and Driekop pipes of the eastern Bushveld are known to have been highly enriched in platinum[16,17]. Two environments which tend to carry elevated concentrations of platinum have been noted. These are, firstly, pegmatoid portions of dunite, and secondly, fragments of chromitite layers which are preserved in the pipes[17].

We agree that the distinction between platiniferous and platinum-poor pegmatoids[15] is probably not justified petrogenetically[18]. We suggest that the action of CO bearing fluids, as outlined above, might be a new angle with which to view the mineralization and might also provide a genetic linkage between the platiniferous, and the non-platiniferous pipes.

Many of these dunite pipes (both platiniferous and non-platiniferous) are known to contain amounts of native graphite[17]. This has almost certainly been produced from a volatile phase and indicates that the migration of a carbon-bearing fluid might have been an integral feature in the development of the pipes. We suggest that it is the action of CO, which transfers PGE from the residual melt into the volatile fluid, and, then the manner in which these volatile PGE compounds react with existing phases in the pipe (notably spinel), which might exercise an important control on the final distribution of any PGE mineralization.

Several authors have noted that the dominance of PGE alloys and the lack of, more common PGE sulphides, in chromitites in or near the pipes might indicate that sulphur has been lost by oxidation from these layers[18,19]. This oxidation could be accomplished by a subsolidus reaction involving pyrrhotite and chromite, producing a more Fe-rich chromite and releasing sulphur[18], or by some interaction with volatile fluids[19]. The chromitite bands would then appear to be zones of localized oxidation. PGE carbonyls are very sensitive to oxidation and passage through these chromitite layers could cause them to be destabilized, breaking down to the PGE metal and CO. Platinum might then be fixed on excess Fe generated by the breakdown of sulphide to form the Pt-alloy dominated assemblage which seems to be a feature of the platiniferous pipes.

Our proposed model is summarized in Figure 3. The eastern Bushveld dunite pipes (Driekop, Mooihoek and Onverwacht) are believed to differ from those in the west, only in the fact that they expose mineralization near the base of the fluid channelway, where volatiles have moved through both residual melt and any chromitite trapping layers, for an extended period of time. In contrast, the larger, and supposedly "platinum-poor" pipes of the western Bushveld expose higher levels of pipes which have roots at depth and have obviously developed further from the base of the structure. Geophysical modelling, suggests that it is likely that they pass through at least the and UG 1 and MG chromitites before they reach the upper regions of the Critical Zone[20]. They appear barren in the upper levels presently exposed at surface and in mine workings. However, we consider it highly possible that any PGE associated with the volatile fluids has been stripped out by chromitites deeper in the stratigraphy and that little PGE remains in the volatile phase when it reaches the upper Critical Zone via these channelways. Thus while the upper levels of the pipes are clearly not extensively mineralized we would predict PGE mineralization of the type seen in the eastern Bushveld, associated with chromitites at much deeper levels in the pipe.

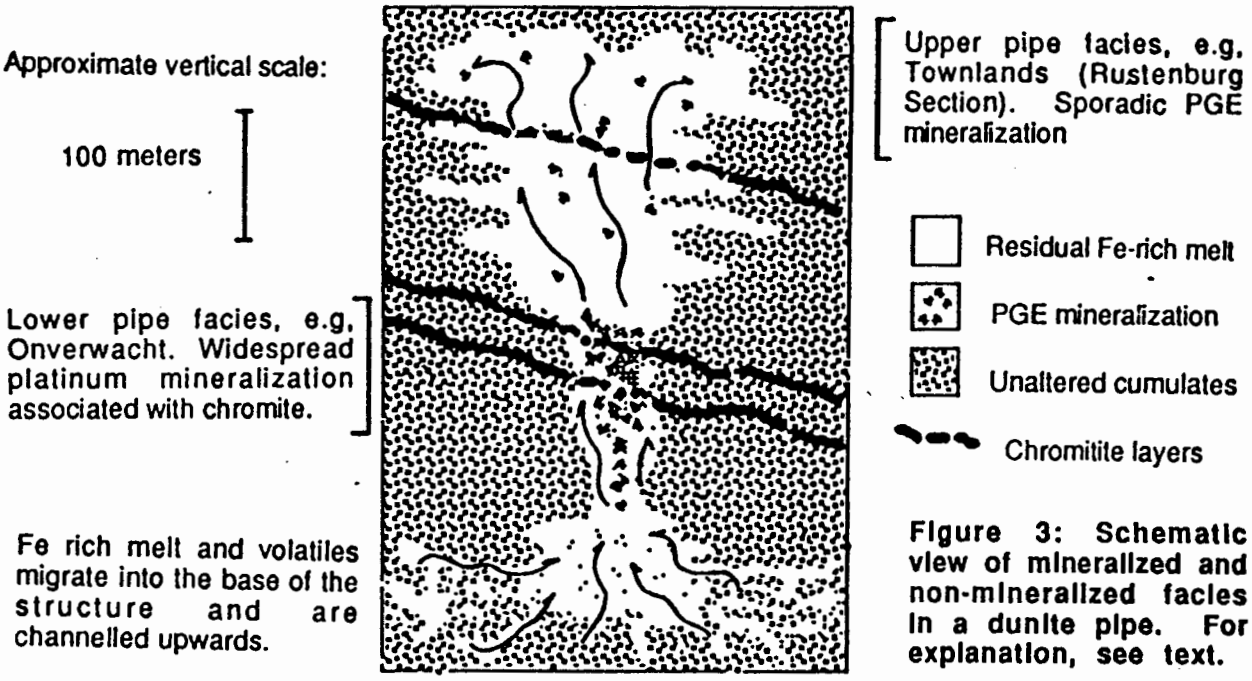

Figure 3: Schematic view of mineralized and non-mineralized facies in a dunite pipe. For explanation, see text.

Summary

When carbon is spiked into nickel sulphide fire-assay samples, less PGE and Au are collected into the sulphide button than is the case with normally prepared samples. We suggest that CO is generated during fusion and that the PGE can be mobilized under assay and also under typical magmatic conditions as carbonyls. Many of these species are highly volatile and they could be carried over considerable distances by magmatic gases. Chromitite layers, via localised oxidation conditions, might act as a collector of these volatile PGE compounds.

Acknowledgements

We thank R.K.W. Merkle and E.D. Kinloch for their patient reviews and very constructive criticism. Financial support for the first author is provided by a J.W. Jagger scholarship from the University Of Cape Town.

References

1. Mond, L., Langer, C, and Quinke, F. (1890). The action of carbon monoxide on nickel. J. Chem. Soc., 57, 749-753.

2. Mond, L., Hirtz, H., and Cowap, M.D. (1910). Some new metallic carbonyls. J.Chem. Soc., 97, 798-810.

3. Hieber, W. (1970). Metal carbonyls, forty years of research. Adv. Organomet. Chem., 8, 1-28.

4. Mathez, E.A., Dietrich, V.J., Holloway, J.R., and Boudreau, A.E. (1989). Carbon distillation in the Stillwater Complex and evolution of vapour during crystallization of Stillwater and Bushveld magmas. J. Petrol., 30, 153-173.

5. Mathez, E.A. (1988a). Vapour associated with mafic magma and controls on its composition. Rev. Econ. Geol., 4, 21-31.

6. Lindsay, N.M. (1989). The processing and recovery of the platinum-group elements. Unpubl. PhD thesis, University of the Witwatersrand, 322pp.

7. Steele, T.W., Levin, J., and Copelowitz, I. (1975). The preparation and certification of a reference sample of precious metal ore. Nat. Inst. Metall. Rept., 1696, Randburg, 50pp.

8. Davies, G., and Tredoux, M. (1985). The platinum-group element and gold contents of marginal rocks and sills the Bushveld Complex. Econ. Geol., 80,838-848.

9. Sato, M., and Wright, T.L. (1966). Oxygen fugacities directly measured in magmatic gases. Science, 153, 1103-1105.

10. French, B.M. (1966). Some geological implications of equilibrium between graphite and a C-H-O gas phase at high temperatures and pressures. Rev. Geophysics, 4, 223-253.

11. Anderson, S., Landquist, B.I., and Norskov, J.K. (1977). Possible mechanism for the catalytic action of nickel surfaces on the reaction $CO = C + CO_2$. Proceedings, 7th Int. Vacuum Congress, Vienna, 815.

12. Delahay, G., and Duprez, D. (1989). Effect of sulphur on the coking of rhodium in the steam reforming of 1-methylnaphthalene. Appl. Catal., 53, 95-105.

13. Hieber, W., and Fischer, H. (1941). Ruthenium carbonyl. Chem. Abstr., 35, 5657.

14. Cotton, F.A., and Wilkinson, G. (1980). Advanced Inorganic Chemistry. (4th edition), Wiley, New York, 1396pp.

15. Viljoen, M.J., and Scoon, R.N. (1985). The distribution and geologic features of discordant bodies of iron-rich ultramafic pegmatite in the Bushveld Complex. Econ. Geol., 80, 1109-1128.

16. Wagner, P.A. (1929). The platinum deposits and mines of South Africa. Oliver and Boyd, Edinburgh, 329pp.

17. Stumpfl, E., and Rucklidge, J.C. (1982). The platiniferous dunite pipes of the eastern Bushveld. Econ. Geol., 77, 1419-1431.

18. Mathez, E.A. (1988b). Interactions involving fluids in the Stillwater and Bushveld complexes: observations from the rocks. Rev. Econ. Geol., 4, 167-179.

19. Kinloch, E.D., and Peyerl, W. (1990). Platinum-group minerals in various rock types of the Merensky Reef: genetic implications. Econ. Geol., 85, 537-555.

20. Viljoen, M.J., Hieber, R., and Peyerl, W. (1983). The geology of the Townlands dunite/pegmatoid pipe, Rustenburg section of Rustenburg Platinum Mines. Abstract, Symposium on the Bushveld Complex, Univ. Pretoria, 94-97.

Appendix 6 : Summary Of Sample Numbers And Codes For Kimberlite And Alkali Rock Samples.

	Intrusion	Sample Number	Age	Group	Reference
Africa					
	Frank Smith	FSK-1	114 Ma	I	B
	Jagersfontein	Jagers-46	86 Ma	I	B
	Wesselton	Wessel-422	86 Ma	I	C
	Premier	CBS Prem. Grey CBS Prem. Piball JJG/243 Carb. Dyke	1180 Ma	I	A
	Monastery	Mon-1	83 Ma	I	B
	Benfontein	173/33/k18/45	?	I	H
	Vioolskraal	173/26/k46/3	?	I	G
	Hartebeesfontein	Hartebees-16	74 Ma	I	G
	Sutherland	Suth 259 Suth 261 Suth 266	75 Ma	I	D
	CKP-9	CKP-9	87 Ma	I	B
	HPK-13	HPK-13	70 Ma	I	E
	Finsch	Finsch 445	118 Ma	II	B
	Roberts Victor	RoVic 112	126 Ma	II	B
	Sanddrift	173/33/k12/45	118 Ma	II	G
	Slypsteen	173/26/k24/5	?	II	G
	Eendekuil	173/18/k2/2	114 Ma	II	G
	Lace K2	Lace-2	140 Ma	II/I	C
	Droogfontein	Droog-9	176 Ma (?)	II/I	G
	Melton Wold	173/27/k9/18	145 Ma	II/I	G
	Pampoenpoort	Pamp-6	103 Ma	I/II	G
Brazil					
	Tres Ranchos	TRX	95 Ma	II/I	F
	Limeira	PDZ	95 Ma	II/I	F
	Japecanga	JAP-60	109 Ma	I/II	F
	Pantano	PAN	87 Ma	II/I	F
	Pres. Olegario	POL	85 Ma	II/I	F
	Carmo Paranaiba	CPB	85 Ma	II/I	F
	Sucesso	SUC-G (R)	118 Ma	II/I	F

References:
A: Robinson (1975)
B: Smith et al. (1985)
C: Shee (1986)
D: Viljoen (1988)
E: Spriggs (1988)
F: Bizzi et al. (1993a)
G: Skinner et al. (1993)
H: Dawson and Hawthorne (1973)